ASSESSMENT OF DIMETHYL SULPHIDE ODOROUS EMISSIONS RELEASED DURING THE UNDERGROUND COAL EXTRACTION IN COAL MINE VELENJE

Gregor Uranjek

Doctoral Dissertation
Jožef Stefan International Postgraduate School
Ljubljana, Slovenia

Supervisor: Asst. Prof. Dr. Jože Kotnik, Jožef Stefan International Postgraduate School, Jožef Stefan Institute, Ljubljana, Slovenia
Co-Supervisor: Prof. Dr. Radmila Milačič, Jožef Stefan Institute, Ljubljana, Slovenia

Evaluation Board:
Prof. Dr. Milena Horvat, Chair, Jožef Stefan International Postgraduate School, Jožef Stefan Institute, Ljubljana, Slovenia
Dr. David Heath, Member, Jožef Stefan International Postgraduate School, Jožef Stefan Institute, Ljubljana, Slovenia
Prof. Dr. Gordan Bedeković, Member, Department of Mining Engineering and Geotechnics, Faculty of Mining, Geology and Petroleum Engineering, University of Zagreb, Croatia

MEDNARODNA PODIPLOMSKA ŠOLA JOŽEFA STEFANA
JOŽEF STEFAN INTERNATIONAL POSTGRADUATE SCHOOL

Gregor Uranjek

ASSESSMENT OF DIMETHYL SULPHIDE ODOROUS EMISSIONS RELEASED DURING THE UNDERGROUND COAL EXTRACTION IN COAL MINE VELENJE

Doctoral Dissertation

OCENA EMISIJ VONJAV NA OSNOVI SPROŠČANJA DIMETIL SULFIDA PRI PROCESU PODZEMNEGA ODKOPAVANJA PREMOGA V PREMOGOVNIKU VELENJE

Doktorska disertacija

Supervisor: Asst. Prof. Dr. Jože Kotnik, Jožef Stefan International Postgraduate School, Jožef Stefan Institute, Ljubljana, Slovenia

Co-Supervisor: Prof. Dr. Radmila Milačič, Jožef Stefan Institute, Ljubljana, Slovenia

Ljubljana, Slovenia, March 2024

Acknowledgments

First, I would like to thank my dissertation supervisor Asst. Prof. Dr. Jože Kotnik and co-supervisor Prof. Dr. Radmila Milačič for their excellent support, help and guidance during my studies. Also, I would like to thank my industry supervisor Dr. Simon Zavšek for his help and guidance during the first half of my studies.

I would like to thank the members of the evaluation board, Prof. Dr. Milena Horvat, Dr. David Heath and Prof. Dr. Gordan Bedeković, for reviewing and evaluating the work in this thesis.

This study was conducted in the framework of the project ″Young researchers from Industry 2010″ and its operation was partly financed by the European Union, European Social Fund. I am grateful to the Velenje Coal Mine, which provided the necessary assets and data, and especially to the mine ventilation team of the Velenje Coal Mine for their technical support and for the necessary mine ventilation parameters. I am also grateful to Dr. David Heath and Prof. Dr. Sevket Durucan for all suggestions and recommendations.

I want to express special gratitude to Prof. Dr. Milena Horvat and Prof. Dr. Radmila Milačič for their outstanding support and help when most needed, which helped me maintain the will and determination to finish this work.

Lastly but most importantly, I would like to thank from the bottom of my heart my loved ones for being the most supportive. None of this would have been possible if my Tina had not stood by my side and taken care of our family while I was away.

Abstract

Underground coal extraction at Coal Mine Velenje occasionally gives rise to odour complaints from local residents and irritates and disturbs the miners at work in the mine.

This work describes a robust quantification of odorous emissions of mine sources and a model-based analysis aimed to establish a better understanding of the sources, concentrations, dispersion, and possible control of odorous compounds during the coal extraction process.

Major odour sources during underground mining are released volatile sulphur compounds from coal seam that have characteristic malodours at extremely low concentrations at $\mu g/m^3$ levels. Analysis of 1028 gas samples taken over a six-year period (2008-2013) revealed that dimethyl sulphide (DMS, $(CH_3)_2S$) is the major odour active compound present in the mine, being detected on 679 occasions throughout the mine. While hydrogen sulphide (H_2S) and sulphur dioxide (SO_2) were detected 5 and 26 times.

Analysis of gas samples has shown that main DMS sources in the mine are coal extraction locations at longwall faces and development headings and that DMS is also released during transport from the main coal transport system.

The dispersion simulations of odour sources in the mine have shown that the concentrations of DMS at median levels can represent relatively modest odour nuisance. While at peak levels, the concentration of DMS remained sufficiently high to create an odour problem both in the mine and on the surface. Overall, dispersion simulations have shown that ventilation regulation on its own is not sufficient as an odour abatement measure.

Povzetek

Podzemno pridobivanje premoga v Premogovniku Velenje občasno povzroča pritožbe lokalnih prebivalcev zaradi neprijetnih vonjav. Neprijeten vonj v premogovniku lahko tudi draži in moti rudarje pri delu.

To delo opisuje robustno kvantifikacijo emisij neprijetnega vonja iz premogovnika in analizo na podlagi disperzijskega modela vonjav premogovnika, katere cilj je vzpostaviti boljše razumevanje virov, koncentracij, disperzije in možnega nadzora neprijetnih vonjav med postopkom pridobivanja premoga.

Glavni viri neprijetnega vonja med podzemnim odkopavanjem so sproščanje hlapnih žveplovih spojin iz premogovnega sloja, ki imajo značilen vonj pri izredno nizkih koncentracijah na ravneh $\mu g/m^3$. Analiza 1028 vzorcev plina, odvzetih v šestletnem obdobju (2008–2013), je razkrila, da je dimetil sulfid (DMS, $(CH_3)_2S$) glavna aktivna spojina z vonjem, ki je prisotna v premogovniku. V celotnem premogovniku je bila zaznana 679-krat. Medtem ko sta bila vodikov sulfid (H_2S) in žveplov dioksid (SO_2) zaznana 5-krat, oz. 26-krat.

Analiza vzorcev plina je pokazala, da so glavni viri DMS v rudniku lokacije pridobivanja premoga. To so odkopi, kjer se odkopava premog in delovišča za izdelavo jamskih prog, ki so izdelane v premogu. DMS se sprošča tudi med transportom iz glavnega transportnega sistema premoga.

Simulacije disperzije virov neprijetnega vonja v premogovniku so pokazale, da lahko pri srednjih ravneh (median) koncentracij DMS emisije predstavljajo razmeroma blag neprijeten vonj. Ko je na najvišjih ravneh (97,5. percentilu) koncentracij DMS, lahko emisije neprijetnega vonja povzročajo težave tako v samem premogovniku kot tudi na površju, na področju bližnjih naselij. Na splošno so simulacije disperzije neprijetnega vonja pokazale, da regulacija sistema zračenja premogovnika sama po sebi ne zadostuje kot ukrep za odpravo neprijetnih vonjav.

Contents

List of Figures

List of Tables

Abbreviations

AFC . . . armoured face conveyor
BSL . . . beam stage loader
CH_3SH . . . methanethiol, methyl mercaptan
CH_4 . . . methane
CMV . . . Coal Mine Velenje
CO_2 . . . carbon dioxide
COS . . . carbonyl sulphide
CS_2 . . . carbon disulphide
DMDS . . . dimethyl disulphide
DMS . . . dimethyl sulphide $(CH_3)_2S$)
DMSP . . . dimethylsulfonopropionate
GC-FID . . . gas chromatography with flame ionization detector
GC-FPD . . . gas chromatography with flame photometric detector
GC-MS . . . gas chromatography with mass spectrometry
GC-SCD . . . gas chromatography with sulphur chemiluminescence detector
HSS . . . hydraulic shield supports
H_2S . . . hydrogen sulphide
LTCC . . . longwall top coal caving
OAV . . . odour activity value
OTD . . . odour detection threshold
RSC . . . reduced sulphur compounds
SO_2 . . . sulphur dioxide
TLV . . . threshold limit value
TRS . . . total reduced sulphur compounds
VMM . . . Velenje mining method
VOC . . . volatile organic compounds
VSC . . . volatile sulphur compounds

Glossary

Airways	Any passage through which air is carried. In an underground mine, airways are usually mine objects such as gateroads, shafts, drifts, slopes, etc.
AFC	Mechanized longwall systems is an armoured face conveyor (AFC). In addition to carrying coal from the face, the AFC serves as the guide for the longwall shearer, which rides on it. The most modern design of AFC utilises a side discharge arrangement to push the coal directly onto the beam stage loader (BSL). This design is most suited to coal with large lumps. This design can also transport a higher capacity of coal.
Auxiliary ventilation	Portion of the main ventilating current directed to face the dead end (e.g. development headings) entry by means of an auxiliary fan and tubing.
Belt conveyor	A looped belt on which coal or other materials can be carried and which is generally constructed of flame-resistant material or of reinforced rubber or rubber-like substance.
BSL	When the coal is transported by the AFC along the longwall face, it reaches the beam stage loader at the end of the face. The beam stage loader is simply a chain conveyor that transports coal from the AFC to the main belt conveyor. Also incorporated into the beam stage loader is a small crusher to reduce the particle size of the coal for easier transportation.
Coalification	The metamorphic processes of forming coal.
Coal mine	An area of land and all structures, facilities, machinery, tools, equipment, shafts, slopes, tunnels, excavations, and other property, real or personal, placed upon, under, or above the surface of such land by any person, used in extracting coal from its natural deposits in the earth by any means or method, and the work of preparing the coal so extracted, including coal preparation facilities. British term is "colliery".
Coal reserves	Measured tonnages of coal that have been calculated to occur in a coal seam within a particular property.
Development heading	Underground work carried out for the purpose of opening up a mineral or coal deposit. Includes shaft sinking, crosscutting, drifting and raising.
Downcast shafts	A shaft where the fresh air enters the mine or workings.
Drift	A horizontal underground opening that follows along the length of a vein or rock formation as opposed to a crosscut which crosses the rock formation.
Gateroads	Underground roadways in the mine which are driven to the back of each longwall panel before longwall mining begins.
Goaf	The term applied to that part of the mine from which the coal has been removed and the space can be filled up with waste (in the case of VCM, there is no filling up of space). Also called gob.
Hanging wall	The rock or coal on the upper side of a vein or ore deposit.
Lignite	A low-rank coal with a relatively high moisture content and relatively low heat/energy content.
Open pit mine	A mine that is entirely on surface. Also referred to as open-cut or open-cast mine.

Shaft	A vertical or inclined excavation in rock for the purpose of providing access to an orebody. Usually equipped with a hoist at the top, which lowers and raises a conveyance for handling workers and materials/a primary vertical or non-vertical opening through mine strata used for ventilation or drainage and/or for hoisting of personnel or materials; connects the surface with underground workings.
Shearer	A mining machine for longwall faces that uses a rotating action to "shear" the material from the face as it progresses along the face.
Slope	Primary inclined opening connecting the surface with the underground workings.
Spoil piles	Overburden and reject materials piled or deposited during surface mining. Material excavated from an excavation, trench, tunnel, or underground shaft.
Stockpile	Broken ore heaped on surface, pending treatment or shipment.
Upcast shafts	A shaft through which air leaves the mine.

Chapter 1

Introduction

1.1 Odour from the Processes of Underground Coal Extraction in Coal Mine Velenje

The Coal Mine Velenje (CMV) produces up to 3 million tonnes of lignite annually, which is fully utilised for the production of electricity at the Šoštanj thermal power plant.

The process of underground lignite exploitation requires effective mine ventilation of all gateroads and other underground facilities (total length approx. 50-60 km) at all times. The aim is to provide a ventilated working microclimate that is healthy and favourable for all mine personnel and that is safe to operate under the conditions that eliminate the possibility of explosive mine atmosphere formation. This is achieved by diluting the concentrations of all gases to levels that are considered non-hazardous to human health. The major releasing coal gases by quantity are odourless methane (CH_4) and carbon dioxide (CO_2).

In the CMV, the exhaust main ventilation system is used to deliver and distribute fresh air from the surface through downcast three shafts, two drifts and intake airways to the working sites, and then the polluted air passes back to the surface through return airways and two upcast shafts with ventilation stations, which are sucking air out of the mine, creating a depression in mine, and thus drive-directs ventilation (from 330 to 420 m^3/s 24 hours a day, every day of the year.). Ventilation stations with main fans are located in the vicinity of Šoštanj (Šoštanj ventilation station) and Velenje (Pesje ventilation station).

The coal extraction process occasionally also emits unpleasant odours in the mine and via the ventilation network to the surface. Emitted odorous compound on the surface from the ventilation stations gives rise to occasional complaints from people in nearby settlements because of detected unpleasant smell.

The mixtures of gases, which are perceived as odours, affect the human olfactory and taste perception of the environment. In the case of unpleasant odours they may have a disturbing effect. Although odours are usually not toxic (individual toxic sulphur gases generally have very low odour detection threshold at $\mu g/m^3$ range, rather than the mandatory limit values for simply odorous pollutants at mg/m^3 range), they can significantly affect the quality of working conditions in the mine, which may consequently affect the concentration and safety awareness during work in the mine and the quality of life of the population in surrounding areas.

The potential odour sources in the mine are locations where there is intervention in the coal seam – i.e. coal extraction process; longwall faces and development headings. Coal gases are emitted from extracted crushed coal and from coal seam where the underground facilities are not insulated – protected from spontaneous combustion of coal (coal seam). Extracted coal from the longwall faces and development headings is then transported via a chain/rubber conveyor system to the surface. Gases are also emitted from the coal during transportation. All emitted gases are diluted with mine ventilation and dispersed with airflow via return airways and upcast shafts to the surface. To a much lower extent the odorous gases are also emitted from the coal stockpile on the surface.

The systematic gases monitoring on CMV, and odour properties of detected gases show that the volatile sulphur compounds (VSC) are the main source of unpleasant odours. The emitted VSCs are formed and stored in coal during the coalification processes. Due to the reactivity and solubility of VSCs, their release and transformation following coal production are also possible.

In the CMV mine atmosphere, gas concentrations are monitored either continuously (CH_4, CO_2, CO) by a network of gas sensors or periodically (CH_4, CO_2, $(CH_3)_2S$ (DMS), H_2S, O_2, CO, H_2, NO, NO_2,

SO_2) or with analytical tests performed on collected air samples in the laboratory using gas chromatography with flame ionization detector (GC-FID) and with flame photometric detector (GC-FPD) and electrochemical sensors.

The odorous gases identified in the mine are the VSCs: DMS, H_2S and SO_2. H_2S and SO_2 gases are usually not detected, which is considered expected under normal conditions. Measurements of VSCs in the mine are particularly exposing DMS concentrations[1], which are regularly detected (with periodic monitoring) at concentrations higher than 2.58 mg/m^3.

During a one-year period from August 2010 to July 2011, the DMS in the main air exiting roadways has always been detected, except in the Pesje pit during the period between August 2010 and January 2011. The highest DMS concentration in the Pesje pit was in April 2011 (113.8 mg/m^3 with airflow of 145.5 m^3/s) and in the Preloge pit in July 2011 (42.6 mg/m^3 with airflow of 248.2 m^3/min). H_2S and SO_2 gases were not detected during the period from August 2010 to July 2011, which is considered normal.

The main odorous characteristics of DMS and also other VSCs are notoriously unpleasant smells and very low odour detection thresholds: in µg/m^3 range.

The presence of DMS in the mine was first noted in the late 1980's as an unpleasant odour when the access roadways for the upper NW part of the coal seam were being developed. Later, in the 1990's, DMS was once again encountered when CO gas sensors sounded without any visible indication of a significant oxidation process, which was later found to be due to the cross-sensitivity of the CO sensors to DMS. Currently, coal production is increasingly centred in this area and odour complaints are expected to increase in the future.

The underground extraction process is dynamic and is not constant, especially regarding coal production intensity. The technology cycles on the longwall face and the development headings include a lot of technological operation rather than coal extraction (crushing) with cutting and top coal caving. The natural characteristics of coal, extraction dynamics and ventilation design are the main influencing factors on the emission dynamics of coal gases. In parallel to this, the possible formation and transformation of odorous compounds depend upon the coal composition and lithology, the intensity of coal production, the airflow quantity, and mine atmosphere conditions as well as the presence of water.

Better understanding of VSCs and especially DMS presence in mine air is fundamental. The study and analysis of factors that are responsible for the presence and amount of released individual VSC and correlations between factors are necessary.

[1] Gases concentrations are, where it makes sense, converted from ppmv to mg/m^3 according to Equation (3.2 (see Chapter 3.2) at normal conditions (temperature 20°C and pressure 1013.25 mbar).

1.2 Literature Preview of the Researched Topic

The text related to Section 1.2 is based on our published article [1].

Coal (lignite) excavation at Coal Mine Velenje (CMV) occasionally emits unpleasant odours, which can affect a miner's attention and hence safety awareness. Furthermore, fugitive odour emissions have a negative effect on the quality of life for local communities, which has become an increasing source of complaints. For these reasons, CMV has been carrying out research into techniques of controlling its odour emissions. This requires an understanding of the specific mining processes, identifying and quantifying the sources of odour and the odour active compounds responsible [2]. Experience (distinctive smell to mine operatives) and historical gas concentration measurements have shown that the main odours at the mine are due to volatile sulphur compounds (VSCs). These compounds have extremely low odour detection thresholds ($\mu g/m^3$), which are many times lower than their toxic threshold limit value (TLV) in mg/m^3 range [3].

The appearance of a distinctively unpleasant smell which is detected by mine operatives and provokes complaints of local communities is always connected with increased DMS concertation (monthly and additional control measurements) in the mine. Also, the distinct smell is similar as the one from released gas mixture of DMS and nitrogen from the gas cylinder.

The main VSC at CMV is dimethyl sulphide (DMS), while hydrogen sulphide (H_2S) and sulphur dioxide (SO_2) are less significant. The odour thresholds of detected VSCs are: SO_2 2.32 mg/m^3, H_2S°0.58 $\mu g/m^3$ and DMS 7.75 $\mu g/m^3$ [4]. DMS has a distinctively offensive smell similar to a combination of decaying cabbage, seaweed, garlic, sulphur, and glue [[5], [6]] and has negative hedonic characteristics [7]. The origin of the DMS in the lignite seam is yet to be fully understood, but it is believed that it originates from the early stages of coal formation during the decay of organic matter [8]. DMS is produced during the anaerobic microbial decomposition of methoxylated aromatic compounds present in the freshwater sediments [9] such as the lignite-bearing Pliocene sediments of the early Velenje basin [[10], [11]]. Therefore, it is believed that the DMS is retained during the rapid accumulation and burial of plant material and subsequent coal formation only to be released during coal extraction.

An extensive body of literature exists concerning odour theory, including odour perception [[12], [13]], odour parameters [[14]; [15], [16], [17]], analytical methods [[18], [19], [20], [21]], olfactometric techniques [[18], [22], [14], [17], [20], [21]], electronic nose [[20], [23], [24]], sampling and emission rate determination of odour sources [[25], [26], [27], [28], [29], [30], [20], [31]], monitoring methods [[32], [33]], and atmospheric dispersion modelling [[34], [35], [36], [37] [21], [38]].

Odour theory is presented in more detail in Appendix A: Odour perception, measurement, and modelling.

Most studies, excluding those on odour theory, relate to industries that have well defined odour nuisance issues, e.g., the agricultural and livestock industry [[25], [36], [39]], waste water treatment plants [[6], [34],], municipal waste sites, recycling facilities, transfer stations, composting facilities [[20], [40], [41]], and industrial plants such as paper pulp mills, petroleum refineries, food processing, leather manufacturing, smelting of non-ferrous ores, steel mills, the manufacture of certain abrasives, paint manufacture, rendering, sulphur dioxide scrubbing, starch manufacturing [42] and, tobacco factory [43], biogas production [44], etc.

On the other hand, little information is available concerning fugitive emissions of odorous gasses from mining activities in general. In addition, addressing potential odour issues as part of making an impact assessment is relatively new in planning coal mining projects. Odour dispersion modelling has been performed as part of an air quality impact assessment for a new ventilation shaft at the Illawarra coal mine, NSW, Australia [45]. For modelling purposes, the mine used cumulative odour measurements taken in the mine's ventilation air from existing ventilation shafts. Gas compositional analysis revealed that the volatile organic compounds (VOC) were mostly below the limits of detection and did not pose an odour issue. Similarly, the Tasman Underground Mine (NSW, Australia) when seeking consent to extend their underground mine operations, also performed an air quality assessment on account that the development of the mine could potentially produce odorous emissions from the existing and proposed ventilation shafts [46]. No odour impact, based on either the levels of odorants in the ventilation shafts or in the actual coal seam, was detected. The Wilpinjong Coal Mine (NSW, Australia) analysed ambient air quality as a response to complaints by local residents [47]. All active odour compounds were below the human odour detection threshold, and it is not clear from the study which odorants were responsible for the complaints. The Kanmantoo Copper Mine (SA, Australia) has performed a study for environment protection and rehabilitation [48] while seeking consent for extending

the life of open-pit mine for excavation and production of copper-gold concentrate. Odour monitoring results have confirmed the predicted odour dispersion model and showed that odour is not anticipated to result in negative impacts from the mining operations. The study of environmental impact of gold mines in Oman, and the pollution impact by heavy metals [49] also, included odour measurements from water from a nearby well used for irrigation. The odour from the water was not detected. Surprisingly, none of these studies included DMS in their analyses despite its low odour threshold.

For the assessment of potential health hazard due to the H_2S emissions from the mine with underground copper ore deposit extraction [50] also air samples and dispersion modelling were included. Room pillar technology is used to extract copper ore in the underground part of the mine. Mine ventilation is provided with four main fans with nominal capacity 400 m^3/s each. The fans are connected to individual diffusers with outlets at the height of 36.3 m, the surface area of the outlet cross-section is S = 46.6 m^2. During normal use, 3 fans are operative. For the determination of H_2S, 20 samples were collected in the diffusors and 24 samples were collected in nearby settlements with distances between 2 and 5 km. Maximum measured concentration of H_2S in the emitter was 286 $\mu g/m^3$. In Poland, the reference values for H_2S that are unlikely to cause adverse health effects in the general population are 5 $\mu g/m^3$ (averaged over the period of the year) and 20 $\mu g/m^3$ (averaged over one hour). At selected sites H_2S concentrations did not exceed 20 $\mu g/m^3$ in 1-hour air samples, and 5 $\mu g/m^3$ in 5-hour air samples. Maximal modelled 1-hour H_2S concentrations of 10 x 10 km2 area were 1.91 $\mu g/m^3$. While there were no exceedances of health hazard H_2S concentrations, there were regular complaints of unpleasant sensation of smell from nearby settlements. According to the data obtained from the Ministry of Environment in 2013, as much as 1,323 air pollution complaints were recorded in Poland and 65.7% referred to odour.

Nevertheless, using the human senses is of fundamental importance for safe mining. For millennia, the miners were relying on their senses and knowing their working environment. Gas awareness training programs, including detection methods and the use of monitoring devices, are one of many essentials for each miner and safe mining, and the sense of smell (and taste) is one of the most important senses for the detection of imminent hazards at a workplace to detect-smell changes in mine air which usually means presence of hazardous gases such as smoke due to the oxidation process (e.g. mine fire), gases from blasting with explosives, gases from the motors with internal combustion, etc. Knowing the odour characteristics of gases that may be present in a working environment is important for all working places, not just in mining. The odour characteristics of a specific compound can be used also for triggering an additional emergency response to visual and audible alert systems. A zinc-copper mine in Australia is deploying stench gas (ethyl mercaptan & R134A propellant) as their emergency alert system [51]. Mining personnel is trained to recognize the odour as a warning system. In addition, stench gas system is also used in some mines where the odourless methane is prevalent.

In the underground coal mines, before the modern monitoring sensors were available, the rate of progress from spontaneous heating to spontaneous combustion was based on observation and sensing of mine environment. As spontaneous heating starts and develops in a mine it produces effects which enable an experienced miner to detect it in most cases before it becomes a blazing fire, although in case where oxidation is very rapid, it is not always the case. The visible and sensed stages of spontaneous heating are [52]: 1st stage – sweating, or deposition of moister on coal seam (roof, sides, etc.). 2nd stage – "gob stink" produced. 3rd stage – paraffin or petrol smell produced. 4th stage – burnt tar smell produced. 5th stage – smoke appears. 6th stage – flame is visible. It is called gob stink because the coal oxidation usually occurs in the goaf or gob area (old works) and has a very distinct odour. An experienced miner can smell if even the faintest trace occurs, and this is an absolutely infallible proof that heating started.

Some studies related to mining can be found, which are not directly implicating odour issues. However, from the odorous gases' concentrations in air and from their odour thresholds it is clear that the odour issue potentially does exist.

One of the consequences of coal mining is the exposure of the coal to air and moisture resulting in the ignition of the coal through the processes of chemisorption, oxidation, and spontaneous combustion. The ignition of coal is a global concern and burning coal may cause significant environmental problems by the solid (coal-fire gas minerals) and gas by-products [53].

Weathering of coal starts immediately after the coal is won from the coal seam unless precautions are taken to prevent its exposure to oxygen (air) and changes in temperature and humidity. The exposure of coal to and its subsequent reaction with the oxygen in air is recognized as the most important contributor to weathering. The reaction of the coal with oxygen occurs readily at ambient temperature, results primarily in oxidation of the coal organic constituents, and leads to an increase in the oxygen content and a decrease in the atomic hydrogen-to-carbon ratio

of the coal. In general, the chemical structural changes that accompany coal oxidation at low temperatures (from ambient temperatures to 200°C) by molecular oxygen are strongly dependent upon coal rank, particle size, oxygen partial pressure, moisture content, and temperature. Another contributor to weathering are the stresses caused by cyclic sorption and desorption of moisture which produce fissures and cracks that mechanically weaken the coal. This decrepitation phenomenon is referred to as slackening. The thermal cycling of coal also contributes to slackening. Slackening is much more rapid and extensive for lignite and subbituminous coals than for higher rank coals. Slackening can also accelerate oxidation by increasing the exposed surface area of the coal to air. Oxidation reduces the calorific value of coal. The oxygen content of freshly mined and crushed lignite coals can increase several percent in a matter of weeks when the coal is stored in air at ambient temperature. Such rapid oxidation can lead to spontaneous combustion of the coal under certain storage conditions [54].

The sulphur is present in coal as organic sulphur (an integral part of the coal structure), pyritic (generally discrete pyrite and marcasite particles or 'lumps') and sulphate (as salts of metals such as calcium or iron) [55]. The sulphur (pyritic) presence in coal (and in metal ores) also greatly contributes to the weathering and spontaneous combustion of the coal [56].

The study of coal pyrolysis concluded that the effects of atmospheres (N_2 and mixtures of 90 % N_2 and 10 % H_2, CO_2, CO, CH_4) the evolution of common sulphur gases at pyrolysis (H_2S, COS, CH_3SH, CS_2, SO_2) [57] and in addition of different atmospheres also different forms of sulphur in coal are influencing on sulphur gases evolution. It was shown that the methanethiol (CH_3SH) evolution during coal pyrolysis, just as H_2S evolution, is affected by not only pyrolysis conditions, but also coal properties (organic sulphurs, H_2S is also formed at decomposition of pyrite).

In the study of by-products of spontaneous combustion of coal in the Witbank and Sasolburg coalfields of South Africa also thirteen gas samples were collected from fumaroles associated with an actively burning coal fire from both coalfields [53].

Emitted gases consisted of a complex mixture of hydrocarbons, halocarbons, greenhouse gases, and toxic concentration of CO, benzene, xylene, and toluene. Four principal groups of chemicals were identified during analyses: aromatic compounds, aliphatic hydrocarbons, halogenated hydrocarbons, and greenhouse and other gases.

Benzene, toluene, ethylbenzene, xylenes, ethyl toluene, and trimethylbenzene were the main detected aromatic compounds with maximum concentrations above their odour thresholds. Also, carbon disulphide was detected above its odour threshold.

Maximum temperature of gas samples was 630°C. The sulphates do not release as sulphur dioxide until 1060 °C.

Open-cut coal mining produces large quantities of waste material that must be disposed of around the mine site. Some of this material may be sufficiently reactive to begin to self-heat which can ultimately lead to spontaneous combustion in the spoil piles at some mines.

Spontaneous combustion results from self-heating which is caused mainly by the oxidation of coal and other carbonaceous materials. If the heat generated by this reaction is trapped, such as in a spoil pile, the temperature of the material will begin to rise and if unchecked it may ultimately ignite.

The reactivity of the materials sent to spoil varies considerably; coal is the most reactive material whereas materials that contain no carbon, e.g., sandstone, rocks and soil and clay, are inert. In general, the reactivity of a material depends on its carbon content. Large amounts of reactive carbonaceous materials in spoil increase the risk of spontaneous combustion. Spontaneous combustion in open-cut coal mines poses several potentially serious safety and environmental problems including emissions of CO, SO_2, H_2S, polynuclear aromatic hydrocarbons and volatile organic compounds [58].

Based on a review of 21 annual environmental reports and complaints registers of coal mines in Australia (Table 1.1), most odour complaints result from spontaneous combustion of coal seam in underground and open cut mines, spoil piles open cut mines and deposited coal and also from blasting fumes from used explosives in open cut mines.

Table 1.1: Review of 21 annual environmental reports and complaints registers of coal mines in Australia.

Coal mine	Type	Period	Num. of environmental complaints	Source of odour complaints	Sulphur like odour

		[year/month]	Reference	Total environmental complaints	Odour complaints	Spontaneous combustion	Blasting fumes	Unknown	
Mushwellbrook	open cut	2016	[59]	93	78	76		2	34
		2017	[60]	88	58	52		6	32
		2018	[61]	54	37	32		5	7
		2019	[62]	32	17	17			8
Austar	underground	2020	[63]	2	1	1			
Wambo	open cut and underground	2014	[64]	31	3		3		
		2019	[65]	6	1		1		
Mt Artur	open cut	2014	[66]	271	0				
Tahmoor	underground	2018	[67]	4	2			2	
		2019	[68]	9	1			1	
Canyon	open cut	2006-2009	[69], [70], [71], [72]	4	0				
Moolarben	open cut and underground	2011/9-2012/8	[73]	359	0				
		2019	[74]	38	1			1	
Drayton	open cut	2013	[75]	23	11			11	
		2015	[76]	15	2			2	
		2016	[77]	5	1			1	
Duralie	open cut	2016/7-2017/6	[78]	17	3	3			3
		2018/3-2019/2	[79]	4	4	4			
SUM				**1055**	**220**	**185**	**4**	**31**	**84**

For 21 yearly periods of 9 coal mines 1055 environmental complaints were reported and of that 21 % complaints were related to odour issue and 38 % of odour complaints reported sulphur like odour. To a large extent, the number of complaints depends on the distance of the coal mine from the settlements and from nature and rate of emissions.

Air quality monitoring in Muswellbrook coal mine in 2018 and 2019 also included 1-hour and 24-hour concentrations measurements of H_2S and SO_2. On all three monitoring locations, in 2018, the highest monthly 1-hour and 24-hour concentrations of H_2S were 177.2 µg/m^3 and 44.7 µg/m^3, mean values of the highest monthly 1-hour and 24-hour concentrations were 35.3 µg/m^3 and 6.9 µg/m^3 and the lowest values of the highest monthly 1-hour and 24-hour concentrations were 3.8 µg/m^3 and 2.0 µg/m^3. The highest monthly 1-hour and 24-hour concentrations of SO_2 were 354.44 µg/m^3 and 144.4 µg/m^3, mean values of the highest monthly 1-hour and 24-hour concentrations were 128.2 µg/m^3 and 32.2 µg/m^3 and the lowest values of the highest monthly 1-hour and 24-hour concentrations were 21.1 µg/m^3 and 8.8 µg/m^3. On all three monitoring locations, in 2019, the highest monthly 1-hour and 24-hour concentrations of H_2S were 428.3 µg/m^3 and 33.6 µg/m^3, mean values of the highest monthly 1-hour and 24-hour concentrations were 48.9 µg/m^3 and 7.7 µg/m^3 and the lowest values of the highest monthly 1-hour and 24-hour concentrations were 4.0 µg/m^3 and 1.6 µg/m^3. The highest monthly 1-hour and 24-hour concentrations of SO_2 were 417.6 µg/m^3 and 68.2 µg/m^3, mean values of the highest monthly 1-hour and 24-hour concentrations were 169.2 µg/m^3 and 26.1 µg/m^3 and the lowest values of the highest monthly 1-hour and 24-hour concentrations were 30.1 µg/m^3 and 12.5 µg/m^3. Monitoring results show that regarding odour threshold in 2018 and 2019, the odour of H_2S was potentially always detected and SO_2 was never sensed.

The literature review carried out in 2011/2012, 2015 and 2020/2021 points out that almost no research exists of DMS emissions from mining activities. The only published work referring DMS to mining activities is from oil sand mine operations in the Fort McKay area in Alberta (Canada) and from those performed by CMV.

In the air quality investigation in a 30 km radius around Fort McKay a five-year monitoring period was performed due to the countless environmental complaints regarding oil sand mining activity in the area [80]. During the monitoring period between 2010 and 2014, there were 172 complaints and 165 were related to odours. Between 47 priority odorant candidates was also DMS. The investigation focused on six oil sand mines and one in situ facility. Selected were 16 continuous monitoring points and various others sampling points. Ambient air from sampling canisters of 1-hour and 24-hour samples was analysed for 60 volatile organic compounds and 20 reduced sulphur compounds. The DMS presence was analysed in 126 samples and was never detected (detection limit was 1 ppbv = 2.58 µg/m^3). Compounds that exceeded an odour threshold from multiple samples were hydrogen sulphide, carbon disulphide, dimethyl disulphide, 2-methyl thiophene, 3-methyl thiophene, methyl mercaptan, acrolein, acetaldehyde, naphthalene, benzaldehyde, isoprene, methyl ethyl ketone, n-propyl benzene, p-ethyl toluene, 2-ethyl hexanol,

2-ethyl hexanal, nonanal, 1-ethyl-4-methylbenzene, alpha pinene. SO_2 is a health concern as it affects pulmonary function. There have been no exceedances of the 458.4 µg/m^3 hourly average, 127.9 µg/m^3 24-hour average, or 21.3 µg/m^3 annual average in the community of Fort McKay. Three hourly average and one 24-hour average exceedance were noted in the 30 km study area for the study period.

The only published studies referring to DMS emissions from coal mining activities are those performed on coal from the Velenje Coal Mine of gaseous sulphur emissions (COS, CS_2 and DMS) from coal stockpiles [8], [81] and a study on the levels of DMS in the return airway of a longwall face [82], which were briefly summarized in an IEA Clean Coal Centre report [83]. The estimated daily emissions of COS and CS_2 for the whole stockpile in the sampling period were 20 g of CS_2 and 70 g of COS (gas concentrations were in µg/m^3 range). The DMS concentrations fell to less than 2.58 mg/m^3 within a few days as it is only released from freshly loaded coal. The measured DMS concentration levels in the mine air, which were sampled once a week for 15 consecutive weeks in the return airway of a longwall face during coal production, ranged from 55.47 to 128.48 mg/m^3. During a series of in-situ coal desorption tests made in 1998 and 1999 (5 boreholes and 10 desorption tests [84]), DMS was detected in all but one sample (max. concentration 516 mg/m^3), while H_2S was <1.42 mg/m^3. The odorous emissions from sources in the CMV and on the surface were systematically addressed in [85].

In the industrial or agricultural processes such as pulp and paper manufacturing, oil or petroleum refining, food decay, composting, landfilling, fish processing, sewage and wastewater treatment, leather manufacturing, paint, rendering plants, sulphur dioxide scrubbing, and starch manufacturing plants, DMS is a typical gaseous odour pollutant [[6], [42]]. Therefore, the removal or degradation of DMS odorant before exhausting into the atmosphere is of great significance for improving the local air quality. DMS has the unique capability of enhancing and intensifying other odours. Due to this property, it is used in warning odorants and odour masking agents [42].

DMS is also a substantial contributor of the aroma to some food items, such as beer [86], [87], red wines [88], truffles [89], milk [90], many vegetables and fruits (tomatoes, sweetcorn, grapes, asparagus, and brassicas), honey [[86], [91]], chewing gum [42], cheddar cheese [92], etc.

One of the most significant discharges of DMS and other RSCs (H_2S, CH_3SH, $(CH_3)_2S_2$) can be from Kraft pulp mills [42]. There are many sources in the mill. Some sources emit a small gas volume with high concentrations (blow heat recovery; turpentine recovery vent; evaporator hotwell vent; and foul condensate storage tank), while others have large volumes with low concentrations (brown stock washer filtrate, tanks, and hood; weak and strong black liquor storage tanks; knotter hood; black liquor oxidation vent; and contaminated condensate tanks). Typical DMS concentrations of a high-volume source are 0.52 mg/m^3 and 38,700 mg/m^3 for a low volume source.

Ambient air samples were collected at several locations in the community around a major Canadian pulp and paper plant over a period of several months, before and after major process changes [93]. In the spring of 2006, they permanently closed one of two Kraft pulp mills on site and shut down a chemical recovery boiler and associated black liquor oxidation systems. The concentrations of H_2S, methyl mercaptan (CH_3SH), DMS, and dimethyl disulphide (DMDS) were compared before and after the process changes. DMS was found to be the most abundant reduced sulphur compound in ambient air before the changes with an average concentration of 3.84 µg/m^3. The sum of concentrations of all gases was 6.73 µg/m^3. After the changes, the average concentrations of DMS decreased by 70 % and the sum of concentrations decreased by 43 %. A total of 18 samples were collected on 9 different days before shutdown and then 39 samples were collected on 21 different days.

Health risk assessment of environmental exposure to malodorous sulphur compounds in central Slovakia in the Ružomberok area, due to the exposure of emissions from the kraft process pulp mill factory [94], was based on measurements of total reduced sulphur compounds (TRS) and separately H_2S in ambient air collected on nine locations which were systematically selected based on geographic, demographic, climate factors and emission dispersion study. During six years for TRS point monitoring 5423 samples were collected. The average weighted mean, max and 95 percentile values from monitoring campaigns were 5.8, 26.7 and 13.0 µg/m^3. Maximum concentration was 68.0 µg/m^3. During four years for H_2S point monitoring 4487 samples were collected. The average weighted mean, max and 95 percentile values from monitoring campaigns were 2.0 µg/m^3, 5.4 µg/m^3 and 3.8 µg/m^3. Maximum concentration was 21.1 µg/m^3. No adverse health effects are expected under 2 µg/m^3.

At landfill sites over 300 trace compounds have been identified in landfill gas. Unpleasant odours are usually associated with the sulphur containing compounds, primarily mercaptans and sulphides. The vast range of trace compounds measured in landfill gas reflects both the anaerobic

decomposition processes taking place in the waste mass and the wide range of chemicals introduced via the industrial and commercial waste streams [41]. DMS is a common odorant in landfill gas typically found in a concertation range between 0.02 mg/m^3 and 135 mg/m^3.

The study of sulphur source from livestock production in Denmark exposes H_2S as a major sulphur source. Finisher pig production is estimated to be the largest source of atmospheric sulphur in Denmark [95]. The only other sulphur compounds measured consistently in the ppb range are methanethiol and DMS, but these only constitute about 2 to 5 % of H_2S. Measurement campaigns were carried out over a 6-year period from 2009 to 2015 on five pig production facilities. The measured concentrations DMS were between 4.39 µg/m^3 and 10.58 µg/m^3.

In the study of identification of volatile sulphur odorants 253 samples were collected from ageing wastewater biosolids, whose production has been steadily increasing with commissioning of new wastewater treatment plants because of increasing population as well as more stringent effluent treatment and discharge standards. DMS was one of three VSCs (out of ten) that were identified by both analyses used in the study (GC-SCD and GC-MS). The maximum DMS value was 4.53 x 10^3 µg/m^3 and was the second highest maximum value after H_2S whit a value equal to 59.9 x 10^3 µg/m^3 [6].

The 2018 study of identification of odour sources in two biogas plants in Poland showed DMS concentrations up to 1.26 mg/m^3 [96].

Physical-chemical and biological techniques are now available for removing odours from air streams including: biofilters, biotrickling filters, membrane bioreactors, wet scrubbing, adsorption, and chemisorption, and more recently, methods based on photo-dissociation, electron beam irradiation, corona discharge decomposition and catalytic and ozone oxidation [7]. However, DMS is one of the least biodegradable compounds among the odorous sulphur containing gaseous pollutants; consequently, it always needs improved systems out of the conventional biological setups. And the elevated temperatures (45–75°C) in some DMS emission processes, such as pulp and paper manufacturing and composting, can directly decrease the removal efficiency of odours. Moreover, the long-term performance of the biological systems is easily reduced due to many physical and chemical parameters including acidification, pressure drops, fouling, accumulation of inhibiting salts, and drying of the filter bed. Traditional physical-chemical approaches to DMS removal mainly include wet scrubbing, adsorption, and chemisorption [42].

One of the largest available odour control systems designed to serve, for example, a water treatment plant, consists of a series of either bio-filters or chemical scrubber units with capacities of up to 69.4 m^3/s [97]. In underground coal mining, cumulative airflow rates are extreme and at CMV they are between 340–420 m^3/s. Clearly, the existing systems could not possibly handle the large volumes of exhaust gases emitted from a coal mine and either new or upgraded solutions must be developed. In addition, odorous mine gas emissions depend on many factors, including the natural characteristics of the coal, presence of odour active compounds in the coal seam and old mine workings, production and ventilation design, and coal production intensity. For these reasons, it is a challenge to predict their actual concentration.

The objectives of this study were to recognize and estimate the main odour sources in the mine and to construct a ventilation model of CMV to perform model-based odour analysis.

This was achieved by taking into consideration the characteristics of mine ventilation, mine gateroad system (airways), and estimated odorous emissions of mine sources in order to establish a better understanding of the sources, dispersion, and ventilation-based control options to reduce the presence of odour active compounds released during the coal extraction process.

1.3 Properties of Identified VSCs in Coal Mine Velenje

Except for SO_2, the identified VSCs in the mine (DMS, H_2S) [82], [98]] and on the stockpile (DMS, H_2S, CS_2 and COS) [8], [81] belong to the family of reduced sulphur compounds (RSC). Physical and chemical properties of DMS, H_2S, CS_2 and COS are presented in Appendix B: Physical and chemical properties of H_2S, CS_2 and COS.

Reduced sulphur compounds (RSC) are a group of inorganic and organic chemicals containing sulphur atoms in their lowest oxidation state (S^{-2}). The group includes hundreds of individual species, of which only a few commonly occur in air. Considering toxic properties, commercial use, and concentration level in the atmosphere, the most important substances within the RSC group are H_2S, methyl mercaptan (CH_3SH), DMS, DMDS, CS_2 and COS. Of these six, H_2S, methyl mercaptan, DMS and DMDS are the four reduced sulphur species most often emitted from

industrial operations and are present in air. Even when other RSC are present, these four substances generally account for 95% of the RSC in the air. The remaining RSC species are generally present in small amounts and are usually present only at specific locations [99].

In the study of distribution characteristics of DMS, CS_2, H_2S, DMDS, and methyl mercaptan (CH_3SH) and their photochemical reactions in landfill air [7], the photochemical conversions of RSC to a further oxidized form were analysed. SO_2 were evaluated in the landfill site using a photochemical box model. This study indicated that the chemical species of RSC, which may exert influences on the SO_2 production depending on sampling conditions, were found to include DMS, DMDS, and H_2S. In general, the RSC contribution to the observed SO_2 levels was insignificant in the sampling sites investigated. Overall, the extent of the RSC oxidation to the observed SO_2 varied dramatically during the sampling period. The photochemical conversion of the RSC in the landfill environment can account for about 15% of the observed SO_2, on average. There was a strong correlation between DMS and SO_2 concentration levels during the study period.

Combined effects of H_2S, DMS, COS, and CS_2 are minor in relation to the oxidized forms of sulphur represented in SO_2 and sulphates. Biogenic sulphur emissions are related to either the aerobic generation of methylated sulphur forms during normal metabolism or to H_2S and DMS generation during anaerobic decomposition of organic residues.

Most of the global biogenic sulphur emissions have been observed over open oceans and coastal waters. In addition to oceans, other natural sources of RSC include volcanoes, biomass burning, and soil, oceans, marshes, and tidal flats where anaerobic decay of organic matter is taking place, also above exposed faces of sulphur-containing oil and coal deposits.

The primary anthropogenic sources of reduced sulphur compounds include Kraft pulp mills, natural gas wells, processing of natural gas and crude oil at upstream stages and downstream refining, smelting of non-ferrous ores, steel mills, the manufacture of certain abrasives, livestock farming, and sewage treatment facilities [42].

1.3.1 Dimethyl sulphide

DMS is a climatically important VSC produced by the breakdown of Dimethylsulfonopropionate (DMSP), which is produced by oceanic phytoplankton. DMS is the most abundant form of volatile sulphur in the ocean and is the main source of sulphuric species in the atmosphere over the unpolluted ocean. Therefore, oceanic phytoplankton plays an important role in the biogeochemical cycle of sulphur, providing a link between the oceanic and atmospheric sulphur cycle through the release of DMS. The oxidation of DMS in the troposphere leads to the formation of sulphate aerosols which can act as cloud condensation nuclei (CCN), which has important consequences on the radiative budget of the earth. The hypothesis known as CLAW hypothesis suggests that homeostatic feedback may exist between oceanic phytoplankton and climate through the production of DMS. Observations in unpolluted areas over the Southern Ocean have indeed found correlations between DMS surface concentrations and CCN population. However, crucial uncertainties remain in the pathway of atmospheric DMS and its contribution to CCN population as well as in the physiological function and production of DMSP and the processes leading to DMS [100], [8].

Since 1987, when the authors published the CLAW hypothesis, the researchers are trying to find the realistic model of “DMS cycle” in the atmosphere regarding biological production of DMS and its fate in the atmosphere.

Major atmospheric sinks for DMS are reactions with OH and NO_3. In marine environments, NO_3 levels are typically low and DMS is removed primarily by OH in the chemical reactions [99]:

$$OH + CH_3SCH_3 = CH_3SCH_2 + H_2O \tag{1.1}$$

and

$$\mathrm{OH} + \mathrm{CH_3SCH_3} = \mathrm{CH_3S\ (OH)\ CH_3} \tag{1.2}$$

The photochemical degradation of DMS in the atmosphere results in the production of SO_2. The series of reactions are shown below:

$$\begin{gathered}\mathrm{CH_3SCH_2} + O_2 = \mathrm{CH_3SCH_2OO}\ \mathrm{CH_3SCH_2OO} + \mathrm{NO} = \mathrm{CH_3SCH_2}O + \mathrm{NO_2} \\ \mathrm{CH_3SCH_2}O = \mathrm{CH_3S\ HCHO}\ \mathrm{CH_3}S + \mathrm{NO} = \mathrm{CH_3SNO}\end{gathered} \tag{1.3}$$

$$CH_3S + O_2 = (CH_3SO_2) = CH_3 + SO_2$$

Other significant sinks of DMS in the atmosphere are oxidations by O_3 [101] and BrO [101], [102].

The rate constant for the vapor-phase reaction of DMS with photochemically produced hydroxyl radicals has been measured as 4.6 x 10^{-12} cm^3 molecule/sec at 298 K. This corresponds to an atmospheric half-life of about 3.5 days at an atmospheric concentration of 5x 10^5 hydroxyl radicals per cm^3. A diurnal cycle of DMS concentration has been reported, which is thought to be consistent with the removal of DMS during the daytime by hydroxyl radical reaction. The half-life for DMS reacting with atomic oxygen in the atmosphere has been estimated to be 6.2 days based on a reaction rate constant of 5.16 x 10^{-11} cm^3 molecule/sec at 298 K and an average ambient atomic oxygen concentration of 2.5 x 10^4 molecule/cm^3. The half-life for night-time reaction of DMS with gaseous nitrate radicals in air is on the order of several hours in a clean atmosphere and an hour in a moderately polluted atmosphere (over the continental US). The atmospheric half-life in the presence of nitrate radicals has been estimated to be about 28 minutes at an atmospheric concentration of 5 x 10^8 nitrate radicals per cm^3 [42].

In the study of DMS in the return airway of a longwall face in CMV [82], also the stability of DMS in the Tedlar® gas sampling bags was tested. A gas sampling bag was filled and flushed several times before use with synthetic air (20% oxygen and 80% nitrogen). Afterwards the bag was filled with DMS standard with a concentration of 19.9 ppm and analysed every day by the gas chromatograph. During the analysis the gas standard in a gas sampling bag was stored in a dark place to avoid the UV-induced photodecomposition. The test results in

Table 1.2 show that DMS in Tedlar® gas sampling bags is stable for at least 4 days.

Table 1.2: Time-concentration profile of DMS standard in gas sampling bags [82].

Time [h]	Concentration of DMS [ppm]
0	19.9
24	19.9
48	19.9
72	19.9
96	19.9
120	18.3
144	16.7

During the study of effects of process changes on concentrations of individual malodorous sulphur compounds in ambient air near a Kraft pulp plant in Thunder Bay, Ontario, Canada [93] also the stability of RSCs in the Teflon sampling bags was assessed.

A gas mixture was introduced containing 2.1 ppb H_2S, 4.7 ppb CH_3SH, 1.5 ppb DMS, and 1.0 ppb DMDS in a clean Teflon bag and then periodically withdrawing aliquots which were analysed to monitor the changes in concentration with time. These initial concentrations were representative of concentrations measured in actual ambient air samples. Figure 1.1 shows the composition of the gas mixture as a function of time. Any change from the initial concentration was due to decomposition of RSC compounds in the gas phase or adsorption on the bag walls. The concentration of DMS was found to remain constant for more than 3.5 hours. Similar results were obtained when the initial concentrations were doubled.

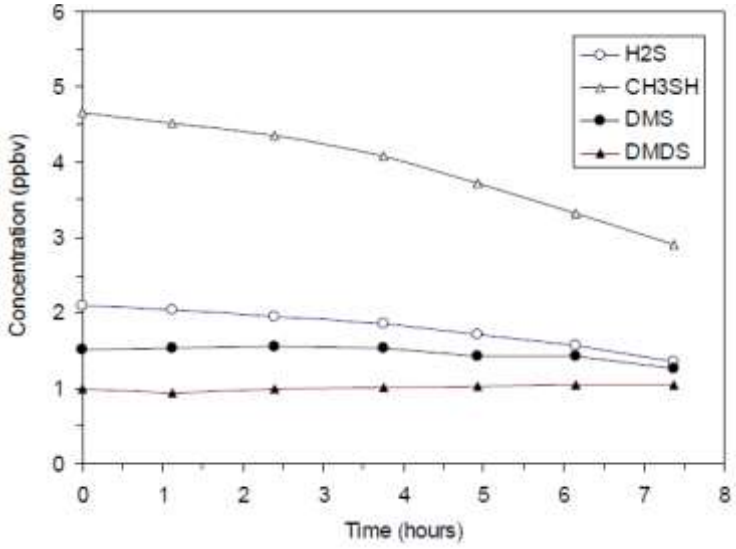

Figure 1.1: Stability of TRS compounds in a Teflon sampling bag [93].

Additional details regarding the upper research are presented in

Table 1.3.

Table 1.3: Additional details from research regarding DMS stability over time.

Paper	Purpose of citation	Sampling	Analytical analysis approach	Results
Determination of dimethyl sulphide in a coal mine atmosphere by gas chromatography [82]	DMS stability test	Laboratory test Sampling in one 2 L Tedlar bag of a preprepared gas mixture from a gas cylinder	GC-FPD Analysis every 24 hours, starting at 0 hours	After 120 hours, the DMS concentration decreased to 48.0 mg/m^3, and after 144, hours it decreased to 43.1 mg/m^3 DMS stable for 4 days
Measuring odours in the environment vs. dispersion modelling: A review. Atmospheric Environment [93]. Emissions of reduced sulphur compounds from the surface of primary and secondary wastewater clarifiers at a Kraft Mill [103].	Stability test of reduced H_2S, methyl mercaptan (CH_3SH), DMS and dimethyl disulphide (DMDS)	Laboratory test One sampling Teflon bag with a gas mixture containing 3.0 µg/m^3 H_2S, 9.4 µg/m^3 methyl mercaptan, 3.9 µg/m^3 DMS, and 3.9 µg/m^3 DMDS Second sampling Teflon bag with doubled initial concentrations in a gas mixture.	GC-PFPD and interfaced with a cryogenic trap The absolute instrument sensitivity was 1.3 µg/m^3 for H_2S, 1.0 µg/m^3 for methyl mercaptan, 0.24 µg/m^3 for DMS, and 0.04 µg/m^3 for DMDS. In less than 7 and a half hours there were 7 analyses, starting at 0 hours	All compounds remained within 10% of the initial concentrations for at least 3 hours. DMS was constant at least 3.5 hours and DMDS for more than 7 hours. Similar results were obtained when the initial concentrations were doubled.

1.3.2 Hydrogen sulphide

H_2S does not absorb solar radiation reaching the troposphere and thus is photochemically stable. The atmospheric lifetime of H_2S is affected by ambient temperature and other ambient conditions including humidity, sunlight, and presence of other pollutants. The decreased temperatures and sunlight as well as decreased levels of hydroxide radicals in northern regions in winter increase the atmospheric residence time of H_2S [42].

Once released into air, H_2S will behave like many other gaseous pollutants and be dispersed and eventually removed. Residence times in the atmosphere range from about one day to more than 40 days, depending on season, latitude, and atmospheric conditions.

H_2S released to the atmosphere is oxidized in reactions with $OH^\bullet$ radicals. The probable mechanism of this hydrogen absorption reaction is as follows [99]:

$$H_2S+OH^\bullet=H_2O+SH^\bullet \quad (1.4)$$

The $SH^\bullet$ radical is oxidized to a transient molecule HSO_3, and then to sulphuric acid (H_2SO_4) as a final product. Other parallel reactions of H_2S with other oxidants such as NO_2, O_2 and O_3 are not important, being much slower than oxidation with $OH^\bullet$ radical.

1.3.3 Carbon disulphide

CS_2 reacts in the atmosphere with photochemically produced hydroxyl radicals; the half-life for this process is estimated to be 5.5 days. It has a weak UV adsorption band at 317 nm, suggesting a potential for direct photolysis.

The rate constant for the vapor-phase reaction of CS_2 with photochemically-produced hydroxyl radicals is 2.9 x 10^{-12} cm^3 molecule/sec at 297 K. Observed temporal variability and vertical gradients suggest that the tropospheric lifetime of CS_2 is rather short [99].

1.3.4 Carbonyl sulphide

The atmospheric lifetime of COS, based on removal via the gas-phase reaction with photochemically produced hydroxyl radicals and oxygen, direct photolysis, and unknown removal processes invoked to balance the sulphur cycle, is approximately two years. Studies have shown that COS may be adsorbed from the atmosphere by plants and by moist soil, the latter due to microbial uptake. Experimental rate constants for the gas-phase reaction of COS with photochemically produced hydroxyl radicals range from 6.08 x 10^{-12} cm^3 molecules/sec to 8.8 x 10^{-15} cm^3 molecules/sec and translate to atmospheric half-lives ranging from 500 days to 6.5 years. COS is not expected to undergo direct photolysis in the troposphere, but it may in the stratosphere [[99].

COS is the most abundant and long-lived reduced sulphur gas in the troposphere, an important precursor for the stratospheric sulphate aerosol layer and thus has an impact on the earth's radiation budget as well as on ozone destruction [104].

1.4 Coal Mine Velenje

Coal Mine Velenje (Figure 1.2) is one of the largest modern deep mines in Europe. It mines the largest Slovenian lignite deposit, which is one of the thickest known coal seams in the world [105]. Over the past 149 years of operation, the mine has produced more than 259 million tonnes of coal and still has exploitable coal reserves of another 96 million tonnes.

The production of lignite uses state-of-the-art technology and produces up to 3 million tonnes of lignite annually, which is fully utilised for the production of electricity at the neighbouring Šoštanj thermal power plant [106].

Figure 1.2: Geographic location of the Velenje Coal Basin. The two main fan stations (exhausting) are shown in blue and fresh air intakes are shown in red (situation in October 2012).

1.4.1 Geology of the Velenje basin

The Velenje coal seam is located in the northern territory of Slovenia near the town of Velenje (Figure 1.2). The coal seam extends under almost the entire Šaleška Valley, it is bowl shaped, 8.5 km long and 1.5-2.5 km wide, and the average depth of the seam is 300 m (between 200-600m deep). Coal seam is on average 60 m tick and the maximal thickness of 165.8 m is proven by drilling [[105], [10], [11]]. The Velenje coal basin is positioned in the Velenje-Dobrna depression between the Smrekovec fault in the north and the Šoštanj fault in the south (Figure 1.3). The paleontological analyses set the Velenje coal seam between the middle and upper Pliocene period approximately 2.5 million years ago [105] which is young considering that the majority of lignite deposits formed during the Tertiary period.

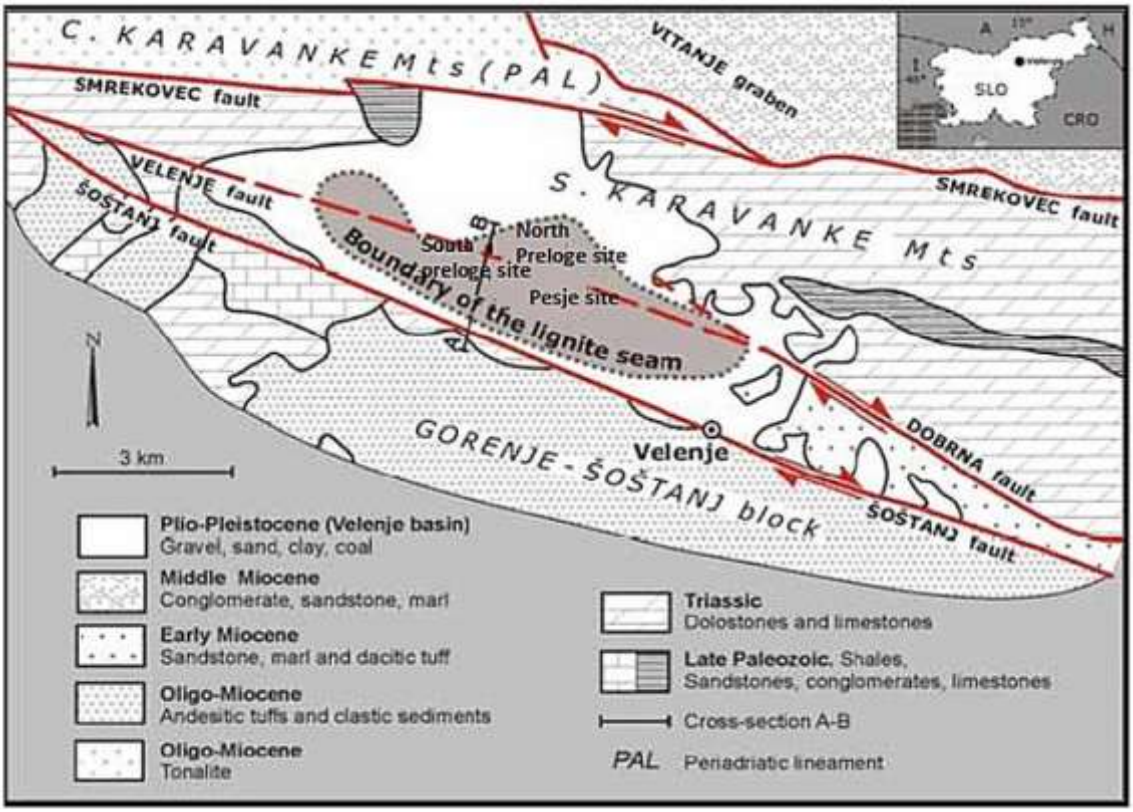

Figure 1.3: Geological map of the Velenje basin area [105].

The Velenje basin is filled with Plio-Pleistocene sediments of terrestrial coarse-grained basalt beds with fine-grained marshy sediments more than 1000 m thick. The lignite seam lies in the Pliocene strata (Figure 1.4 and Figure 1.5). Under the lignite seam, the Pliocene strata is up to 50 m thick and consists of shales, clay, coal, and lignite. Above the Pliocene strata lie up to 250 m thick green sandy silts. Along the Smrekovec fault at the southern edge of the Basin, andesite bodies lie at the bottom of the Basin, while on the northern parts of the Velenje basin, in the footwall, Triassic dolomites and limestone can be found close to the Velenje fault [105].

With the hypothesis that the andesite tuffs, identified in logged cores from boreholes drilled deep beneath the coal seam, lie at the same altitude as the external tuffs, then it can be concluded that the northern wing of the Šoštanj fault has dropped by at least 1500 m in depth relative to the southern part of the fault [107]. The rise in the northern part of the Velenje fault means that the coal seam is situated on the triad layers.

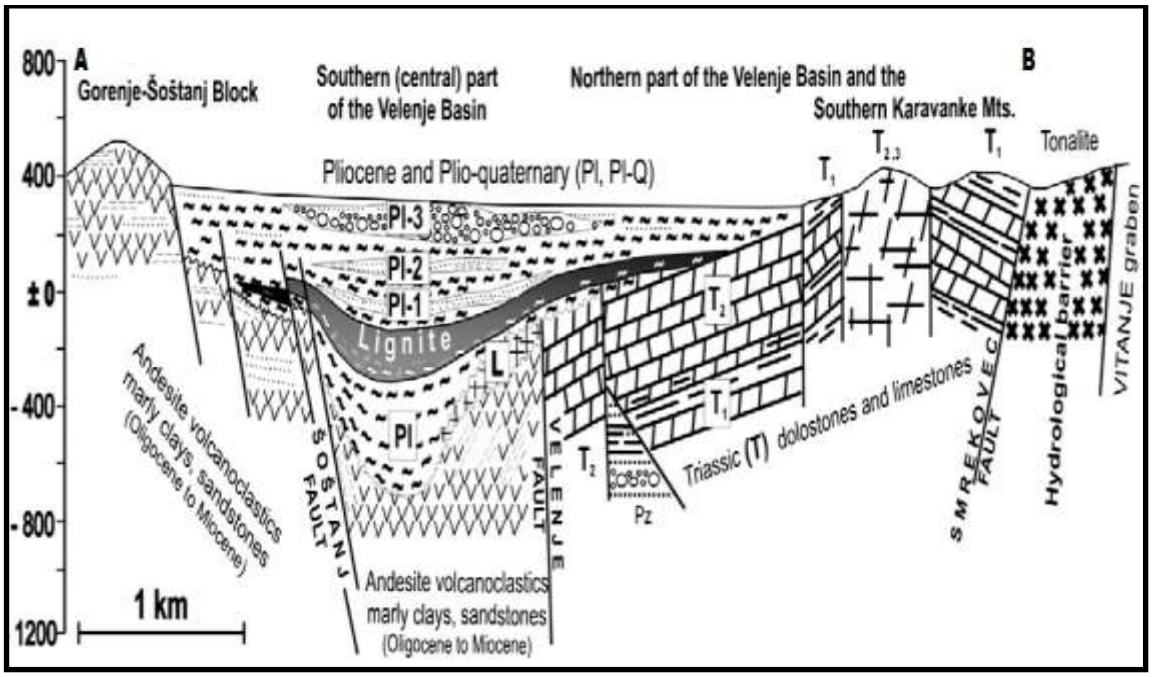

Figure 1.4: Schematic geological cross-section of the Velenje basin [105].

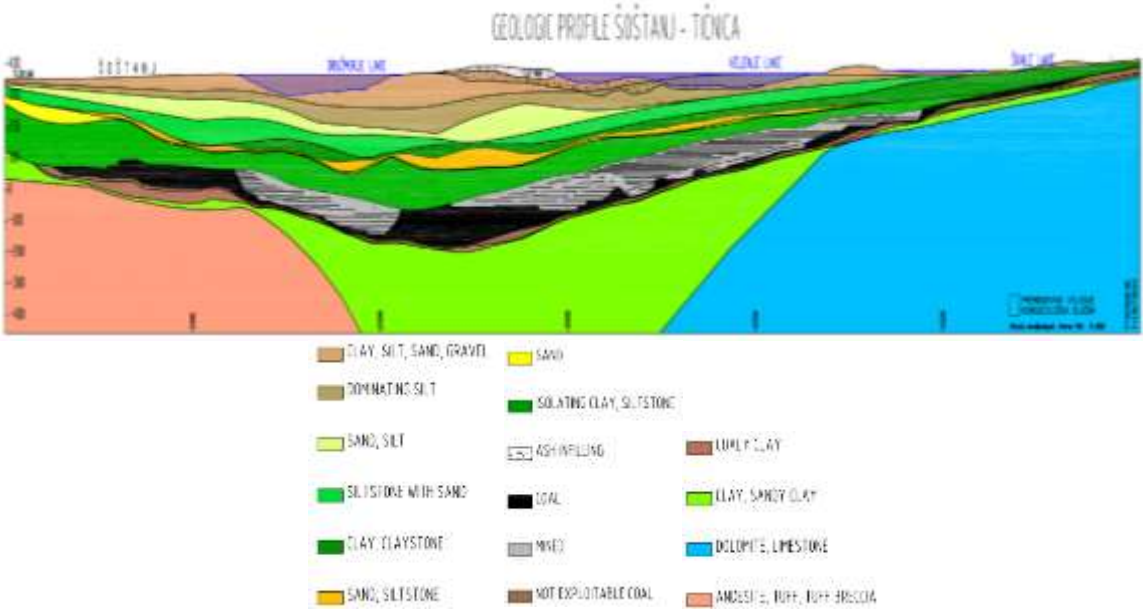

Figure 1.5: Geological map of the Velenje basin area [105].

1.4.2 Velenje mining method

The special longwall mining method nowadays used in the CMV is known as the Velenje Mining Method (VMM) and is unique in the world mining technology with beginnings in 1947 [108] when longwall faces were introduced in the mine. After 1952, the longwall mining method with classic under-structure prevailed. The exceptional thickness of the Velenje lignite seam prompted the Velenje miners to investigate the possibilities of extracting as much coal as possible while investing the least necessary amount of mining work. Therefore, they divided the coal seam into several levels at heights (Figure 1.6) still manageable in view of the related natural characteristics and technical possibilities. The highest located levels in the coal seam are mined first (Figure 1.6 and Figure 1.8), from the hanging-wall layers towards the footwall relatively good conditions are maintained for setting up necessary underground accession facilities at lower levels. The mining operations on the upper levels do not disturb the lower laying coal to any considerable degree [106].

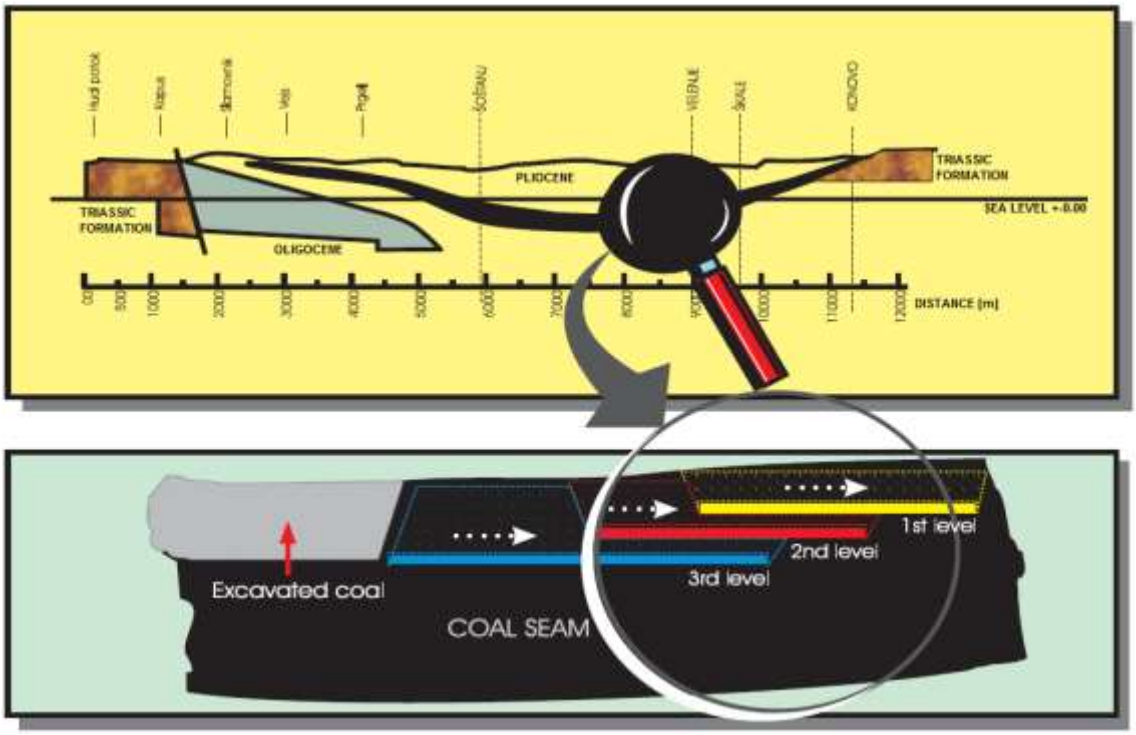

Figure 1.6: Longitudinal section of the coal seam and the sequence of extraction [109].

Development of the longwall mining method in Velenje focused on two variants: so-called horizontal concentration and vertical concentration, which led to a basic concept (Figure 1.8) of VMM that the area of coal exploitation extends above the longwall support system that is protecting the area of the coal face, while the natural forces of the higher lying geological strata are exploited for breaking and crushing the coal seam above the support system. The top coal caving process is then followed by caving-in of hanging-wall layers. At the beginning, the increased heights were provided by blasting off the ceiling section above the classic support system with friction legs and steel beams. In the early 1970's, CMV started using various types of mechanised hydraulic face support [108].

Based on continuous research, the method has undergone various organisational and technological improvements. With a better understanding of the geomechanical processes in coal mining, several improvements have been made in order to increase the coal production. With this method, the primary and secondary stress conditions and their transformations are used, which cause breaking and crushing of the coal seam, plastic transformations of the protective clay layer and bending and subsiding of soil layers lying above [110]. With the introduction of criteria for safe coal extraction beneath the aquifer layers, allowing the continuously variable determination of permissible extraction heights according to the depth of the face, the thickness of the insulation layer, the water pressure in the aquifer and the relative position of the face in the coal seam, the difference between the horizontal and vertical concentration is disappearing. VMM is also defined as a longwall mining method with increased or variable extraction heights, respectively.

The VMM is a combination of multi-level mining and longwall top coal caving (LTCC). From the top of the thick seam to the bottom, the coal deposit is divided into a series of mining levels ranging from 10 to 20 m thick, mined in a time sequence (

Figure 1.7 and Figure 1.8) with at least six months between the mining of each underlying longwall panel [111]. At each mining level, the lower part of the seam (3–4 metres high) is cut by a shearer under the hydraulic shield supports (HSS) while the upper section (7–17 metres) is caved. Caving of the top coal is achieved by the use of shield supports with an extending canopy which allows up to 4 m face advance, through several cuts at the face, before the extending arm is collapsed and the top coal is caved in phases. A more detailed description of the VMM can be found in [109].

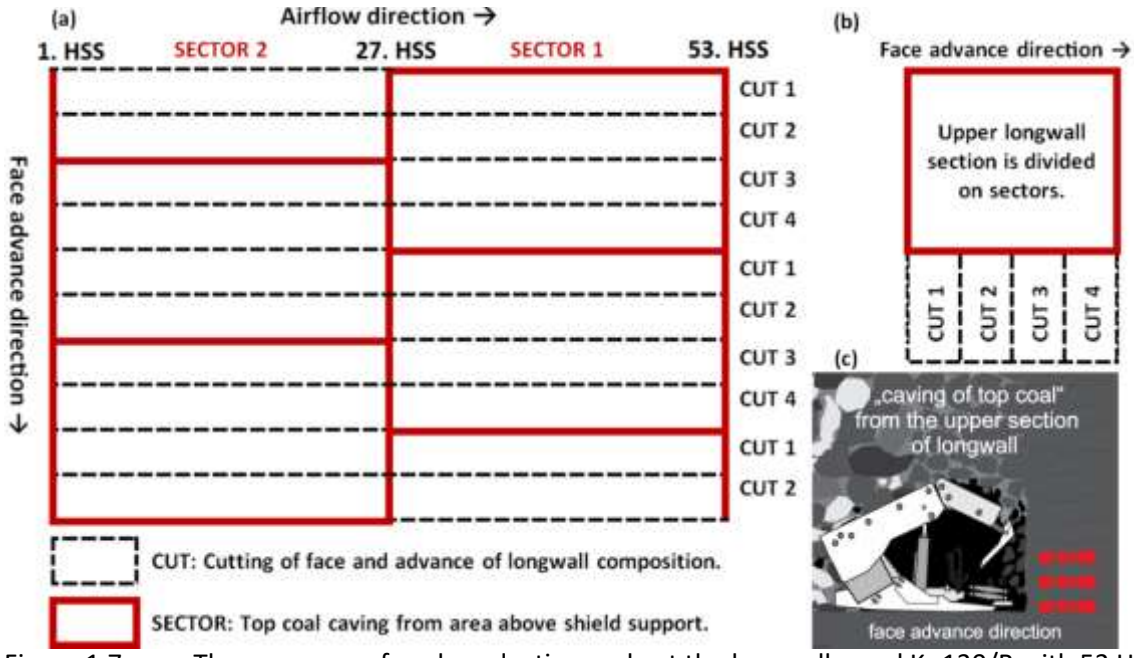

Figure 1.7: The sequence of coal production cycle at the longwall panel K.-130/B with 53 HSS units: plain (a) and side (b) views of a sequence of cuts and top coal caving of upper sectors, (c) top coal caving process at Coal Mine Velenje (adapted from [106]).

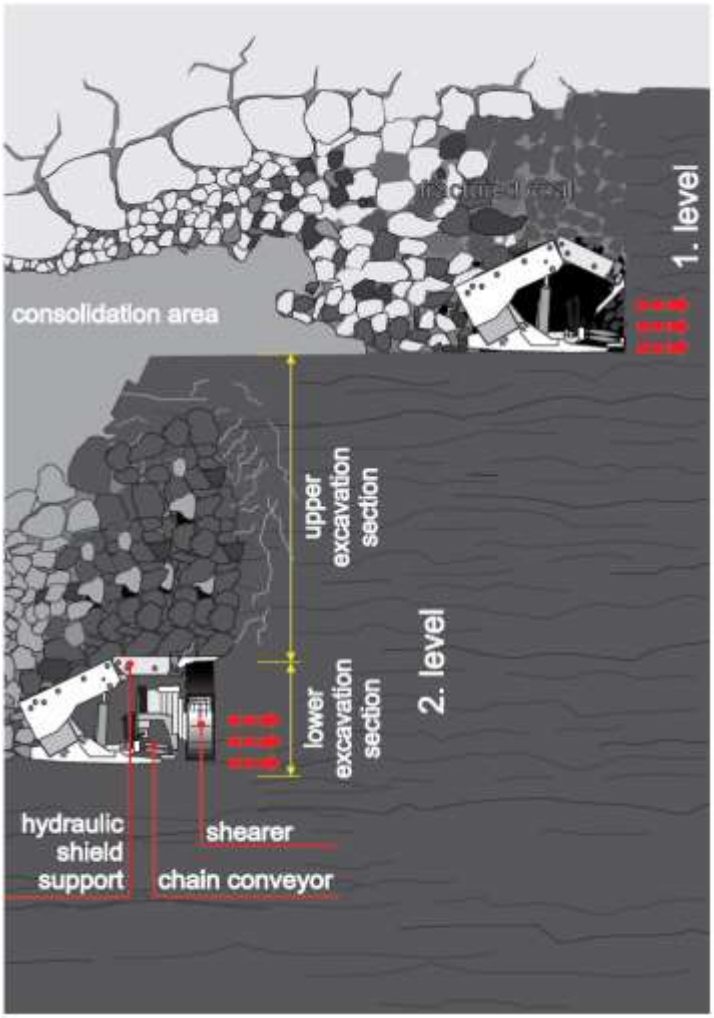

Figure 1.8: Scheme and the sequence of level extraction according to VMM [110].

The controlled top coal caving process is achieved with specially designed "carrying and shielding" HSS units (Figure 1.8), adapted for the VMM.

Technologically, besides the criteria for safe coal extraction, the extraction heights are limited also with mining losses which are increasing with increased extraction heights. At 20 m extraction height there are approx. 25 % extraction losses in normal conditions [108].

The technological cycle of longwall extraction according to VMM consists of the following working phases [108]:

- *dismantling the steel arch supports of gateroads at junctions,*
- *transporting the steel arch supports,*
- *cutting the longwall face with a shearer,*
- *advancing the armoured face conveyor (AFC) and beam stage loader (BSL)),*
- *advancing the hydraulic shield supports,*
- *top coal caving of a* specific sector (*Figure 1.7*),
- *shortening of the rubber conveyor, pipelines, and power lines in gateroads.*

The major production working phases are coal seam cutting and top coal caving (Figure 1.7 and Figure 1.8).

VMM is a completely mechanised method (Figure 1.9) with high productivity when natural factors provide the efficient top coal caving stage. The basic technology parameters of VMM since the 1990's and to the present are:

- *length of the faces: 110-230 m,*
- *extraction heights: from 5 m to 20 m,*
- *daily coal production from one longwall face: up to 16,800 t (28 July 2005),*
- *daily coal production: up to 33,000 t (11 September 1997),*
- *annual coal production: 2.5-4.25 million tons (5.1 million tons in 1985).*

In terms of organisation and technological solutions, the VMM has been constantly upgraded since its beginnings and has become well known worldwide and considered as the most important method of excavating thick coal seams. In technological and organisational terms, this method is constantly being optimised, particularly in terms of increasing the production, increasing the yield of a seam, the safety of the employees and the humanisation of the work [110].

Figure 1.9: Longwall face extraction process (work phase: simultaneously coal seam cutting with a shearer and loading on the BSL) in the CMV.

1.4.3 Development headings (gateroad building)

Underground objects (gateroads, shafts, drifts, etc.) are developed for a variety of purposes. In mines development headings provide mine access for men and materials, ore and waste hoisting, and ventilation paths (airways).

The extraction of tick coal seam in CMV is carried out from up to the bottom of the seam and it is based on the retreating extraction direction of longwall faces. All access gateroads are built before the start of the longwall face and with face advancement the gate gateroads are simultaneously liquidated. The cross section (13–18 m^2) and support system of gateroads in CMV are defined according to their intended use and lifetime, and of building conditions. CMV underground structures are divided into three groups [112]:

- *the main gateroads,*

- *the access gateroads and*
- *the gateroads.*

The general support system of gateroads (Figure 1.10) consists of combinations of supporting elements such as a steel arch support, wooden panels and composite arches with filling the voids with fly ash, water, and cement mixture to achieve continuous contact between the support system and coal for improved stability, and in particularly for preventing the development of spontaneous combustion in the coal seam.

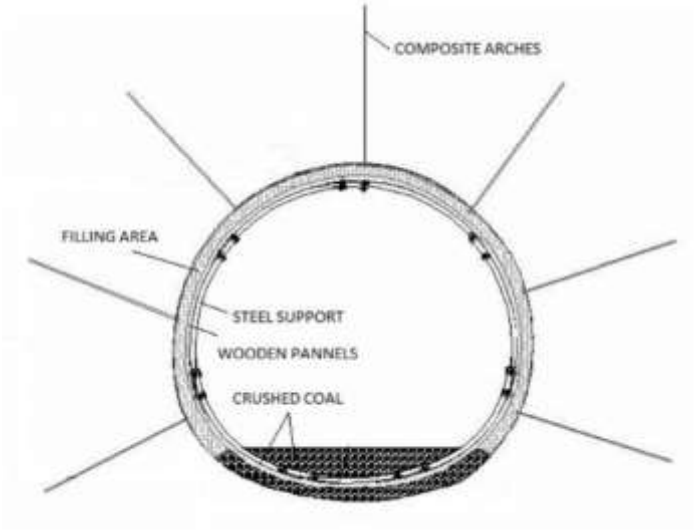

Figure 1.10: General cross section and support elements of the gateroad in CMV [112].

The cutting of gateroad's profile with a roadheader (Figure 1.11) is usually performed in three phases, which are divided into the ceiling, side, and floor of the profile. The step of advancement depends on the conditions in the working area, ranging from 0.8 m to 1.6 m [112].

Figure 1.11: Development heading: cutting of the floor part of gateroad's profile with a roadheader GPK PV.

1.4.4 Coal composition and lithology

It is known from experience of miners and supervisors, engineers of CMV that DMS appearing varies from not present (not detected) to present and to annoying in specific areas of the coal seam. Where DMS occurs in higher concentrations dark coal (darker than other lithotypes) with

fine texture is usually extracted. Nowadays, coal production is increasingly concentrated on such areas.

Based on extraction experiences in CMV it can be assumed that DMS is present only in some parts of the lignite seam. The fine texture coal (detrite) was found (excavated) throughout the whole seam (the detrite lithotype is usually surrounding xylite lithotype coal [10]). Apparently, there must also be some other coal composition characteristics (conditions) in the peat and coal formation period. It is known that coals are also containing different forms of sulphur. The sulphur is present in coal as organic sulphur (an integral part of the coal structure), pyritic (generally discrete pyrite and marcasite particles or 'lumps') and sulphate (as salts of metals such as calcium or iron) [55]. The average sulphur content in the CMV coal seam is 1.7 % (from more than 1600 coal analysis) [10].

The most common lignite lithotypes in CMV are detrite (D), xylo-detrite (xD), detro-xylite (dX) and xylite (differentiated into three dimensions (X, XX and XXX).

Detrite (D; composed of particles smaller than 1 mm) is composed of fine detrital homogeneous plant material that represents a matrix between larger fragmental components. In the sense of constituent elements, the elements were very small plant particles that mostly cannot be differentiated macroscopically. Fine detrite is dark brown to black. Xylo-detrite (xD) and detro-xylite (dX) are lithotype components composed of xylitic fragments and the very closely surrounding fine detrital matrix. Thus, both components are composed of two constituent elements and are considered as bi-elemental lithotype components. Xylite (in three classes by size: X - 64-512 mm; XX – 512-2048 mm; XXX – larger than 2048 mm) is a well-known synonym for large brown pieces of wood (branches, stems, stumps, trunks) lying within fine detrital matrix [10].

The lignite clearly exhibits a fragmental/detrital appearance. The scale is applied to describe size limits of the lignite's constituting components in Figure 1.12.

MACROPETROGRAPHIC PATTERN Core diameter 63 mm	LITHOTYPE COMPONENTS (classes in vol. %)	CODE textural	
	Sand and silt	1	
	Clay	1.5 (w) 2	
	Mineral-rich lignite	combination	
	X	3 (w)	
	X and dX	3.5 (w)	
	dXxD > 85 D < 15	4 (w)	
	dXxD 60-85 D 15-40	5	5.5
	dXxD 40-60 D 40-60	6	6.5
	dXxD 15-40 D 60-85	7	7.5
	dXxD 5-15 D 85-95	8	9
	D > 95	9.5 (w)	
	Gelification - weak g	10	
	Gelification - pronounced G	15 (w)	

Figure 1.12: Schematic presentation of lithotype components (graphics on the left), classes of lithotype composition (in the middle), and "textural" code values for separate compositional classes (on the right) that CMV lignite coal corresponds to [10].

In 1997, a study of adsorption and desorption of gases on samples of different lithotypes of lignite was performed. As a result, their laboratory experiments showed significantly contrasted adsorption and desorption properties of different lithotypes of lignite. For example, the specific surface of pores of homogenous fine detrital lignite amounts to more than 180 m^2/g, whereas that of xylite to "only" 35 m^2/g, mainly related to differences in porosity parameters [10].

Despite an extensive study of lithotype characterization of Velenje coal seam mainly from structural boreholes samples (surface and underground boreholes) and from faces of underground mine workings, the detailed lithotype model of coal seam could not be made, because of varying conditions during peat formation and coal genesis (topography, vegetation, water presence, subsidence, tectonics). However, the general model presumes that during peat formation on the surface tree-rich plant was mostly growing at the foothills and dwarf plants mainly in the middle of the area. Also, subsidence was the fastest at the middle of the basin. A very simplified illustration is presented in Figure 1.13 of the marginal tree-rich versus inner basin dwarf plants distribution as presumed in the development of the Velenje peat accumulation. Subsidence was the highest in the inner part of the basin, causing inclination of the strata at the margins and creating accommodation space in the interior [10].

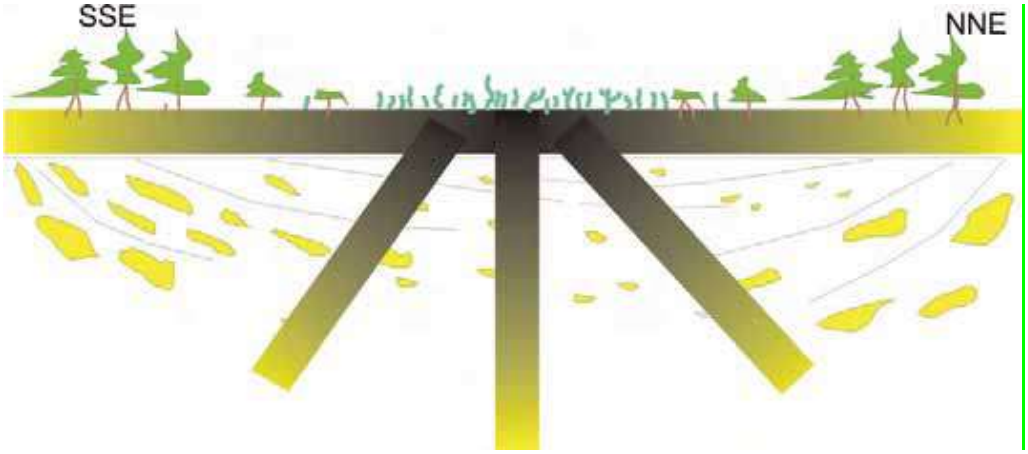

Figure 1.13: Very simplified illustration of tree-rich versus inner basin dwarf plants distribution as presumed in the development of the Velenje peat accumulation [10].

Studies of the Velenje lignite (geo-mechanical, structural geology, coal petrology, isotopic and geochemistry) have revealed that knowledge regarding the petrographic heterogeneity of lignite is crucial for understanding the complex gas properties and gas behaviour during mining within the lignite seam ([10], [11]).

1.4.5 Mine ventilation

A special part of the mining is mine ventilation. It can be described as the lifeblood of a mine, the intake airways being arteries that carry oxygen to the working areas and the returns veins that carry diluted pollutants all the way to the outside atmosphere.

The primary objective of a mine ventilation system is the provision of acceptable working mine atmosphere with the supply of fresh air and the dilution and removal of pollutants within the boundaries of regulated limits. In addition to gas dilution and removal, a ventilation system is responsible for the maintenance of a satisfactory climate and dust control [113]. Fans located either in the mine or on the surface provide the necessary airflow and are an essential part of the mine ventilation system. As the mine is developed and the expanses underground increase, the ventilation system must also be able to adapt over time to the changing conditions. A great deal of engineering goes into developing a mine ventilation system to incorporate all these factors [114].

The primary means of producing and controlling the airflow are also illustrated in Figure 1.14. The main fans handle all of the air that passes through the entire system. The necessary connections between intake and return airways are regulated with ventilation doors. When these are no longer required for access or ventilation, they must be blocked by stoppings in order to prevent short-circuiting of the airflow. Abandoned areas of a mine are to be isolated from the current ventilation infrastructure with seals and filled with non-flammable material (e.g., water-coal ash-cement-based fill in CMV). Where access must remain available between an intake and a return airway, a stopping may be fitted with ventilation doors. Ventilation doors are usually built as a set of at least two or more to form an airlock. This prevents short-circuiting when one door is opened for passage of vehicles or personnel. Ventilation doors are also used as regulators for adjusting the desired airflow value. Also, a variety of other forms of passive regulator is used in the mine. Where intake and return airways are required to cross over each other, then leakage between is controlled by the use of air crossings which separate both airstreams.

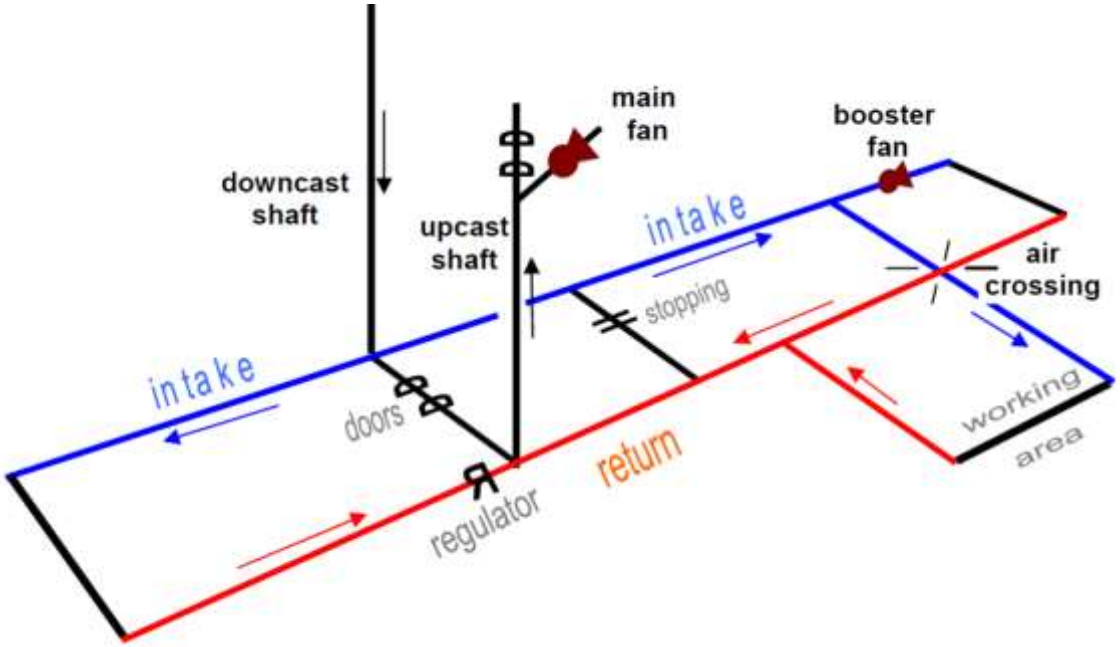

Figure 1.14: Typical elements of a main ventilation system [115].

The main ventilation system is responsible for the delivery and distribution of fresh air around the main mine ventilation network. This is principally achieved by the correct choice of the number, type, and location of main surface or near surface fans. The main fans provide ventilation to the mine by either exhausting the polluted air out of the mine or by forcing fresh clean air into the mine. In the ventilation of many large and extensive mining operations a combined force/exhaust (push/pull) main fan ventilation combination is employed [113]. The main factors to be considered in the choice between the force/exhaust configurations [115] are gas control, transportation, maintenance, and performance (efficiency). In Slovenia, the exhaust main mine ventilation system is mandatory in coal mines.

Also, part of the main ventilation system are booster fans. Booster fans are used where a mine network may extend to a greater depth or lateral extent to exploit additional reserves, the main fans may not be able to produce the pressures required to distribute the required fresh air. A common solution is to install additional subsurface booster fans to assist in the distribution of fresh air by providing the pressure required to overcome the additional resistance afforded by the extended circuit. Booster fans provide a high outlet velocity creating an excess of momentum that exerts a forward force on the normal airflow [113].

Mine ventilation at CMV is one of the major processes of coal extraction, requiring the continuous and effective ventilation for all the gateroads and underground facilities (between 50 and 60 km). The ventilation of the CMV is operated continuously with a capacity between 340 m^3/s and 420 m^3/s.

Forced mine ventilation is driven by two main ventilators and series of auxiliary ventilators in mine areas without flow-through ventilation. The shafts and fans are located in the vicinity of the Šoštanj power plant (Šoštanj ventilation station) and near the settlement of Pesje (Pesje

ventilation station). The fans of ventilation stations on the surface power the mine ventilation by creating depression (partial vacuum) with air suction from the mine. Created pressure differences then enable the movement and direct the air flows in airways trough the mine. CMV has five surface air intakes of fresh air with three down cast shafts and two drivages connected to the surface. Figure 1.15 shows the air intakes and exits on the surface and underground facilities of CMV. Šoštanj ventilation station provides approximately two-thirds of required airflow and the Pesje ventilation station provides the remaining one-third.

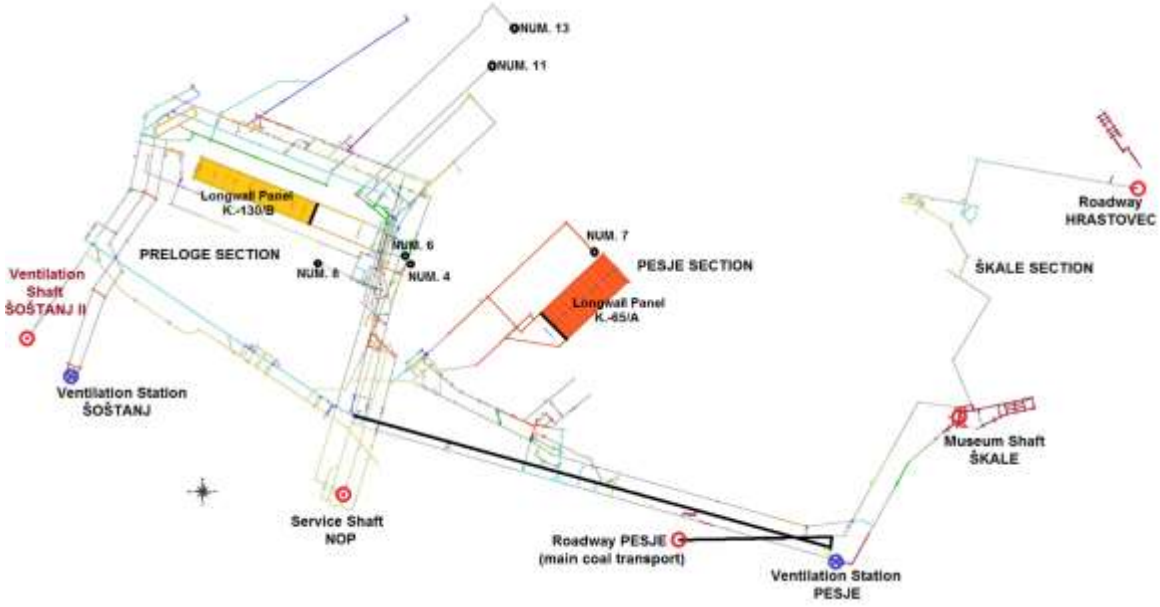

Figure 1.15: Mine plan in October 2012 illustrating the mine ventilation network, the two active longwall panels and the main coal transport gateroad. The two main exhaust fans are indicated as ventilation stations. The five fresh air intakes are also marked. The development headings are also numbered as sources for DMS emission.

Chapter 2

Aims and Hypothesis

The purpose of this study is to develop and implement a robust odour emission monitoring system based on the real time gases concentration measurements and collect the necessary data and develop an understanding of occurrence in the process of underground coal extraction (Velenje mining method) and dispersion of odorous compounds in the mine ventilation system. The monitoring results form the basis for the correlation study between influencing factors and for the numerical modelling of the mine ventilation parameters with a focus on predicting concentrations of pollutants in the underground facilities over time.

Therefore, the main aims of this dissertation are as follows:

Collection and analysis of existing data of ventilation parameters of the mine ventilation system.

Collection and analysis of existing data on gaseous emissions from the coal extraction areas, air exit gateroads (return gateroads) and air exit shafts with a focus on mine gases that cause odour.

Analysis of odour sources in the process of longwall coal mining.

Correlation analysis of monitored gaseous emissions in relation to working phases of the top coal caving extraction process (in the Velenje Coal Mine it is known as the "Velenje mining method").

Numerical modelling of mine ventilation in relation to monitored results with a focus on predicting concentrations of pollutants in the underground spaces over time.

Test of DMS stability in mine atmosphere for the period of traveling time when DMS is released from the longwall faces and ventilated to the surface.

This dissertation will investigate the following hypotheses:

Odorous gases are emitted from the coal seam mainly during the phases of coal extraction.

The release of CH_4 and CO_2 concentrations is highly correlated with specific phases of the coal extraction process.

DMS concentration has different release characteristics than CH_4 and CO_2 concentrations during coal extraction.

DMS concentrations in the mine are dependent on many parameters including natural characteristics of the coal, presence of odour active compounds in the coal seam and old mine workings, production and ventilation design, and coal production intensity.

DMS is the most abundant SVC and the most influential in the occurrence of odour in the mine.

DMS is stable and does not decay when released from the mine sources into the mine atmosphere and is diluted only with the mine ventilation during traveling from the source to the surface.

The longwall faces, development headings and main coal transportation system are the main odour sources in the mine.

Ventilation-based control options to reduce the presence of odour-active compounds released during mining of coal are alone not sufficient.

Chapter 3

Materials and Methods

3.1 Monthly Gas Sampling Data Analysis

The text related to Section 3.1 is based on our published article [1].

As the first step in this study, the long-term monthly monitoring data of gases concentrations in the mine atmosphere were analysed in order to determine the main odorants in the mine, their source, and to estimate emissions.

Monthly chemical analysis of mine gasses is carried out to control gas concentrations in mine air and includes the following gases: CH_4, CO_2, DMS, H_2S, SO_2, O_2, CO, H_2, NO, NO_2 and N_2.

The N_2 content of the mine gas is the difference between the sum of the monitored gases and from 100% [116]. The concentrations of CH_4, CO_2, DMS and H_2S were determined using gas chromatography. The test method PM 3.01 was used for CH_4, CO_2 (GC - FID) while the test method PM 3.02 was used to determine H_2S and DMS (GC – FPD), [116]. The concentrations of O_2, CO, H_2, NO, NO_2, SO_2 were determined using a gas meter with a built-in electrochemical sensor (Echo d.o.o., Slovenia). Oxygen and CO concentrations were determined using the PM 3.03 test method, while the remainder were determined using the PM 3.04 test method. All three methods were developed by Erico – since 2017 is named Eurofins Erico [116] and are granted by an accreditation body (i.e., Slovenian Accreditation).

These mine air samples were collected in 2 L Tedlar® sampling gas bags and analysed in the laboratory within 24 hours [116]. The monitoring sites were selected systematically in such a way that all coal production activities can be controlled. Air samples were collected in the return airflows of all main work sites in the mine and in all main returns of mine ventilation. Samples were not collected simultaneously at specific monthly monitoring campaigns.

The monitored gases were divided into odorous and odourless gases. The limits of detection of odorous gases were: DMS 2.58 mg/m^3, SO_2 2.67 mg/m^3, H_2S 1.42 mg/m^3, NO 1.25 mg/m^3 and NO_2 1.91 mg/m^3. Out of odorous gases NO and NO_2 were never detected. Therefore, only monitored sulphur gases were analysed.

Based on monthly monitoring data, the characteristic gases concentrations of mine odour sources were statistically determined for identified mine sources. For model entry values, two levels of mine odour sources were quantified: median sources (50th percentile) and peak sources (97.5th percentile).

Additionally, the odour activity values (OAV) were calculated considering characteristic concentrations and ODT [5]:

$$\text{OAV} = \frac{\text{Concentration}}{\text{Odour detection threshold (ODT)}} \ [/] \tag{3.1}$$

The OAV represents relative importance of an individual compound in a usually complex odour mixture. The OAV is defined as the ratio of the concentration of a single compound to the odour threshold for that compound. Conceptually, the larger the OAV, the more likely that compound will contribute to the overall odour of a complex odour mixture [[117], [118]]. The odour concentration, usually expressed in odour units (OU/m^3), is numerically equal to the dilution factor necessary to reach the odour threshold that is the minimum concentration perceived by 50% of population. According to European standardization, 1 OU/m^3 is defined as the amount of odorant that, when evaporated into 1 m^3 of gas air at standard conditions, causes a physiological response from a panel (detection threshold) equivalent to that of n-butanol (reference gas) evaporated into

1 m^3 of neutral gas [119]. Considering the definitions of odour concentrations and OAV in case of air mixture with only one odorant, the values of odour concentration and OAV are equal.

3.2 DMS Monitoring Campaign on Longwall Panel K.-130/B

Research described here aimed at carrying out a detailed investigation into the variability in the levels of DMS and the correlation between DMS and other monitored parameters during different production phases at a longwall face (
Table 3.1). For this purpose, a continuous monitoring DMS sensor was added to the routine gas monitoring system at the out by end of the return gateroad of longwall panel K.-130/B (Figure 3.1, position “f”).

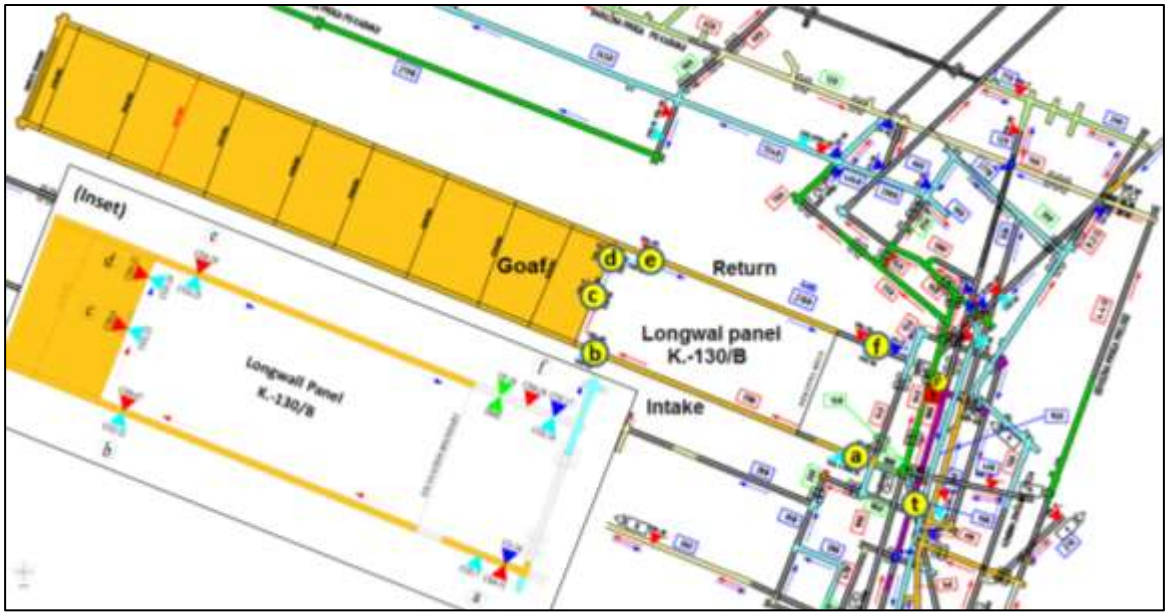

Figure 3.1: Longwall panel K.-130/B showing sensor positions a to f (in more detail on the inset) and the coal tonnage monitoring station t (longwall face as on 15 October 2012).

The longwall panel K.-130/B was selected because it is located in an area where odour is often detected. The longwall panel (93 m x 690 m, average excavation height 10 m), consisting of 53 hydraulic shield supports, was located in the southeast part of CMV (Figure 3.1). Coal was extracted between 29 May 2012 and 9 January 2013, a total of 151 work days. Total production was 1,179,627 metric tonnes of coal. During this period, the longwall face advanced 224.6 m. All sensors were connected to the “Safety and Technology Information System” through the mine's main fibre optic data transfer line. The data was processed at one-minute intervals using the dedicated database integration software “Query” (Schneider Electric Software, France). This produced 1,440 data points per day for each sensor. This frequency of sampling gave a manageable volume of processed data (approx. 133,800 readings per sensor).

Gas monitoring was performed over 62 production days (4 October 2012–5 January 2013). The gas sensors used included GMM 05.05 (DMS, see Figure 3.12 in Chapter 3.3.1), GMM 04.04(CO_2), GMM 01.04(CH_4), GMM 03.05 (CO2) and WMA 15.07.5 (air velocity) supplied by Woelke Industrieelektronik GmbH of Germany. A coal production sensor (type KPV-02 continuous belt scale, Siemens, Germany) was positioned at location “t” to measure tonnage.

Table 3.1: Position and description of sensors on longwall panel K.-130/B.

LOCATION	NAME	MEASURED PARAMETER	DESCRIPTION
a	CH_4-51	CH_4 concentration [%]	Intake roadway: unloading area for steel arch supports; approx. 15 m from the junction where the mine air enters the longwall panel.

	CO_2-7	CO_2 concentration [%]	
	CO-24	CO concentration [ppm]	
b	CH_4-67	CH_4 concentration [%]	Intake roadway: between the primary coal crusher on stage loader and the longwall face.
	CO_2-22	CO_2 concentration [%]	
c	CH_4-6	CH_4 concentration [%]	Longwall face: in the middle of face mounted on the 27th shield support.
	CO_2-23	CO_2 concentration [%]	
d	CH_4-22	CH_4 concentration [%]	Longwall face: towards the end of the longwall face mounted on the 46th shield support.
	CO_2-24	CO_2 concentration [%]	
e	CH_4-29	CH_4 concentration [%]	Return roadway: approx. 20 m from the face end and after the auxiliary fan discharge point (6,67 m^3/s).
	CO_2-25	CO_2 concentration [%]	
f	CH_4-24	CH_4 concentration [%]	Return roadway: approx. 50 m from the out by end.
	CO_2-34	CO_2 concentration [%]	
	CO-17	CO concentration [ppm]	
	VP-34	Airflow speed [m/s]	
	DMS	DMS concentration [ppm]	
t	PRO-32	Coal tonnage [t]	Belt conveyor 70J: next in line of the belt conveyor in the main intake roadway.

As presented in detail in Table 3.1, the monitoring system used allowed for real-time surveillance of gas levels in the intake and return gateroads as well as the longwall face. Since the gas sensors display measured gases concentrations in ppmv (DMS, CO) and in % (CH_4, CO_2) units, the conversion to mg/m^3 at normal conditions (temperature 20°C and pressure 1013.25 mbar) was calculated where necessary with the following equation:

$$ppmv = mg/m^3 \times \frac{22.4}{M} \times \frac{(273+T)}{273} \times \frac{P}{1013} \quad (3.2)$$

where:

M …molecular weight of a substance

22.4 (L) …the volume of 1 mol at 1 atmospheric pressure at 0°C

273 (K) …K stands for Kelvin

1013 (mbar) …One atmospheric pressure

P …the atmospheric pressure at the point of measurement (mbar).

Then the conversions gave the following values in mg/m^3: 1ppm=2.583 mg/m^3 for DMS, 1%= 6,672.2 mg/m^3 for CH_4 and 1%= 18,306.9 mg/m^3 for CO^2.

The collected data was analysed in MS Excel. Table 3.2 shows the analysed sensors and their differences.

Table 3.2: Analysed sensors and their differences.

Num.	Parameter
1	DMS
2	CO_17
3	CO_24
4	CH4_51
5	CO2_07
6	CH4_67
7	CO2_22
8	CH4_06
9	CO2_23
10	CH4_22
11	CO2_24
12	CH4_29
13	CO2_25
14	CH4_24
15	CO2_34
16	PRO32_SUM
17	[t/min]
18	VP_34
19	[m3/min]
20	CO (17-24)
21	1=CH4 (67-51)
22	1=CO2 (22-07)
23	2=CH4 (06-67)
24	2=CO2 (23-22)
25	3=CH4 (22-06)
26	3=CO2 (24-23)
27	4=CH4 (29-22)
28	4=CO2 (25-24)
29	5=CH4 (24-29)
30	5=CO2 (34-25)
31	2+3=CH4 (22-67)
32	2+3=CO2 (24-22)
33	2+3+4=CH4(29-67)
34	2+3+4=CO(25-22)
35	2+3+4+5=CH4(24-67)
36	2+3+4+5=CO(34-22)

For a correlation between variables x and y, the formula for calculating the sample Pearson's correlation coefficient is given by [120]

$$r_{xy} = \frac{\sum_{i=1}^{n}(x_i - \bar{x})(y_i - \bar{y})}{\sqrt{\left[\sum_{i=1}^{n}(x_i - \bar{x})^2\right]\left[\sum_{i=1}^{n}(y_i - \bar{y})^2\right]}} \quad (3.3)$$

where x_i and y_i are the values of x and y for the i-th individual.

The strength of specific correlations was estimated with the calculated hourly values of correlation coefficients according to Table 3.3.

Table 3.3: "Rule of Thumb" for interpreting the value of a correlation coefficient [120].

Size of Correlation	**Interpretation**
0.90 to 1.00 (-0.90 to –1.00)	Very high positive (negative) correlation
0.70 to 0.90 (-0.70 to -0.90)	High positive (negative) correlation
0.50 to 0.70 (-0.50 to -0.70)	Moderate positive (negative) correlation
0.30 to 0.50 (-0.30 to -0.50)	Low positive (negative) correlation
0.00 to 0.30 (0.00 to -0.30)	Little if any correlation

In the analysis of the correlations two approaches were used to capture the nature of the coal extraction process and its intensity.

In the first part, the focus was on the releasing properties of DMS during mine extraction process in relation to working phases of the Velenje mining method – longwall top coal caving extraction process, and to study the interdependences between monitored parameters. The analysis considers a period from 5 October 1012 (6:00) to 25 October 2012 (6:00). The correlation analysis of specific pairs of sensors in relation to working phases of extraction process was based on monitored values and the actual workflow on longwall face. The working phases were established on the base of daily reports of longwall face mining supervisors. Every work shift the mining supervisor has produced a graph of the workflow (part of a daily report), which serves for daily chronological overview of the main extraction features on longwall face (Figure 3.2).

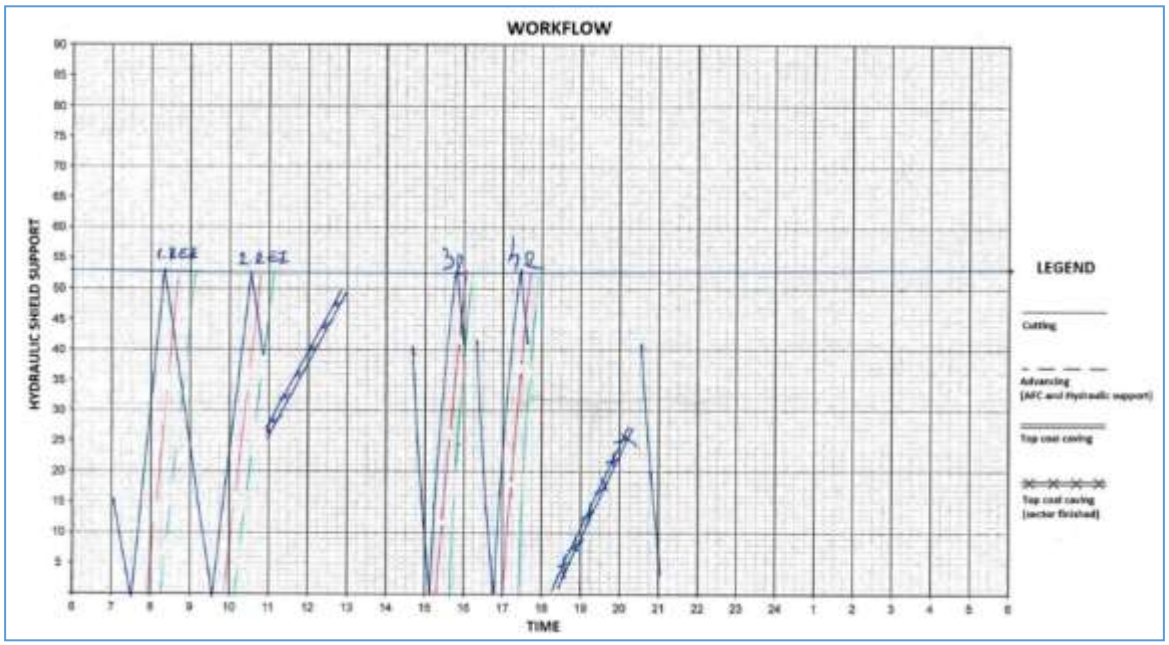

Figure 3.2: Workflow report on longwall face of K.-130/B panel on 12 October 2012. The extraction on the longwall face of the whole analysed period was carried out in two eight-hour shifts per working day.

From the workflow in Figure 3.2 it is visible that working phases on 12 October 2012 follow as envisaged in the technological process (see Figure 1.7 in Chapter 1.4.2); after two cuts with the shearer and advancing of transporters (AFC and BSL) and hydraulic shield supports, the top coal caving part of one sector follows. The production on the longwall face was active in the first and second work shift, the third shift was not in operation as planned according to production of other longwall faces on CMV and coal consumption of Šoštanj thermal plant.

In the second part of the correlation, analyses focused on the releasing properties of DMS during the mine extraction process in relation to production intensity. The whole monitored period (4 October 2012–5 January 2013) was divided in half-hour intervals and arranged according to production intensity (as tonnage in 30 minutes) in intervals 0, 1-100, 101-200, 201-300, 301-400, 401-500, 501-600 and 601-671 (671 t/30min was max. value). For each of 4,462 half-hour intervals half-hour characteristic values of monitored parameters were calculated: minimum, average, maximum, standard deviation, median, percentiles (2.5%, 25%, 75%, 97.5%) and for the production rate (intensity) [t/30min]. The half-hour interval was selected to better capture the production and non-production working phases. In reality, the individual working phases according to VMM (see Chapter 1.4.2) are not generally carried out according to the hour-to-hour schedule but the durations are working conditions specific.

3.3 The Experiment of Dimethyl Sulphide Stability in Coal Mine Velenje

The main objective of the DMS stability experiment in the mine atmosphere was to additionally confirm the literature preview (see Chapter 1.3.1) if the DMS concentrations after releasing from the coal seam (during coal extraction) in the air stream of an airway are reducing only with dilution because of mine ventilation or is there additional decay while DMS is ventilated and diluted from the mine source to the surface. That is, to release and control artificial DMS source in the mine and measure DMS concentrations on the way while DMS travels through the mine. Monitoring locations must be positioned in a way that from collected data it is possible to determine the traveling time of DMS and to detect possible changes of DMS concentrations or DMS mass flow between monitoring locations. The underground mine consists of a network of gateroads which are also airways for ventilation network.

The experiment was designed in a way that it was possible to simulate the duration of the DMS journey from the longwall face in Coal Mine Velenje when it is released from the coal during extraction and all the way to the surface through the network of airways as it leaves the mine atmosphere.

The traveling time of released DMS from the longwall faces to the surface was modelled in Ventsim™. Modelling results (presented in detail in Chapter 4.4.1) show that DMS is traveling from the longwall faces and to the surface between 556 to 750 seconds (approx. between 9.5 and 12.5 minutes).

The major obstacle of this mine experiment is the mine atmosphere itself with the mine ventilation and airways network and released mine gases. For the successful experiment, the airway with a sufficient length and low airflow velocity is necessary and in addition there must be no releases of DMS along the airways.

For example, the airway with 12 m^2 cross-section (in general, cross-sections in CMV varies between 12 and 17 m^2) and minimum airflow velocity 0.2 m/s by Slovenian mine legislation would have 2.4 m^3/s (144 m^3/min). There are no airways with such low airflow velocity in the Velenje coal mine with appropriate length.

After inspecting approx. 60 km airways of the Velenje coal mine it was clear that the airway with the characteristics that are closest to desired characteristics was and to this day still is “Južna talninska zveza” with the length approx. 600 m and built with bricks (secondary support system), which practically prevents the realising of mine gases in the airway. In 2015, the airway had airflows between 8.33 and 10 m^3/s (500 and 600 m^3/min) and air flow velocities between 0.7 and 0.8 m/s. With additional measures just before the test, such as additional sealing of ventilation regulation doors and mounting, i.e., a mine parachute to reduce airflow rate in the return of airway “Južna talninska zveza”. With additional measures the airflow velocity fell to 0.5 m/s and airflow to 6 m^3/s (360 m^3/min).

After the first unsuccessful experiment in 2015 in the “Južna talninska zveza” airway it became clear that a successfully executed experiment will be a very demanding task. Not only because the sufficient dosage of artificial DMS source from gas cylinder. But even more, how to set up the DMS sensor in an airway with a 12 m^2 cross-section to collect average DMS concentration knowing that DMS is much heavier (2.58 kg/m^3) than air (1.29 kg/m^3)? In theory, that would be possible with a cross-section reduction (constriction) to at least 1 m^2 just before each monitoring location in the form of a funnel. But in the operational underground mine where each airway has a special meaning for mine operation that is not possible. Also, there were other obstacles which need to be accounted for as measuring characteristics of DMS sensors. The sensor’s accuracy is optimal after several minutes after they are induced with airflow that contains DMS.

The only practical solution to transport DMS into the mine with the known mixture is by gas cylinders. The producer of gas mixtures (Linde) prepared the DMS mixture with a maximum concentration of 0.2% and 99.8 % nitrogen at pressure 150 bar and volume of gas cylinder 40 litres. That is 6000 litres or 6 m^3 of mixture with 2000 ppm of DMS. Higher concentrations of DMS in a cylinder are not possible due to the explosion characteristics of DMS. DMS mixture with air is explosive with DMS concentrations between 2.2 and 19.7 %.

This means that in an airway with a 12 m^2 cross-section and airflow velocity 0.5 m/s, one gas cylinder can provide approx. 10 ppm DMS source in an airway for only 200 seconds or 3.33 minutes.

Since there was still a demand for the test to be conducted in a mine atmosphere, the search for a solution focused on how to minimize airflow and air velocity in the mine.

The solution was found in an auxiliary ventilation system. Auxiliary ventilation refers to the systems that are used to supply air to the working faces of blind headings. There are two primary

forms of ducted auxiliary ventilation, namely the force and exhaust systems. Figure 3.3 illustrates a typical force and exhaust layout of ducted systems. Also, at ducted systems overlapping systems are possible [115].

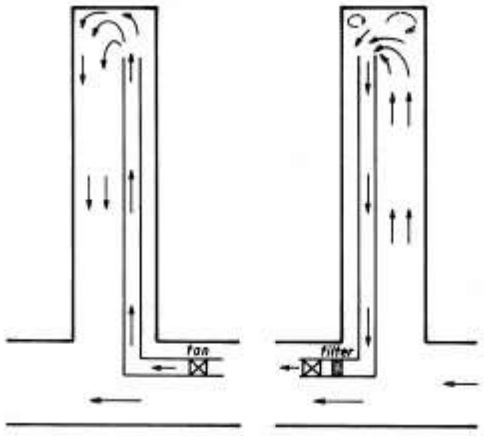

Figure 3.3: Typical force (left) and exhaust (right) layout of ducted systems [115].

In Slovenian coal mines with a "methane regime" the fan and duct systems with a force layout for auxiliary ventilation of development headings are preferred by the mining legislation. The reason is that at an exhaust layout increased concentrations of methane could occur at a level of potentially explosive atmosphere (5–15%) in the duct, by sucking the surrounding atmosphere of the duct intake, which means that the fan must be immediately switched off from the electrical supply. The safety switched off methane level is 1.5 %. In such a case, the ventilation of the development heading would be interrupted.

The use of the environment of ducting in case of an experiment brings many advantages. The duct with 0.6 m in diameter means nearly 98 % cross-section reduction. This means that with airflow velocity 0.6 m/s in ducting, one gas cylinder can provide approx. 10 ppm DMS source in ducting for almost 2 hours.

The control of airflow velocity and consequently the airflow rate with the fan connected to the ducting is much easier than the control of airflow velocity of an airway main fan regulation and auxiliary regulation in the airway of the experiment and airways that have the greatest impact on the location we want to regulate. Also, the regulation of one airway has impact on the whole area ventilated with one main fan.

And, on the soft ducting of force auxiliary ventilation it is easy to apply cross-section reductions (constrictions) where needed.

The downside of the layout with ducting in comparison to airway is that the airway has no losses of mass flow. Meanwhile, the leakage of mass flow at the joints of ducting is common at 5 % of mass flow losses per 100 m. Which means that it is not possible to control mass flow of DMS after it is released from the cylinder and the success of the experiment depends on DMS concentration measurements only.

The leakage within the mine ventilation network represents any interconnections between intakes and returns or groups of airways which should be minimized and, if possible, geographically separated. All airflows through interconnections must be minimized with doors, stoppings, or seals, which must be constructed and maintained to a good standard [115]. The significant leakage can also represent the poorly maintained fan and duct auxiliary systems (e.g., loose coupling of joints, tearing of a duct) of development headings which can increase with length of the development advance. The volumetric efficiency [115] of a mine is defined as:

$$VE = \frac{Airflow\ usefully\ employed}{Total\ airflow\ trough\ main\ fans} \times 100\% \tag{3.4}$$

The problem of mass flow loss was investigated in more detail with the help of a simulation in the Ventsim™ software. And also to study how the ducting will behave under experiment conditions. The whole report of leakage simulation is presented in Appendix C: Modelling of leakage of mass flow from the ducting.

Targeted traveling time was at least 750 seconds or 12.5 minutes. At airflow velocity 0.6 m/s at least 450 m long ducting is needed. The targeted air flow velocity in ducting is much lower than at actual ventilation of the development heading.

In CMV airflow rates are between 4.0 and 9.2 m^3/s (according to ventilation data from October 2012) which corresponds to velocities between 8.0 and 18.3 m/s in ducting 0.8 m in diameter. In case of ventilation of development headings, the rubber ducting is always inflated because of the flow pressure.

Simulations showed that in case of a setup as on development headings (example 1, see Appendix C):

- *The total loss of mass flow is 14.3 % or 2.6 % per 100 m of ducting (mass flow losses are comparable to the losses of ducting of brand-new ducts. In CMV mass flow losses were measured as low as 2% per 100 m.*

- *The maximum leakage at the first joint is 0.0206 kg/s and the minimum leakage at the last joint is 0.0017 kg/s. The difference between minimal and maximal leakages is 91.7 %.*

In case of a setup similar to the planned experiment with reduction cross-section reductions at the end of ducting with the auxiliary fan set to only 3 % power to achieve targeted average airflow velocity (example 2, see Appendix C):

- *Because of such low fan power which gives such low airflow rate, at a joint approx. at the middle of ducting, the leakage becomes reverse and the "airway starts to leak in the ducting". In reality, the ducting starts collapsing when the total pressure in ducting is lower than the total pressure in the airway. This manifests in a collapse of the soft ducting that is used for the forced auxiliary ventilation layout. This phenomenon also appeared at pre-tests in the previous experiment in January 2018. The collapsing of the ducting in simulation and in reality, is prevented with the cross-section reduction at the end of ducting.*

In case of a setup as of similar setup as at planed experiment with bigger (than example 2) reduction cross-section reductions at the end of ducting with the auxiliary fan set to 6 % power to achieve targeted average airflow velocity (example 3, Appendix):

- *The auxiliary fan was set to only 6 % power to overcome additional resistance due to shock losses of cross-section reduction.*

- *Due to the cross-section reduction (additional resistance) total loss of mass flow is 28.1 % or 5.1 % per 100 m of ducting.*

- *The maximum leakage is 0.0014 kg/s and minimum leakage is 0.0011 kg/s. The difference between leakages is 21.4 %. The difference is much smaller than in example 1. If only the first three decimal places are considered, the mass flow losses at all joints are equal. This shows that cross-section reductions help with averaging of mass flow leakages if we assume that each joint of duct is geometrically the same. Taking into account the simulation results, in theory, it is possible to make all joints with the same rate of mass flow leakage with adding additional reduction.*

Also, simulations show that cross-section reduction – constriction at the end of ducting is necessary to inflate the soft ducting and with that to achieve a steady cross section along the entire length.

3.3.1 The location and layout of the experiment

The selection of location of the experiment's site was based on airway length which could provide long enough traveling time and that its remote location would not interfere with the production. The previous location was in a return airway of longwall panel CD3/G in preparation. At the beginning of 2018, it turned out that there was not enough time between the completion of the return airway and the start of the longwall face to reconcile the ambiguities and carry out the experiment.

Based on experiences gained from previous experiments, for the new location of the experiment, I was looking for a long enough airway, which is as far away as possible from the coal production processes and in which I can install ventilation ducting just for the experiment. One of

the two main returns of the Škale pit was selected in the northeast part of Coal Mine Velenje, which is ventilated through the Pesje ventilation station (Figure 3.4).

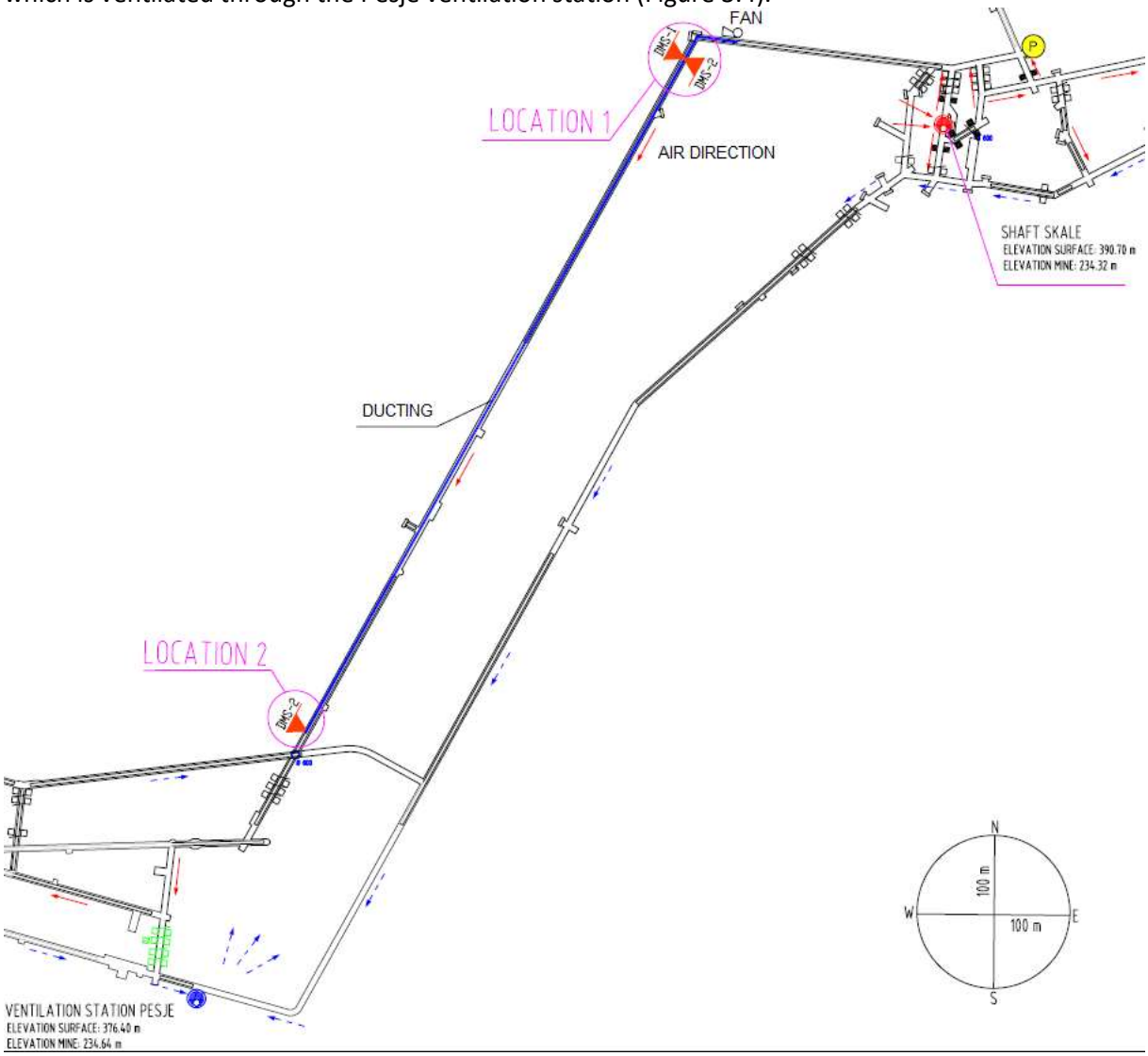

Figure 3.4: Locations of the test site in the mine with locations of DMS sensors and the ducting with auxiliary fan.

For the experiment the force auxiliary ventilation layout is selected. The main reason is that at the force auxiliary ventilation overpressure is created and gas mixture with DMS would leak out of ducting. At exhaust auxiliary ventilation the leakage would be in the opposite direction. The airflow of the gateroad would leak into ducting and the gas mixture in ducting cannot be constant.

The experiment's layout presented in Figure 3.5 consisted of an approx. 550 m long ducting and pneumatic fan. Distance between Location 1 and Location 2 is 500 m. Location 1 and Location 2 are monitoring locations of the experiment. On the monitoring locations we mounted continuous monitors for DMS concentration sensors (Figure 3.12), "IMG-PAN" anemometers (Figure 3.11, left) and "Almemo" sensors for air pressure, dry temperature, relative humidity, and an anemometer connected to a data logger Almemo 2690-8 (Figure 3.11, right). The DMS sensors are connected to a "Safety and Technology Information System" of CMV, which can, among other things, monitor and save data of approx. 5000 real-time parameters. The data logging device is a part of "IMG-PAN" anemometer.

During the experiment, barometric pressure on the surface was also measured. For the detection of pressure change it is measured every 5 minutes.

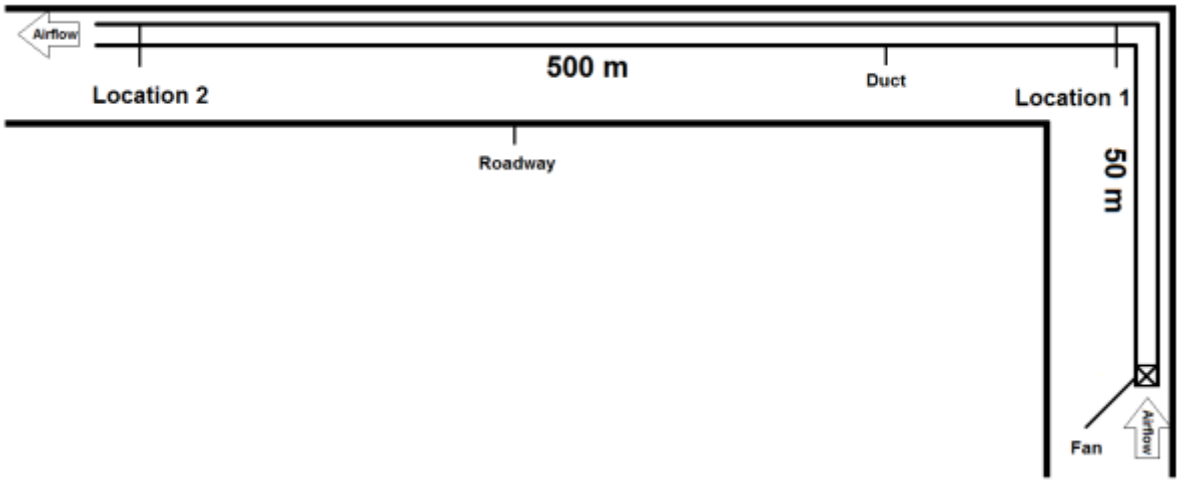

Figure 3.5: Layout of fan and ducting in the airway with monitoring locations.

The airflow in the duct is enabled by a pneumatic fan (Figure 3.6). Pneumatic fan enables the setup of airflow rate with the ball valve (Figure 3.7).

To achieve a traveling time of DMS of at least 12.5 minutes in the 500 m long duct, the average airflow velocity must be less than 0.67 m/s.

The preparation and setup of the actual experiment's layout in the mine is shown in Figure 3.6 to Figure 3.10.

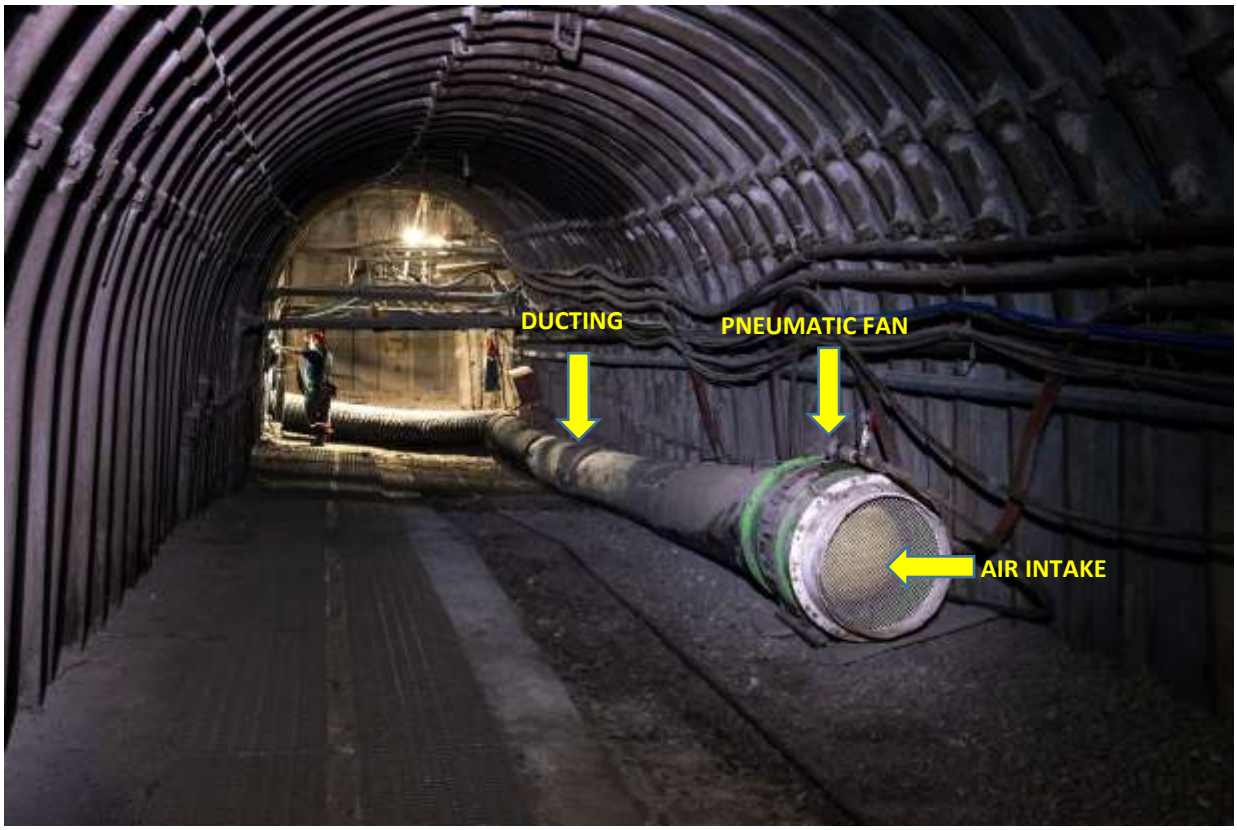

Figure 3.6: View of the beginning of the ducting layout in the airway with pneumatic fan and air intake.

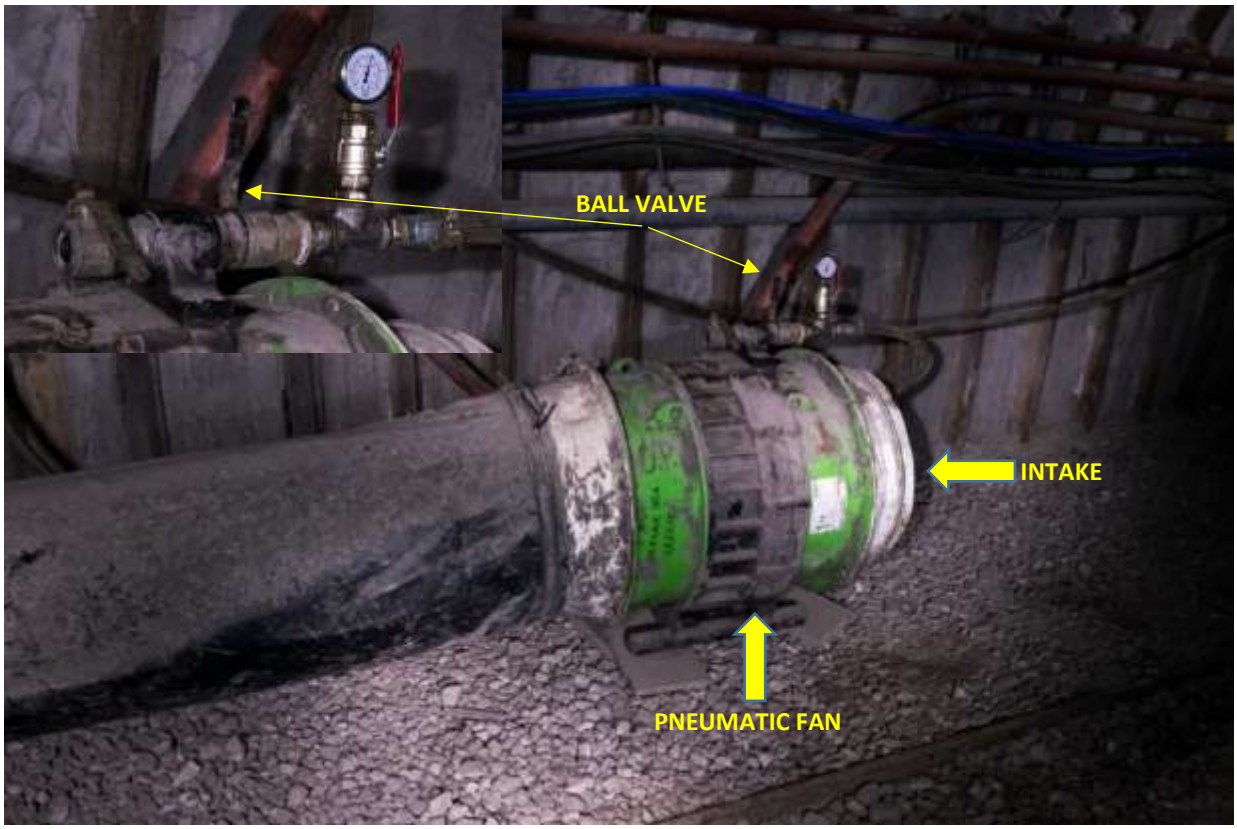

Figure 3.7: Pneumatic fan connected to the duct and ball valve for the regulation of fan power (drive with compressed air) and air flow.

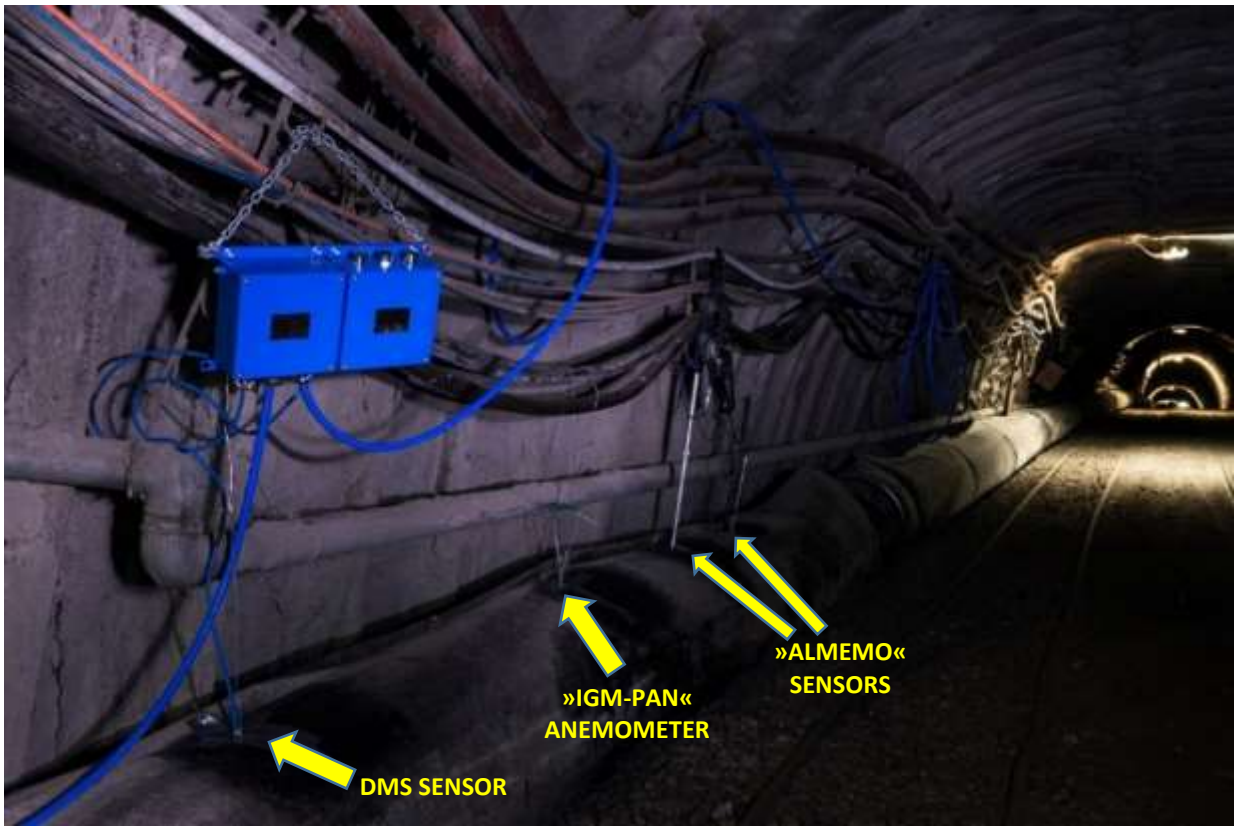

Figure 3.8: Sensors layout of monitoring location 1.

Figure 3.9: View of the ducting layout in the airway. Left figure: view of the ducting layout from monitoring location 1 in the direction of the end. Right figure: view of the ducting layout from the middle towards the end.

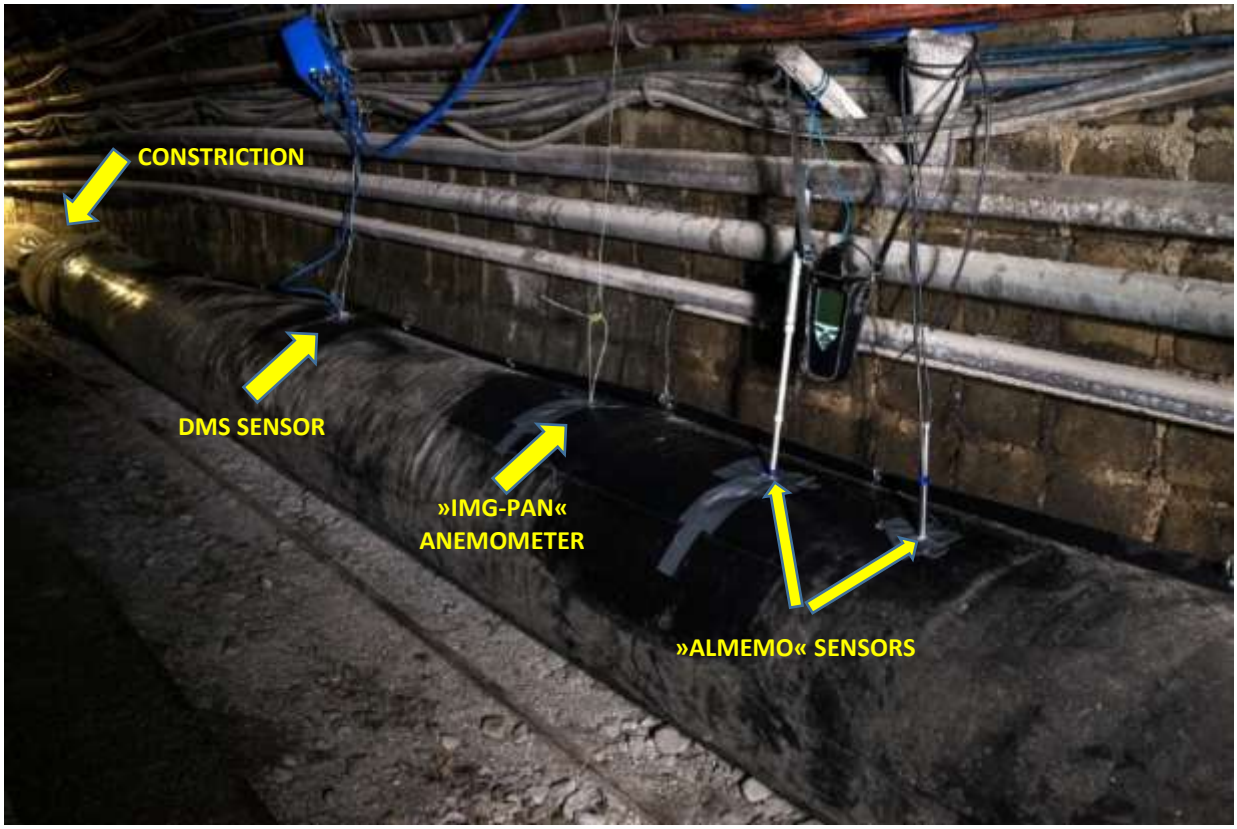

Figure 3.10: Sensors layout of monitoring location 2.

The “IGM- PAN” anemometers were developed and kindly lent to me for the experiment by IMG-PAN (Strata Mechanic Research Institute, Polish Academy of Science). They are also able to monitor methane concentrations.

Figure 3.11: Left: anemometer. Right: Almemo 2690-8 data logger for airflow velocity, temperature, pressure, and humidity sensors.

DMS sensor (Figure 3.12) Type MONIMENT GMM 05.05 was developed on request from CMV for the mine conditions with methane presence (category I M1 Ex ia I Ma), due to the frequent occurrence of DMS in CMV. It continuously measures and monitors dimethyl sulphide – DMS concentrations in mine air. The measurement range lies between 0 to 100 ppm V/V DMS in air. Its temperature and pressure compensated sensor works according to the electrochemical principle.

Figure 3.12: DMS sensor Type MONIMENT GMM 05.05

Figure 3.13 shows Final inspection and setup of ducting and sensors before the start of the experiment with a dosage of DMS into the ducting.

Figure 3.13: Final inspection and setup of ducting and sensors.

3.3.2 Constrictions of ducting

Constriction – reduction of ducting's cross section – is necessary according to simulation and previous tests at the end of the ducting (Figure 3.14). With such an increase of ducting's shock losses the inflation of soft ducting is achieved.

Figure 3.14: View of the end of the ducting layout with part of the layout of monitoring location 2 in the airway with the cross-section reduction or constriction, respectively.

According to https://www.princeton.edu/~asmits/Bicycle_web/transition.html, the air motion is invariably turbulent and if an airway measures 3 m in diameter, then the airflow velocity must be less than 6.6 mm/s (0.015 mph) for it to be laminar. Despite that, the gases concentration readings from continuous monitoring at the beginning and at the end of a return gateroad from longwall face k.-130/B show that some layering of methane and carbon dioxide can appear (see Table 4.4 in Chapter 3.2).

To prevent any layering of gases and to provide a steady gas mixture the constrictions are also placed just before the DMS sensors on monitoring location 1 and 2. Figure 3.14 shows the constriction before monitoring location 2 and just before the end of ducting.

Because the ducting has a leakage of airflow at joints, it is also necessary to provide a steady gas mixture when passing the joints and losing mass flow. For better mixing of airflow smaller constrictions were placed just before joints as shown in Figure 3.15.

Figure 3.15: Constrictions before each joint of ducting between ducts.

3.3.3 Artificial source of DMS

After the ducting and sensors setup, the preparation of cylinder with DMS and nitrogen mixture followed. Then was mounted the reduction valve and the rubber tube with 7.5 mm in diameter (Figure 3.16) was connected with cylinder and inserted in the ducting before the constriction and monitoring location 1.

Before the dosing of DMS in the ducting the actual setup of DMS dosage needs to be done. The targeted dosage in the ducting was between 7 and 10 ppm of DMS. The actual flow velocity of DMS and nitrogen was set up with measurement of flow velocity at the end of the tube connected to the cylinder with Pitot tube (Figure 3.17). Such a procedure was chosen because there are no such reducing valves on the market to regulate such low flow rates.

Figure 3.16: Preparation of a cylinder with DMS and a pressure reducing valve for flow regulation.

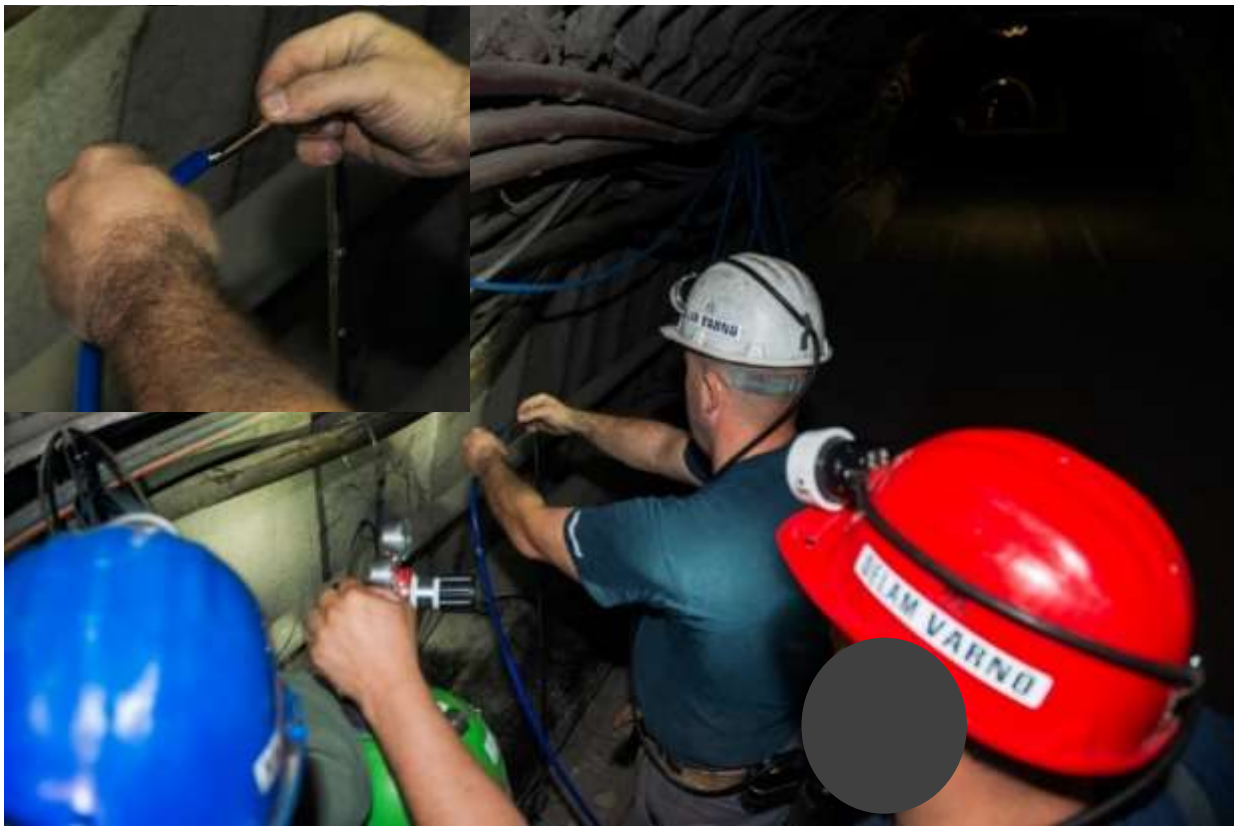

Figure 3.17: Adjusting the flow from the cylinder by carefully opening the pressure reducing valve with simultaneous measurements of flow velocity at the outlet by means of Pitot tube.

Figure 3.18: Inserting the tube connected to the DMS cylinder into the duct approx. 10 m before the DMS sensor on location 1 with respect to the flow direction.

3.3.4 Theory for calculations

The calculations in MS Excel are based on equations for saturation vapour pressure, relative humidity, air densities (actual and apparent) [115]:

For saturation vapour pressure e_{sd} equation at specific air (dry bulb) temperature t in °C, which is for usual mining range of 10 to 40°C, the curve fitting procedure gives

$$e_{sd}=610.162\times\exp\left[\frac{17.291\times t}{237.481+t}\right]\ [\text{Pa}] \tag{3.5}$$

an excellent accuracy of within 0.01 percent for that range. Which gives better accuracy (0.06 percent) than the widely used equation for range 0 to 60°C. Then the curve fitting procedure from standard tables of Goff and Gratch produced in 1945 gives

$$e_{sd}=610.6\times\exp\left[\frac{17.27\times t}{237.3+t}\right]\ [\text{Pa}] \tag{3.6}$$

Relative humidity rh in percent expresses the degree of saturation of space. It is defined as

$$rh=\frac{e}{e_{sd}}\times 100\ [\%] \tag{3.7}$$

e being vapour pressure in Pa.

The actual specific volume of moist air, V_m is

$$V_m=287.04\frac{T}{(P-0.378\times e)}\ [\text{m}^3/\text{kg of moist air}] \tag{3.8}$$

and specific volume of dry air (apparent), $V_{m\,(apparent)}$ is

$$V_{m\ (apparent)}=287.04\frac{T}{(P\text{-}e)}\ [m^3/\text{kg of dry air}] \tag{3.9}$$

In these equations, temperature T is in degrees Kelvin and barometric pressure P in Pascals. The relationship between density and volume is reciprocal. That gives us actual density ρ_m of the moist air

$$\rho_m=\frac{(P\text{-}0.378\times e)}{287.04\times T}\ [\text{kg of moist air}/m^3] \tag{3.10}$$

and apparent density of dry air $\rho_{m\ (apparent)}$

$$\rho_{m\ (apparent)}=\frac{(P\text{-}e)}{287.04\times T}\ [\text{kg of dry air}/m^3] \tag{3.11}$$

Most measurements of airflow in ventilation systems are based on the volume of air (m^3) that passes through a given cross section of a duct or airway in unit time (1 second). The units of volume flow, Q, are, therefore, m^3/s. However, for accurate analyses when density variations are to be considered, it is preferable to work in terms of mass flow – that is, the mass of air (kg) passing through the cross section in 1 second. The units of mass flow, M, are then kg/s.

The relationship between volume flow and mass flow follows directly from the definition of density, ρ,

$$\rho=\frac{mass}{volume}\left[\frac{kg}{m^3}\right] \tag{3.12}$$

and

$$\rho=\frac{\text{mass flow}}{\text{volume flow}}=\frac{M}{Q}\left[\frac{\text{kg s}}{\text{s m}^3}\right] \tag{3.13}$$

giving

$$M=Q\times\rho\ [\text{kg}/\text{s}] \tag{3.14}$$

In any continuous duct or airway, the mass flows passing through all cross sections along its length are equal, provided that the system is at steady state and there are no inflows or outflows of air or other gases between the two ends.

3.4 Ventilation/Odour Model of Coal Mine Velenje

The text related to Section 3.4 is based on our published article [1].

The purpose of odour modelling in the mine was to simulate dispersion of odorous gas emissions from its potential sources and to the surface under variable mine ventilation conditions and the characteristic concentrations of odour compounds.

The DMS concentration and odour concentration modelling in the mine is based on mine ventilation model of CMV designed in the Ventsim Visual™ software (Ventsim). The software allows 3D graphical representation of modelling and simulation results for underground ventilation networks with simulated paths and concentrations of smoke, dust, diesel particles, gases, and other contaminants. It is also a powerful tool for planning and analysing emergency situations (such as mine fires), short and long-term planning of ventilation, and the simulation of gas and aerosol concentrations [121].

Since the odour units (OU/m^3) are the number of dilutions of an odorous air to the odour threshold in case of olfactory measurements of odour sources and in case of only single odorant (measured concentration of odorant and ODT), the software can also be adopted for odour dispersion simulations.

The software treats every component in the mine air in the same manner. The concentrations of gaseous compounds are diluted according to the dilution ratios of the return airways and their dilution at airway junctions. For each studied component, a decay mechanism can also be modelled.

The calculation of airflows in a model is based on the Hardy Cross iterative method. The method that is most widely used in computer programmes for ventilation network analysis was originally devised for water distribution systems by Professor Hardy Cross at the University of Illinois in 1936. This was modified and further developed for mine ventilation systems by D.R. Scott and F.B. Hinsley at the University of Nottingham in 1951. However, it was not until digital computers became more widely available for engineering work in the 1960's those numerical methods became truly practicable [115]. The Hardy Cross iterative method is commonly applied to the analysis of the kind of large complex mine networks present within the mining industry in modern times. The method is based upon some underlying principles, which are listed below [113]:

- *For any given arrangement of mine network components (resistances/fans etc.) there is one possible air mass flow distribution throughout that network.*
- *Regardless of the complexity, the network can be broken down into a series of 'nodes', these nodes are connected via gateroads or 'paths' and can have any number of connections.*
- *The method is iterative and therefore the solution is dependent upon the accuracy of the required initial estimate of the variables at each of the nodes and the overall complexity of the network.*

At each of the nodes, the estimated pressure (P) is applied. The unknown flow (Q) through each node is given an error, the addition of which to the assumed value of Q gives the correct value. The error of Q at each node is then successively reduced through the iterative procedure until the entire network balances according to Kirchhoff's laws.

The airflow rate regulator of a specific airway in a ventilation network is determined with shock loss (representing regulators such as ventilation doors) and Atkinson's resistance (R) representing the resistance of an airway. In case when measurements of a regulator's performance are reported as resistances, the Atkinson's resistance can represent also shock losses. Considering the Atkinson's Equation

$$p=RQ^2 \tag{3.15}$$

the parameter R of the airway is the factor that governs the amount of airflow, Q, which will pass when a given pressure differential, p, is applied across the ends of an airway. Atkinson's equation is analogous to Ohm's law regarding the flow of electrical current through circuits. Potential difference (V) is replaced by barometric pressure (P). In the same way that electrical current (I) flows through a circuit as airflows through the mine airways network (Q). Finally, resistance (R) impedes flow in the same manner. Atkinson's expression uses the square of flow

(Q) since the cross-section area is considered, this is irrelevant in terms of electrical circuitry [113]. This simple equation is known as the Square Law of mine ventilation and is probably the single most widely used relationship in subsurface ventilation engineering [115].

The simplicity of the Square Law has been achieved at the expense of precision and clarity. The resistance of an airway, ideally, varies only with the geometry and roughness of that airway. However, the simplest equation of square law [115] hides that R depends also upon the density of the air. Hence, any variations in the temperature and/or pressure of the air in an airway will produce a change in the Atkinson resistance of that airway (the density term is hidden within the definition of Atkinson resistance).

The designed ventilation/odour model of CMV is based on ventilation and mine data from October 2012 using monthly ventilation parameters for the determination of airflow rate airways and represents the situation of mine ventilation in 57.85 km of underground facilities. Ventilation parameters are used each month to create a ventilation map of the CMV, which is a visual representation of the situation in the underground gateroads (airways) and facilities with respect to adjusted airflows, direction of airflow and locations of ventilation regulators: doors, barriers, boreholes, and shafts, auxiliary ventilators, and locations of gas sensors. The adjusted airflow rate of each airway was then determined by considering Kirchoff's first and second law theorems [115].

Gustav R. Kirchhoff was a German physicist who first recognized the fundamental relationships that govern the behaviour of electrical current in a network of conductors. The same basic relationships, now known as Kirchhoff's Laws, are also applicable to fluid networks including closed ventilation systems at steady state [115].

Kirchhoff's first law states that the mass flow (M) entering a junction equals the mass flow leaving that junction [115]:

$$\sum_{j} M=0 \tag{3.16}$$

Where M are mass flows, positive and negative, entering junction j. Assuming uniform density of air at all mass flows that enter or leave the junction, then mass flow [kg/s] can be replaced with airflow quantity (Q) [m^3/s] in the above equation.

The simplest statement of Kirchhoff's second law applied to ventilation networks is that the algebraic sum of all pressure drops around a closed path, or mesh, in the network must be zero, having considered the effects of fans and ventilating pressures [115]:

$$\sum_{j} (p-p_f) - NVP=0 \tag{3.17}$$

Where p is frictional pressure drop [Pa], P_f is rise in total pressure across fan [Pa] and NVP is natural ventilating pressure [Pa].

Kirchhoff's laws can be applied to fluid networks that conduct either compressible or incompressible fluids [115].

The total resistances of the airways in the model are summarized from the "Zračenje" software developed in-house [122].

Figure 3.19, besides the mine gateway system, shows the locations of the main air intakes (service shaft NOP, ventilation shaft Šoštanj II, service shaft Škale, the main coal transport drift and Hrastovec drift), the main air exits – returns (ventilation stations Šoštanj and Pesje), the longwall faces (K-130/B and K-65/A) and the development headings: 4, 6, 7, 8, 11 and 13. The deepest part of the mine is approximately 500 m deep. First, the whole data set was used to create a 3D model that defined every airway according to length, profile (round profiles were used for shafts, boreholes, ducts, and modified profiles for specific types of gateways used in CMV), cross-section, airway type, and total resistance. Other data included the average surface temperatures, both dry (10°C) and wet (7°C), together with temperature and atmospheric pressure (985 mBar). The network air density was calculated from the average monthly temperatures and pressures (1.20 kg/m^3). In the model fixed air flows were used for the upcast ventilation shafts (ventilation station stations), in the airways of the auxiliary ventilators and in the ventilation boreholes (altogether 24 fixed flows). The model does not consider natural ventilation and compressible flows, which only have a significant effect when simulating mines deeper than 500m [121]. All the other software settings were left as default.

In the second step, the airflow rate and directions of airways were modelled, iteratively adjusted for their total resistances and different ventilation regulation measures. To control the

adjusted total resistances, pressure drops on the main fans were considered, which were 3460 Pa at the Šoštanj and 2040 Pa at the Pesje ventilation stations. The exhaust main ventilation at the CMV is provided by two main fans, and a series of smaller auxiliary fans for ventilation of development sections or dead-end headings. The main fans are located at the Pesje and Šoštanj ventilation stations (Figure 3.19). Each fan draws air up from the mine from five surface air intakes (situation as of 2012, Figure 3.19). The main fan located at the Šoštanj station is a Turmag GVhv 31-1800 with nominal power 1800kW (auxiliary fan: the same type), while at the Pesje station a TLT-GAF 34-31 is installed with nominal power 800kW (auxiliary fan: Turmag GLH-28-660 with nominal power 600 kW) [123]. The Šoštanj station provides approximately two-thirds of the required airflow rate, with the Pesje station providing the remaining one-third.

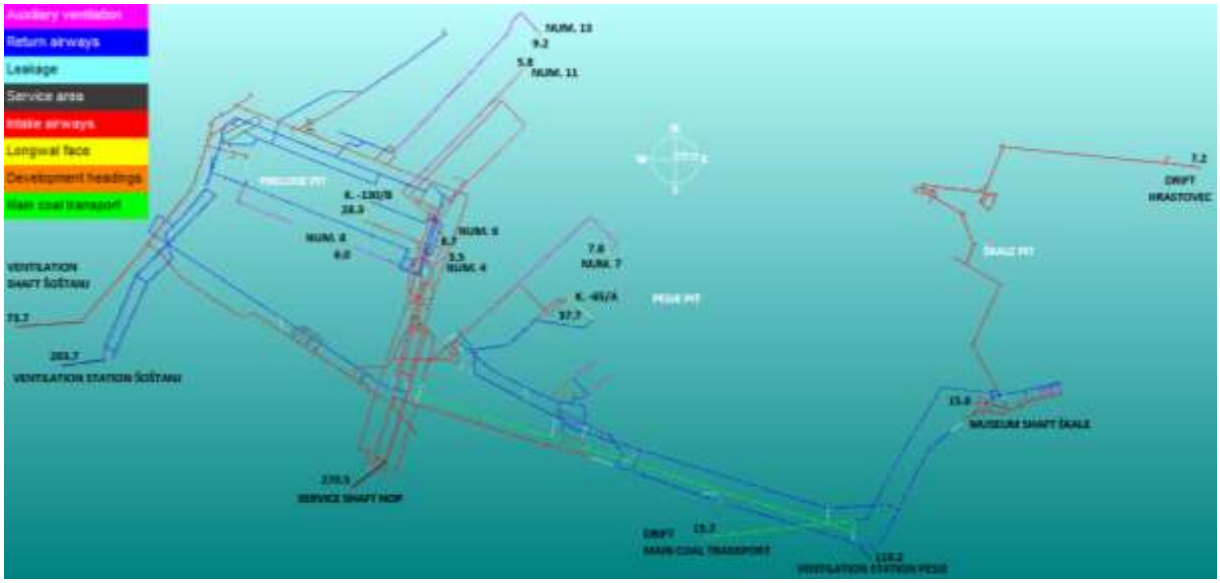

Figure 3.19: CMV plan modelled in VentsimTM as of October 2012 with adjusted airflows (m^3/s). The lines represent the actual gateways in the mine and the colours of the gateways (legend in upper-left corner) show the different types of odour sources and the purpose of gateways regarding the mine ventilation.

The general regulation of mine ventilation is possible by positioning the angles of the main fans blades setup at each ventilation station. The airflow regulation potential with main fans of ventilation stations has a direct effect on dilution potential of every gas or contaminant source in the mine. Main fan at Šoštanj has adjustable blades between angles -10° and +10°, while at Pesje, the main fan has blades that can be adjusted between 20° and +2°. The characteristic curves of fans are presented in Figure 3.20 and Figure 3.21. The main fans characteristic curves [124] are customized in the Ventsim^{TM} for the airflow rate simulation at: Šoštanj (Figure 3.20): -10°, -8°, -6°, -4°, -2°, 0°, +2°, +4°, +6°, +8° and +10° and for Pesje (Figure 3.21): -20°, -18°, -16°, -14°, -12°, -10°, -8°, -6°, -4°, -2°, 0° and +2°. The setup of fan's blades in October 2012 was +1° (Šoštanj) and -11° (Pesje).

Verification of the model was based on the differences between the modelled and calculated airflow rate and between modelled and measured depressions of the main fans. The accuracy of the model, estimated on the basis of calculated and modelled airflows quantities in 226 airways, is ± 0.07 m3/s. The modelled values of the main fan depressions were 3459.7 Pa at Šoštanj and 2040.4 Pa at Pesje stations.

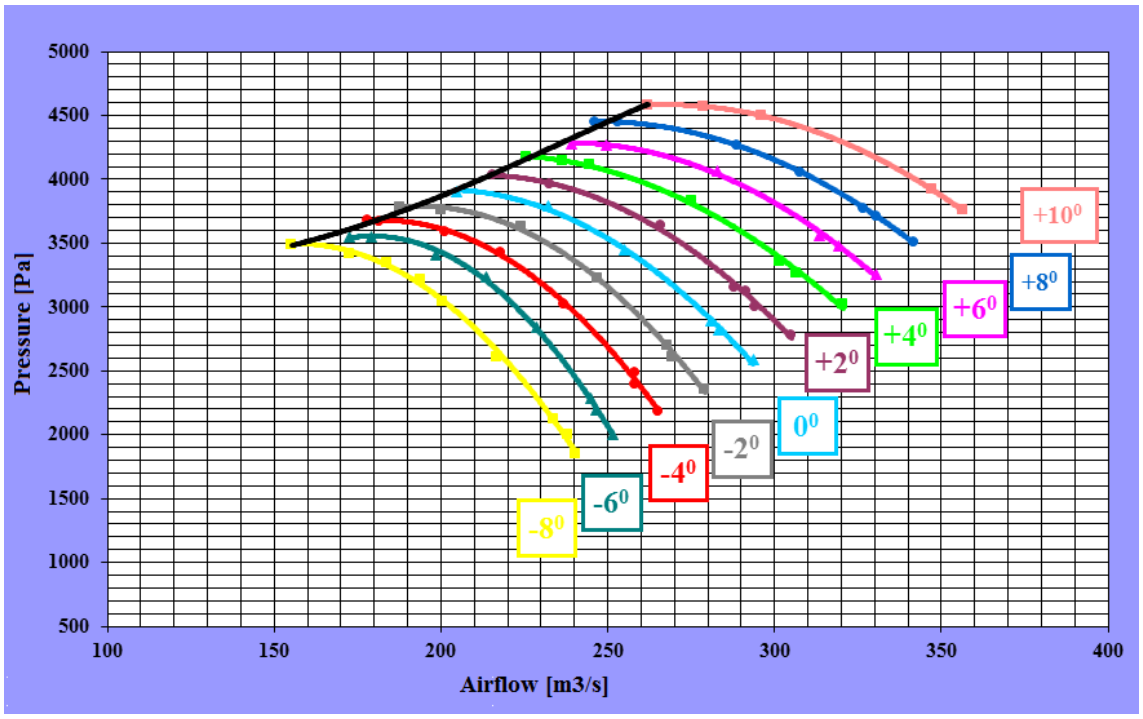

Figure 3.20: Fan characteristic curves at different angles of blades for main fan Turmag GVhv 34-1800 which is stationed in the Šoštanj ventilation station [124].

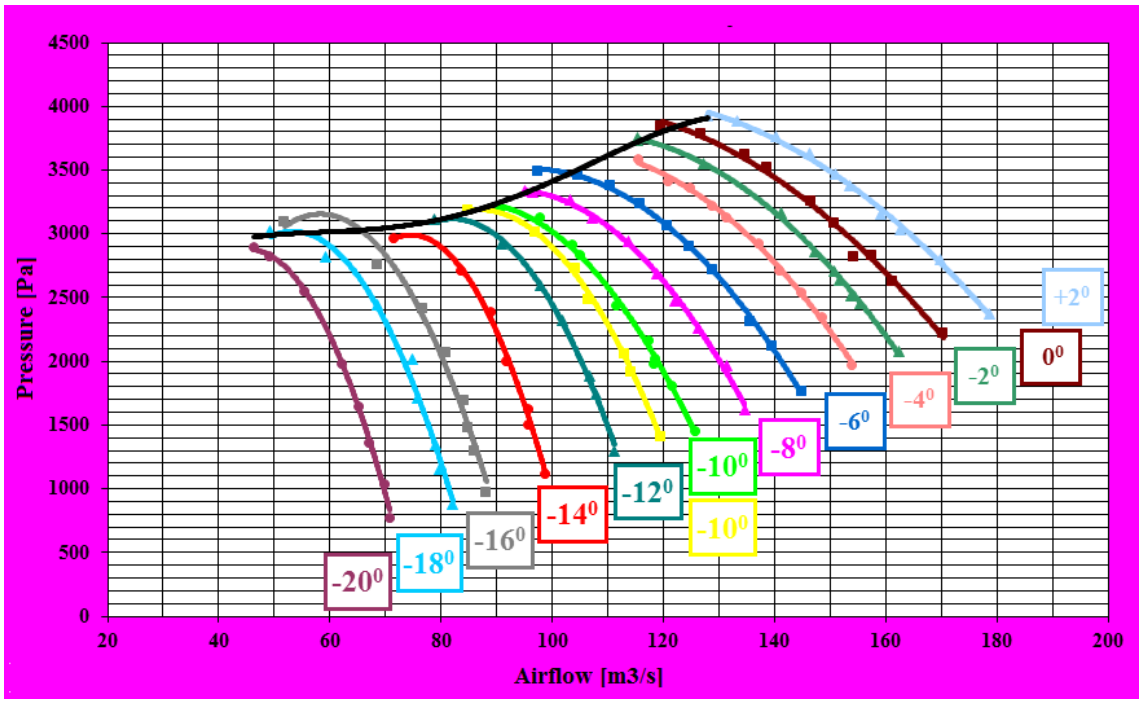

Figure 3.21: Fan characteristic curves at different angles of blades for main fan Turmag GAF 24/13, 3-1 which is stationed in the Pesje ventilation station [124].

The odour model is based on DMS emissions. Odour concentrations of mine odour sources for the model were calculated from characteristic DMS concentrations considering that 1 mg/m^3 = 129 OU/m^3 which is calculated from DMS ODT 0.003 ppm (Nagata, 2003) considering that 1 ppm = 2.583 mg/m^3. Odour emission rates (OU.m^3/s) from the ventilation stations were calculated by multiplying the modelled odour concentrations (OU/m^3) and airflow rate (m^3/s).

Chapter 4

Results and Discussion

4.1 Analysis of Odorous Gas Emissions and Estimation of Odorous Sources

The text related to Section 3.1 is based on our published article [1].

Over a six-year period (2008/1-2013/12), 1,028-point measurements were taken during mine operations. The monitoring sites were selected systematically so that the return airways of all production and development worksites and all main return airways were included. Under normal working conditions at the mine, H_2S (released at the locations where the water is present in the mine, e.g., mine pump stations and SO_2 (oxidation process in coal, e.g., mine fire) are rarely detected. Levels of SO_2 throughout the mine exceeded the limit of detection on only 26 occasions (24 x 2.67 mg/m^3, 1 x 5.34 mg/m^3 and 1 x 10.68 mg/m^3), while H_2S was only detected 5 times (2.41 – 13.63 mg/m^3).

The DMS were detected in 679 out of 1,028 samples in levels of DMS between 2.58 mg/m^3 and >129 mg/m^3 (levels above 129 mg/m^3 were recorded as > 129 mg/m^3). Out of all DMS detections, it was detected 116 times out of 163 measurements on longwall faces, 262 times out of 398 measurements on development headings and 30 times out of 72 measurements on main coal transport. The detection frequency shows that DMS is released during the coal extraction process (also gateways are mostly built in coal seam) and DMS detection at main coal transport shows that DMS is released by desorption processes as the coal is being transported from the mine, similar to desorption from the coal in the stockpiles [81], [83] and CMV coal samples from boreholes in the coal seam [84].

Previous researchers [82] already identified DMS as one of major VSCs in CMV. The analysis results confirmed DMS as one of major VSCs in the mine and the most abundant odorant considering the detection frequency and concentrations of VSCs and the releasing under normal working conditions. Considering the mine locations where the DMS were detected, the DMS mine sources were identified and considering the DMS concentrations values, the DMS mine sources were quantified. The identified main mine DMS sources are the longwall faces (coal extraction working sites), the main coal transport system (a system of rubber belt conveyors that is transporting coal directly to the surface), and the development headings (gateway building working sites). The analysis results of characteristic DMS concentrations and flowrates of DMS sources in return airways of main odour sources are presented in Table 4.1.

Table 4.1: Values of characteristic DMS concentrations with their OAV values and mass flows of DMS in the returns of mine odour sources.

Odour/DMS Source		Longwall face		Main coal transport		Development headings	
Number of samples		163		72		398	
DMS concentration [mg/m³]	OAV	[mg/m³]	OAV	[mg/m³]	OAV	[mg/m³]	OAV
MAX		129.0	16929	87.7	11512	129.0	16929
MEAN		52.7	6910	7.9	1034	23.5	3081
MIN		0.0	0	0.0	0	0.0	0
Std		55.1	7230	15.2	1990	34.5	4525
0.975		**129.0**	16929	**43.9**	5764	**129.0**	16929
0.75		129.0	16929	9.2	1210	30.3	3978
0.5		**31.0**	4063	**0.0**	0	**7.5**	982
0.25		0.0	0	0.0	0	0.0	0
0.025		0.0	0	0.0	0	0.0	0
Average airflow rate [m³/s]		**35.4**		**71.8**		**7.3**	
Median DMS source [mg/s]		**1097**		**0.0**		**55**	
Peak DMS source [mg/s]		**4569**		**3154**		**944**	

The results show great variations of DMS concentrations for each confirmed odour source and also that DMS was present at sources between 44 % and 71 % of the time. For the estimation of characteristic emissions of DMS sources median DMS concentrations at average airflow rates were taken into consideration and for the estimation of DMS sources peak emissions 97.5th percentile DMS concentrations at average airflow rates were taken into consideration. Additionally, for the characteristic DMS concentrations the OAVs were calculated, which shows dilution to threshold ratios. OAV values are very high (maximum OAV value was 16929) due to the very low DMS's ODT even while the DMS concentrations are at trace levels. While even lower ODT of H_2S and considering maximum measured concentration, results in OAV value of 23,500, but it was detected only in 0.5% measurements, while DMS was detected in 66%. The maximum OAV of SO_2 was 5 and was detected in 0.6% measurements.

Longwall faces and development headings as odour sources are regarding ventilation and dispersion relatively simple, not considering the variability of production intensity and the amount of DMS presence in the coal. While the main coal transport system with six successive conveyors of total length 2.6 km and six intakes of fresh air at junctions and connection to the surface (see Figure 1.15 in Chapter 1.4.5), and six leakage connections with main return airways is an odour source with very complex dispersion. All six leakages are dispersed to the Pesje ventilation station. Detected DMS in return airway of main coal transport in Preloge pit shows that it is being released during transport and that also all return airways – leakages in Pesje pit must be considered.

For the main coal transport source in the model it was considered that DMS is released at a constant release rate from the constant mass flow of coal through the whole length. The source in the model was divided into each individual part of main coal transport airways accordingly to their lengths. Each individual part is represented in the model as a partial source of DMS. The simulation results showed that 34.5 % of main coal transport source was dispersed to the Pesje ventilation station and 65.5 % was dispersed to the Šoštanj ventilation station which was detected with monthly measurements. Considering the whole main coal transport DMS emission rate at maximum concentration 87.7 mg/m³ and average airflow rate 71.8 m³/s, then is 6,297 mg/s and is potentially the biggest DMS source versus longwall faces (4569 mg/s) and development headings (944 mg/s). The division of the whole source in the model at leakages from L1 to L6 was 3.5 %, 1.8 %, 6.1 %, 6.7 %, 6.7 % and 9.7 %. Locations of leakages are marked in Figure 4.1 as a green circle.

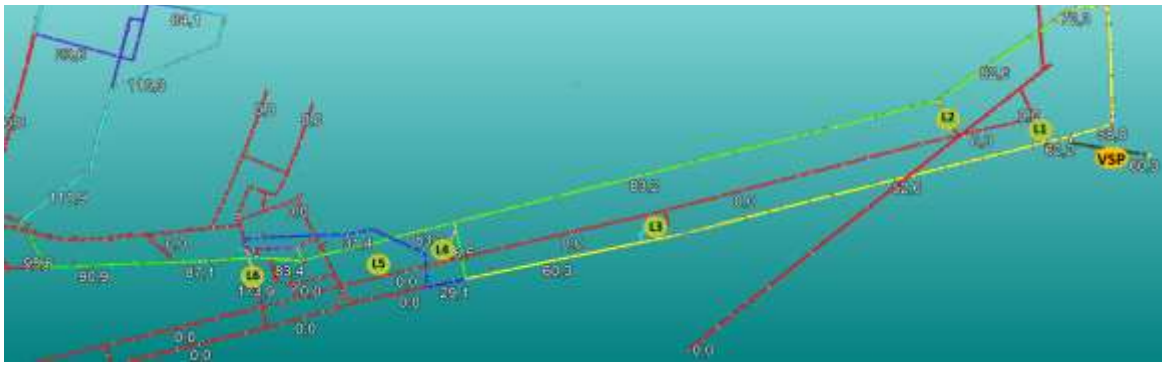

Figure 4.1: Six leakages connections (L1 – L6; marked in figure as green circles) of main coal transport with main return airways. All six leakages are dispersed to the Pesje ventilation station.

4.2 Analysis of the DMS Monitoring Campaign on Longwall Panel K. 130/B

During the three months monitoring period (4 October 2012–4 January 2013), including the no-production shifts and holidays, the average gas concentrations at longwall face K.-130/B were 14.5 mg/m^3 DMS, 3,536.3 mg/m^3 CH_4, and 19,039.2 mg/m^3 CO_2. The average airflow was 27.6 m^3/s and the daily average DMS emission was 33.6 kg/day. Figure 4.2 shows an overview of monitored data with a series of box-and-whisker plots of concentration, production intensity and airflow capacities.

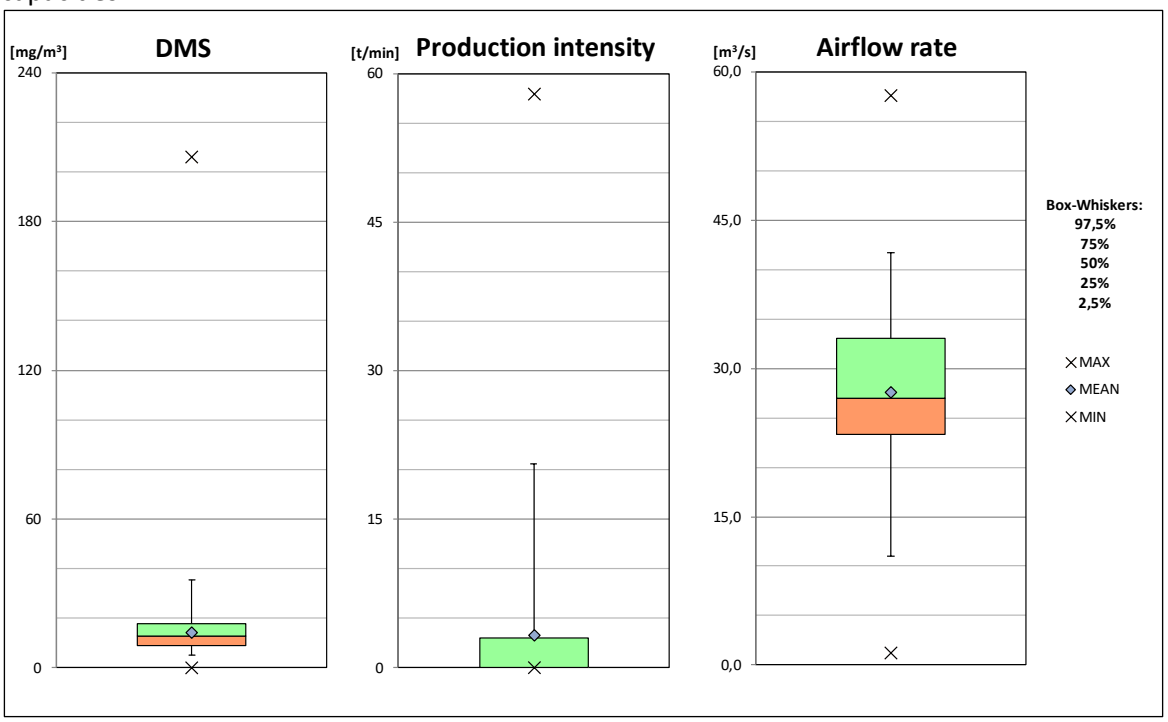

Figure 4.2: Characteristic values and distributions of DMS concentrations (left), production intensity (middle) and airflow capacities (right).

During the monitoring period, the production was limited to two 8-hour work shifts and there was no production as a result of work free days, time taken between work shifts and during support working phases. Overall, zero production accounted for approximately 2/3 of the monitoring period (87967 records out of 133801). The average production intensity was 3.2 t/min (active production (>= 1 t/min): 11.4 t/min) with a peak production intensity reaching above 30 t/min on eight occasions (max: 58 t/min).

The DMS concentration exceeded 50 mg/m^3 on 669 occasions (0.50 %), 100 mg/m^3 50 ppm on 43 occasions (0.03 %) and 150 mg/m^3 on 8 occasions (0.006 %), which accounts for approx. 3 months of the monitoring period. The box whisker plots and summary statistics (Figure 4.2 and Figure 4.3) indicate that high DMS concentrations are recorded only rarely. The lower extreme level (2.5 percentile) at 6.5 mg/m^3 in the return airway suggests the continuous presence of DMS in the return airway (Figure 4.2).

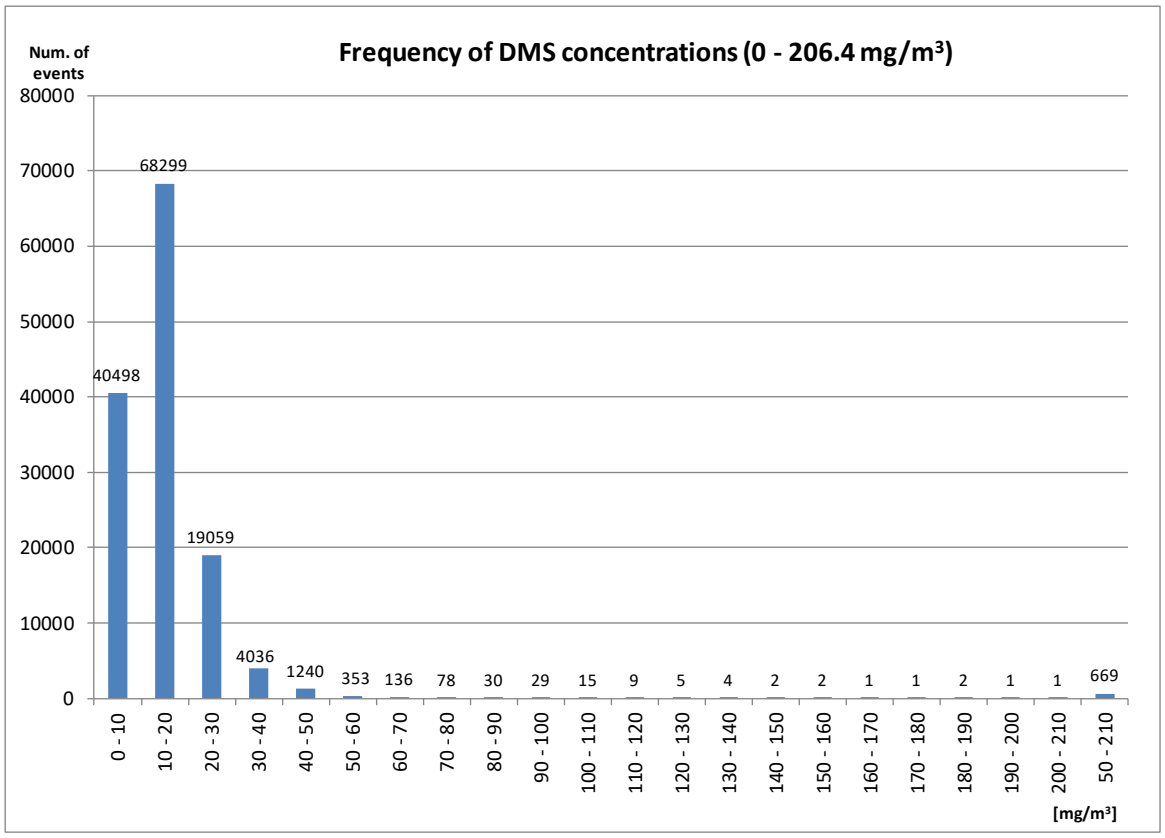

Figure 4.3: Frequency distribution of measured DMS concentrations.

Figure 4.4 shows the variability of daily emission rates of DMS, CO_2 and CH_4 against daily coal production and airflow rates throughout the whole monitoring period.

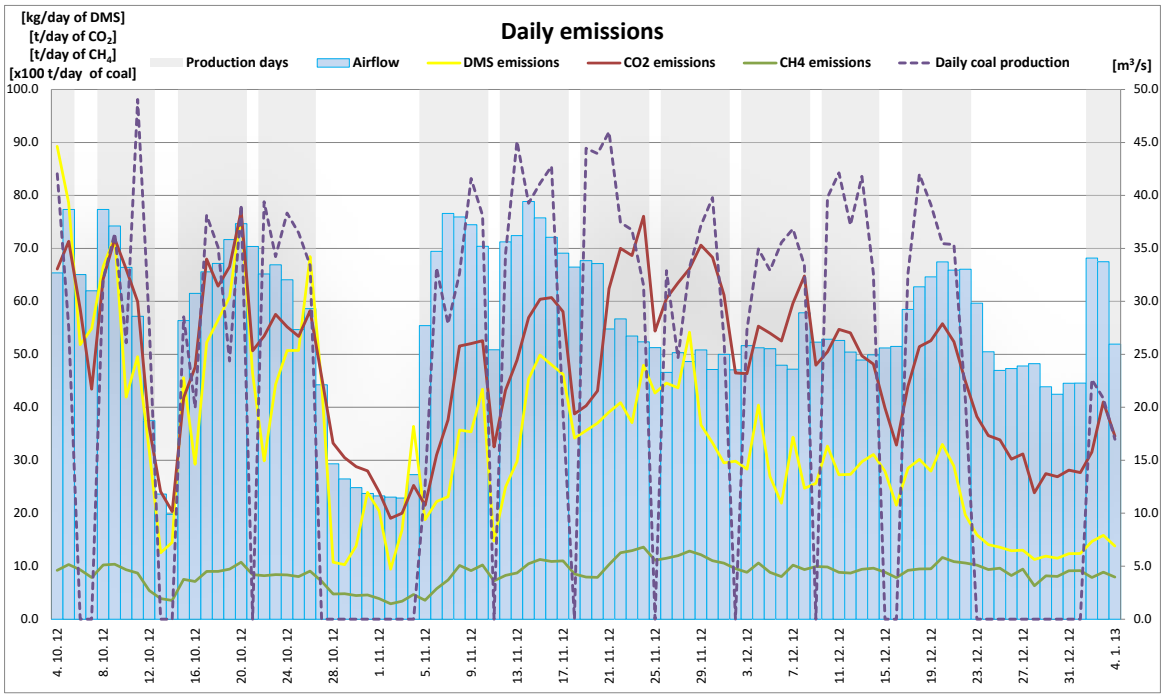

Figure 4.4: Daily DMS, CO_2 and CH_4 emissions against coal production rate at longwall K.-130/B with average daily airflows and production/non-production periods also shown.

At first glance, it is clear from Figure 4.4 that gas emission rate is dependent on coal production and, generally, peaks towards the end of production weeks. There may also be a correlation between DMS and CO_2 and CH_4 emissions. The figure also shows that, depending on the overall gas emission and dilution requirements, ventilation at longwall face K.-130/B was regulated to be relatively lower at some weekends and holiday periods when gas emission rates are low. The two one-week holiday periods with regulated but different ventilation air quantities during 27 October–4 November 2012 and 23 December–1 January 2013 suggest that DMS retention and release mechanism in Velenje lignite may be different than that for other gases and may also be controlled by coal lithology.

A more detailed plot of daily DMS concentration against daily coal production rates shown in Figure 4.5 reveals that a background level DMS concentration existed throughout the three months monitoring period. As shown in Figure 4.5, which presents the DMS concentrations plotted against coal produced every half hour during Monday 15th and Saturday 20th October 2012 respectively, this background level was also recorded during shift changes and non-production shifts each day. Both figures clearly show the correlation between coal production and DMS concentration in the ventilation air. On the other hand, it is noted that peak levels of DMS recorded during different production weeks (or at different positions along the longwall panel), for similar rates of daily coal production, are significantly different (Figure 4.6). This also suggests that changes in dominant lithological component in the Velenje lignite may be one of the controlling factors affecting DMS emission rates from coal (see Chapter 1.4.4).

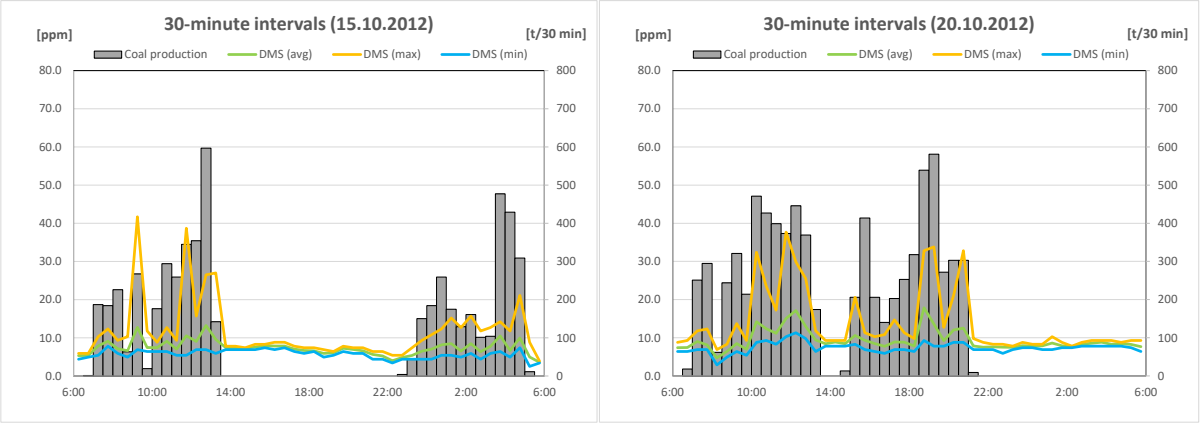

Figure 4.5: Day data K.-130/B of 30-minute intervals: DMS concentrations plotted against coal produced every half hour during Monday 15th and Saturday 20th October 2012, respectively.

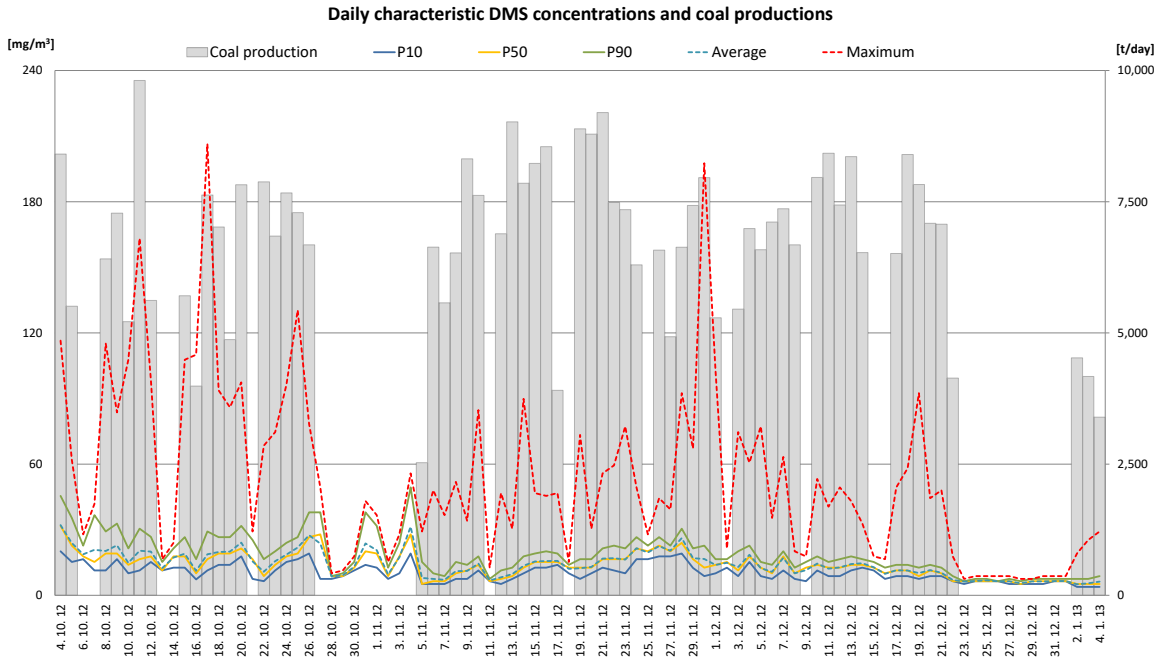

Figure 4.6: Daily DMS concentration data against daily coal production rate at longwall K.-130/B.

The DMS sensor data were analysed with respect to the position and coal production rate along the longwall panel K.-130/B during the monitoring period. As illustrated in Figure 4.7, data interpolated along the face length reveal the variability of emission rates in different parts along the longwall panel. Figure 4.7 (upper) suggests that, at average ventilation rates, the DMS concentration is much higher at certain regions of the panel, and Figure 4.7 (lower) confirms that the content of DMS varies within the coal seam. For example, there are at least three zones (460.5-472.5, 508.2-513.3, 527.8-531.7 m) and probably a thin strip of coal along 575 m with relatively higher in situ DMS content in the coal seam.

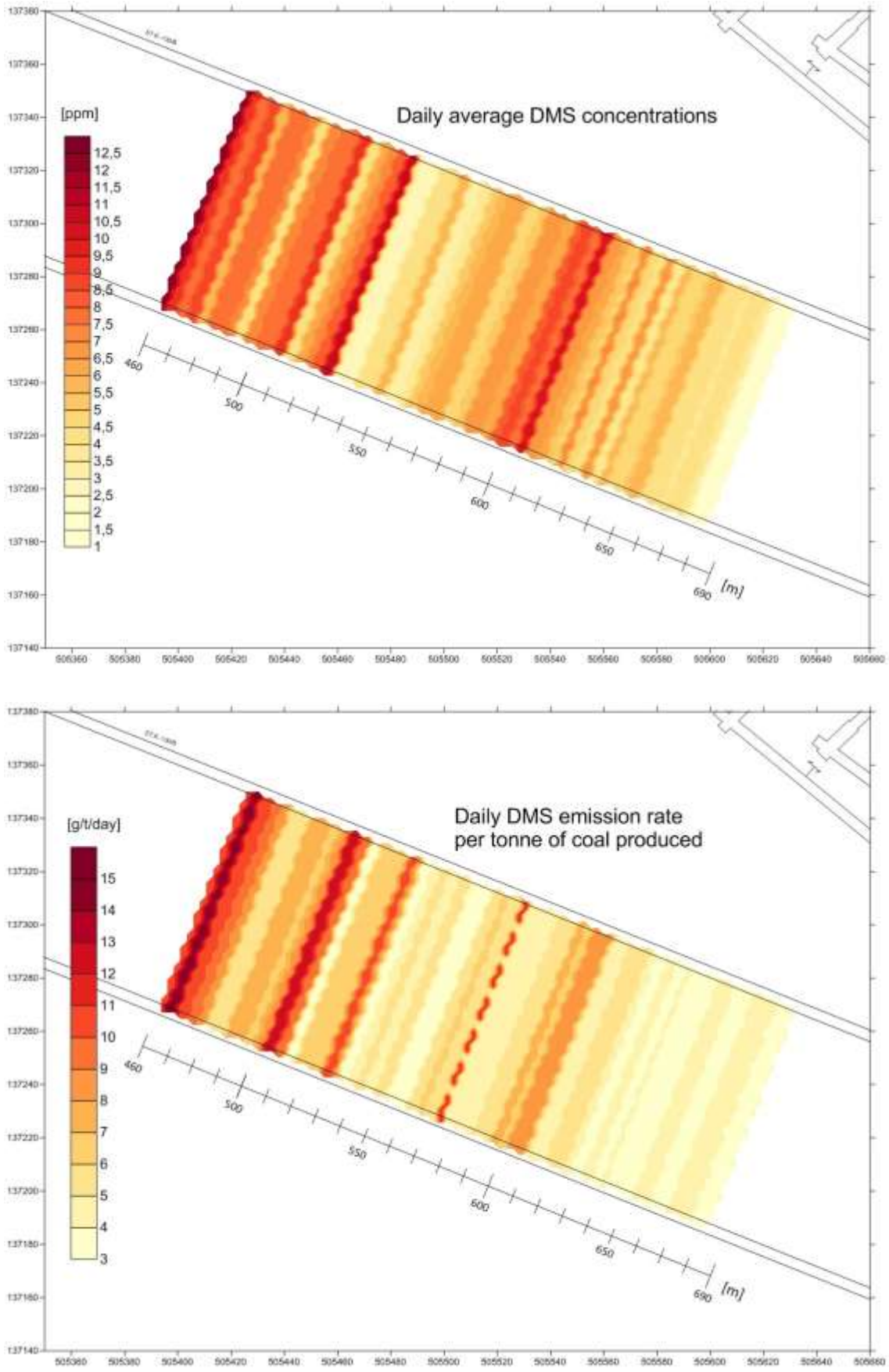

Figure 4.7: Analysis of daily average DMS data illustrating (upper) gas concentrations and (lower) emission rates per tonne of coal produced in longwall panel K.-130/B.

A more detailed analysis of 30-minute intervals for the whole monitoring period (4462 intervals) which were divided into half-hour segments from the start to the end of the monitoring campaign. The airflow rates and gases concentrations and emissions were classified regarding intervals of 30-minute production rates which enables assessment of dependence of background and production rate on gases emissions. The 30-minute intervals were grouped according to production intensity in non-production intervals and intervals with coal production of 1-100, 101-200, 201-300, 301-400, 401-500, 501-600 and 601-671 tons of coal per 30 minutes.

The summary statistics in Figure 4.8 show that there were more non-production intervals (2725) than the intervals with detected production (1737) and that the interval values are decreasing with increased production intensity.

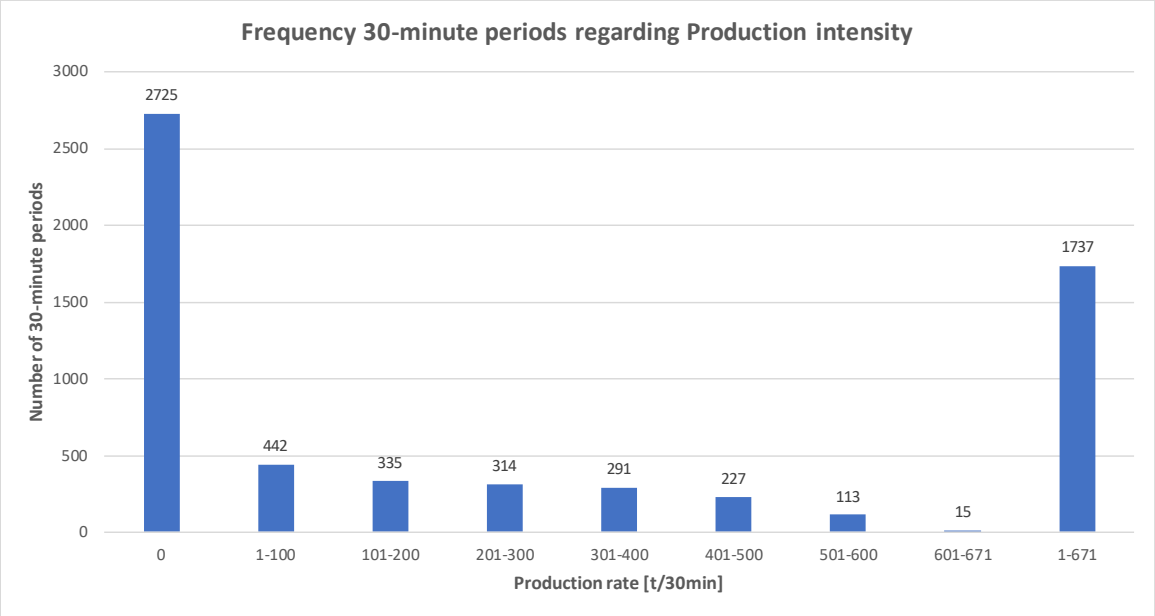

Figure 4.8: Frequency distribution of 30-minute periods grouped according to production intensity.

The detailed results of characteristic values of 30-minute intervals of airflow rates and gases concentrations and emissions grouped regarding production rates are presented in Appendix D: Results of 30-minute intervals and they further confirm that gaseous emissions are also significant when there is no production, and that they increase with increasing production intensity. Figures between Figure 4.9 and Figure 4.11 show the overview of quantification of gaseous emissions regarding production intensity. Figure 4.12 additionally shows average airflow rates regarding intervals of production rates, which reveals the impact on gases concentrations. Also, airflow values show the ventilation regulation impact at periods when longwall face is at standstill and at maximal production rates when additional airflow is necessary to keep the gaseous concentrations in the TLV limits (threshold limit value).

The results show that average DMS emission from longwall face at zero production is 328 mg/s and at maximal production interval it is 680 mg/s. The average CH_4 emission from longwall face at zero production is 94 g/s and at maximal production interval it is 123 g/s. The average CO_2 emission from longwall face at zero production is 477 g/s and at maximal production rate it is 809 g/s. The emissions rates between the production intervals of minimal and maximal production rates are 2.07 for DMS, 1.31 for CH_4 and 1.70 for CO_2. They show a significant release during production standstill and a significant increase of gases emission during coal production.

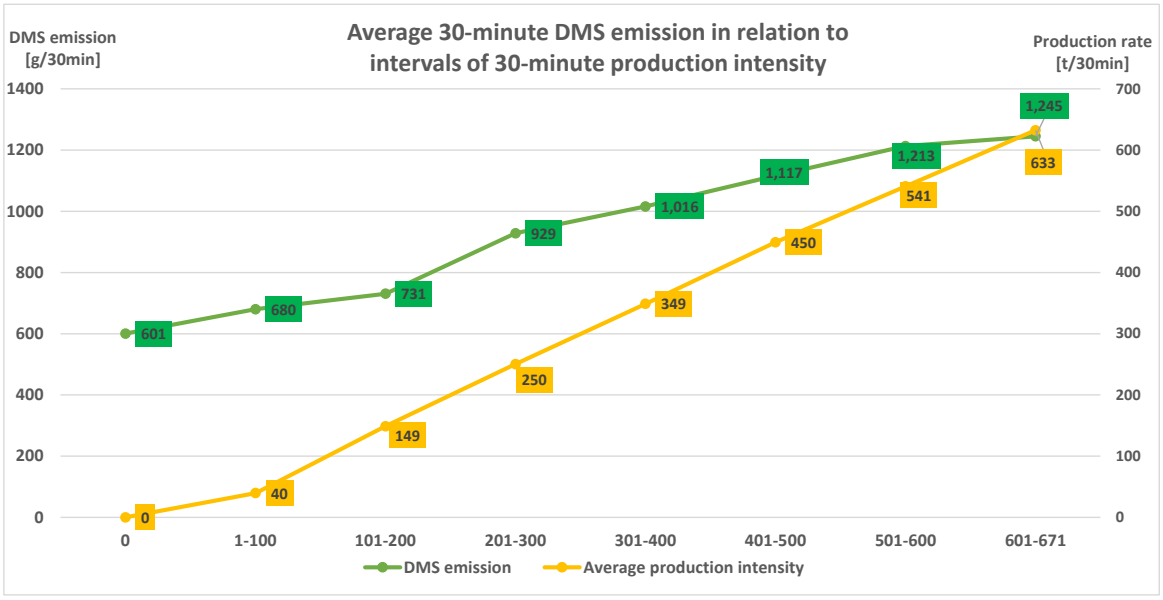

Figure 4.9: Average 30-minute DMS emission in relation to 30-minute production intensity.

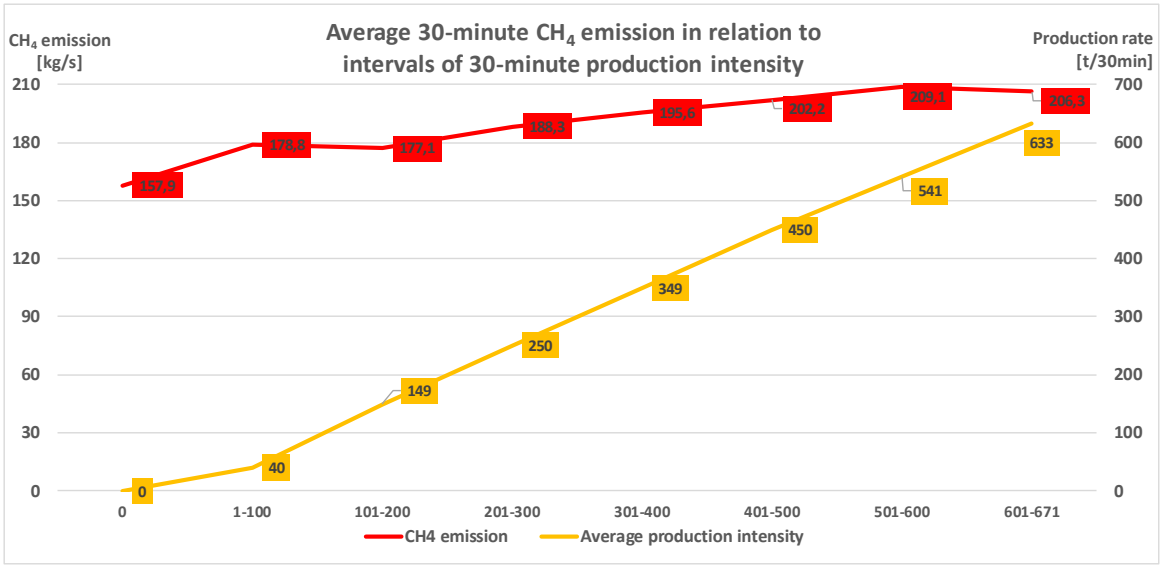

Figure 4.10: Average 30-minute CH_4 emission in relation to 30-minute production intensity.

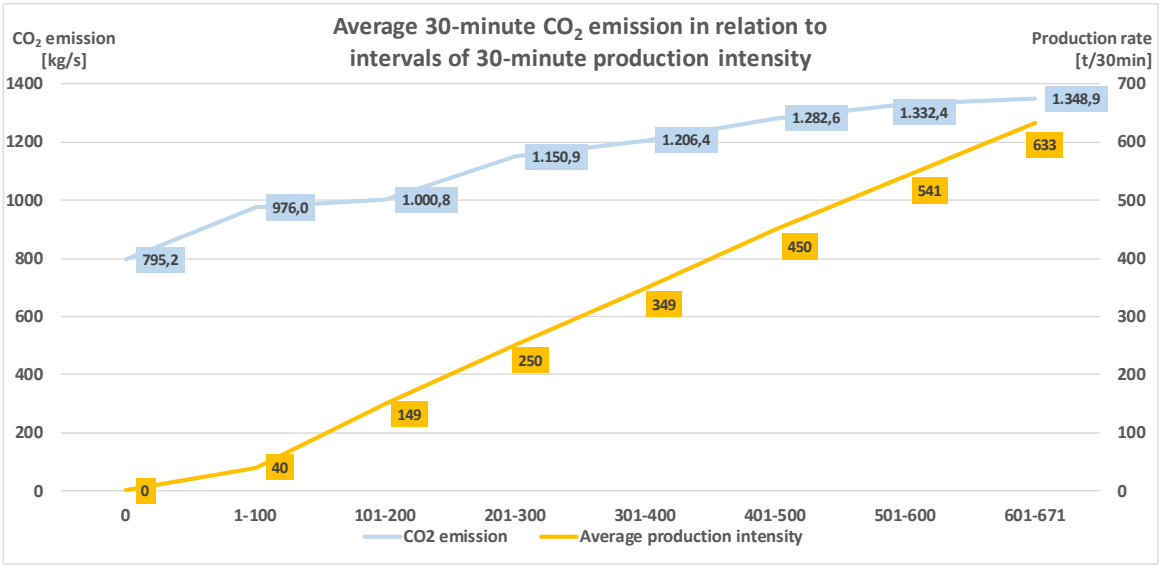

Figure 4.11: Average 30-minute CO_2 emission in relation to 30-minute production intensity.

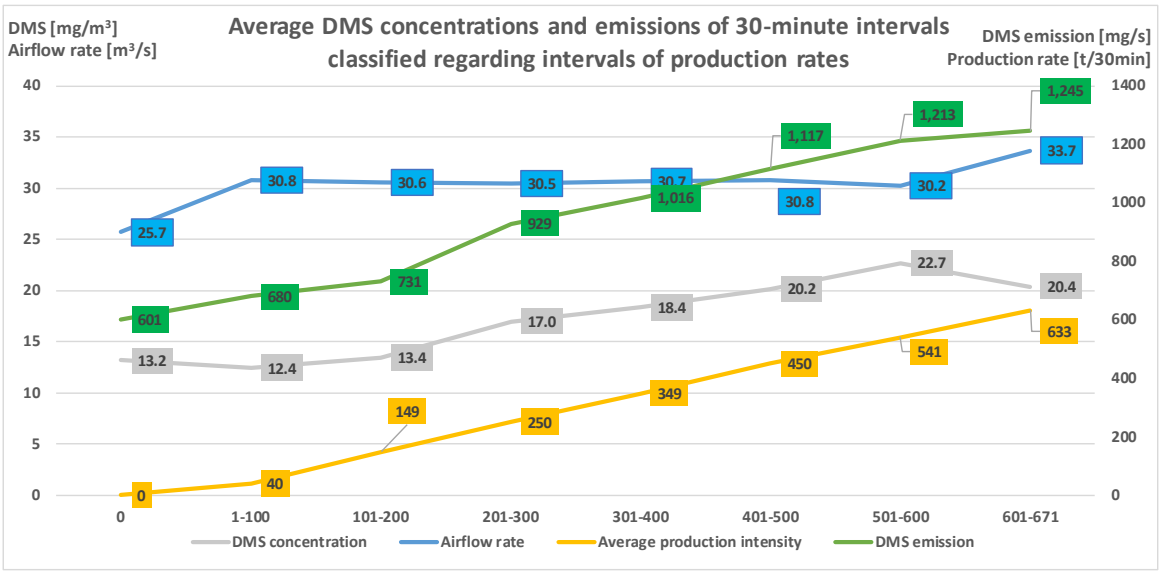

Figure 4.12: Average 30-minute DMS concentrations and emissions with airflow rates in relation to 30-minute production intensity.

The gases emissions ratios in Figure 4.13 show the trend in relation to production intensity. The CO_2:CH_4 emission ratios expected a trend according to recognized releasing characteristics [125] of both gases, that CO_2 stays trapped in coal and while coal is crushed, the ratio increases regarding productions intensity. Both, CO_2:DMS and CH_4:DMS emission ratios show that the releasing of DMS is more controlled with coal crushing by coal production than at the releasing of CH_4 and even of CO_2.

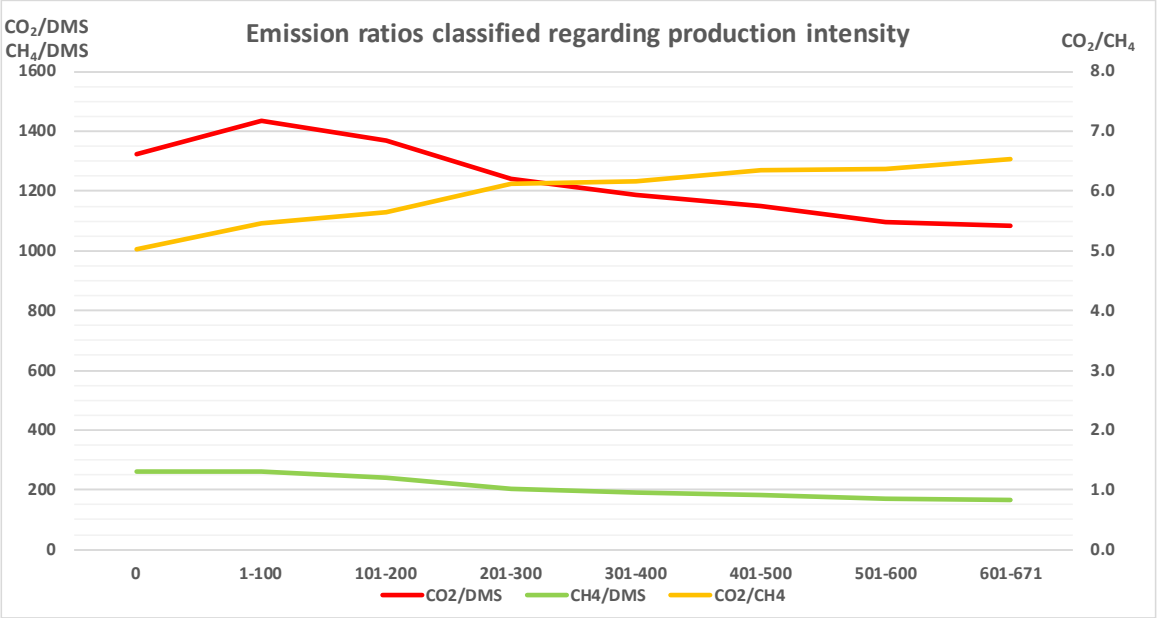

Figure 4.13: Ratios of average gas 30-minute emission rates in relation to 30-minute production intensity.

While trends of average 30-minute gas emissions show positive trends against increasing production intensity, the other characteristic emission values (maximum, minimum, percentile 97.5th and percentile 2.5 th) in Figure 4.14 to Figure 4.16 show interesting results. Otherwise, the trend of other characteristic emissions is generally increasing with production intensity, but it varies considerably while the production intensity is increasing. It indicates that releasing mechanisms of DMS are also significantly controlled by coal lithology. Also, considering the releasing ratios between production intervals and non-production interval (Table 4.2), the DMS releasing is most controlled by coal crushing of all three gases and DMS is released during coal transport to the surface and from the fresh coal (first few days after being transported to surface) on the stockpile concentrations of several mg/m^3 are detected [81]. All stated facts suggest that the releasing mechanism is similar to CO_2. The general releasing mechanisms of CO_2 and CH_4 are explained with previous studies of structural and petrographical changes of Velenje lignite [125] that the CO_2 is mainly adsorbed on the lignite structure or trapped in the coal matrix, while CH_4 is mainly free in the coal fractures.

Table 4.2: Gas emission ratios between production intervals/non-production interval.

Production intensity intervals [t/30min]		0	1-100	101-200	201-300	301-400	401-500	501-600	601-671	1-671
Average production intensity [t/30min]		0	40	149	250	349	450	541	633	242
DMS emission ratios	Production intervals/ non-production interval	1.0	1.1	1.2	1.5	1.7	1.9	2.0	2.1	1.5
CH4 emission ratios		1.0	1.1	1.1	1.2	1.2	1.3	1.3	1.3	1.2
CO2 emission ratios		1.0	1.2	1.3	1.4	1.5	1.6	1.7	1.7	1.4

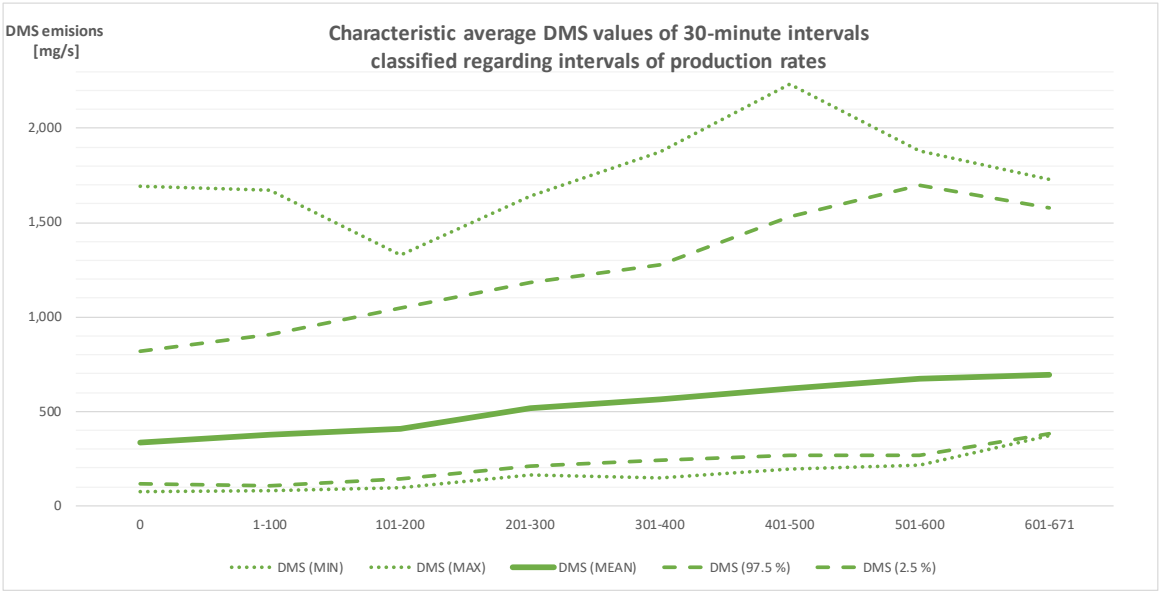

Figure 4.14: Characteristic average 30-minute DMS emissions classified regarding production intensities.

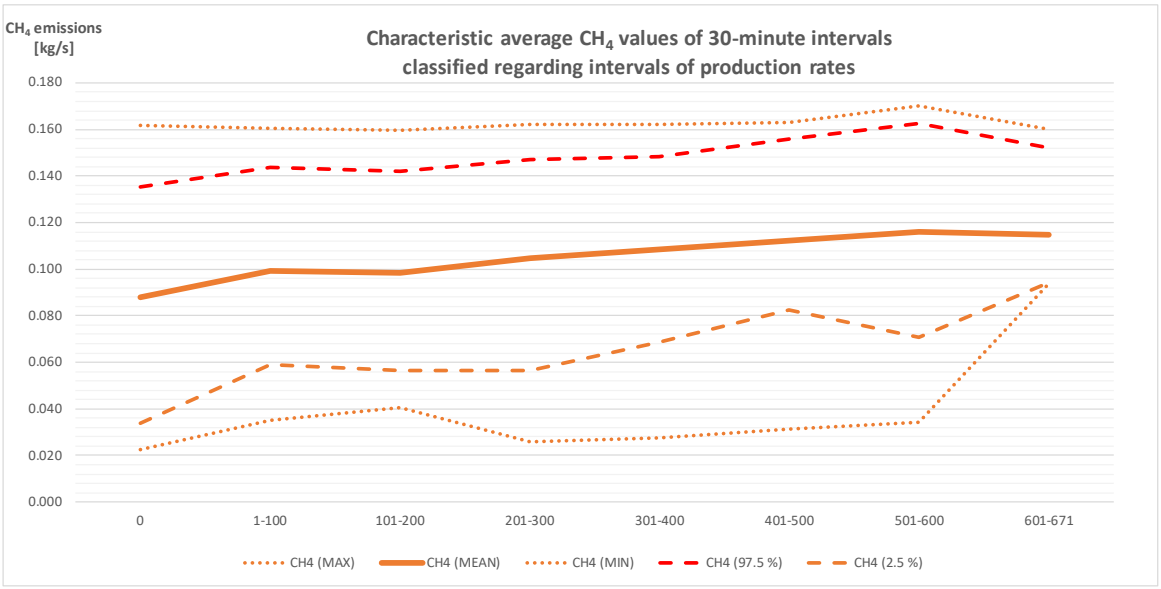

Figure 4.15: Characteristic average 30-minute CH_4 emissions classified regarding production intensities.

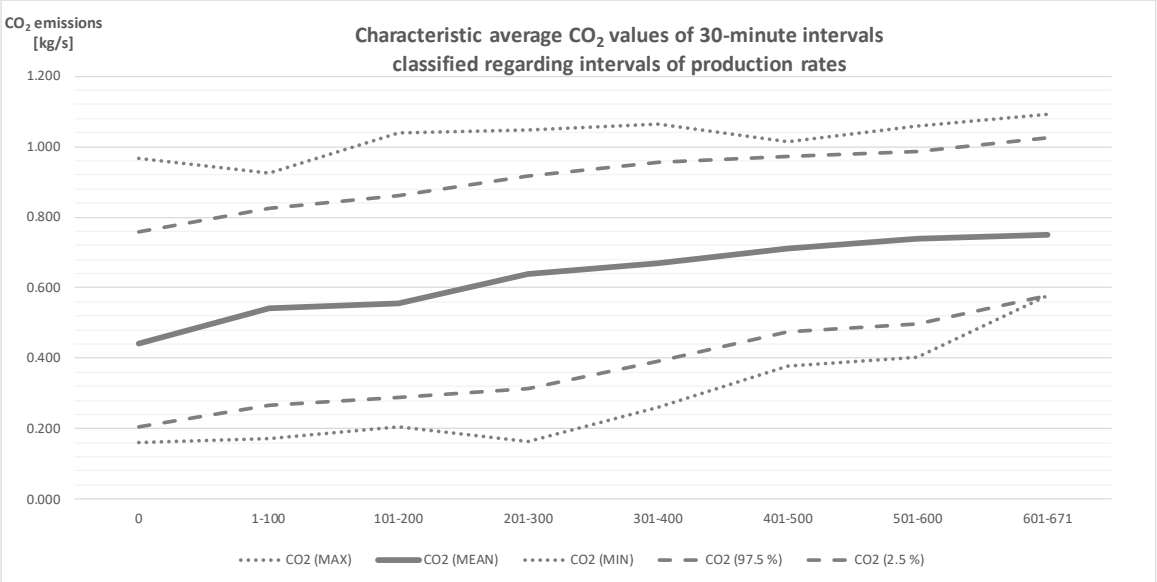

Figure 4.16: Characteristic average 30-minute CO_2 emissions classified regarding production intensities.

To further study the relationships between gases and gases regarding coal production the gases concentrations (DMS [ppmv]; CO_2 and CH_4 [%]) were grouped according to a specific work phase of VMM or according to 30-minute production intensity, respectively.

For correlation analysis of gases concentrations in relation to work phases, the period of 21 days (5 October 2012–25 October 2012) was considered. The procedure of work phases determination and calculation process of hourly correlations between parameters for a specific work phase is presented in Appendix E: The procedure for calculating correlations in relation to working phases of the Velenje mining method.

For the whole monitoring period (4 October 2012–4 January 2013) the correlation analysis was based on 4,462 half-hour intervals which were arranged according to production intensity (as tonnage in 30 minutes) in intervals 0, 1-100, 101-200, 201-300, 301-400, 401-500, 501-600 and 601-671 (671 t/30min was max. value). For each half-hour interval average half-hour emissions of DMS, CO_2 and CH_4 were calculated.

The relationship between CH_4 and CO_2 concentrations was studied at locations **b** to **f**. The data from the sensors at location **a** were excluded due to malfunction. Table 2 shows the calculated average hourly correlation coefficients (r-values) according to individual work phases.

Table 4.3: Average hourly r values of relationships CH_4-CO_2 according to individual work phases. The locations of sensors are presented in Figure 3.1.

Average hourly correlations between CH_4 and CO_2 on sensor locations "b" to "f"						
5. - 25.10.2012 (21 days)	Num. of Events	Location "b"	Location "c"	Location "d"	Location "e"	Location "f"
WORK PHASE		r values				
Cutting	39	0.47	0.62	0.82	0.81	0.84
Advancing	38	0.42	0.63	0.84	0.82	0.83
Caving 1/2	29	0.38	0.66	0.85	0.85	0.83
Caving 2/2	32	0.35	0.66	0.78	0.79	0.81
Not in operation	128	0.09	0.24	0.5	0.62	0.59
Shift change	64	0.25	0.4	0.71	0.75	0.72
Undefined	174	0.2	0.32	0.61	0.52	0.55
PROD. PHASE AVG.	138	0.41	0.64	0.82	0.82	0.83
ALL	504	0.24	0.4	0.65	0.66	0.66

The average r-values at **f** during coal production work phases (cutting, advancing and top coal caving in sectors 1 and 2) were on average 0.83 (0.81 to 0.84) indicating a high correlation between CH_4 and CO_2 and for the work phases "with no coal crushing" (shift change: 0.72; not operating: 0.59) they were significantly lower than for production phases. After the mine team finished the work, the gas concentrations started do decrease. This way the correlations at work phase "shift change" are higher than other "non-production phases".

The average r-value for all working phases was 0.66, i.e., a moderate correlation. The r values increase from **b** to **f** in the direction of the airflow due to the fact that the sensors on each next location regarding airflow direction are detecting gases releasing from bigger part of longwall face. At locations **e** and **f** sensors are detecting all released amounts from the longwall face.

Table 4.4: Ratios of CH_4-CO_2 at each sensor location.

CO_2/CH_4 ratios according to the sensor locations				
Location "b"	Location "c"	Location "d"	Location "e"	Location "f"
7.06	1.84	2.42	2.91	2.38

Interesting releasing behaviour of CO_2 and CH_4 additionally shows the CO_2/CH_4 ratios specific sensors locations (Table 4.4). At location **b**, the ratio (7.06) is more than twice as seen in other locations. This is because the sensors at **b** were positioned between the coal crusher on the BSL conveyor and the longwall face in the transport gate road (intake airway). This means that a significant amount of gases is also released during primary crushing and that the CO_2 and CH_4 are released with differing intensities. The ratio of CO2:CH4 at e (2.91) is higher than at f (2.38) even though both are located in the return airway. This is because the average concentration level of CO_2 was slightly higher at e (CO_2 at e = 1.14%; and CO_2 at f = 1.06%) and the average CH_4 level was slightly lower (location e: 0.39 %; location f: 0.45 %) indicating more stable (more laminar) airflow at the end of the return airway, allowing the layering of gases according to density.

Previous studies of coalbed gases at the CMV show that the average CO_2:CH_4 v/v mixture is approx. 2:1, where the CO_2 is mainly adsorbed on the lignite structure or trapped in the coal matrix, while CH_4 is mainly free in the coal fractures [125]. Also, the emission and mobilization of coal gases from the pillar begin at 100 m to 75 m out from the longwall face due to the pressure wave caused by the advance of the longwall face [126]. This explains why the highest CO_2:CH_4 ratio occurs at **b** (Table 4.4). Study of spatial distribution and origin of coalbed gases at the working faces of the Velenje Coal Basin [127] reports variation in the CO_2:CH_4 ratios from 30:70 vol. % to 100:0 vol. %. The CO_2:CH_4 ratio in different coals (by volume per mass unit of coal) is generally reported to be about 2, while in lignite coals it can be as high as 10 [[10], [128]]. Since there is no information regarding the desorption characteristics of DMS over time from coal, this analysis is

also focused on comparison of already known facts of releasing mechanisms of CO_2 and CH_4 with DMS releasing using monitored data and detailed understanding of the coal production process. The relationship between DMS and CH_4, CO_2, is studied using the data obtained from location **f** (Table 4.5).

Table 4.5: Average hourly r-values of DMS:CO_2 and DMS:CH_4 at location **f** according to each work phase.

Average hourly correlations of DMS/CO_2 and DMS/CH_4 at location "f"			
5. - 25.10.2012 (21 days)	Num. of Events	CH_4	CO_2
WORK PHASE		r values	
Cutting	39	0.56	0.59
Advancing	38	0.57	0.61
Caving 1/2	29	0.58	0.55
Caving 2/2	32	0.56	0.48
Not in operation	128	0.52	0.42
Shift change	64	0.57	0.59
Undefined	174	0.44	0.42
PROD. PHASE AVG.	138	0.57	0.56
ALL	504	0.51	0.48

For DMS:CH_4 and DMS:CO_2, the average hourly r-values during the different production phases were 0.57 and 0.56, respectively, indicating a moderate correlation.

The analysis of correlations between gases and between gases and production intensity is the next study that inspects the releasing behaviours of gases. Included are monitored data of location **f** (gases) and location **t** (production rate). This analysis was included to supplement the previous correlation analysis. It includes the whole duration of the monitoring campaign. Considering 30-minute intervals the error of simultaneous detection in time is not significant as it could be at minute data logging since sensors are not on the same location (see Figure 3.1 in Chapter 3.2). Also, in the analysis of correlations regarding work phases of VMM, the work phases were included if they could be defined on the hour-to-hour basis. If in a specific hour more than one was recognized, they were defined as “undefined”.

Table 4.6 shows the summary of r-values between average 30-minute gas concentrations and 30-minute production intensity.

Table 4.6: Summary of correlation analyses of average 30-minute gas concentrations and 30-minute production intensity.

Production intensity	Number of records	CO_2/CH_4	DMS/CO_2	DMS/CH_4	30-minute production rate		
					DMS	CO_2	CH_4
		r values					
0	**2725**	**0.63**	**0.53**	**0.21**			
1-100	442	0.87	0.59	0.48	-0.18	-0.14	-0.12
101-200	335	0.85	0.54	0.39	0.25	0.17	0.11
201-300	314	0.85	0.40	0.26	0.03	0.06	0.00
301-400	291	0.87	0.45	0.27	0.00	-0.04	-0.03
401-500	227	0.82	0.39	0.25	0.07	0.18	0.18
501-600	113	0.86	0.54	0.34	-0.01	-0.08	-0.08
601-671	15	0.85	0.62	0.33	-0.35	-0.15	0.14
1-671	**1737**	**0.85**	**0.55**	**0.36**	**0.39**	**0.36**	**0.16**
r values	**MAX**	0.87	0.62	0.48	0.39	0.36	0.18
	MIN	0.63	0.39	0.21	-0.35	-0.15	-0.12

Again, analysis shows that generally the correlations between gases are higher during the coal production. The highest correlation is between CO_2 and CH_4 during coal production. The correlations between CO_2 and DMS are similar as in the previous correlation analysis, while this analysis shows less correlation between CH_4 and DMS.

Additionally, Figure 4.17 toFigure 4.19 show in more detail why the correlations between gas concentrations and productions intensity are low or little if any, respectively. While the trend lines show that the emissions are increasing with higher production intensity, figures also show significant variations in gas emissions at specific production intensity and indicate that production intensity is not only a controlling factor of gas emissions.

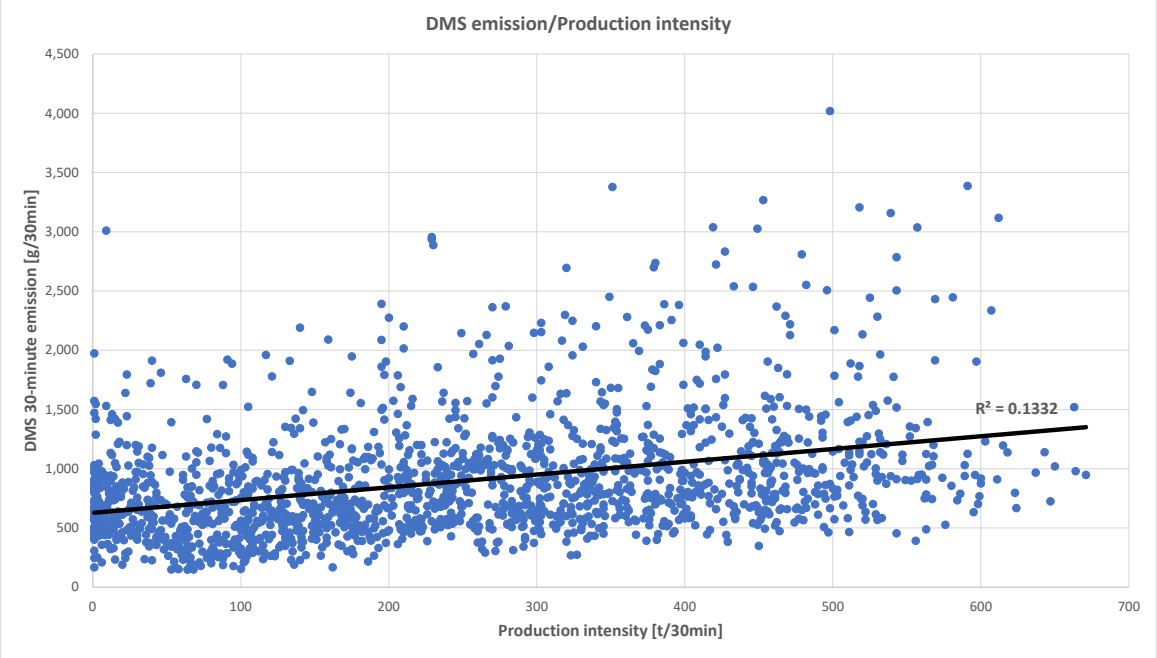

Figure 4.17: Average 30-minute DMS emission vs 30-minute production intensity.

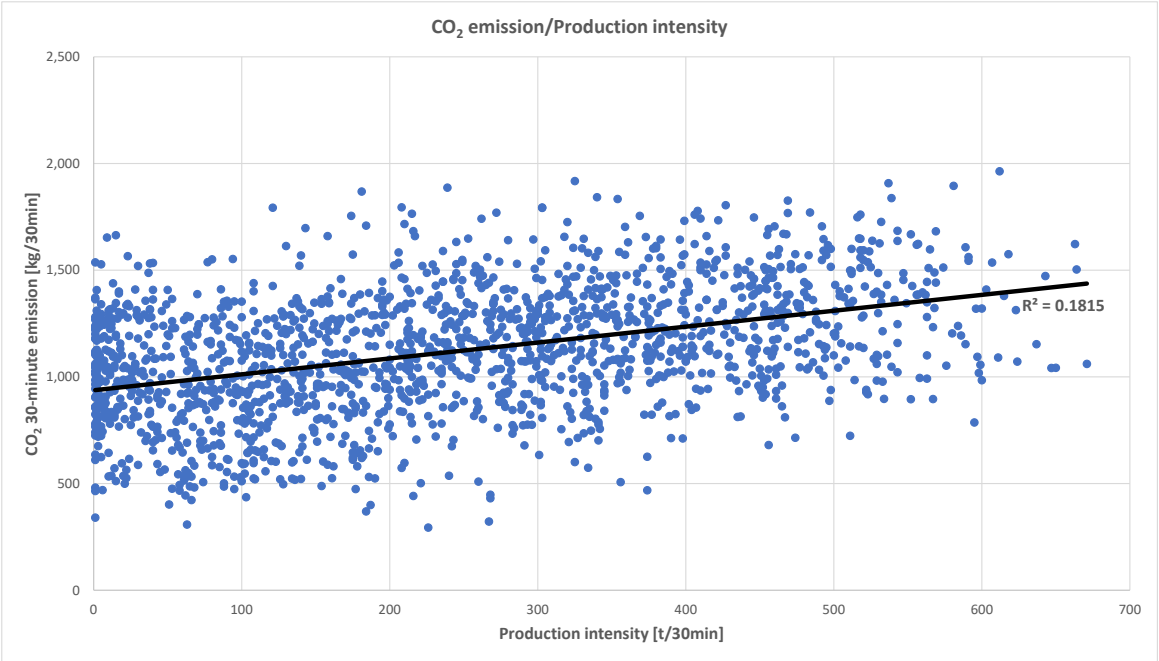

Figure 4.18: Average 30-minute CO_2 emission vs 30-minute production intensity.

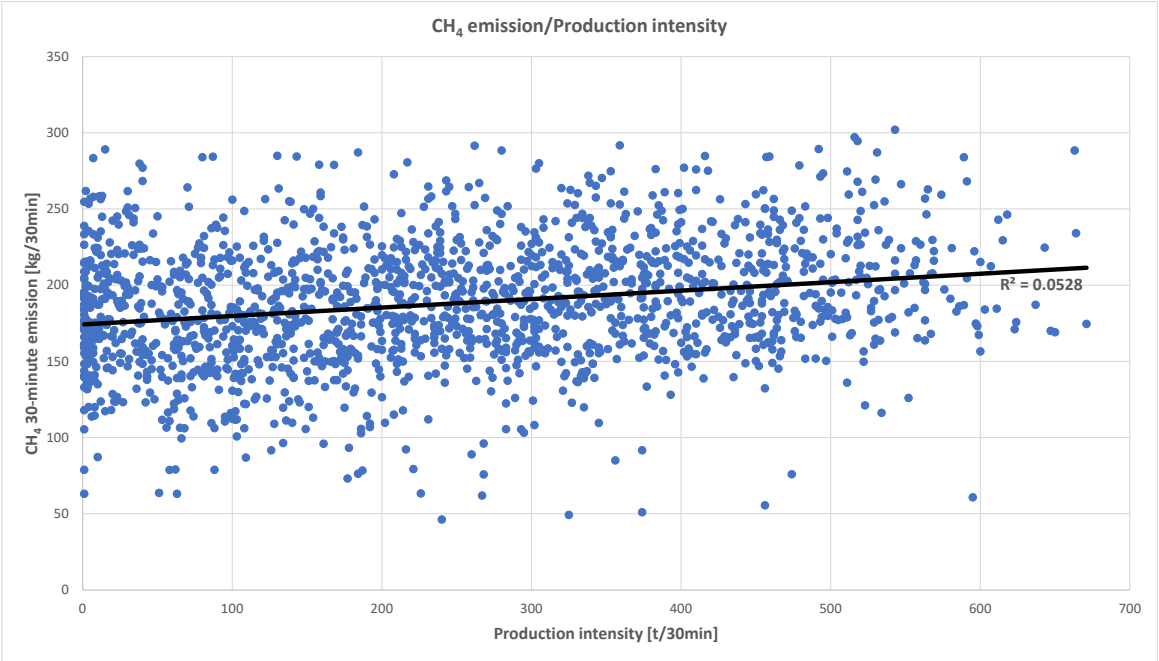

Figure 4.19: Average 30-minute CH_4 emission vs 30-minute production intensity.

Overall, the analyses in this chapter show:

- DMS, CO_2 and CH_4 are released during the coal extraction process with an intervention in the coal seam (coal crushing).
- DMS, CO_2 and CH_4 emissions are controlled with coal production intensity.
- Previous studies of structural and petrographical changes of Velenje lignite and analysis in this work suggest that DMS is also controlled by coal lithology and that the releasing mechanism may be similar to the releasing mechanism of CO_2.
- Concentrations and emissions of gases are also controlled by mine ventilation.
- The releasing of DMS (also CO_2 and CH_4) from the extraction process is a very complex phenomenon. Besides the already stated main controlled gas releasing factors, the general

variability of DMS (also CO_2 and CH_4) emission rates is also governed by other factors of the coal extraction process besides the production intensity or work phases, respectively. The total emission rate is also dependent on the size of the goaf area, the size of the open space behind the shield supports (size of uncollapsed area – for safe mining the continuous collapse of the goaf area in necessary). The instantaneous collapse of the goaf area results in peak detected concentration levels. Also, the peak DMS concentration levels can also be a result of the release from gas from pockets in the coal seam or from accumulated DMS in the old mine work (previous gateroad and previously mined longwall panels in upper levels of coal seam), which can be reached by the top coal caving process as an active longwall face is extracting underneath.

4.3 Results of the Dimethyl Sulphide Stability Experiment in the Mine

4.3.1 First experiment with dosage of DMS

The first experiment with DMS at a new location was conducted on 28 June 2019. The objective of the experiment was to simultaneously monitor DMS concentration, airflow velocity, dry temperature, relative humidity, and total pressure in the duct on both monitoring locations while dosing the DMS from the cylinder into the ducting. The frequency of data logging was 1 second. Monitoring of airflow velocities was conducted with two types of anemometers. One was an anemometer connected to the Almemo data logger which is used in CMV. The second was an anemometer developed by IGM-PAN which can also monitor methane. During the experiment on both monitoring locations methane was not detected.

Before the start of the experiment, the ducting was inspected, and the fan was set in a way that the desired airflow velocity at monitoring location 1 would be approx. 0.65 m/s. While pre-testing the ducting layout we learned that airflow velocity under 0.6 m/s can lead to a collapse of part of the ducting. After the setup of airflow velocity, all the sensors on both monitoring locations were mounted in a ducting. When all the sensors were in place, the cylinder with DMS, reducing valve on the cylinder and connecting tube to the ducting was getting ready. All holes that appeared in the ducting while mounting the sensors in the ducting were carefully sealed. At the monitoring location all sensors were mounted into the ducting in a way that they fitted in one 10 m long duct, so that there were no joints between sensors.

Before inserting the tube into the ducting 10 m before the DMS sensor on monitoring location 1, the desired volume flow from the tube was set by very slowly opening the cylinder by reducing the valve and measuring the flow velocity at the end of the tube with Pitot tube. The desired flow velocity was iteratively calculated based on known diameters of the tube and duct and from the necessary flow rate from the cylinder with concentration 2000 ppm of DMS mixture with nitrogen. The iterative calculation is based on equation of weighted arithmetic mean

$$\overline{x} = \frac{\sum_{i=1}^{n} w_i \times x_i}{\sum_{i=1}^{n} w_i} \tag{4.1}$$

where weights are w_i and the data set is x_i. Then the equation for average DMS concentration DMS_D in the ducting is

$$DMS_D = \frac{Q_F \times DMS_F + Q_C \times DMS_C}{Q_F + Q_C} \ [\text{ppm}] \tag{4.2}$$

where F stands for airflow sucked from the airway and pushed into the ducting with fan and where C stands for content in the cylinder.

The desired DMS concentration of the airflow in the ducting was between 7 and 10 ppm. For that, the required flow velocity at the end of the tube should be between 15 and 21 m/s. The calculation results in MS Excel are presented in Table 1.1. After the final check of ducting and all sensors, the positioning and data logging, the experiment started with inserting the tube and starting to dose DMS into the ducting.

Table 4.7: Iterative calculation of the desired DMS concentration in the ducting.

Flow rate from tube conected to the cylinder		
Diamater [m]	0.0075	0.0075
Cross section [m^2]	0.0000442	0.0000442
Flow velocity [m/s]	**14.62**	**20.91**
Flow rate [m^3/s]	0.000646	0.000924
DMS in cylinder [ppm]	2000	2000
Flow rate in duct		
Daimater [m]	0.6	0.6
Cross section [m^2]	0.2827433	0.2827433
Flow velocity [m/s]	**0.65**	**0.65**
Flow rate [m^3/s]	0.183783	0.183783
Calculated DMS concentration in duct [ppm]	**7.00**	**10.00**

The experiment lasted approx. 50 minutes between 10:50:00 to 11:40:00 [hh:mm:ss]. Table 4.8 and Table 4.9 show the overview of collected data of airflow conditions on both monitoring locations.

Table 4.8: An overview of airflow conditions in the ducting on monitoring location 1 in the period between 10:50:00 to 11:40:00.

LOCATION 1	Velocity [m/s]	Dry temperature [°C]	Relative humudity [%]	Total pressure [mbar]
MAX	0.74	17.3	79.5	991.2
AVERAGE	0.66	17.3	79.1	990.8
MIN	0.58	17.3	79.0	990.7
STD. DEV.	0.02	0.0	0.1	0.1

Table 4.9: An overview of airflow conditions in the ducting on monitoring location 2 in the period between 10:50:00 to 11:40:00.

LOCATION 2	Velocity [m/s]	Dry temperature [°C]	Relative humudity [%]	Total pressure [mbar]
MAX	0.60	17.3	78.7	996.0
AVERAGE	0.56	17.3	78.4	995.6
MIN	0.52	17.3	78.1	995.4
STD. DEV.	0.01	0.0	0.2	0.1

In Table 4.10, monitored results of all anemometers are shown. At location 1, velocities coincide very well, the average velocities are practically identical. At location 2, the average velocity difference is 0.05 m/s or 8.2 %.

Table 4.10: A monitored results overview of all used anemometers at both monitoring locations in the period between 10:50:00 to 11:40:00.

50 minutes	Velocity L1 - Almemo [m/s]	Velocity L2 - Almemo [m/s]	Velocity L1 -IGM [m/s]	Velocity L2 -IGM [m/s]
MAX	0.69	0.65	0.74	0.6
AVERAGE	0.66	0.61	0.66	0.56
MIN	0.63	0.56	0.58	0.52
STD. DEV.	0.01	0.02	0.02	0.01

Airflow velocity monitoring results during the experiment at both monitoring locations are shown in Figure 4.20. All anemometers detected the velocity changes at a similar time. The detected velocity changes show that during the experiment, the pressure in the pneumatic network of CMV was not constant which reflected in the power of the pneumatic fan.

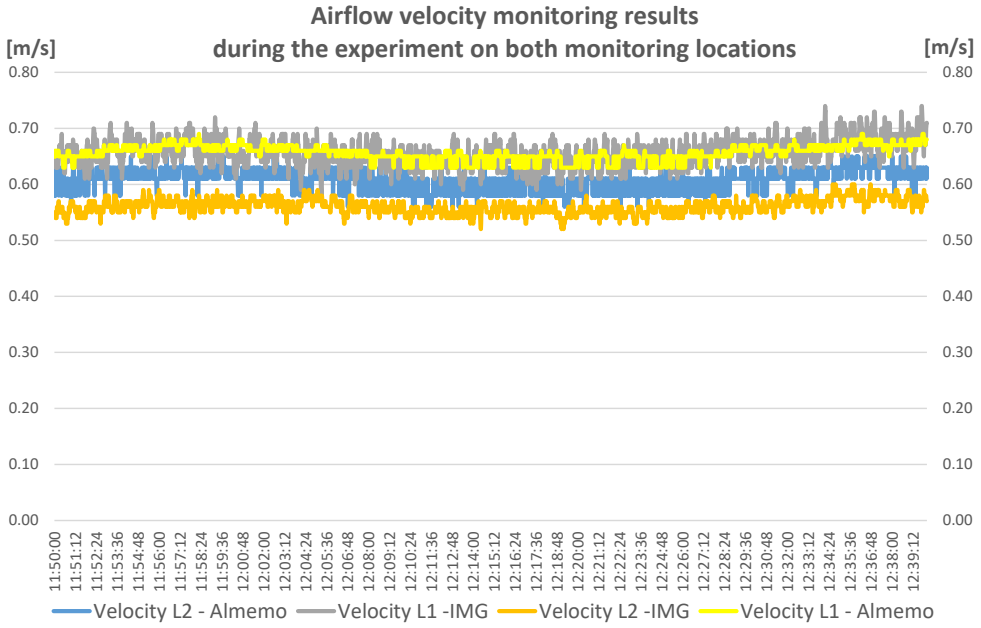

Figure 4.20: Airflow velocity monitoring results during the experiment at both monitoring locations.

The presented diagram of monitoring results of DMS concentrations (Figure 4.21) at both locations during the experiment shows the starts of DMS detection at both locations with an increase of DMS concentrations. The DMS sensors needed approx. 5 minutes to reach the expected values. Similar times are needed also at the sensors test side on CMV. Hereinafter, when DMS sensor at location 1 reaches the expected values, it responds to airflow velocity changes at monitoring location 1. The airflow velocity (airflow rate) at monitoring location 1 and its changes delegate the dilution rate of the DMS from the cylinder after the reduction valve of the cylinder was set.

The DMS 1 sensor started to detect DMS at 11:55:28 and DMS 2 sensor started to detect DMS at 12:09:15. That gives 13 minutes and 47 seconds of traveling time, the time that DMS needed to travel from monitoring location 1 to monitoring location 2.

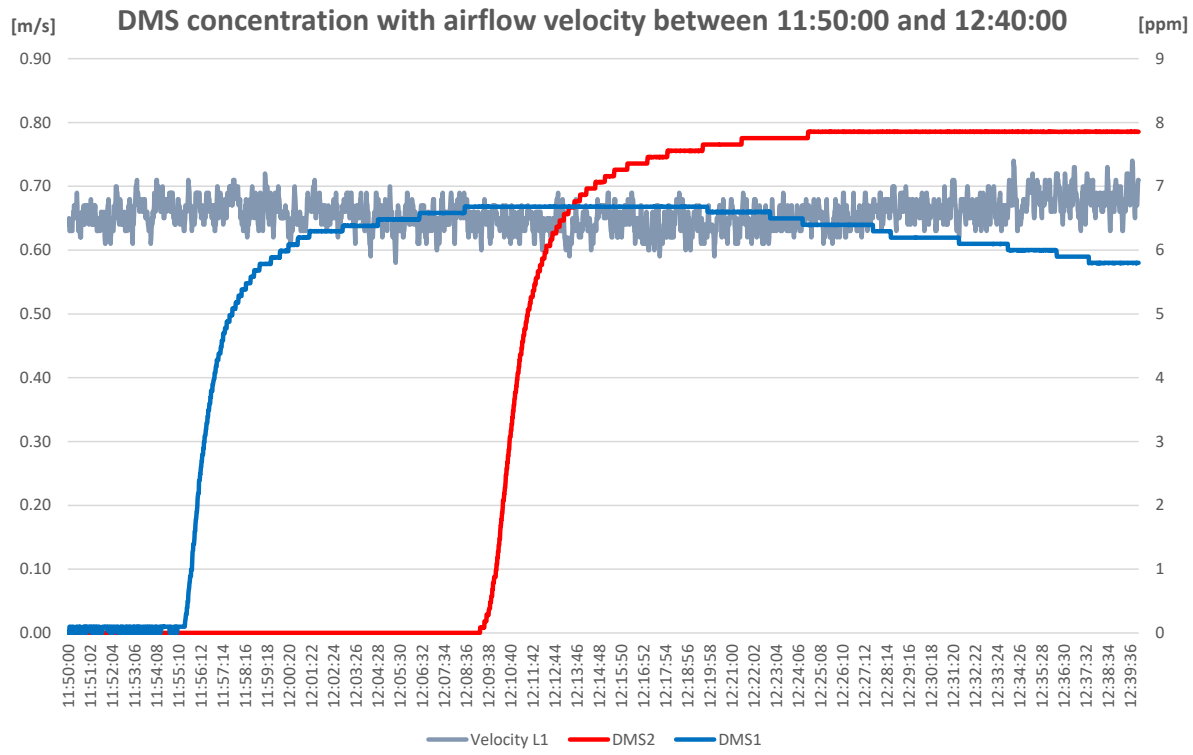

Figure 4.21: DMS concentrations at both locations and airflow velocity at monitoring location 1 during the experiment.

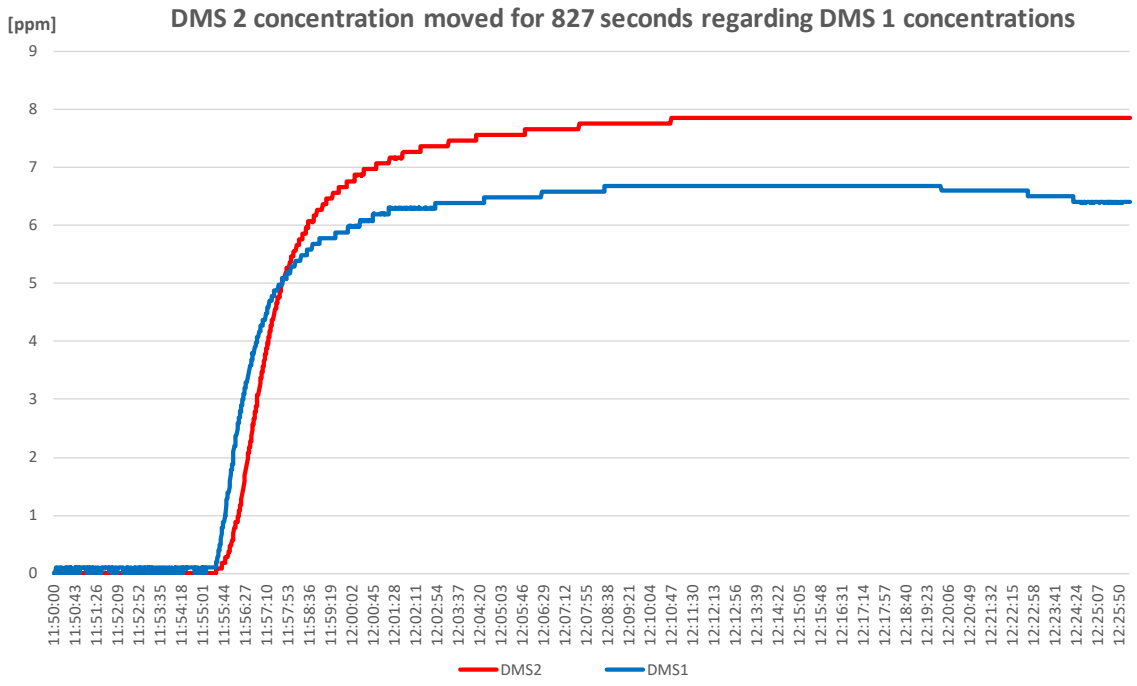

Figure 4.22: Comparison of DMS concentrations at both locations. Measured values of DMS 2 sensor were moved back regarding measured values of DMS 1 sensors for the time of DMS travel, for 827 seconds (13 minutes and 47 seconds).

The review of the 20-minute period of airflow velocity and DMS concentration at monitoring location 1 shows (Figure 4.22) an increase of airflow velocity from 0.64 to 0.69 m/s, for 7.2 %, and

a decrease of DMS concentration from 6.6 to 5.8 ppm, for 12.1%. The airflow velocity change in the inspected period was determined with the help of a linear trendline.

The calculation shows (Table 4.11) that DMS concentration would also decrease for 7.2 % in the 20-minute period.

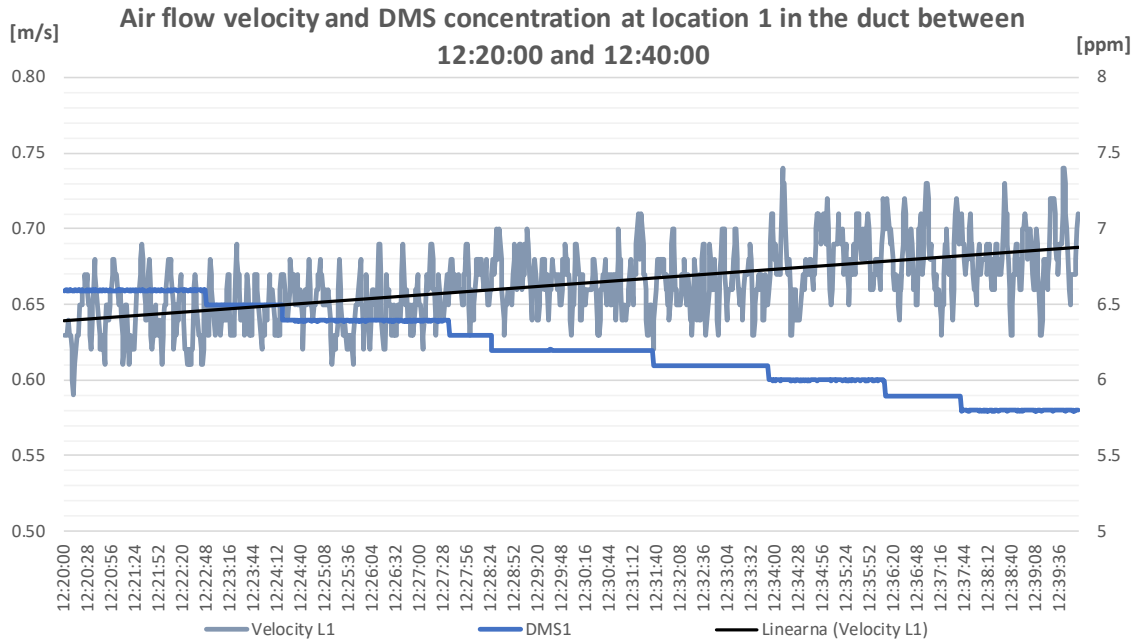

Figure 4.23: 20-minute period of airflow velocity and DMS concentration at monitoring location 1.

Table 4.11: Calculation results of the DMS concentration in the ducting based on an increase of airflow velocity from 0.64 to 0.69 m/s and constant flow velocity from the cylinder.

Flow rate from tube conected to the cylinder		
Diamater [m]	0.0075	0.0075
Cross section [m^2]	0.0000442	0.0000442
Flow velocity [m/s]	**15**	**15**
Flow rate [m^3/s]	0.000663	0.000663
DMS in cylinder [ppm]	2000	2000
Flow rate in duct		
Diamater [m]	0.6	0.6
Cross section [m^2]	0.2827433	0.2827433
Flow velocity [m/s]	**0.64**	**0.69**
Flow rate [m^3/s]	0.180956	0.195093
Calculated DMS concentration in duct [ppm]	**7.30**	**6.77**

The presented diagram of monitoring results of DMS concentrations (Figure 4.21 and Figure 4.22) also shows that at monitoring location 2, DMS concentrations are higher than at monitoring location 1, which is not logical. At most one might expect the contrary, that the DMS concentration would be higher at monitoring location 1 than at monitoring location 2, which would suggest decay of DMS in the time of traveling through the ducting.

Immediately after the mine experiment, the DMS sensors were unmounted and brought to the surface for inspection at the test laboratory for sensors. The concentrations of both sensors showed a concentration of 80 ppm as were the test concentrations of DMS in the test cylinder at the test site. The same procedure was undertaken for sensor calibration of the DMS sensor before the experiment.

Then with the addition of nitrogen into the flow from the test cylinder, the DMS concentration decreased in the range of concentrations similar as in the experiment. Then the DMS sensor from location 1 showed a value of 7.9 ppm and the DMS sensor from location 2 showed a value of 8.9 ppm.

The difference of both DMS concentrations from the monitoring results was inspected in the range of maximum concentrations. The reason are measuring properties of DMS sensors. At the start of detection, they need time to adjust.

For that, an 8-minute period between 12:11:00 and 12:19:00 was selected for monitoring location 1 and between 12:14:47 and 12:32:47 for monitoring location 2, when the conditions in the ducting were most steady. The overview of monitoring results for DMS concentrations and airflow velocities for the 8-minute period is shown in Table 4.12 and Figure 4.24. The average difference of DMS concentrations was 1.176 ppm with standard deviation ± 0.004 ppm.

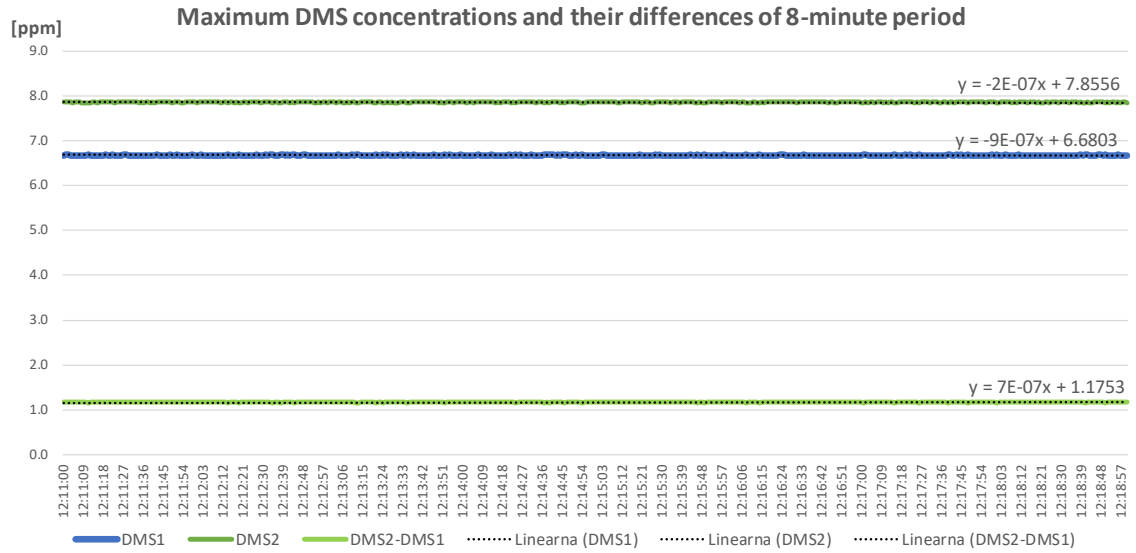

Figure 4.24: Comparison of DMS concentration differences at both locations in the 8-minute period. Measured values of the DMS 2 sensor were moved back regarding measured values of DMS 1 sensors for the time of DMS travel, for 827 seconds (13 minutes and 47 seconds). For monitoring location 1, values are from the period between 12:11:00 and 12:19:00, and for monitoring location 2, values are from the period between 12:14:47 and 12:32:47.

Table 4.12: An overview of DMS concentrations and airflow velocities from both monitoring locations in the period between 12:11:00 and 12:19:00. For monitoring location 1, values are from the period between 12:11:00 and 12:19:00, and for monitoring location 2, values are from the period between 12:14:47 and 12:32:47.

8-minute period L1: (12:11:00 -12:19:00) L2: (12:24:47 -12:32:47)	Velocity L1 - Almemo [m/s]	Velocity L2 - Almemo [m/s]	Velocity L1 -IMG-PAN [m/s]	Velocity L2 -IMG-PAN [m/s]	DMS1 [ppm]	DMS2 [ppm]	DMS2 - DMS1 [ppm]
MAX	0.66	0.63	0.69	0.59	6.68	7.86	1.178
AVERAGE	0.645	0.606	0.643	0.559	6.68	7.86	1.176
MIN	0.63	0.56	0.59	0.54	6.68	7.85	1.166
STD. DEV.	0.01	0.02	0.02	0.01	0.002	0.003	0.004

The calculation of volume flow and mass flows (apparent and actual) at both monitoring locations, and their losses on the way from monitoring location 1 to monitoring location 2, are shown in Table 4.13, where airflow velocities obtained with IMG-PAN anemometers were considered, and Table 4.14 shows calculation results where airflow velocities obtained with Almemo anemometers were considered. When they are considered airflow rates, velocities obtained with IMG-PAN anemometers, the losses are between 12.5 and 13.0 %. And, when they are considered airflow velocities obtained with Almemo anemometers, the losses are between 5.4 and 5.9 %. An overview of monitored airflow velocities and DMS concentrations for the 8-minute period are shown in Table 4.12.

Table 4.13: Calculation results in MS Excel of volume flow and mass flows (apparent and actual) on both monitoring locations, and their losses. Airflow velocities obtained with IMG-PAN anemometers were considered. For monitoring location 1, values are from the period between 12:11:00 and 12:19:00, and for monitoring location 2, values are from the period between 12:14:47 and 12:32:47.

8 minutes - IMG-PAN anemometers	Volume flow [m^3 of air]	Mass flow (apparent) [kg of dry air]	Mass flow (actual) [kg of moist air]
SUM Location 1	87.4	102.2	103.2
SUM Location 2	76.0	89.4	90.3
Location2/Location1	0.870	0.875	0.875

Table 4.14: Calculation results in MS Excel of volume flow and mass flows (apparent and actual) at both monitoring locations, and their losses. Airflow velocities obtained with Almemo anemometers were considered. For monitoring location 1, values are from the period between 12:11:00 and 12:19:00, and for monitoring location 2 ,values are from the period between 12:14:47 and 12:32:47.

8 minutes - IMG-PAN anemometers	Volume flow [m^3 of air]	Mass flow (apparent) [kg of dry air]	Mass flow (actual) [kg of moist air]
SUM Location 1	87.6	102.4	103.5
SUM Location 2	82.4	96.9	97.9
Location2/Location1	0.941	0.946	0.946

4.3.2 Second mine experiment with DMS

The second experiment with DMS was conducted on 14 August 2019. In the first experiment it was discovered that DMS sensors do not show the same values at concentrations range that are planned for the experiment. The setup of DMS sensors was not changed after the first experiment.

The objectives were to repeat the first experiment in similar conditions and to determine the difference of monitored DMS concentrations of both DMS sensors at the same DMS concentration in the mine.

For that, the experiment was conducted in two stages. At the first stage, both DMS sensors were mounted at monitoring location 1. And in the second stage, the DMS sensors were mounted at monitoring location 1 and monitoring location 2.

After the overview of monitoring results of the second experiment was discovered, DMS sensors were accidentally exchanged between the preparation for stage two. The DMS1 sensor from the first experiment was mounted at monitoring location 2 and the DMS2 sensor was mounted at monitoring location 2. However, I labelled DMS sensors in this analysis regarding labels of monitoring locations. The sensor at monitoring location 1 is the DMS1 sensor and the sensor at monitoring location 2 is the DMS2 sensor.

At the monitoring locations we simultaneously monitored DMS concentration, airflow velocity, dry temperature, relative humidity, and total pressure in the duct. The frequency of data logging was 1 second. In stage one, both DMS1 and DMS2 sensors were mounted at monitoring location 1. In stage two, DMS2 sensor has been moved to monitoring location 2.

For the second experiment only anemometers of Almemo system were available. Before each stage of the experiment, the ducting was inspected, and the fan was set in a way that the desired airflow velocity at monitoring location 1 would be approx. 0.65 m/s. The setup of the fan remained the same throughout the experiment.

After the setup of airflow velocity, all the sensors at both monitoring locations were mounted in a ducting. The DMS sensors were mounted regarding the stages of the experiment.

When all the sensors were in place, the cylinder with DMS, reducing valve on the cylinder and connecting tube to the ducting was getting ready. All holes in the ducting that appeared due to the mounting of sensors in the ducting were carefully sealed. At the monitoring location all sensors were mounted into the ducting in a way that they fitted in one 10 m long duct, so that there were no joints between sensors.

Before inserting the tube into the ducting 10 m before the DMS sensor at monitoring location 1, the desired volume flow rate from the tube was set by very slowly opening the cylinder by reducing the valve and measuring the flow velocity at the end of the tube with Pitot tube. The desired flow velocity was iteratively calculated based on known diameters of the tube and duct and from the necessary flow rate from the cylinder with a concentration of 2000 ppm of DMS mixture with nitrogen. The flow velocity was set to 20 m/s. The calculation results in MS Excel for the expected DMS concentration in ducting, at airflow velocity in the duct 0.65 m/s and flow velocity from the tube connected to the cylinder 20 m/s, are shown in

Table 4.15.

Table 4.15: Calculation results of the DMS concentration in the ducting, at airflow velocity in the duct 0.65 m/s and flow velocity from the tube connected to the cylinder 20 m/s.

Flow rate from tube conected to the cylinder	
Diamater [m]	0.0075
Cross section [m^2]	0.0000442
Flow velocity [m/s]	**20**
Flow rate [m^3/s]	0.000884
DMS in cylinder [ppm]	2000
Flow rate in duct	
Diamater [m]	0.6
Cross section [m^2]	0.2827433
Flow velocity [m/s]	**0.65**
Flow rate [m^3/s]	0.183783
Calculated DMS concentration in duct [ppm]	**9.57**

After the final check of the ducting and all sensors, the positioning and data logging, the stage One of the experiment started with inserting the tube and starting to dose DMS into the ducting. The procedure final check was repeated before stage two. Between stages of the experiment, and moving DMS2 sensor to monitoring location 2, only the tube connected to the cylinder was sealed. The setup of the reducing valve of the cylinder fan remained the same throughout the experiment.

Both stages of the experiment, and the time in between, lasted approx. 2 hours and 20 minutes, from 9:40:00 to 12:00:00 [hh:mm:ss]. Table 4.16 and Table 4.17 show the overview of collected data of airflow conditions at both monitoring locations.

Table 4.16: An overview of airflow conditions in the ducting at monitoring location 1 in the period from 9:40:00 to 12:00:00.

LOCATION 1	**Velocity [m/s]**	**Dry temperature [°C]**	**Relative humidity [%]**	**Total pressure [mbar]**
MAX	0.73	17.1	83.7	994.0
AVERAGE	0.67	17.1	82.4	993.6
MIN	0.63	17.0	82.0	993.2
STD. DEV.	0.01	0.01	0.3	0.2

Table 4.17: An overview of airflow conditions in the ducting at monitoring location 2 in the period from 9:40:00 to 12:00:00.

LOCATION 2	**Velocity [m/s]**	**Dry temperature [°C]**	**Relative humudity [%]**	**Total pressure [mbar]**
MAX	0.63	17.5	79.4	994.8
AVERAGE	0.57	17.4	79.1	994.5
MIN	0.52	17.4	78.7	994.1
STD. DEV.	0.02	0.01	0.2	0.1

The presented diagram of monitoring results of DMS concentrations (Figure 4.25) at both locations during the experiment shows both stages of the experiment. At both stages, the DMS sensors needed approx. 5 minutes to reach the expected values. The airflow velocity (airflow rate) at monitoring location 1 and its changes delegate the dilution rate of the DMS from the cylinder after the reduction valve of the cylinder was set.

The traveling time of DMS from monitoring location 1 to monitoring location 2 has been determined in stage two. The DMS 1 sensor started to detect DMS at 10:30:06 and DMS 2 sensor started to detect DMS at 10:44:12. That means 14 minutes and 6 seconds of traveling time (Figure 4.25).

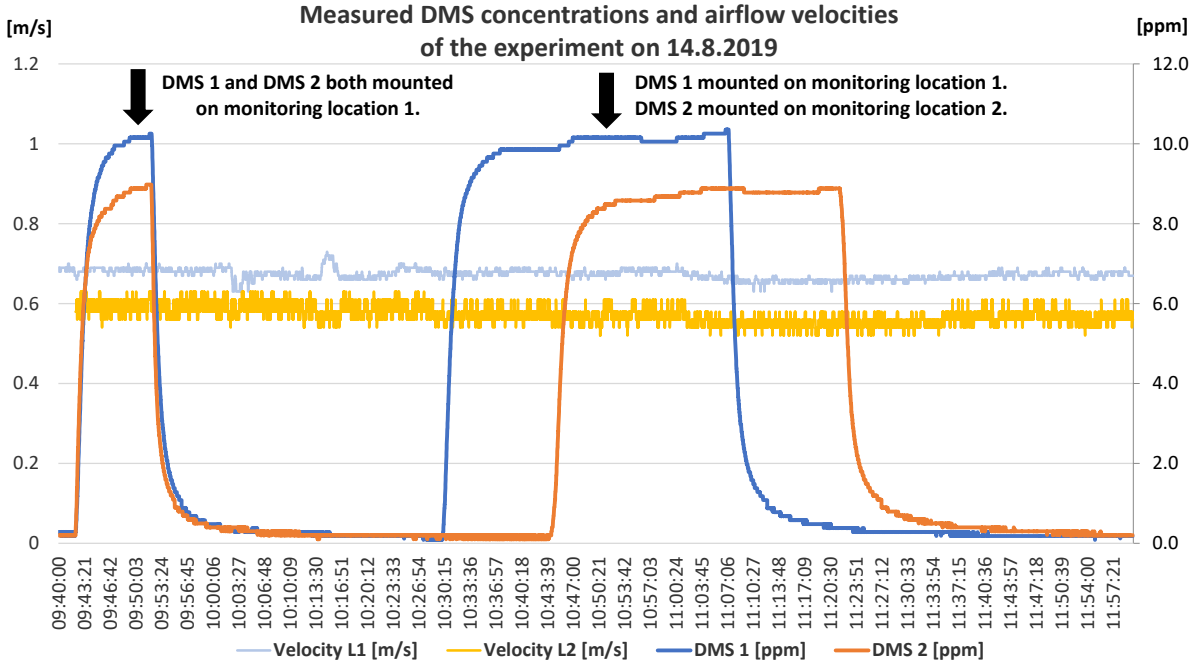

Figure 4.25: DMS concentrations and airflow velocities at both monitoring locations during the experiment.

4.3.2.1 Stage one of the second experiment

The difference of both DMS concentrations was inspected in the range of maximum concentrations. The reason are measuring properties of DMS sensors. At the start of detection, they need time to adjust. At stage one, dosing of DMS lasted for approx. 10 minutes.

For that we selected a 2-minute period between 09:49:22 and 09:51:21 when both DMS concentrations were most steady and a 5-minute period between 09:47:07 and 09:52:06.

The overview of monitoring results for DMS concentrations and airflow velocities for the 2-minute and 5-minute period are shown in Table 4.18 and Table 4.19, and Figure 4.26 and Figure 4.27. The average difference of DMS concentrations was 1.275 ppm with standard deviation ± 0.004 ppm at the 2-minute period, and at the 5-minute period it was 1.276 ppm with standard deviation ± 0.004 ppm.

Table 4.18: An overview of DMS concentrations and airflow velocities at monitoring location 1 for the 2-minute period between 09:49:22 and 09:51:21 of stage one.

STAGE ONE - 2 MINUTES	DMS 1 [ppm]	DMS 2 [ppm]	DMS1-DMS2 [ppm]	Velocity [m/s]
MAX	10.159	8.883	1.282	0.69
AVERAGE	10.156	8.881	1.275	0.68
MIN	10.153	8.877	1.270	0.67
STD. DEV.	0.003	0.003	0.004	0.005

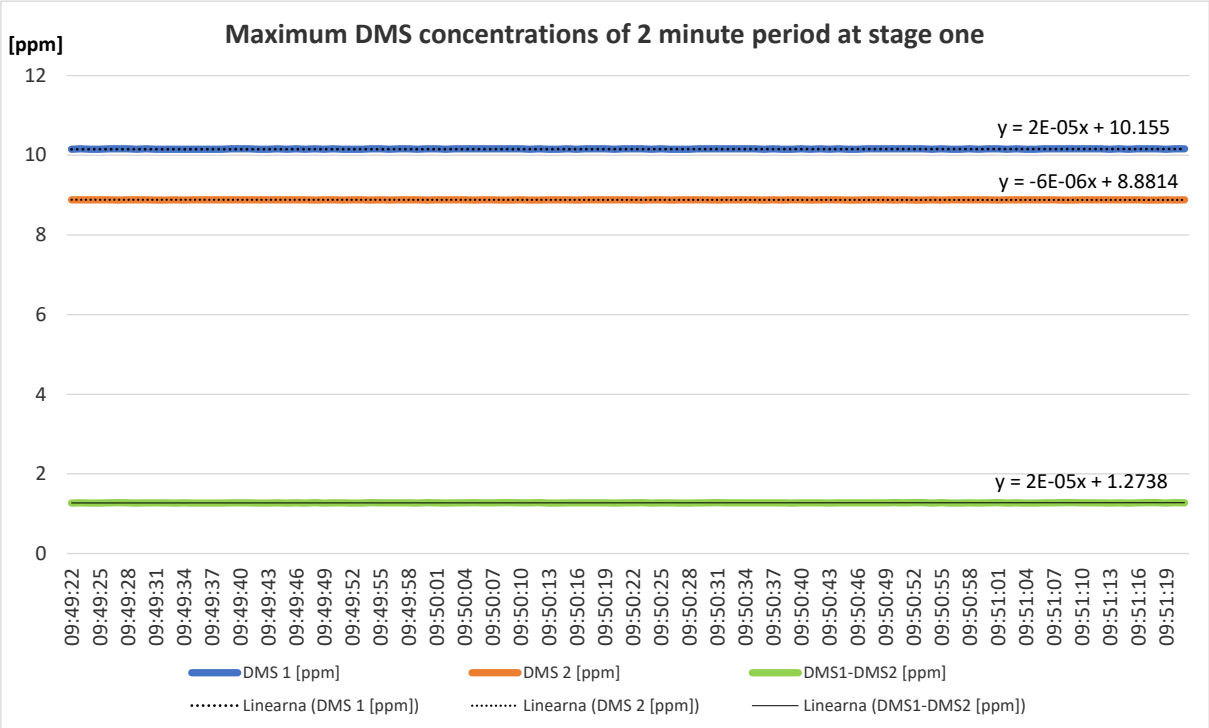

Figure 4.26: Comparison of DMS concentration differences at stage one in the 2-minute period between 09:49:22 and 09:51:21.

Table 4.19: An overview of DMS concentrations and airflow velocity at monitoring location 1 for the 5-minute period between 09:47:07 and 09:52:06 at stage one.

STAGE ONE - 5 MINUTES	DMS 1 [ppm]	DMS 2 [ppm]	DMS1-DMS2 [ppm]	Velocity [m/s]
MAX	10.256	8.980	1.386	0.70
AVERAGE	10.086	8.810	1.276	0.69
MIN	9.853	8.474	1.172	0.67
STD. DEV.	0.101	0.121	0.043	0.01

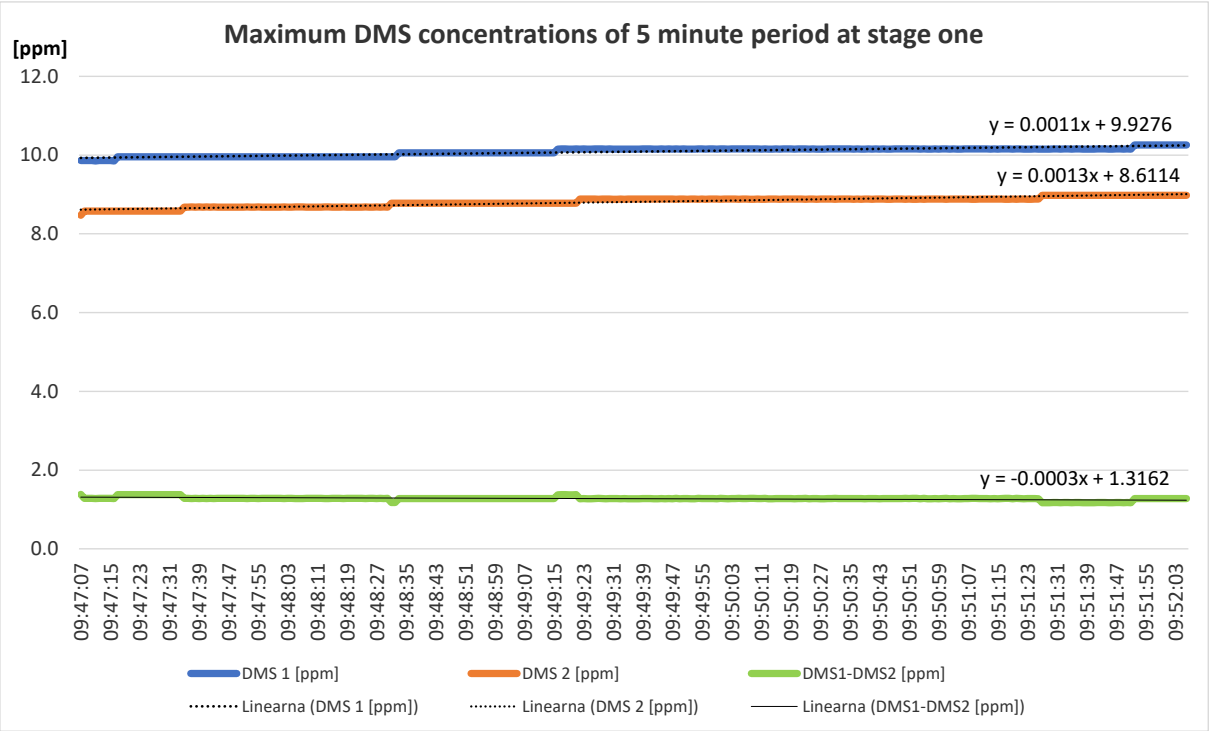

Figure 4.27: Comparison of DMS concentration differences at stage one in the 2-minute period between 09:49:22 and 09:51:21.

4.3.2.2 Stage two of the second experiment

The difference of both DMS concentrations was inspected in the range of maximum concentrations. The reason are measuring properties of DMS sensors. At the start of detection, they need time to adjust. At stage one, dosing of DMS lasted for approx. 37 minutes.

For review we selected a 5-minute period between 10:50:00 and 10:54:59 at monitoring location 1 and between 11:04:06 and 11:09:05 at monitoring location 2, when both DMS concentrations were most steady, and a 10-minute period between 10:50:00 and 10:59:59 at monitoring location 1 and between 11:04:06 and 11:14:05 at monitoring location 2.

The overview of monitoring results for DMS concentrations for the 5-minute and 10-minute period are shown in Table 4.20 and Figure 4.28. The average difference of DMS concentrations was 1.274 ppm with standard deviation ± 0.004 ppm at the 5-minute period, and at the 10-minute period it was 1.282 ppm with standard deviation ± 0.027 ppm.

Table 4.20: An overview of DMS concentrations at both monitoring locations for the 5-minute period between 10:50:00 and 10:54:59 at monitoring location 1 and between 11:04:06 and 11:09:05 at monitoring location 2 at stage two.

STAGE TWO - 5 MINUTES	DMS 1 [ppm]	DMS 2 [ppm]	DMS1-DMS2 [ppm]
MAX	10.159	8.889	1.282
AVERAGE	10.155	8.881	1.274
MIN	10.153	8.877	1.270
STD. DEV.	0.003	0.003	0.004

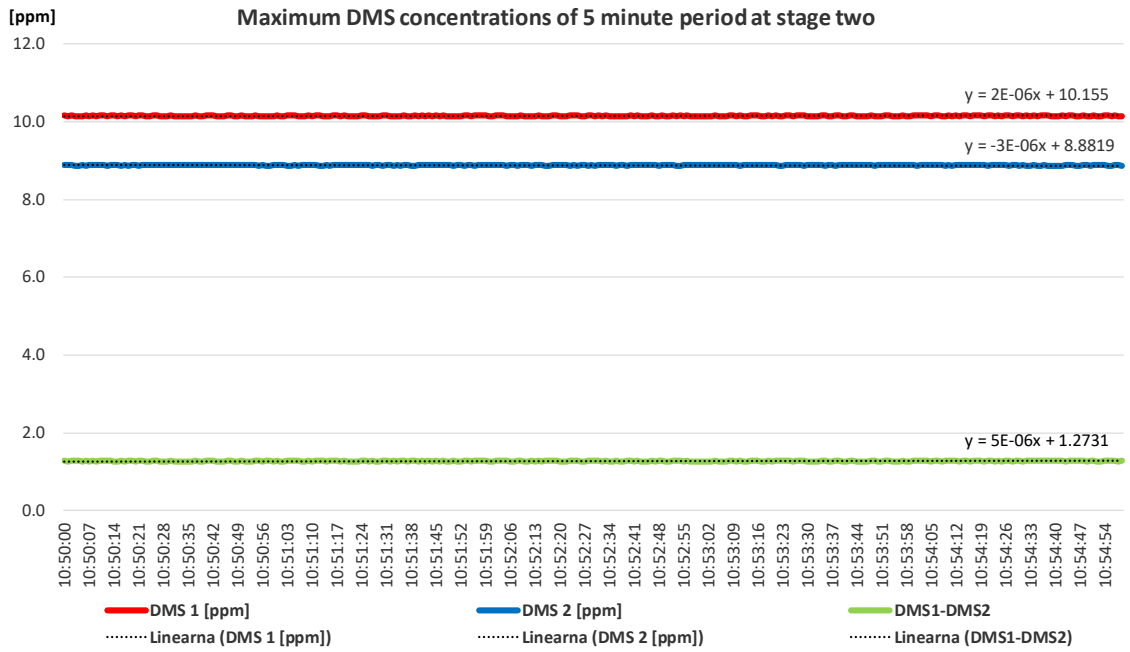

Figure 4.28: Comparison of DMS concentration differences at both locations in the 5-minute period at stage two. Measured values of DMS 2 sensor were moved back regarding measured values of DMS 1 sensors for the time of DMS travel, for 846 seconds (14 minutes and 6 seconds). For monitoring location 1, values are from the period between 10:50:00 and 10:54:59, and for monitoring location 2, values are from the period between 11:04:06 and 11:09:05.

Table 4.21: An overview of DMS concentrations at both monitoring locations for the 5-minute period between 10:50:00 and 10:59:59 at monitoring location 1 and between 11:04:06 and 11:14:05 at monitoring location 2 at stage two.

STAGE TWO - 10 MINUTES	DMS 1 [ppm]	DMS 2 [ppm]	DMS1-DMS2 [ppm]
MAX	10.159	8.889	1.380
AVERAGE	10.115	8.832	1.282
MIN	10.055	8.779	1.264
STD. DEV.	0.049	0.051	0.027

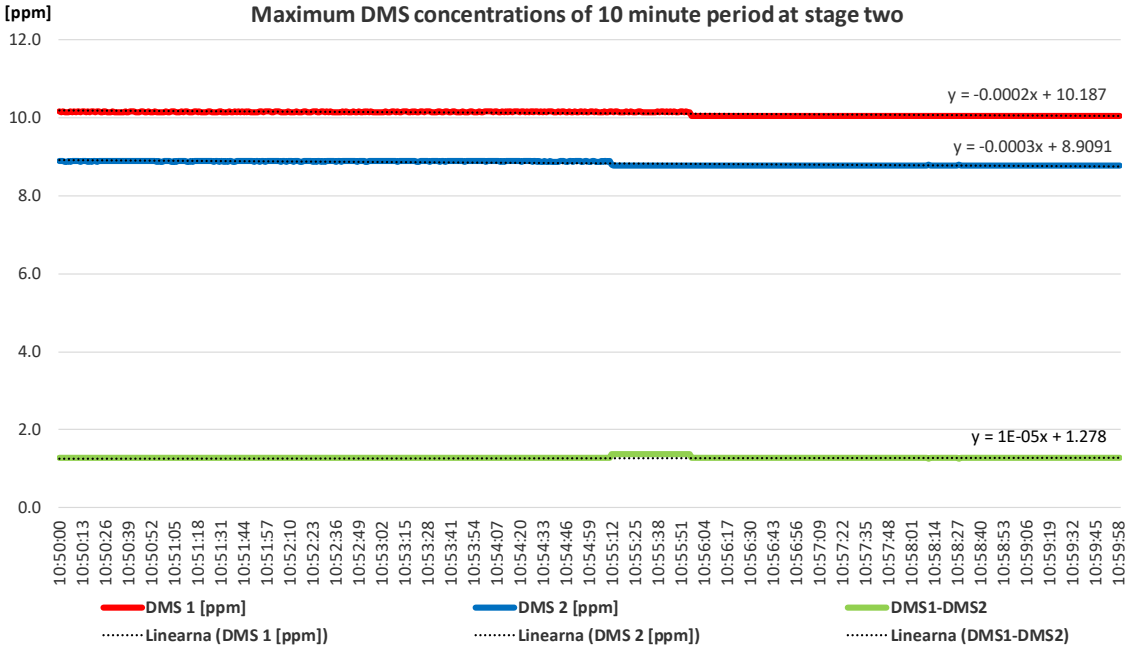

Figure 4.29: Comparison of DMS concentration differences at both locations in the 10-minute period at stage two. Measured values of DMS 2 sensor were moved back regarding measured values of DMS 1 sensors for the time of DMS travel, for 846 seconds (14 minutes and 6 seconds). For monitoring location 1, values are from the period between 10:50:00 and 10:59:59, and for monitoring location 2, values are from the period between 11:04:06 and 11:14:05.

Review of DMS concentrations and airflow velocities at monitoring location 1 during stage two of the experiment (

Figure 4.30) show that conditions were not particularly steady because of airflow velocity changes, which are in an inverse relationship with DMS concentrations.

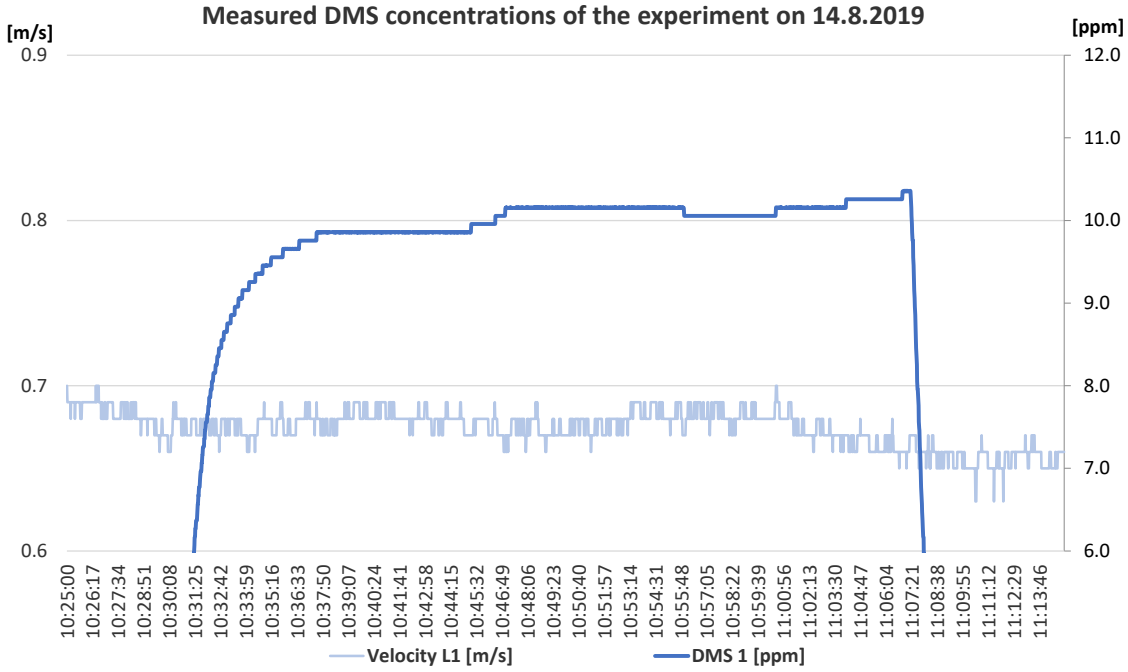

Figure 4.30: DMS concentrations and airflow velocities at monitoring location 1 during stage two of the experiment.

Comparison of DMS concentrations at both locations is shown in Figure 4.31 where the measured values of DMS 2 sensor were moved back regarding measured values of DMS 1 sensors for the time of DMS travel, for 14 minutes and 6 seconds. At the range of maximum DMS concentrations both measured value sets form a similar shape. Which means that both DMS sensors were detecting small changes of DMS concentrations in the airflow, which are dependent on airflow rate changes (airflow velocity changes) at the point of DMS dosing.

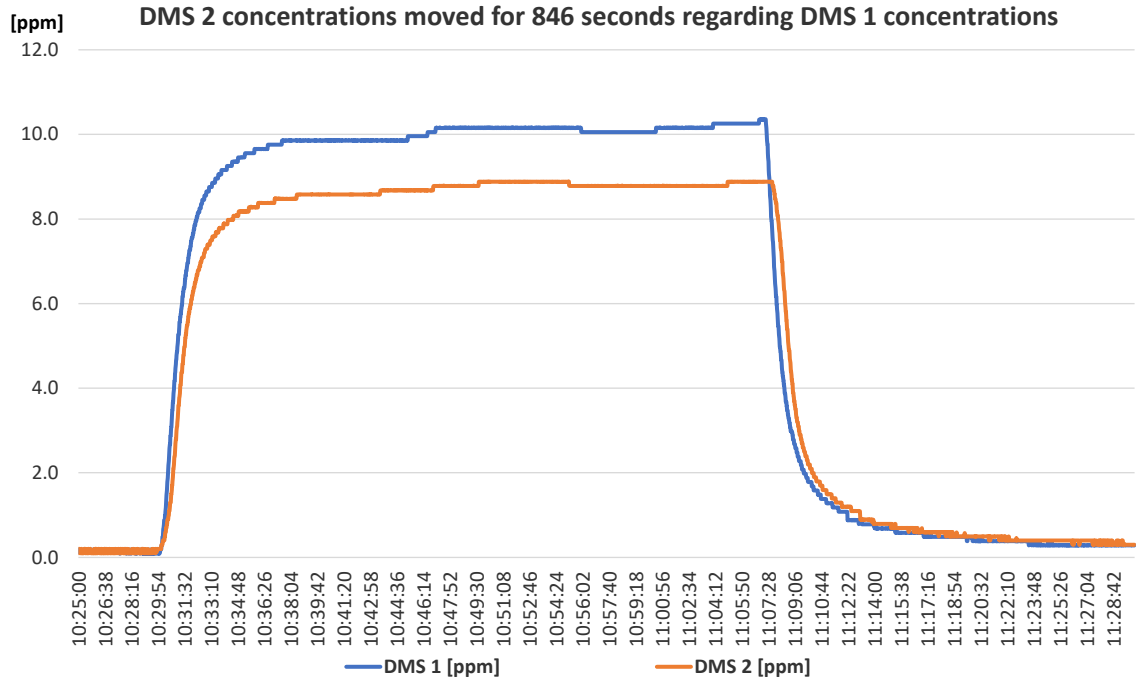

Figure 4.31: Comparison of DMS concentrations at both locations. Measured values of DMS 2 sensor were moved back regarding measured values of DMS 1 sensors for the time of DMS travel, for 846 seconds (14 minutes and 6 seconds).

The calculation results of volume flow, mass flows (apparent and actual) and DMS mass flow on both monitoring locations during the 10-minute period (same period as was inspected for differences of DMS concentrations), and their losses on the way from monitoring location 1 to monitoring location 2 are shown in Table 5.37.

For the calculation of DMS mass flow, average DMS concentrations of the 10-minute period were considered and for the conversion from DMS concentration in ppm to mg of DMS, 1 ppm = 2.583 mg/m^3 was considered.

Table 4.22: The calculation results of volume flow, mass flows (apparent and actual) and DMS mass flow at both monitoring locations during the 10-minute period, and their losses on the way from monitoring location 1 to monitoring location 2.

10-minute period	Volume flow [m^3/s]	Mass flow (apparent) [kg of dry air]	Mass flow (actual) [kg of moist air]	DMS [mg]
SUM Location 1	115.4	135.5	136.9	2777
SUM Location 2	97.0	113.8	114.9	2333
Losses [%]	16.0	16.0	16.0	16.0

Table 4.23: The calculation results of DMS mass flow from the cylinder in the 10-minute period, at flow velocity from the tube connected to the cylinder 20 m/s.

DMS mass flow from tube conected to the cylinder in 10-minute period	
Diamater [m]	0.0075
Cross section [m^2]	0.0000442
Flow velocity [m/s]	**20**
Flow rate [m^3/s]	0.000884
DMS in cylinder [ppm]	2000
Conversion factor: 1ppm=2.58 mg/m^3	
Calculated DMS mass flow from the cylinder [mg]	**2735**

In Table 20, calculated results in MS Excel of DMS mass flow from the cylinder in the 10-minute period are presented. The comparison of DMS mass flows from the cylinder and in the ducting at monitoring location 1 shows 1.5% difference.

From the results of mine experiments (first and second stage) it can be concluded:

- *The monitoring results of airflow velocities show that significant differences between measurements may arise. In the first experiment where two anemometers per location were available, at location 2 the average velocity difference was 0.05 m/s or 8.2 %, respectively. There are many reasons that can lead to such inaccuracy. Such measurements, when sensors are inserted in the duct, are especially demanding regarding positioning. And anemometers of all sensors used in the experiment are the most sensitive to the positioning in the duct. They must be positioned perpendicular to the airflow and in the centre of the cross section, as the velocity is not uniform across the cross section. The velocity is the highest at the centre and the lowest at the sides where the air is slowed down by friction. The accuracy of volume flow and mass flow thus depends on the accuracy of measured airflow velocity.*

- *The monitoring results of DMS concentrations of the second experiment and their differences show that DMS concentrations can be considered as identical at both monitoring locations. At the most steady conditions, at stage one, when both DMS sensors were at location 1, the average concentration of DMS1 sensor was 10.156 ppm, average concentration of DMS2 sensor was 8.881 and average difference DMS1 – DMS2 was 1.275 ppm. At the most steady conditions, at stage two, after DMS2 sensor was moved at location 2, the average concentration of DMS1 sensor was 10.155 ppm, average concentration of DMS2 sensor was 8.881 ppm and average difference DMS1 – DMS was 1.274 ppm.*

- *Modelling of traveling times from the longwall faces to the surface with the Ventsim Visual software (for airflows as in October 2012) shows that DMS is traveling from the longwall faces to the surface between 556 to 750 seconds.*

- *Traveling time of DMS from location 1 to location 2, based on the start of DMS detection at both locations, was at the first experiment 827 seconds and at the second experiment it was 846 seconds.*

- *From the monitoring results of DMS concentrations of the second experiment and their differences, and from DMS traveling time in the second experiment, it can be concluded that DMS is stable in the mine air and is not decaying for at least 846 seconds.*

4.4 Simulations in the Ventilation/Odour Model

4.4.1 Dispersion analysis of DMS from the odour sources

In this study of DMS dispersion from the odour sources through the return airways and to the surface dispersion characteristics of DMS was analysed. The analysis is based on topography and topology of CMV ventilation network and simulation results of CMV ventilation model in Ventsim^{TM}: DMS concentrations, spread times of DMS from the sources, airflow rates, airflow speeds.

Longwall faces

The **longwall face k.-130/B** is considered as a major potential odour source in the Preloge pit in relation to DMS concentrations and airflow rates. Regarding ventilation longwall face was considered as the critical point (bottle neck) of ventilation in the Preloge pit. For the analysis of dispersion characteristics we used three simulation scenarios with different fan blade settings: position for maximum airflow capacity (+10°), position for minimum airflow capacity (-10°) and fixed flow for the situation as in October 2012 (+1°). The DMS source was determined for each simulation according to the average values from DMS monitoring.

The dispersion characteristics from the source in the mine are besides the source characteristics mainly dependent on the topography and topology of ventilation network and its ventilation regulation. Figure 4.32 and Figure 4.33 show the topology of dispersion of gases from the longwall face k.-130/B to the surface. The numbers present the sequence of dilutions, separation and combining of the airways in which the DMS was detected accordingly to the simulation. The dilutions and mixing in the direction of airflow was on every junction of airways at which follows additional dilution and/or mixing.

Table 4.24: Dispersion characteristics of DMS from longwall face k.-130/B and to the surface: DMS concentrations in airways in relation to sequence of dilutions and regulation of the Šoštanj ventilation station (angle of fan's blades).

Dispersion characteristics of odour source from longwall face k.-130/B in Preloge Pit																	
Ventilator blades set on -10°						Ventilator blades set on + 1° (fixflow)						Ventilator blades set on + 10°					
Sequence of dilutions		Cross connections		DMS [mg/ m^3]		Sequence of dilutions		Cross connections		DMS [mg/ m^3]		Sequence of dilutions		Cross connections		DMS [mg/ m^3]	
1				18.86		1				14.21		1				12.14	
2				14.46		2				11.37		2				10.07	
3				13.69		3				10.59		3				9.30	
4				13.69		4				10.33		4				8.78	
5				10.07		5				8.01		5				6.97	
6				9.04		6				7.23		6				6.20	
7				8.27		7				6.46		7				5.68	
8				7.75		8				5.94		8				5.17	
9				6.20		9				4.91		9				4.39	
10				5.42		10				4.39		10				3.87	
11a	5.42					11a	4.13					11a	3.62				
12a	4.13					12a	3.10					12a	2.84				
13a	3.87	13a-11b	3.62	11b	5.42	13a	3.10	13a-11b	3.10	11b	4.13	13a	2.84	13a-11b	2.84	11b	2.58
14a	3.62			12b	4.39	14a	2.84			12b	3.62	14a	2.58			12b	3.10
15a	3.36					15a	2.58					15a	2.32				
16a	2.84	16a-13b	2.84	13b	4.13	16a	2.32	16a-13b	2.32	13b	3.10	16a	2.07	16a-13b	2.32	13b	2.84
17a	2.84			14b	3.87	17a	2.32			14b	3.10	17a	2.07			14b	2.84
18a	1.29	18a-15b	1.29	15b	3.87	18a	1.03	18a-15b	1.03	15b	3.10	18a	1.03	18a-15b	1.03	15b	2.58
19a	1.29					19a	1.03					19a	1.03				
20a	0.52	20a-16b	0.52	16b	3.62	20a	0.52	20a-16b	0.52	16b	2.84	20a	0.52	20a-16b	0.52	16b	2.58
21a	0.52	21a-17b	0.52	17b	3.10	21a	0.52	21a-17b	0.52	17b	2.58	21a	0.52	21a-17b	0.52	17b	2.32
22		0.52/ 3.10				22		0.52/ 2.58				22		0.52/ 0.2.07			
23		1.81				23		1.55				23		1.29			

Table 4.25: Dispersion characteristics of DMS from longwall face k.-130/B and to the surface: traveling times at junctions in relation to regulation of the Šoštanj ventilation station (angle of fan's blades).

Dispersion characteristics of odour source from longwall face k.-130/B in Preloge Pit																			
Ventilator blades set on -10°						Ventilator blades set on + 1° (fixflow)						Ventilator blades set on + 10°							
Sequence of dilutions		Cross connections		Spread time [s]		Sequence of dilutions		Cross connections		Spread time [s]		Sequence of dilutions		Cross connections		Spread time [s]			
1				49		1				35		1				30			
2				146		2				110		2				96			
3				190		3				144		3				123			
4				243		4				182		4				159			
5				297		5				223		5				194			
6				324		6				243		6				212			
7				347		7				260		7				227			
8				357		8				268		8				234			
9				365		9				274		9				239			
10				391		10				294		10				256			
11a	447					11a	336					11a	293						
12a	459					12a	372					12a	324						
13a	513	13a-11b	528	11b	590	13a	385	13a-11b	396	11b	471	13a	336	13a-11b	346	11b	411		
14a	539			12b	541	14a	438			12b	407	14a	382			12b	355		
15a	587					15a	444					15a	383						
16a	635	16a-13b	700	13b	562	16a	477	16a-13b	538	13b	423	16a	417	16a-13b	472	13b	369		
17a	664			14b	573	17a	499			14b	431	17a	436			14b	376		
18a	692	18a-15b	739	15b	600	18a	521	18a-15b	559	15b	452	18a	455	18a-15b	489	15b	395		
19a	732					19a	552					19a	483						
20a	764	20a-16b	829	16b	659	20a	577	20a-16b	629	16b	498	20a	505	20a-16b	550	16b	436		
21a	798	21a-17b	903	17b	698	21a	604	21a-17b	686	17b	528	21a	528	21a-17b	601	17b	462		
22		704/ 805				22		610/ 533				22		532/ 467					
23		733				23		556				23		487					

Table 4.26: Characteristic lengths of DMS dispersion path from longwall face k.-130/B and to the surface.

Sequence of dilutions	Lengths [m]
1-10	1211.7
10-13a	492.0
13a-11b	51.9
11b-22	1262.8
17b-22	52.9
22-23	235.9
10-11b	541.6
13a-22	1425.6
21a-22	60.5
16a-13b	45.4
18a-15b	49.9
20a-16b	56.0
21a-17b	45.2
Fastest	**3254.3**
Slowest	**3402.8**

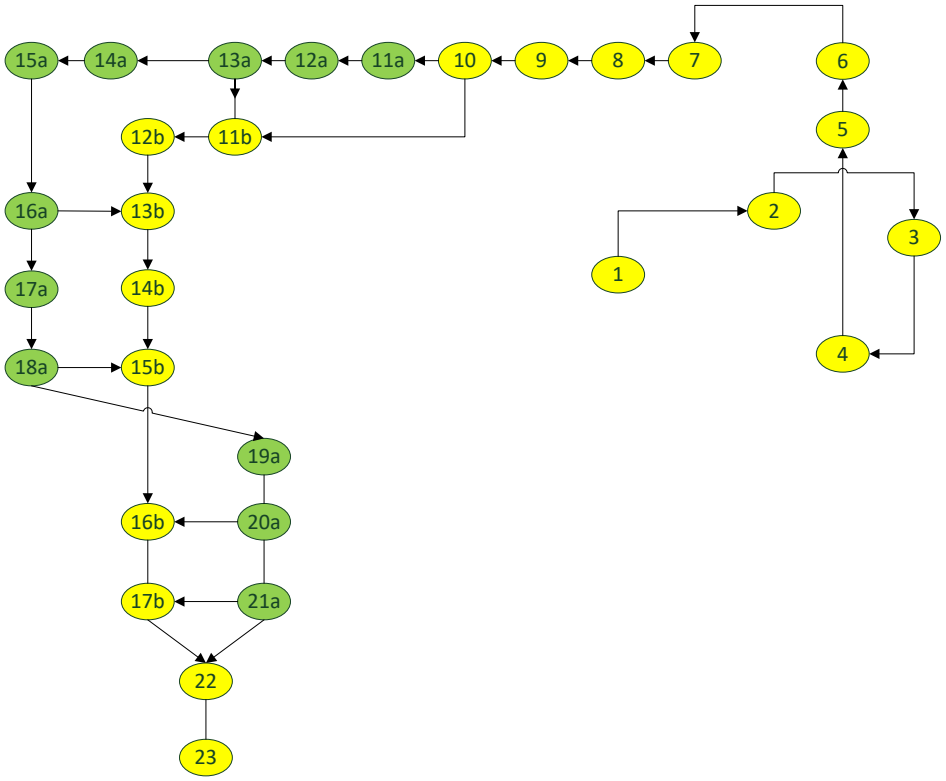

Figure 4.32: The topology of dispersion characteristics from longwall face k.-130/B: the path of the highest DMS concentrations is marked with yellow and lower concentrations with green.

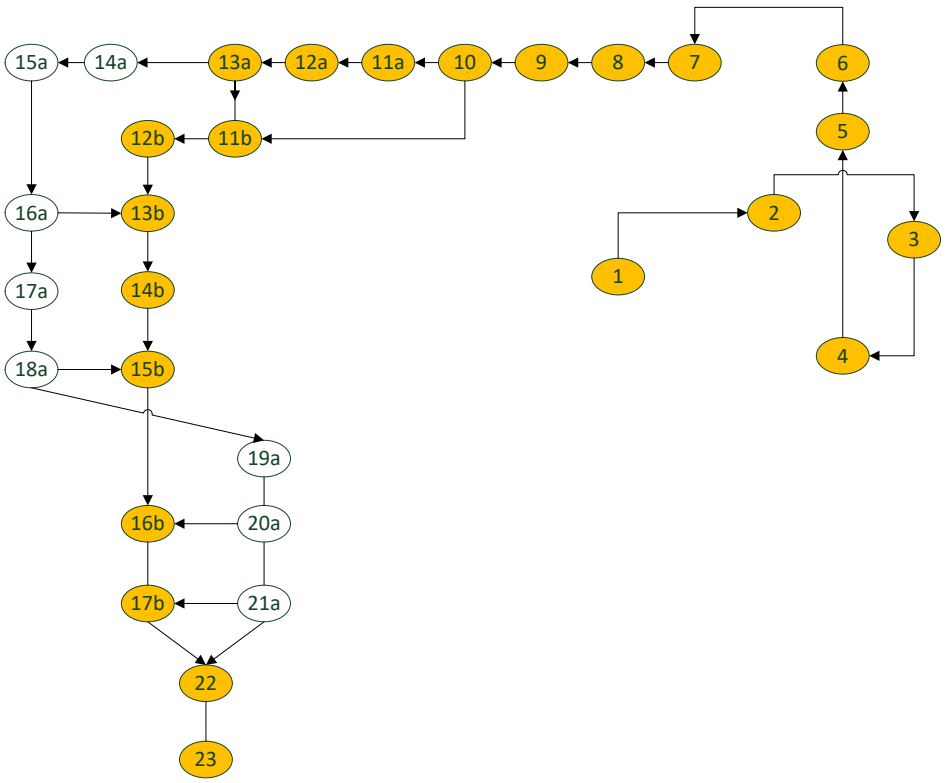

Figure 4.33: The topology of dispersion characteristics from longwall face k.-130/B: the fastest path of DMS dispersion (orange).

Figure 4.32 and Figure 4.33 show that airflow from the longwall face k.-130/B was divided in two branches “a” and “b” in point “10” and merged back in point “22”.

Figure 4.32 shows dispersion path of DMS highest concentrations (yellow colour) and lower concentrations (green colour). Before branches were merged back in point “22”, the DMS concentration in branch “a” was 4 to 6 times smaller than in branch “b”.

In terms of quality of dilution, the DMS concentration was approx. halved at point “6” (50 % of source concentration) and then again at points “12a” and “12b” (75% of source concentration).

Table 4.25 shows the traveling (spread) times of DMS dispersion from the longwall face to the surface. Table 4.26 shows the characteristic lengths of DMS dispersion paths. Figure 4.33 shows the topology of the fastest path of DMS dispersion from the longwall face to the surface in terms of traveling (spread) times (orange colour). The fastest traveling times were between 487 and 733 s and the slowest spread times were between 626 and 938 s.

The **longwall face k.-65/A** was recognized as a major odour source in the Pesje pit in relation to DMS concentrations and airflow rates. Regarding ventilation longwall face was considered as the critical point (bottle neck) of ventilation in the Pesje pit. For the analysis of dispersion characteristics three simulation scenarios with different fan blade settings were used: position for maximum airflow capacity (+10°), position for minimum airflow capacity (-10°) and fixed flow for situation as in October 2012 (+1°). The DMS source was determined for each simulation according to the average values from DMS monitoring.

Figure 4.34 and Figure 4.35 show the topology of dispersion of DMS from the longwall face k.-65/A. The numbers present the sequence of dilutions, separation and combining the airways in which the DMS was detected according to the simulations. The dilutions and mixing in the direction of airflow was on every junction of airways.

Table 4.27: Dispersion characteristics of DMS from longwall face k.-65/A and to surface: DMS concentrations in airways in relation to the sequence of dilutions and regulation of the Šoštanj ventilation station (angle of ventilator’s blades).

Dispersion of odour source from longwall face k.-65/A in Pesje Pit																	
Fan blades set on -10°						Fan blades set on + 1° (fixflow)						Fan blades set on + 10°					
Sequence of dilutions		Cross connections		DMS [mg/m³]		Sequence of dilutions		Cross connections		DMS [mg/m³]		Sequence of dilutions		Cross connections		DMS [mg/m³]	
1				19.6		1				10.6		1				7.7	
2				14.5		2				8.5		2				6.7	
3				13.7		3				8.0		3				6.5	
4				11.9		4				7.0		4				5.4	
5				11.9		5				6.5		5				4.9	
6				11.4		6				6.2		6				4.6	
7				10.6		7				5.9		7				4.6	
8a	10.59			8b		8a	5.94			8b	5.94	8a	4.65			8b	4.65
9a	9.56	9a-10c	9.82	9b	0.27	9a	5.68	9a-10c	5.68	9b	1.03	9a	4.39	9a-10c	4.39	9b	0.77
10a	9.56			10b	0.27	10a	5.68			10b	1.03	10a	4.39			10b	0.77
		10c-11b	9.04					10c-11b	5.17					10c-11b	3.87		
11a	9.30			11b	1.81	11a	5.42			11b	0.77	11a	4.13			11b	0.52
12a	7.23			12b	5.68	12a	4.91			12b	3.10	12a	3.87			12b	2.32
				13b	5.68					13b	3.10					13b	2.32
14			5.94/5.42			14			3.87/2.84			14			3.10/2.07		
15			5.68			15			3.36			15			2.58		

Table 4.28: Dispersion characteristics of DMS from longwall face k.-130/B and to surface: traveling times at the points of dilutions in relation to the regulation of the Šoštanj ventilation station (angle of fan's blades).

Dispersion of odour source from longwall face k.-65/ A in Pesje Pit																		
Fan blades set on -10°						Fan blades set on + 1° (fixflow)						Fan blades set on + 10°						
Sequence of dilutions		Cross connections		Spread time [s]		Sequence of dilutions		Cross connections		Spread time [s]		Sequence of dilutions		Cross connections		Spread time [s]		
1				79		1				43		1				32		
2				186		2				110		2				84		
3				318		3				192		3				148		
4				353		4				213		4				465		
5				466		5				276		5				212		
6				538		6				316		6				242		
7				559		7				327		7				251		
8a	604			8b	648	8a	353			8b	386	8a	270			8b	297	
9a	649	9a-10c	655	9b	726	9a	380	9a-10c	384	9b	483	9a	290	9a-10c	293	9b	333	
10a	1086			10b	952	10a	624			10b	562	10a	474			10b	431	
		10c-11b	701					10c-11b	399					10c-11b	315			
11a	1186			11b	991	11a	679			11b	584	11a	516			11b	447	
12a	1226			12b	794	12a	703			12b	467	12a	534			12b	358	
				13b	1001					13b	589					13b	451	
14		1282/ 1012				14		737/ 595				14		561/ 456				
15		1035				15		608				15		466				

Table 4.29: Characteristic lengths of dispersion path of DMS from longwall face k.-65/A and to surface.

Sequence of dilutions	Lengths [m]
1-7	1332.5
7-9a	282.4
9a-11b	96.9
11b-14	944.1
14-15	136.5
7-11b	590.3
9a-14	1291.7
Fastest	**2792.4**
Slowest	**3003.4**

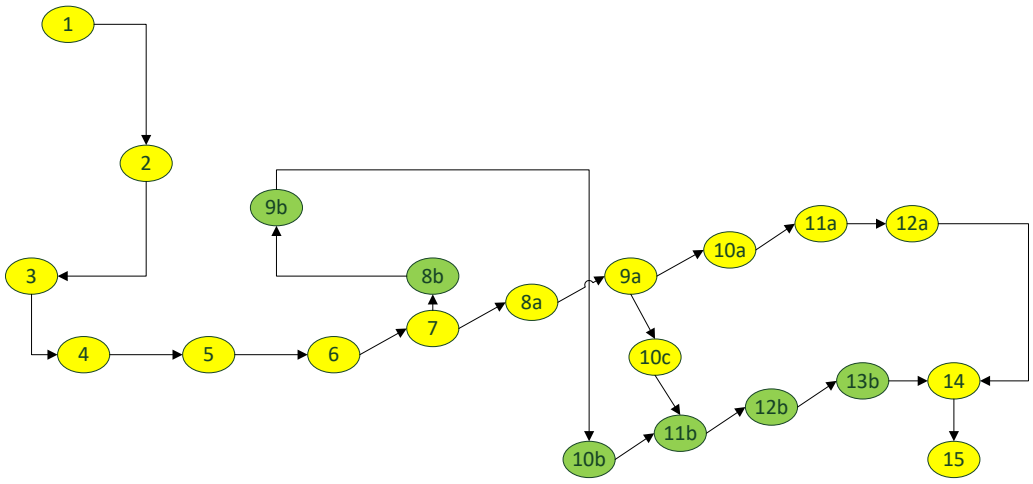

Figure 4.34: The topology of dispersion characteristics from longwall face k.-65/A: the paths of the highest DMS concentrations are marked with yellow and lower concentrations with green.

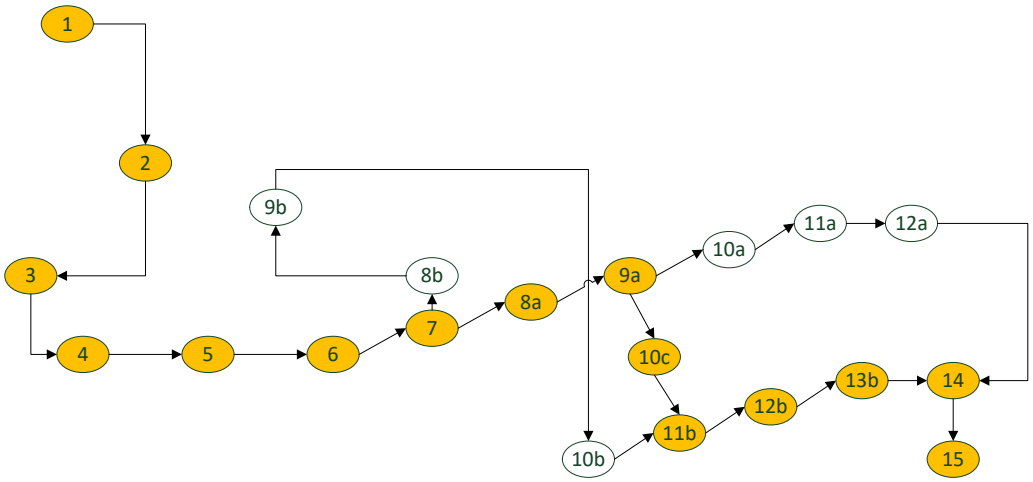

Figure 4.35: The topology of dispersion characteristics from longwall face k.-65/A: the fastest path of DMS dispersion (orange).

Table 4.27 and Table 4.28 show the main simulation results in relation to dispersion characteristics at different regulation settings of the Pesje ventilation station.

Figure 4.34 and Figure 4.35 show that airflow from the longwall k.-65/A was divided in two branches “a” and “b” in point “7” (between 3.2 and 3.6 % of total airflow capacity at the Pesje ventilation station) and were joined in point “14”. In between the division and the merger there was one cross connection (9a-10c-11b) whereby the airflow was directed from branch “a” to branch “b”: the DMS was directed from “a” to “b” (between 1.6 ppm and 3.5 ppm and airflows between 25.0 and 26.3 % of total airflow capacity at the Pesje ventilation station).

Figure 4.34 shows dispersion path of DMS highest concentrations (yellow colour) and lower concentrations (green colour). The concentrations were lower in branch “b” because of dilution with airflow without DMS until the cross connection in point “11b” where the part of branch “a” was joined. In terms of quality of DMS concentration dilution until point “7” the concentrations were between 54 and 60 % of the source. In branch “b” until point “11b” the concentrations decreased between 6.7 and 9.2 % of the source. DMS concentrations in the ventilation station were between 28.9 and 33.3 % of the source.

Table 4.28 shows the traveling (spread) times of DMS dispersion from the longwall face to the surface. Table 4.29 shows the characteristic lengths of DMS dispersion paths. Figure 4.35 shows the fastest path (orange colour).

The fastest traveling times were between 466 and 1035 s and the slowest spread times were between 698 and 1325 s.

Development headings

The gateroads are usually built in the coal seam. In October 2012, all six development headings were building gateroads and gateways in the coal seam and all six development headings 4, 6, 7, 8, 11 and 13 were recognized as a protentional odour source (locations are shown in Figure 3.19, see Chapter 3.4). The specific development heading was considered as a smaller source in relation to the longwall face. Coal production calculated from the daily advances and gateroad's cross-sections varied between 150 and 240 t/day and airflow rates of auxiliary fans varied between 3.5 and 9.2 m^3/s.

Table 4.30 to Table 4.35 show the simulations results of DMS dispersion from the source and to the surface at different regulations of fan's blades of ventilation stations Šoštanj and Pesje. Presented are characteristic DMS concentrations and airflow rates on the source, at the end of auxiliary ventilation and on the ventilation stations and characteristic fastest traveling times at the end of auxiliary ventilation and when emitted on the surface. For the analysis of dispersion characteristics three simulation scenarios were used with different fan blade settings: position for maximum airflow capacity (+10°/+2°), position for minimum airflow capacity ((-10°/-20°) and fixed flows for the situation as in October 2012 (+1°/-11°).

The DMS source was fixed at 25.83 mg/m^3 for all six development faces. The fixed concentration of DMS was selected for a more transparent comparison between development faces. Airflow rates of the development faces were fixed in the model.

Table 4.30: Simulation results of dispersion characteristics from development face "number 7" to the surface in relation to the regulation of ventilation stations Šoštanj and Pesje.

Development heading »number 7«				
Regulation of main fan's blades: Šoštanj/Pesje		-10°/-20°	Fixed(+1°)/ Fixed(-11°)	+10°/+2°
DMS [mg/m³]	Source	25.8	25.8	25.8
	End of auxiliary ventilation	9.6	5.2	3.9
	Ventilation station Pesje	2.8	1.8	1.3
Airflow rate [m³/s]	Source	7.8	7.8	7.8
	End of auxiliary ventilation	21.2	40.1	53.9
	Ventilation station Pesje	71.2	119.2	154.1
Dilution ratio	End of auxiliary ventilation	2.7	5.1	6.9
	Ventilation station Pesje	9.1	15.2	19.7
Traveling time [s]	End of auxiliary ventilation	1119	1119	1119
	Ventilation station Pesje	2367	1836	1668

Table 4.31: Simulation results of dispersion characteristics from development face “number 4” to the surface in relation to the regulation of ventilation stations Šoštanj and Pesje.

Development heading »number 4«				
Regulation of main ventilator's blades: Šoštanj/Pesje		-10°/-20°	Fixed(+1°)/ Fixed(-11°)	+10°/+2°
DMS [mg/m³]	Source	25.8	25.8	25.8
	End of auxiliary ventilation	10.3	7.7	6.7
	Ventilation station Šoštanj	0.5	0.3	0.3
Airflow rate [m³/s]	Source	3.5	3.5	3.5
	End of auxiliary ventilation	8.7	11.6	13.3
	Ventilation station Šoštanj	206.6	263.7	296.1
Dilution ratio	End of auxiliary ventilation	2.5	3.3	3.8
	Ventilation station Šoštanj	59.0	75.3	84.6
Spread time [s]	End of auxiliary ventilation	190	190	190
	Ventilation station Šoštanj	1030	827	751

Table 4.32: Simulation results of dispersion characteristics from development face “number 6” to the surface in relation to the regulation of ventilation stations Šoštanj and Pesje.

Development heading »number 6«				
Regulation of main ventilator's blades: Šoštanj/Pesje		-10°/-20°	Fixed(+1°)/ Fixed(-11°)	+10°/+2°
DMS [mg/m³]	Source	25.8	25.8	25.8
	End of auxiliary ventilation	8.8	7.0	6.2
	Ventilation station Šoštanj	0.8	0.8	0.5
Airflow rate [m³/s]	Source	6.7	6.7	6.7
	End of auxiliary ventilation	19.9	25.0	28.0
	Ventilation station Šoštanj	206.6	263.7	296.1
Dilution ratio	End of auxiliary ventilation	3.0	3.8	4.2
	Ventilation station Šoštanj	31.0	39.6	44.4
Spread time [s]	End of auxiliary ventilation	157	157	157
	Ventilation station Šoštanj	932	750	680

Table 4.33: Simulation results of dispersion characteristics from development face “number 8” to the surface in relation to the regulation of ventilation stations Šoštanj and Pesje.

Development heading »number 8«				
Regulation of main ventilator's blades: Šoštanj/Pesje		-10°/-20°	Fixed(+1°)/ Fixed(-11°)	+10°/+2°
DMS [mg/m³]	Source	25.8	25.8	25.8
	End of auxiliary ventilation	9.3	7.2	6.5
	Ventilation station Šoštanj	0.8	0.5	0.5
Airflow rate [m³/s]	Source	6.0	6.0	6.0
	End of auxiliary ventilation	16.8	21.1	23.6
	Ventilation station Šoštanj	206.6	263.7	296.1
Dilution ratio	End of auxiliary ventilation	2.8	3.5	3.9
	Ventilation station Šoštanj	34.4	43.9	49.4
Spread time [s]	End of auxiliary ventilation	490	490	490
	Ventilation station Šoštanj	1071	937	885

Table 4.34: Simulation results of dispersion characteristics from development face “number 11” to the surface in relation to the regulation of ventilation stations Šoštanj and Pesje.

Development heading »number 11«				
Regulation of main ventilator's blades: Šoštanj/Pesje		-10°/-20°	Fixed(+1°)/ Fixed(-11°)	+10°/+2°
DMS [mg/m³]	Source	25.8	25.8	25.8
	End of auxiliary ventilation	2.1	1.5	1.5
	Ventilation station Šoštanj	0.8	0.5	0.5
Airflow rate [m³/s]	Source	5.8	5.8	5.8
	End of auxiliary ventilation	70.3	92.3	104.8
	Ventilation station Šoštanj	206.6	263.7	296.1
Dilution ratio	End of auxiliary ventilation	12.0	15.8	18.0
	Ventilation station Šoštanj	35.4	45.2	50.8
Spread time [s]	End of auxiliary ventilation	1239	1239	1239
	Ventilation station Šoštanj	1610	1526	1493

Table 4.35: Simulation results of dispersion characteristics from development face “number 13” to the surface in relation to the regulation of ventilation stations Šoštanj and Pesje.

Development heading »number 13«				
Regulation of main ventilator's blades: Šoštanj/Pesje		-10°/-20°	Fixed(+1°)/ Fixed(-11°)	+10°/+2°
DMS [mg/m³]	Source	25.8	25.8	25.8
	End of auxiliary ventilation	23.8	18.1	16.8
	Ventilation station Šoštanj	1.0	0.8	0.8
Airflow rate [m³/s]	Source	9.2	9.2	9.2
	End of auxiliary ventilation	11.8	13.2	14.0
	Ventilation station Šoštanj	206.6	263.7	296.1
Dilution ratio	End of auxiliary ventilation	1.3	1.4	1.5
	Ventilation station Šoštanj	22.5	28.8	32.3
Spread time [s]	End of auxiliary ventilation	1279	1279	1279
	Ventilation station Šoštanj	1897	1739	1680

The simulation results presented in tables from 32 to 37 show that:

- *The development headings are smaller sources of DMS in comparison to longwall faces in relation to values of DMS concentration and airflow rates.*
- *All development headings except Num. 7 were diluted with the Šoštanj ventilation station.*
- *The dilution ratios of DMS sources at the ventilation stations of all scenarios were between 9.1 and 84.6.*
- *Ventilation of development headings can be subject to airflow recirculation at lower airflow rates of ventilation stations as in the case of Num. 13 at minimum main ventilators setup -10°/-20° when the ventilation was not sufficient and caused that auxiliary fan was also sucking air from the airflow that came from the development face. Because of that, DMS concentration on the development heading increased from 10 to 11.8 ppm.*
- *The traveling (spread) times from the development headings were between 680 and 2367 s. The traveling times were longer between 234 and 1333 s than of longwall face k.-65/A and between 193 and 1637 s longer than on longwall face k.-130/B. Due to the practically the same cross-section of airways and lower auxiliary ventilation flow rates than at flow through ventilation, the airflow velocities in airways were between 0.4 and 0.7 m/s. The air from development faces travelled in the airways with auxiliary ventilation between 16.8 and 83.0 % of total traveling times to the surface.*

Main coal transport

The main coal transport system consists of 6 successive rubber conveyors which transport the whole coal production to the surface (Figure 4.36). The total length of conveyors is 2605 m (Table 4.36). According to the monthly measurements, the DMS were still desorbed from the transported coal along the entire length (see Chapter 4.1).

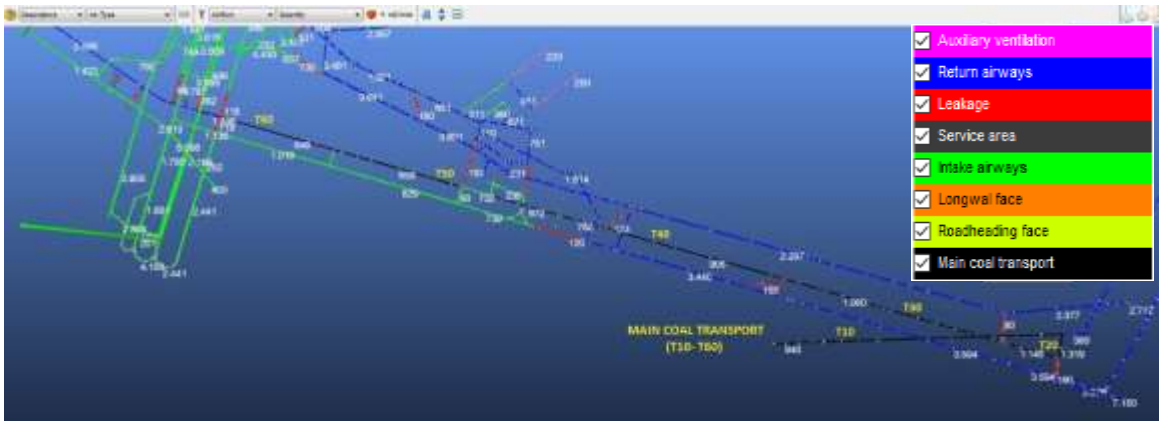

Figure 4.36: Main coal transport with a system of six rubber conveyors (T10-T60) with modelled airflows.

The main coal transport system was recognized as the most complex potential odour source because DMS is released while the coal is being transported to the surface and due to the topology of the source as shown in Figure 4.37. In relation to ventilation the main coal transport has 11 junctions and connection to the surface (»0« in Figure 4.37) of which 5 dilutions are at junctions and intake on the surface (red colour) with air of no DMS and 6 divisions of airflow (blue colour) which are connected with the main return airways of the Pesje pit (»P«). The airflow from the junction »11« is directed to the Šoštanj ventilation station and is further diluted in junctions of main return airways of the Preloge pit (»Š«).

The main influences on the odour intensity/DMS content (releasing intensity) is the amount of coal on the conveyors and ventilation capacities.

Table 4.36: Lengths and transport velocities of conveyors of the main coal transport system.

Main coal transport system		
Conveyor name	Length [m]	Velocity [m/s]
T10	657	3.29
T20	50	3.32
T30	543	3.05
T40	470	3.05
T50	600	3.05
T60	285	3.05
SUM/AVERAGE	2605	3.14

Source dispersion characteristics in Figure 4.37 show the dispersion complexity of the source. The source is being dispersed through the junctions to the returns of both ventilation stations. For a detailed analysis of source dispersion of the main coal transport, the ventilation/odour model was used. For the source dispersion, the length of the main coal transport was considered in a way that the whole source from the main coal transport was divided to sources of individual parts of airways accordingly to their lengths (Table 4.37). Due to the model characteristics each airway is divided into individual parts.

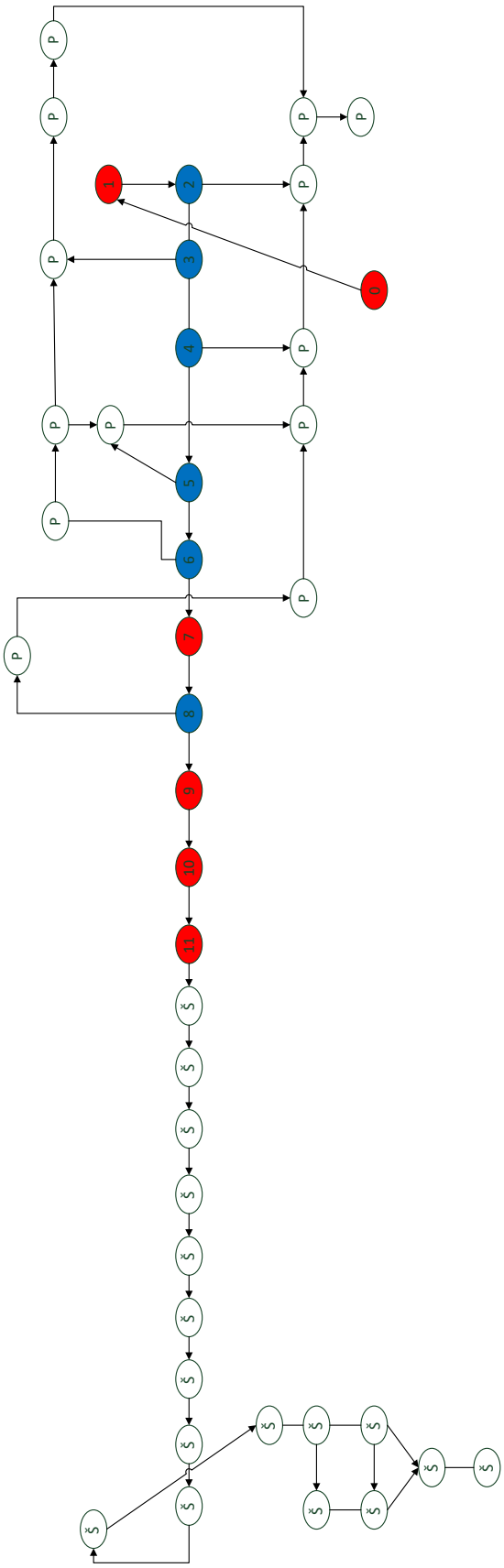

Figure 4.37: The dispersion topology of the main coal transport potential DMS (odour) source.

Table 4.37: Division of the main coal transport contaminant source for the simulation of dispersion in the model.

Lengths in the model [m]	Source adjusted to lenght [mg/s]	Airflow rate [m^3/s]	Concentration at the source [mg/m^3]
42.1	16,168.7	15.7	1,033.1
24.5	9,409.3	15.7	601.2
23.8	9,140.5	15.7	584.1
29	11,137.6	15.7	711.7
60	23,043.2	15.7	1,472.4
125.4	48,160.4	15.7	3,077.3
39.6	15,208.5	15.7	971.8
88.6	34,027.2	15.7	2,174.3
120.6	46,316.9	15.7	2,959.5
60.2	23,120.1	15.7	1,477.3
7.2	2,765.2	15.7	176.7
47.7	18,319.4	22.0	833.3
8	3,072.4	19.0	161.7
41.9	16,091.9	19.0	846.9
37.7	14,478.8	19.0	762.0
17.3	6,644.1	19.0	349.7
5.6	2,150.7	17.7	121.7
18.4	7,066.6	17.7	400.0
31.1	11,944.1	17.7	676.1
45.7	17,551.3	17.7	993.5
37.4	14,363.6	17.7	813.0
38.1	14,632.5	17.7	828.3
53.6	20,585.3	17.7	1,165.2
11.6	4,455.0	17.7	252.2
34.8	13,365.1	17.7	756.5
55.6	21,353.4	17.7	1,208.7
36.6	14,056.4	17.7	795.6
55.4	21,276.6	17.7	1,204.3
24.8	9,524.5	17.7	539.1
27.2	10,446.3	15.1	692.6
139.8	53,690.8	15.1	3,559.6
70	26,883.8	15.1	1,782.4
40.7	15,631.0	15.1	1,036.3
99.9	38,367.0	15.1	2,543.7
8.1	3,110.8	15.1	206.2
39.5	15,170.1	13.0	1,163.9
8.4	3,226.1	13.0	247.5
48.1	18,473.0	13.0	1,417.4
12.1	4,647.1	13.0	356.6
78.5	30,148.2	11.2	2,691.8
19.9	7,642.7	11.2	682.4
36.6	14,056.4	11.2	1,255.0
23.6	9,063.7	11.2	809.3
13.2	5,069.5	12.2	415.5
20.7	7,949.9	12.2	651.6
30.4	11,675.2	12.2	957.0
10.3	3,955.8	11.0	360.2
56.1	21,545.4	11.0	1,961.6
62.5	24,003.4	11.0	2,185.4
80.3	30,839.5	11.0	2,807.8
32.7	12,558.6	11.0	1,143.4
41.8	16,053.5	11.0	1,461.6
28.4	10,907.1	11.0	993.1
87.8	33,719.9	14.1	2,385.8
95.1	36,523.5	14.1	2,584.2
108.4	41,631.5	14.1	2,945.6
51.1	19,625.2	22.3	882.0
10.3	3,955.8	22.3	177.8
2,603.80	**1,000,000.00**	**SUM**	

For the contaminant source emission in the model 1,000,000.0 mg/s was selected which was divided accordingly to lengths and then concentrations at the sources in the airways were calculated. The simulation of the main coal transport source showed that the concentrations in

the upcast shafts of ventilation stations were 2899.1 mg/m^3 at flowrate 119.2 m^3/s in Pesje and 2487.5 mg/m^3 at flowrate 263.7 m^3/s in Šoštanj. Calculated total emission of both ventilation stations was 1,001,534.1 mg/m^3. The difference between source emission and emissions from the ventilation stations is 0.15 % due to the iterative calculation of the model. The simulation shows that 65.5 % of the main coal transport source is dispersed to the surface through the Šoštanj ventilation station and 34.5 % through the Pesje ventilation station. That means that monthly measurements in the return of the main coal transport measure only 65.5 % of the whole source.

Table 4.38 shows the shares of the whole source of main coal transport that must be considered in the model for the simulation of DMS dispersion. Partial sources of the connections (leakages) between the main coal transport and main returns of Pesje pit represent the part of whole source which is emitted through the Pesje ventilation station. Differences between source emissions of leakages and emissions from the Pesje ventilation station are 0.5 % due to the iterative calculation of the model.

Table 4.38: Shares of the whole source of the main coal transport of the connections (leakages) between the main coal transport and main returns of the Pesje pit.

Num. of leakage	Leakage [m^3/s]	Concentration in the airway of the leakage [mg/m^3]	Emission of the leakage [mg/s]	Share of the total source [%]
1	3.0	11,598.8	34,796.46	3.49
2	1.3	13,719.2	17,834.96	1.79
3	2.6	23,473.5	61,030.97	6.12
4	2.0	33,294.2	66,588.38	6.68
5	4.0	16,607.5	66,430.00	6.66
6	2.7	35,993.1	97,181.26	9.75
SUM			343,862.03	34.50

Table 4.39 and Table 4.40 show the modelling results of scenarios in relation to the angle of the main fans on both ventilation stations. For the contaminant source the single point source at the drive of conveyor T10 was selected (end of coal transport in the mine at the contact at the surface). The single point source was selected to study the traveling times of the contaminant from the source to the surface.

The results show that emissions of contaminants are potentially traveling from the source and to the surface – Šoštanj ventilation station – for the longest time. The traveling times from conveyor T10 varied from 1566 s to 7409 s and from conveyor T60 from 260 s to 417 s (Table 4.39). Analysis of traveling times show that air was traveling the majority of the time through the main coal transport: between 83.4 and 94.4 % of traveling time. While the length of the main coal transport represents 52 % (2605 m) of total traveling length 4995 m to the Šoštanj ventilation station. Traveling times through airways depend on the airway's lengths and airflow velocities in the airways. Traveling times for mine ventilation situation as in October 2012 (fixed/fixed) were from conveyor T10 up to 521 s to the Pesje ventilation station and up to 1923 s to the Šoštanj ventilation station.

Table 4.39: Simulation results of dispersion characteristics from the main coal transport: spread times of DMS from the source and to the surface.

Angle of fan's blades [°]		Main coal transport - traveling (spread) times [s]				
Vent. stat. ŠOŠTANJ	Vent. stat. PESJE	T10	T30	T60	Vent. stat. ŠOŠTANJ	Vent. stat. PESJE
fixed	fixed	339	414	1634	1923	521
+10	fixed	316	367	1306	1566	483
-10	fixed	459	540	3297	3699	623

fixed	**+2**	328	384	1776	2080	452
fixed	**-20**	411	476	1531	1821	726
-10	**+2**	412	489	6992	7409	538
+10	**-20**	339	414	1634	1923	521
-10	**-20**	542	631	2524	2909	827
+10	**+2**	295	344	1384	1650	420

Table 4.40: Simulation results of dispersion characteristics from the main coal transport: characteristic airflows.

Angle of fan's blades [°]		**Main coal transport – airflows [m^3/s]**				
Vent. stat. ŠOŠTANJ	**Vent. stat. PESJE**	**T10**	**T30**	**T60**	**Vent. stat. ŠOŠTANJ**	**Vent. stat. PESJE**
fixed	**fixed**	15.7	19.0	28.3	263.7	119.2
+10	**fixed**	17.7	22.2	35.4	297.8	119.2
-10	**fixed**	12.2	13.6	15.3	205.6	119.2
fixed	**+2**	17.1	19.7	26.7	263.7	154.9
fixed	**-20**	13.6	17.8	30.6	263.7	70.9
-10	**+2**	13.6	14.2	14.4	204.6	156.2
+10	**-20**	15.5	20.8	38.7	300.1	70.5
-10	**-20**	10.3	12.6	18.4	206.6	71.3
+10	**+2**	19.0	22.8	33.4	296.1	154.1

Simulation results of the airflow rates show the regulation capacity of the ventilation network. Regulation capacity regarding the situation as in October 2012 for conveyor T10 is +21.3 % and -41.7 % of 15.7 m^3/s, for conveyor T30 +19.8 % and -43.1 % of 19.0 m^3/s and for conveyor T60 +36.9 % and -59.4 % of 28.3 m^3/s.

If there are no jams or defects on the main coal transport system, according to the characteristics in Table 4.36, the coal travels for 837 seconds or approximately 14 minutes.

4.4.2 Airflow regulation potential of ventilation stations in CMV

The airflow regulation potential with main fans of ventilation stations has a direct effect on the dilution potential of every gas or contaminant source in the mine. In this chapter, airflow changes were simulated and analysed on the longwall faces, in the main coal transport gateroads and in main intakes and returns of air in the CMV while regulating the angles of blades of main fans in ventilation stations Šoštanj and Pesje.

The fixflow setting on ventilation stations represents the ventilation situation in October 2012. The regulation of CMV ventilation is generally optimized for dilution of main coal gases CO_2 and CH_4 on the longwall faces and air exit airways which are "bottle necks" of the ventilation network.

Development faces results (also potential odour sources) are not included because they were ventilated with auxiliary fans with fixed capacities between 3.5 and 9.2 m^3/s (fixflows in the model) and are not affected by the regulation of main fans.

The analysis was done on the basis of 31 simulations results (Table 4.41, Table 4.42 and Table 4.47) in Ventsim^{TM} with the regulation of main fans in the ventilation model. The regulation with auxiliary fans and ventilation objects (e.g., ventilation doors) was not performed because at auxiliary fans actual airflow rates are used (monthly measurements) and ventilation objects were optimized for maximal airflow rates on longwall faces.

Table 4.41: The airflow rates of main air intakes and returns of CMV and returns of longwall faces and main coal transport in relation to the regulation of fan's blades at the Šoštanj ventilation station.

Ventilation station Šoštanj - blades position [°]	Airfow rates [m^3/s]									
	Longwall face k.- 130/ B	Longwall face k.- 65/ A	Main coal transport	Vent. Stat. Šoštanj	Vent. Stat. Pesje	Air intake Šoštanj II	Air intake NOP	Air intake Škale	Air intake main coal transport	Air intake Hrastovec
-10	20.3	37.5	58.3	205.6	119.2	59.8	231.9	14.4	12.2	6.6
-8	22.7	37.6	62.9	222.8	119.2	63.8	243.3	14.8	13.2	6.8
-6	24.0	37.6	65.5	232.5	119.2	66.2	249.8	15.0	13.8	6.9
-4	25.1	37.7	67.6	240.4	119.2	68.0	255.1	15.2	14.3	7.0
-2	26.4	37.7	70.1	249.8	119.2	70.3	261.3	15.4	14.8	7.1
0	27.6	37.8	72.9	258.7	119.2	72.4	267.3	15.6	15.4	7.2
+ 2	28.8	37.8	74.6	266.7	119.2	74.4	272.6	15.8	15.8	7.3
+ 4	29.9	37.9	76.7	274.7	119.2	76.3	277.9	16.0	16.3	7.4
+ 6	30.7	37.9	78.4	280.9	119.2	77.8	282.0	16.2	16.7	7.4
+ 8	31.9	38.0	80.6	289.1	119.2	79.8	287.5	16.4	17.2	7.5
+ 10	33.1	38.0	82.9	297.8	119.2	81.9	293.2	16.6	17.7	7.6
Fixflow (+ 1)	**28.3**	**37.8**	**73.8**	**263.7**	**119.2**	**73.6**	**270.6**	**15.8**	**15.7**	**7.2**

Table 4.42: The airflow rates of main air intakes and returns of CMV and returns of longwall faces and main coal transport in relation to the regulation of fan's blades at the Pesje ventilation station.

Ventilation station Pesje - blades position [°]	Airfow rates [m³/ s]									
	Longwall face k.- 130/ B	Longwall face k.- 65/ A	Main coal transport	Vent. Stat. Šoštanj	Vent. Stat. Pesje	Air intake Šoštanj II	Air intake NOP	Air intake Škale	Air intake main coal transport	Air intake Hrastovec
-20	28.1	20.2	75.4	263.7	70.9	71.5	231.4	12.3	13.6	5.7
-18	28.1	24.0	75.0	263.7	81.4	71.9	239.9	13.1	14.1	6.1
-16	28.2	26.1	74.8	263.7	87.2	72.2	244.6	13.3	14.3	6.3
-14	28.2	29.6	74.5	263.7	96.8	72.6	252.4	14.1	14.8	6.6
-12	28.3	33.6	74.1	263.7	107.8	73.1	261.4	14.9	15.2	6.9
-10	28.3	38.5	73.7	263.7	120.9	73.7	272.0	15.9	15.7	7.3
-8	28.4	40.3	73.6	263.7	127.5	74.0	276.1	16.3	15.9	7.4
-6	28.4	42.7	73.4	263.7	132.5	74.3	281.4	16.7	16.2	7.6
-4	28.5	45.5	73.1	263.7	140.2	74.6	287.6	17.3	16.5	7.9
-2	28.5	47.4	73.0	263.7	145.2	74.9	291.6	17.7	16.7	8.0
0	28.5	49.0	72.8	263.7	149.5	75.1	295.1	18.0	16.9	8.2
+ 2	28.5	50.9	72.5	263.7	154.9	75.4	299.5	18.4	17.1	8.3
Fixflow (-11)	**28.3**	**37.8**	**73.8**	**263.7**	**119.2**	**73.6**	**270.6**	**15.8**	**15.7**	**7.2**

Table 4.43: The differences of airflow rates (according to fixflow) of main air intakes and returns of CMV and returns of longwall faces and main coal transport in relation to the regulation of fan's blades at the Šoštanj ventilation station.

Ventilation station Šoštanj - blades position [°]	Differences of airfow rates in relation to fan's blades regulation [m³/ s]									
	Longwall face k.- 130/ B	Longwall face k.- 65/ A	Main coal transport	Vent. Stat. Šoštanj	Vent. Stat. Pesje	Air intake Šoštanj II	Air intake NOP	Air intake Škale	Air intake main coal transport	Air intake Hrastovec
-10	-8.0	-0.3	-15.5	-58.1	0.0	-13.9	-38.7	-1.4	-3.5	-0.7
-8	-5.7	-0.2	-10.9	-40.9	0.0	-9.8	-27.2	-1.0	-2.5	-0.5
-6	-4.3	-0.2	-8.3	-31.2	0.0	-7.5	-20.8	-0.7	-1.9	-0.4
-4	-3.2	-0.1	-6.2	-23.3	0.0	-5.6	-15.5	-0.6	-1.4	-0.3
-2	-2.0	-0.1	-3.7	-13.9	0.0	-3.4	-9.2	-0.4	-0.8	-0.1
0	-0.7	0.0	-0.9	-4.9	0.0	-1.2	-3.3	-0.1	-0.3	0.0
+ 2	0.4	0.0	0.8	3.1	0.0	0.7	2.1	0.1	0.2	0.0
+ 4	1.5	0.1	2.9	11.0	0.0	2.6	7.3	0.3	0.7	0.1
+ 6	2.4	0.1	4.6	17.2	0.0	4.1	11.5	0.4	1.0	0.2
+ 8	3.6	0.2	6.8	25.5	0.0	6.1	16.9	0.6	1.5	0.3
+ 10	4.8	0.2	9.1	34.2	0.0	8.2	22.7	0.8	2.0	0.4
Fixflow (+ 1)	**28.3**	**37.8**	**73.8**	**263.7**	**119.2**	**73.6**	**270.6**	**15.8**	**15.7**	**7.2**

Table 4.44: The differences of airflow rates (according to fixflow) of main air intakes and returns of CMV and returns of longwall faces and main coal transport in relation to the regulation of fan's blades at the Pesje ventilation station.

Ventilation station Pesje - blades position [°]	Differences of airfow rates in relation to fan's blades regulation [m³/ s]									
	Longwall face k.- 130/ B	Longwall face k.- 65/ A	Main coal transport	Vent. Stat. Šoštanj	Vent. Stat. Pesje	Air intake Šoštanj II	Air intake NOP	Air intake Škale	Air intake main coal transport	Air intake Hrastovec
-20	-0.3	-17.6	1.6	0.0	-48.3	-2.2	-39.1	-3.5	-2.1	-1.5
-18	-0.2	-13.8	1.2	0.0	-37.8	-1.7	-30.6	-2.7	-1.6	-1.2
-16	-0.2	-11.7	1.0	0.0	-32.0	-1.4	-25.9	-2.4	-1.3	-0.9
-14	-0.1	-8.2	0.7	0.0	-22.4	-1.0	-18.2	-1.7	-0.9	-0.7
-12	-0.1	-4.2	0.4	0.0	-11.4	-0.5	-9.2	-0.9	-0.5	-0.3
-10	0.0	0.7	-0.1	0.0	1.8	0.1	1.5	0.1	0.1	0.1
-8	0.0	2.5	-0.2	0.0	8.4	0.3	5.6	0.5	0.3	0.2
-6	0.1	4.9	-0.4	0.0	13.3	0.6	10.8	1.0	0.5	0.4
-4	0.1	7.7	-0.7	0.0	21.0	1.0	17.0	1.5	0.8	0.7
-2	0.1	9.6	-0.8	0.0	26.0	1.2	21.0	1.9	1.0	0.8
0	0.1	9.6	-0.8	0.0	26.0	1.2	21.0	1.9	1.0	0.8
+ 2	0.2	13.2	-1.3	0.0	35.7	1.7	28.9	2.6	1.4	1.1
Fixflow (-11)	**28.3**	**37.8**	**73.8**	**263.7**	**119.2**	**73.6**	**270.6**	**15.8**	**15.7**	**7.2**

Table 4.45: The differences of airflow rates in % (according to fixflow) of main air intakes and returns of CMV and returns of longwall faces and main coal transport in relation to the regulation of fan's blades at the Šoštanj ventilation station.

Ventilation station Šoštanj - blades position [°]	Airfows changes in relation to fan's blades regulation [%]									
	Longwall face k.- 130/ B	Longwall face k.- 65/ A	Main coal transport	Vent. Stat. Šoštanj	Vent. Stat. Pesje	Air intake Šoštanj II	Air intake NOP	Air intake Škale	Air intake main coal transport	Air intake Hrastovec
-10	-28.4	-0.7	-21	-22	0	-18.9	-14.3	-8.8	-22.3	-9.2
-8	-19.9	-0.5	-14.8	-15.5	0	-13.3	-10.1	-6.2	-15.7	-6.2
-6	-15.2	-0.4	-11.3	-11.8	0	-10.2	-7.7	-4.7	-11.9	-4.8
-4	-11.4	-0.3	-8.4	-8.8	0	-7.6	-5.7	-3.6	-8.8	-3.5
-2	-6.9	-0.2	-5	-5.3	0	-4.5	-3.4	-2.2	-5.3	-1.8
0	-2.5	0	-1.2	-1.9	0	-1.6	-1.2	-0.8	-1.8	-0.5
+ 2	1.5	0	1.1	1.2	0	1	0.8	0.4	1.2	0.5
+ 4	5.4	0.2	4	4.2	0	3.6	2.7	1.6	4.3	1.8
+ 6	8.5	0.3	6.2	6.5	0	5.6	4.2	2.5	6.6	2.8
+ 8	12.6	0.4	9.2	9.7	0	8.3	6.3	3.7	9.7	4.4
+ 10	16.9	0.6	12.3	13	0	11.2	8.4	5.1	13	5.5
Fixflow (+ 1)	**28.3**	**37.8**	**73.8**	**263.7**	**119.2**	**73.6**	**270.6**	**15.8**	**15.7**	**7.2**

Table 4.46: The differences of airflow rates in % (according to fixflow) of main air intakes and returns of CMV and returns of longwall faces and main coal transport in relation to the regulation of fan's blades at the Pesje ventilation station.

Ventilation station Pesje - blades position [°]	Airfows changes in relation to fan's blades regulation [%]									
	Longwall face k.-130/ B	Longwall face k.-65/ A	Main coal transport	Vent. Stat. Šoštanj	Vent. Stat. Pesje	Air intake Šoštanj II	Air intake NOP	Air intake Škale	Air intake main coal transport	Air intake Hrastovec
-20	-0.9	-46.4	2.2	0	-41	-2.9	-14.5	-21.9	-13.1	-20.8
-18	-0.7	-36.5	1.6	0	-32	-2.3	-11.3	-17.2	-10	-15.9
-16	-0.6	-30.9	1.4	0	-27	-1.9	-9.6	-15.4	-8.4	-12.5
-14	-0.4	-21.7	1	0	-19	-1.4	-6.7	-10.5	-5.8	-9.2
-12	-0.2	-11	0.5	0	-10	-0.7	-3.4	-5.6	-2.9	-4.2
-10	0	1.8	-0.1	0	1	0.1	0.5	0.8	0.5	0.9
-8	0.1	6.7	-0.3	0	7	0.4	2.1	3.2	1.8	3
-6	0.2	13	-0.6	0	11	0.8	4	6.1	3.4	5.8
-4	0.4	20.5	-0.9	0	18	1.3	6.3	9.6	5.3	9.2
-2	0.4	20.5	-0.9	0	18	1.3	6.3	9.6	5.3	9.2
0	0.5	25.3	-1.1	0	22	1.7	7.8	11.9	6.6	11.3
+ 2	0.7	34.8	-1.7	0	30	2.3	10.7	16.4	9.1	15.5
Fixflow (-11)	**28.3**	**37.8**	**73.8**	**263.7**	**119.2**	**73.6**	**270.6**	**15.8**	**15.7**	**7.2**

Table 4.47: The comparison of airflow rates of longwall faces and ventilation stations at different settings of the main fans: fixflow in ventilation shafts or modelled fan's characteristics.

Ventilation station Šoštanj - blades position [°]	Ventilation station Pesje - blades position [°]	Airflow rates [m³/s]			
		Longwall face k.-130/B	Longwall face k.-65/A	Vent. Stat. Šoštanj	Vent. Stat. Pesje
-10	**-10**	20.3	38.5	205.5	121.7
+10	**-10**	33.1	38.4	297.8	120.3
+2	**-10**	28.8	38.5	266.7	120.9
fixflow	**-10**	28.3	38.5	263.7	120.9
+2	**-20**	28.8	20.3	269.6	71.0
+2	**+2**	28.7	50.9	265.2	154.9
+10	**+2**	33.1	50.8	296.1	154.1
+2	**fixflow**	28.8	37.8	266.8	119.2
Fixflow (+1)	**Fixflow (-11)**	**28.3**	**37.8**	**263.7**	**119.2**

The simulation results presented in Tables Table 4.41 to Table 4.47 show that:

- *Regulation effect of the Šoštanj ventilation station on total return airflow rate: (max – min) airflow rate = 92.2 m³/s and dilution ratio (max/min) = 1.45. Regulation effect regarding actual airflow rates as in October 2012: (max – actual) airflow rate = 34.1 m³/s and dilution ratio (max/actual) = 1.13.*
- *Regulation effect of the Pesje ventilation station on total return airflow rate: (max – min) airflow rate = 84.0 m³/s and dilution ratio (max/min) = 2.19. Regulation effect regarding actual airflow rates as in October 2012: (max – actual) airflow rate = 35.7 m³/s and dilution ratio (max/actual) = 1.30.*
- *The Šoštanj ventilation station has between 33 % and 420 % higher airflow rates capacity than the Pesje ventilation station.*
- *Regulation effect of the Šoštanj ventilation station on airflow rate on longwall face k.-130/B: (max – min) airflow rate = 12.8 m³/s and dilution ratio (max/min) = 1.63. Regulation effect*

regarding actual airflow rates as in October 2012: (max – actual) airflow rate = 4.8 m^3/s and dilution ratio (max/actual) = 1.17.

- *Regulation effect of the Pesje ventilation station on airflow rate on longwall face k.-65/A: (max – min) airflow rate = 30.7 m^3/s and dilution ratio (max/min) = 2.52. Regulation effect regarding actual airflow rates as in October 2012: (max – actual) airflow rate = 13.1 m^3/s and dilution ratio (max/actual) = 1.35.*

- *The dilution ratio between longwall face k.-130/B and total return airflow of the Šoštanj ventilation station was up to 14.67 and if we consider the airflow rate of longwall face k.-65/A as in October 2012 (28.3 m^3/s), the dilution ratio was up to 10.51.*

- *The dilution ratio between longwall face k.-65/A and total return airflow of the Pesje ventilation station was up to 7.66 and if we consider the airflow rate of longwall face k.-65/A as in October 2012 (37.8 m^3/s), the dilution ratio was up to 4.10.*

- *The dilution ratio with airflow regulation in the exit airway of the main coal transport in the Preloge pit with the Šoštanj ventilation station was up to 1.42 while the dilution ratios at the ventilation station of airflow from the longwall face were between 3.53 and 3.59.*

- *The dilution ratios of development headings at the Pesje ventilation station ranged between 9.04 and 19.77. Only the airflow from development heading num. 7 was ventilated with the Pesje ventilation station.*

- *The dilution ratios of specific development heading at the Šoštanj ventilation station ranged between 58.74 and 85.04. The airflows from development headings num. 4, num. 6, num. 8, num. 11 and num. 13 were ventilated with the Šoštanj ventilation station. The dilution ratios for all development heading ranged between 7.43 and 10.76.*

- *The dilution ratio with airflow regulation in exit airway of the main coal transport in the Preloge pit with the Šoštanj ventilation station was up to 1.42 while the dilution ratios at the ventilation station of airflow from the longwall face were between 3.53 and 3.59.*

- ***Simulation results show that the ventilation system of CMV does not have the capacity to effectively dilute odour sources. Maximum dilution of the simulation ratio was 85.04. For example, to dilute the general detection limit on CMV 2.58 mg/m^3 (1 ppm) of DMS in ambient air under the threshold detection level (0,008 mg/m^3), the dilution ratio must be at least 333.***

4.4.3 Simulations of DMS and odour concentrations

The text related to Section 4.4.3 is based on our published article [1].

The odour model is based on DMS emissions. The model is considered inert since it assumes that all the sources of DMS do not decay over time. It is known that DMS in the atmosphere does decay through reactions with photochemically produced hydroxyl (OH) and nitrate (NO_3) radicals, ozone (O_3) and nitrogen dioxide (NO_2) [[42], [129]]. A typical atmospheric half-life for DMS in the environment is from several hours to 3.5 days. In addition, photochemical oxidation, although important on the surface, is not considered relevant in the underground mine.

Results of the DMS study in the return airways of longwall faces in CMV [82] also showed that DMS with a concentration of 51.3 mg/m^3 in Tedlar gas sampling bag filled with synthetic air (20% oxygen and 80% nitrogen) is stable for at least 4 days.

During the study of effects of process changes on concentrations of individual malodorous sulphur compounds in ambient air near a Kraft pulp plant in Thunder Bay, Ontario, Canada [[93], [103]] also the stability of reduced sulphur compounds in the Teflon sampling bags was assessed. A gas mixture also containing 3.87 µg/m3 of DMS was introduced in a clean Teflon bag and then aliquots were withdrawn periodically which were analysed to monitor the changes in concentration over time. The concentration of DMS was found to remain constant for more than 3.5 hours. Similar results were obtained when the initial concentrations were doubled. More detailed results are described in Chapter 1.3.1.

Additionally, the experiment of DMS stability in the mine was conducted to test the decaying properties in the mine air for the time that DMS travels from the longwall faces to the surface. The experiment has additionally confirmed that DMS is not decayed in the mine during release from the longwall face to the surface. The detailed results of the experiment are presented in detail in Chapter 4.3.

Simulations of traveling (spread) times of DMS from the sources to the surface at operational air flowrate as of October 2021 showed that traveling times from longwall faces were between 556 s and 750 s, from development headings they were between 750 s and 1,836 s and from the main coal transport they were between 521 s and 1,923 s. The longest traveling time 7,409 s or 2.1 hours was from the main coal transport at the simulation where the main fan blades at the Šoštanj ventilation station were set to -10° (minimum air flowrate) and at the Pesje ventilation station to +2°. The extreme traveling time is due to the changed airflow directions in some airways and dispersion through the Pesje ventilation station instead of the Šoštanj ventilation station as normal.

Based on the cases described above and modelled traveling times, no decay mechanisms of DMS were considered in the model. The identified odour sources were the longwall faces K.-130/B and K.-65/A, road building faces 4. 6, 7, 8, 11 and 13 and the main coal transport system. In the model, sources are represented as point sources for each source, except at the main coal transport, where the whole source in the model represents 7-point sources at the return airway of the main coal transport and at 6 leakages (Figure 4.38, bottom figure).

For the study of DMS and odour dispersion analysis 8 simulation scenarios were considered, four for DMS and four for odour dispersion. Simulations tested the dispersion of characteristic DMS and odour concentrations at median and peak levels and all characteristic concentrations at the operational airflow rate as of October 2012 and at maximum possible airflow rate due to the main fans characteristics (Šoštanj station at +10° and Pesje station +2°). The evaluation of the DMS sources is based on the analysis of monthly gases measurements (see Chapter 4.1) The monitoring locations from 1 to 50 and ventilation stations Šoštanj and Pesje in the model (Figure 4.38) were systematically selected to follow all dilutions in return airways from the sources and to the surface.

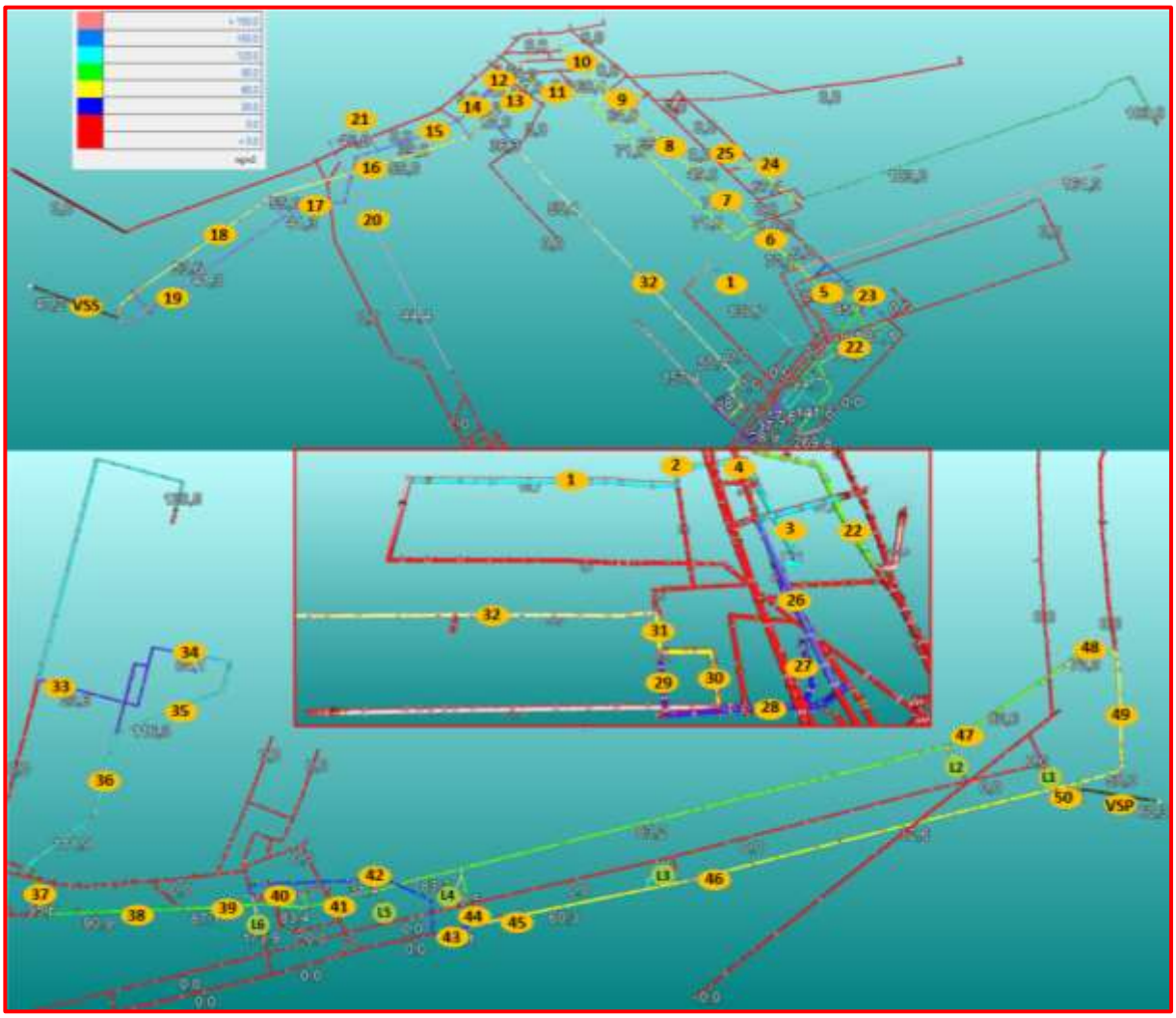

Figure 4.38: The monitoring location of simulations in the Preloge pit (upper) and the Pesje pit (bottom) with the simulated DMS concentrations at peak DMS sources. In the middle, enlargement of the longwall panel k.-130/B area is presented.

The simulation results are presented in Table 4.48, and in Figure 4.39, simulation results of median and peak DMS concentrations at operational airflows. In the model, the airflow rates at the Šoštanj ventilation station varied between 205.6 and 297.8 m^3/s and, at the Pesje ventilation station, the airflow rates varied between 70.9 and 154.9 m^3/s.

Table 4.48: The simulation results at the monitored locations.

Monitored location	Operational airflows					Maximum airflows					Odour/DMS Reduction
	[m³/s]	Median concentrations		Peak concentrations		[m³/s]	Median concentrations		Peak concentrations		
		[mg/m³]	[OU/m³]	[mg/m³]	[OU/m³]		[mg/m³]	[OU/m³]	[mg/m³]	[OU/m³]	[%]
1	35.0	31.3	4,044	130.7	16,885	39.3	27.9	3,604	116.3	15,024	10.9
2	37.3	29.4	3,798	122.6	15,838	41.9	26.1	3,372	109.0	14,081	11.2
3	39.0	28.1	3,630	117.4	15,166	44.7	24.5	3,165	102.2	13,203	12.9
4	50.4	22.0	2,842	94.7	12,234	56.7	19.5	2,519	83.8	10,826	11.4
5	61.8	18.4	2,377	85.6	11,058	69.5	16.4	2,119	75.7	9,779	11.2
6	92.2	13.2	1,705	72.2	9,327	103.6	11.7	1,511	64.1	8,281	11.3
7	57.5	13.0	1,679	71.0	9,172	64.4	11.5	1,486	62.9	8,126	11.5
8	76.5	10.5	1,356	65.7	8,488	86.4	9.2	1,189	57.9	7,480	12.1
9	77.5	10.3	1,331	64.8	8,371	87.4	9.1	1,176	57.2	7,389	11.7
10	36.6	9.6	1,240	60.4	7,803	41.7	8.5	1,098	53.2	6,873	11.7
11	91.3	10.1	1,305	59.1	7,635	102.9	8.9	1,150	52.1	6,731	11.9
12	39.6	7.5	969	47.0	6,072	44.8	6.7	866	42.1	5,439	10.5
13	100.8	9.7	1,253	57.0	7,364	112.8	8.6	1,111	50.5	6,524	11.4
14	86.1	4.6	594	41.2	5,322	96.3	4.2	543	37.4	4,832	9.0
15	75.7	4.4	568	39.8	5,142	85.4	4.0	517	36.1	4,664	9.2
16	114.2	9.1	1,176	55.0	7,105	127.1	8.1	1,046	48.9	6,317	11.0
17	149.5	2.2	284	41.8	5,400	166.0	2.1	271	37.6	4,857	7.3
18	127.5	8.4	1,085	53.6	6,924	141.7	7.5	969	47.7	6,162	10.9
19	136.1	2.2	284	41.8	5,400	151.3	2.1	271	37.6	4,857	7.3
20	71.1	0.0	0	44.4	5,736	77.4	0.0	0	40.7	5,258	8.3
21	73.8	0.0	0	42.8	5,529	80.5	0.0	0	39.2	5,064	8.4
22	11.6	4.7	607	81.1	10,477	13.1	4.2	543	72.2	9,327	10.8
23	12.6	2.0	258	34.1	4,405	13.7	1.8	233	31.5	4,069	8.8
24	14.0	3.9	504	67.4	8,707	16.2	3.4	439	58.3	7,532	13.2
25	19.0	2.9	375	49.8	6,433	22.0	2.5	323	43.0	5,555	13.7
26	25.0	2.2	284	37.7	4,870	27.6	2.0	258	34.1	4,405	9.3
27	6.9	1.7	220	28.9	3,733	7.8	1.5	194	26.3	3,398	10.4
28	15.1	1.9	245	33.3	4,302	17.4	1.7	220	30.0	3,876	10.2
29	9.1	1.5	194	26.5	3,423	10.7	1.3	168	22.7	2,933	13.8
30	21.1	4.0	517	68.8	8,888	23.4	3.6	465	62.7	8,100	9.4
31	30.2	3.2	413	55.9	7,222	34.1	2.9	375	50.2	6,485	9.8
32	33.5	2.9	375	50.4	6,511	37.8	2.6	336	45.2	5,839	10.3
33	40.1	1.4	181	23.6	3,049	53.3	1.0	129	17.7	2,287	26.8
34	37.7	15.9	2,054	84.1	10,865	50.4	11.9	1,537	63.0	8,139	25.1
35	46.9	24.5	3,165	116.3	15,024	59.6	19.3	2,493	91.7	11,846	21.2
36	49.2	23.4	3,023	111.9	14,456	62.6	18.4	2,377	88.1	11,381	21.3
37	57.6	20.0	2,584	95.6	12,350	73.6	15.7	2,028	74.9	9,676	21.6
38	60.6	19.0	2,455	90.9	11,743	80.4	14.4	1,860	68.7	8,875	24.3
39	63.3	18.2	2,351	87.1	11,252	83.8	13.8	1,783	65.8	8,500	24.3
40	20.7	3.2	413	15.5	2,002	26.6	2.5	323	11.7	1,511	23.2
41	62.3	17.4	2,248	83.4	10,774	81.8	13.3	1,718	63.7	8,229	23.6
42	25.2	2.7	349	31.4	4,056	32.8	2.0	258	24.0	3,100	24.7
43	27.2	2.5	323	29.1	3,759	35.6	1.8	233	22.1	2,855	26.0
44	30.1	15.3	1,977	88.5	11,433	38.4	11.8	1,524	68.1	8,798	23.0
45	57.3	9.2	1,189	60.3	7,790	74.0	7.0	904	46.0	5,943	23.8
46	59.9	8.8	1,137	62.6	8,087	77.4	6.7	869	47.8	6,175	23.6
47	39.5	15.8	2,041	82.6	10,671	51.9	12.3	1,589	63.9	8,255	22.4
48	45.2	13.9	1,796	72.3	9,340	57.6	11.1	1,434	57.6	7,441	20.2
49	56.3	11.1	1,434	58.0	7,493	72.0	8.9	1,150	46.1	5,955	20.2
50	62.9	8.4	1,085	62.2	8,035	81.4	6.4	827	47.5	6,136	23.7
VSP	**119.2**	**9.7**	**1,253**	**60.3**	**7,790**	**153.3**	**7.5**	**969**	**46.9**	**6,059**	**22.5**
VSS	**263.7**	**5.2**	**672**	**47.2**	**6,098**	**293.0**	**4.7**	**607**	**42.5**	**5,490**	**9.8**
AVERAGE		**10.0**	**1,293**	**63.6**	**8,212**		**8.4**	**1,080**	**53.6**	**6,922**	**15.4**

The simulation results reveal a high odour concentration despite the low DMS concentrations also at median sources because of the low odour detection threshold of DMS. Odour concentration from median sources at ventilation stations means that the odorous emissions at the Šoštanj ventilation station must be diluted to the odour detection threshold for additional 672 times by the atmosphere and at the Pesje ventilation station for additional 1,253 times. The odorous emission from the Šoštanj ventilation station at odour concentration 672 OU/m^3 and airflow rate 263.7 m^3/s was 177,145 OU.m^3/s and odorous emission from the Pesje ventilation station at odour concentration 1253 OU/m^3 and airflow rate 119.2 m^3/s was 149,370 OU.m^3/s.

While the emissions from Šoštanj are higher, the concentrations are lower due to the higher dilution rates of sources due to the 2.2 times higher airflow rate than in Pesje. For the longwall face k.-130/B in the Preloge pit, the dilution rate to the surface was 9.3, and for the longwall face k.-65/A in the Pesje pit, it was 3.2. Dilution ratios for development heading in the Preloge pit were between 28.7 and 75.3 and in the Pesje pit only development heading no. 7 was dispersed to Pesje with dilution ratio 15.2. At median sources the main coal transport was not recognized as DMS/odour source as more than 50 % DMS was not detected. The dilution ratio at peak sources was 3.7 in Šoštanj and between 29.8 and 91.7 in Pesje.

In comparison, the odour emission modelling of the newly planned ventilation shaft at the Illawarra coal mine, NSW, Australia [45], showed that an odour source equivalent to 219,500 $OU.m^3/s$ predicted that odour concentrations 3 OU/m3 would exceed only 1% of the time, which is in accordance with the local odour regulations. In Slovenia, there are no odour regulations. If only the levels of odour emissions of CMV are compared, without taking into consideration the atmospheric conditions and the vicinity of settlements, at the median odour sources no odour complaints are expected. On the other hand, at peak sources, which is considered the “worst case scenario”, the odorous emissions from Šoštanj with 1,607,932 $OU.m^3/s$ (at odour concentration 5,490 OU/m^3 and airflow rate 293.7 m^3/s) and from Pesje with (at odour concentration 6,059 OU/m^3 and airflow rate 153.3 m^3/s) 928,558 $OU.m^3/s$ are likely to lead to odour complaints. If would consider scenario with only one longwall face at peak levels, the emission rate would be 580.242 $UO.m^3/s$. Figure 4.39 presents a graphical visualization of the main results of characteristic DMS mine sources estimation, and characteristic odour emissions on the surface.

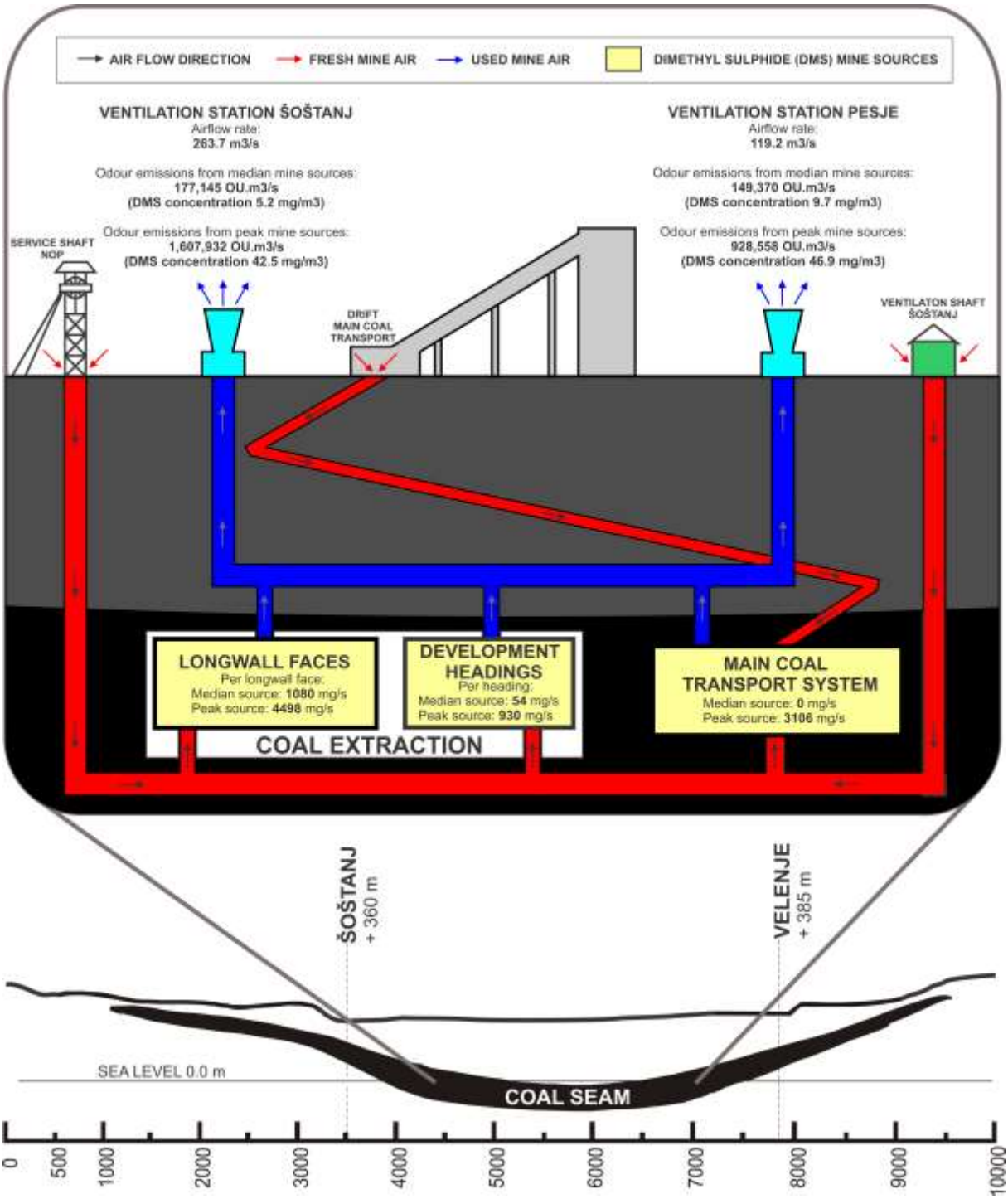

Figure 4.39: Graphical visualization of the main results of assessment of DMS odorous emissions during the coal extraction process in CMV.

Simulations of the regulation of the main fans at peak levels to provide maximum airflow rate resulted in an overall additional reduction of concentrations for 15.4 % on average. The ventilation reduction potential of concentrations regarding operational airflow rate as of October 2012 in the Preloge pit was 10.6 % and 22.9 % in the Pesje pit. At peak sources, the average concentrations were 9.3 times higher than at median sources at monitored locations and total emissions of peak sources were 7.8 times higher than of median sources.

The characteristic levels of DMS (Table 4.48) show great variations. At peak concentrations, the longwall face source is 4.2 times higher than at median concentrations, and at the development heading source, it is 17.2 times higher. Main coal transport is not considered as DMS

source at median levels and at peak levels it is potentially the biggest source in the mine. The results indicate that DMS is not released only with the extraction at longwall faces and development heading but it is also released from the coal while it is being transported to the surface. It is likely to be adsorbed on the lignite structure or trapped in the coal matrix, similarly as CO_2 [125]. From an adsorption/desorption study [10] of gases from different lithotypes of the Velenje lignite it was observed that the different lithotypes have significantly contrasting desorption properties related to differences in porosity. The specific surface area of pores in homogenous fine detrital lignite is more than 180 m^2/g and 35 m^2/g for xylite. Released DMS amount from sources greatly varies due to natural characteristics of the coal, presence of DMS in coal, production and ventilation design, and coal production intensity.

The odour concentrations estimation of mine air is based on the DMS concentrations and its odour detection threshold. Simulation results show odour concentrations at ventilation stations between 672 OU/m^3 and 7,790 OU/m^3. So far, rare separate point odour concentration measurements (according to standard EN 13725) at CMV's ventilation stations were conducted. The monitored odour concentration levels were similar to modelled levels. Four separate odour concentration measurements at ventilation stations [130] in 2016 gave odour concentrations between 850 OU/m^3 and 4,500 OU/m^3, and on 26 November 2007, three measurements [131] showed odour concentrations between 3,900 OU/m^3 and 8,400 OU/m^3.

Chapter 5

Conclusions

The text related to Chapter 5 is based on our published article [1].

There is almost no information concerning the fugitive emissions of DMS and odours in general from underground coal mining activities.

In this work we addressed this by describing and quantifying a dispersion of odorous gases released from sources of CMV by focusing on the analysis of gases monthly measurements in the mine and simulations of characteristic emissions of odorous compounds with a mine ventilation model constructed in Ventsim^{TM}.

This research, based on the analysis of monthly gas measurements, confirmed DMS as one of major VSCs in the mine and the most abundant odorant considering the detection frequency and concentrations of VSCs and the releasing under normal working conditions. DMS is a major potential odorant in the CMV released during the coal extraction process and during the transport to the surface from identified and quantified mine odour sources: longwall faces, development headings and main coal transport.

The DMS monitoring campaign on the longwall panel during coal extraction also showed great variability of DMS, CO_2 and CH_4 emissions.

The analyses of point monitoring showed that the main controlling factors affecting the levels of DMS in the return airways during normal conditions are the DMS content in the coal seam and its coal lithology, production intensity and airflow capacities.

The analyses of 30-minute intervals showed that gas emissions are increasing with production intensity and the levels of DMS are most controlled by production intensity, the extent of coal crushing.

Knowledge of petrographic heterogeneity of the Velenje coal seam from previous research and understanding the releasing characteristics of CO_2 and CH_4 suggest that the significant variability of DMS levels can be controlled by coal lithology. Correlation analyses show that during coal production CO_2 and CH_4 are most similarly released with high correlation while DMS correlated with CO_2 moderately and lowly with CH_4 indicated more similar releasing to CO_2 than CH_4. And knowing from monthly gas measurements that DMS is released also during coal transport and previous researchers measured significant DMS levels released from the coal stock pile also indicated that DMS similarly like CO_2 could also be mainly adsorbed on the lignite structure. At the releasing characteristic of DMS it must also be considered that DMS concentrations are in mg/m^3 levels while CO_2 and CH_4 are detected in g/m^3 levels, and also, it is known from experiences that DMS was not always detected in the coal seam while CO_2 and CH_4 were.

This work also experimentally proved that there is no DMS decay in the mine after the releasing from the longwall face and during the traveling to the surface with mine ventilation. The mine environment itself was found to be very challenging in terms of how to control the DMS concentration of an artificial source while collecting the necessary data in the gateroad that is long enough and which allows low enough airflow speed and is without loss of mass flow (no junctions) and without the release of gases on the way. After several unsuccessful attempts in the mine and after it was clear that the experiment cannot be conducted in any gateroad in the mine, the setup of the experiment was then directed into the ventilation ducting, which takes control over the mine conditions. Because the use of ducting also meant losses in mass flow, the modelling of mine experiment's setup and leakage of ducting channel in Ventsim^{TM} was applied. After a series of simulations in three examples of setups for the experiment it was proposed and successfully executed to test a constant gas mixture throughout the ducting channel despite the leakage of mass with systematically placed cross-section reductions at the end of the ducting channel, before the monitoring locations and before the ducting joints, to

ensure the inflation of ducting and to provide mixing of the gases mixture before the monitoring and before the mass flow loss at the joints.

The dispersion simulations of odour sources based on DMS concentrations in the mine show that median emissions represent relatively modest odour nuisance. While during peak emissions in the exit airways odour is potentially high to be disturbing and on the surface at the ventilation stations would be subject to odour complaints from the local residents. The simulation where odour levels were additionally reduced with increasing airflow rate with the regulation of main fans showed that it is not an effective measure for mitigating odorous emissions, while measures of reducing coal production would impose severe economic penalties.

Since DMS is not regularly monitored in mines and levels significantly vary due to the described control factors, the future work will focus on real-time monitoring of DMS levels extended on all mines and the study of its correlations to the coal extraction process in order to better understand and more accurately estimate odorous emissions from specific work phases of the coal extraction process. The DMS content in the seam is related to the petrographic heterogeneity of the coal, future research will thus involve investigating the coal desorption characteristics of DMS from coal.

In addition, to effectively address the odour issue at the CMV, especially in relation to fugitive odour emissions at the surface and for the design of technical measures for odour control, monitoring, and dispersion modelling of odour sources on the surface are necessary hereafter.

However, underground coal mines are not widely recognized as an odour nuisance, and the development of technical abatement solutions to control odour from coalmining operations, especially given the large volume of ventilated air produced by the mine, will need more recognition of the problem and more support in order for it to be solved.

Appendix A

Odour Perception, Measurement, and Modelling

A.1 Overview

This section presents a literature review of odour theory, how humans detect and percept odour and how the nature of odour is being handled by the science. The odour is subjective because the main sensor is human nose, and the sense of smell varies greatly between humans. Every odorous mixture has a unique smell and threshold. For these reasons, the primary consideration of odour science is to address the odour as objectively as possible. This section includes a look at the subjective and objective odour parameters which characterize the odour detection and perception. There are many divisions of odour measurement techniques because some of them can fall in more than one category. They are generally divided into analytical and sensory measurement techniques and methods, where analytical techniques give the concentrations of chemical species and sensory methods (olfactometry) use human nose to estimate the psychological response to a particular mixture. The next important part is odour sampling of different odour sources which is then analysed in laboratories. The focus of sampling technologies is on the averaging of the situation by prolonging the sampling time and on the fate of samples when reactive compounds are part of the emitted mixture. The last part discusses the estimation of dispersion of odour emissions on the surface, which is mainly based on atmospheric dispersion modelling. To successfully measure odour emissions of a particular source and assess its emission, it is essential to know about the releasing process and environment in which the odour is being dispersed.

A.2 Odour Perception

Olfaction, the sense of smell, is the most complex and unique in structure and organization and also the least understood of the five senses. While human olfaction supplies 80% of flavour sensations during eating, the olfactory system plays a major role as a defence mechanism by creating a natural aversion response to malodours and irritants. Human olfaction is a protective sense, protecting from tainted food and matter, such as rotting vegetables, putrefying meat, and fecal matter. This is accomplished with two main nerves. The olfactory nerve (first cranial nerve) processes the perception of chemical odorants. The trigeminal nerve (fifth cranial nerve) processes the irritation or pungency of chemicals, which may or may not be odorants [12].

During normal nose breathing only 10% of inhaled air passes up and under the olfactory receptors in the top, back of the nasal cavity. When a sniffing action is produced, either an involuntary sniff reflex or a voluntary sniff, more than 20% of inhaled air is carried to the area near the olfactory receptors due to turbulent action in front of the turbinates. These receptors, in both nasal cavities, are ten to twenty-five million olfactory cells making up the olfactory epithelium (Figure 5.1). Cilia on the surface of this epithelium have a receptor contact surface area of approximately five square centimetres due to the presence of many microvilli on their surface. Supporting cells surrounding these cilia secrete mucus, which acts as a trap for chemical odorants [12].

Chemical odorants pass by the olfactory epithelium and are dissolved into the mucus at a rate dependent on their water solubility and other mass transfer factors. The more water-soluble the chemical, the more easily it is dissolved into the mucus layer. Sites on the olfactory cells, assisted by specialized proteins, receive the chemical odorant. The response created by the reception of a chemical odorant depends on the mass concentration, i.e., the number of odorant molecules. Each reception creates an electrical response of the olfactory nerves. A summation of these electrical signals leads to an action potential. If this action potential has high enough amplitude (i.e., threshold potential), then the signal is propagated along the nerve, through the ethmoidal bone between the nasal cavity and the brain compartment where it synapses with the olfactory bulb [13].

All olfactory signals meet in the olfactory bulb where the information is distributed to two different parts of the brain. One major pathway of information is to the limbic system, which processes emotion and memory response of the body. This area also influences the signals of the hypothalamus and the pituitary gland, the two main hormone control centres of the human body. The second major information pathway is to the frontal cortex. This is where conscious sensations take place as information is processed with other sensations and is compared with cumulative life experiences for the individual to possibly recognize the odour and make some decision about the experience [12].

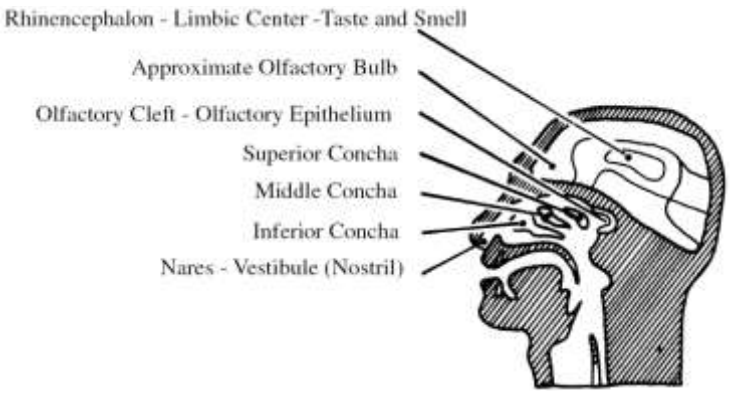

Figure 5.1: Human olfactory system [12].

Usually, an odorous stimulus is a combination of many scents. As in the case of animal production facilities. The effect of one odour on another may be related to differences in the water solubility of the two odours resulting in a number of possible outcomes. Flowery, fruity odorants tend to have higher molecular weights. Aldehydes, esters, alcohols, ethers, halogens, phenols, and ketones have more pleasant aromas than the lower molecular-weight carboxylic acids, nitrogenous compounds (not associated with oxygen), and sulphur-containing compounds. Blending of the two odours may occur, producing an odour with properties of both the original and properties unique to the newly developed odours. One odour may dominate another, or at least periodically, or the two odours may be smelled concurrently as individual odours. The complex nature of how odorants interact with each other is the primary challenge in determining how best to prevent odour formation [12].

As perceived by humans, odours have five basic properties that can be quantified [15]:

- *intensity,*
- *degree of offensiveness,*
- *character,*
- *frequency, and*
- *duration.*

All of which contribute to the neighbour's attitude towards the odour as well as the business generating the odour. It is generally accepted that the extent of objection and reaction to odour

by neighbours is highly variable. The reaction can be based on previous experience, relationship to the odour-producing enterprise and the sensitivity of the individual. Weather (temperature, humidity, wind direction) affects the volatility of compounds, preventing or enhancing movement into the gaseous phase where an odour can be dispersed downwind. Most of us will accept even a strong odour for a short period of time, provided we do not have to smell it often. But we have a threshold for the frequency and duration of the odour, above which our tolerance is exceeded, and we view the odour as a nuisance. These thresholds, however, are person specific. While it is the frequency and duration of an odour that often triggers a nuisance complaint, odour measurement procedures typically focus on the first three traits (intensity, offensiveness, and character). From a human health standpoint, exposure time is an essential measure in predicting any negative effects that may occur and this encompasses frequency and duration as well as concentration (intensity).

As a result, regulatory procedures often include concentration, frequency, and duration as part of the compliance protocol [15].

A.3 Odour Parameters

Odour is measurable using scientific methods. Odour testing has evolved over time with changes in terminology, methods, and instrumentation. Odour terminology is linked to standard methods and the instrumentation used in these standard methods. A clear understanding of odour terminology is needed in order to discuss the uses of odour measurements [14].

The objective parameters of perceived odour are [14]:

Odour Concentration – measured as dilution ratios and reported as detection threshold or recognition thresholds or as dilution-to-threshold (D/T) and sometimes assigned the pseudo-dimension of odour units per cubic meter.

Odour Intensity – reported as equivalent ppm butanol, using a referencing scale of discrete butanol concentrations.

Odour Persistence – reported as the dose-response function, a relationship of odour concentration and odour intensity.

Odour Character Descriptors – what the odour smells like using categorical scales and real exemplars (e.g., fruity → citrus → lemon: from a real lemon).

These odour parameters are objective because they are measured using techniques or referencing scales dealing with facts without distortion by personal feelings or prejudices. Additional measurable, but subjective, parameters of perceived odour are [14]:

Hedonic Tone – pleasantness vs. unpleasantness.

Annoyance – interference with comfortable enjoyment of life and property.

Objectionable – causes a person to avoid or causes physiological effects.

Strength – word scales like "faint to strong".

These odour parameters are subjective because individuals rely on their interpretation of word scales and on their personal feelings, beliefs, memories, experiences, and prejudices to report them. Written guidelines for subjective odour parameter scales assist individuals (citizens and air pollution inspectors) in reporting observed odour; however, the nature of these parameters remains subjective [14].

A.3.1 Odour concentration - thresholds

The most common odour parameter determined by odour testing is odour concentration. The characteristic odour concentrations are called "odour thresholds". Odour thresholds are minimal detectable concentrations at specific odour characteristics (detection or recognition). They are usually reported as odour units (OU), defined as the volume of dilution (non-odorous)

air divided by the volume of odorous sample air at either detection or recognition. Most often, odour threshold is used to mean detection threshold (DT), which identifies the concentration at which 50 % of a human panel can identify the presence of an odour or odorant without characterizing the stimulus. Detection threshold is the term most frequently used when discussing odour research. The recognition threshold (RT) is the concentration at which 50 % of the human panel can identify the odorant or odour, such as the smell of ammonia or peppermint [14], [17].

Another threshold on the odorant concentration gradient is a "health symptoms threshold" (HST) as shown in Figure 5.2. The individual citizen may reach some point on the concentration gradient of the odorant at which non-specific symptoms begin, such as headache, nausea, itchy eyes, etc. The “health symptoms threshold” can be higher on the odorant concentration gradient than the detection and recognition thresholds and may be higher than the annoyance threshold (AT). The “health symptoms threshold" is probably time and duration dependent (i.e., similar to the toxicological paradigm) and would be based on the individual's health history, body mass and other conditions of their body, i.e., immune system, general physical and mental "wellbeing" [14].

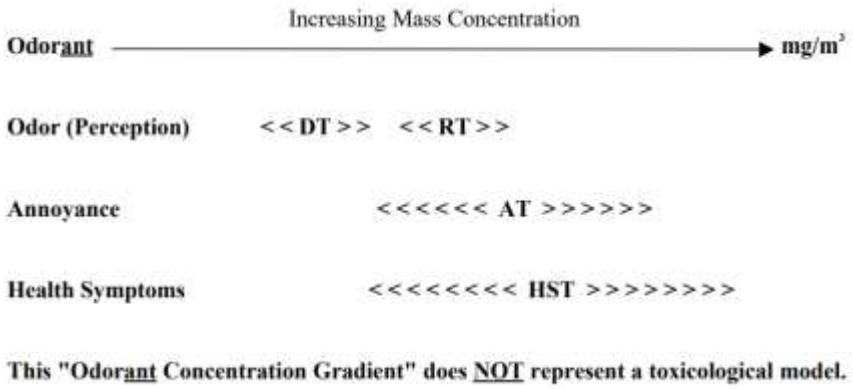

Figure 5.2: Odorant concentration gradient for one individual odorant [132].

A.3.2 Odour intensity

Perceived odour intensity is the relative strength of the odour above the recognition threshold (suprathreshold). The assessor compares the observed intensity of an odorous air sample to a specific concentration level of the standard odorant (usually n-butanol) from the olfactometer device which presents the continuous flow of sample or standard odorant, respectively. The butanol referencing method of quantifying odour intensity is the most commonly used method in evaluating environmental odours. Butanol concentrations are a referencing scale for purposes of documentation and communication in a reproducible format. For this method, the odour intensity result is expressed in parts per million (ppm) of n-butanol. Another important aspect of the butanol intensity referencing scale is the variety of available scales (Figure 5.3) [14].

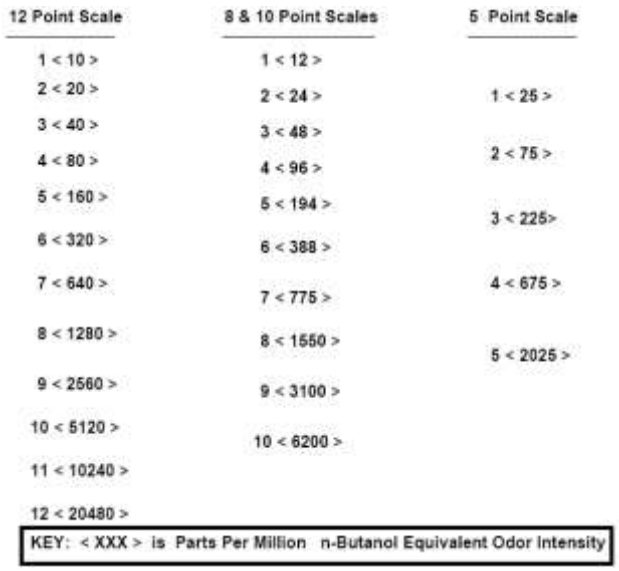

Figure 5.3: Butanol-based odour intensity referencing scale [14].

A larger value of butanol means a stronger odour. A small value of butanol means a weaker odour. Odour intensity is the strength of the perceived odour sensation. It is related to the odorant concentration.

Odour is a psychophysical phenomenon. Psychophysics involves the response of an organism to changes in the environment perceived by the five senses. Examples of psychophysical phenomenon include how the human body perceives sound loudness, lighting brightness, or odour intensity [14].

In the 19th century, E. H. Weber proposed that the amount of increase in a physical stimulus, to be just perceivably different, was a constant ratio. This relationship can be expressed as [14]:

$$\frac{\Delta I}{I}=\frac{\Delta C}{C}=k \tag{5.1}$$

Where I is the stimulus intensity, C is the measurable amount or concentration of stimulus, and k is a constant that is different for every sensory property and specific stimulus.

As an example, this expression means that there would be the same perceived increase in intensity when changing a concentration of sugar in water from 10% to 11% as when changing the concentration from 20% to 22%.

In 1860, G.T. Fechner expressed the Weber law somewhat differently by plotting the perceived intensity versus the stimulus magnitude on a semi-log scale, also known as the Weber-Fechner law [133]:

$$I=k\cdot \log C+n \tag{5.2}$$

In the 1950's and 1960's, through his work at Harvard University, S. S. Stevens proposed that apparent odour intensity grows as a power function of the stimulus odorant. Stevens showed that this Power Law (Steven's Law) follows the equation [14]:

$$I=k\cdot C^{n} \tag{5.3}$$

Where I is the odour intensity, C is the mass concentration of odorant (e.g., milligrams/cubic meter, mg/m^3), and k and n are constants that are different for every specific odorant or mixture of specific odorants.

In odour science the Beidler model is also used [133]:

$$I=\frac{k_1 nC}{1+nC} \tag{5.4}$$

When plotted on a log-log scale this equation is a straight line (Figure 5.4). The x-axis is the mass concentration (mg/m^3) of the single odorant. The upward slope of the graph illustrates that the odour intensity of the single odorant increases as the mass concentration increases. The slope of the power law is less than one for odour since it takes a larger and larger increase in concentration to maintain a constant increase in perceived intensity. Steven's Law has been used most often in modern odour science [14].

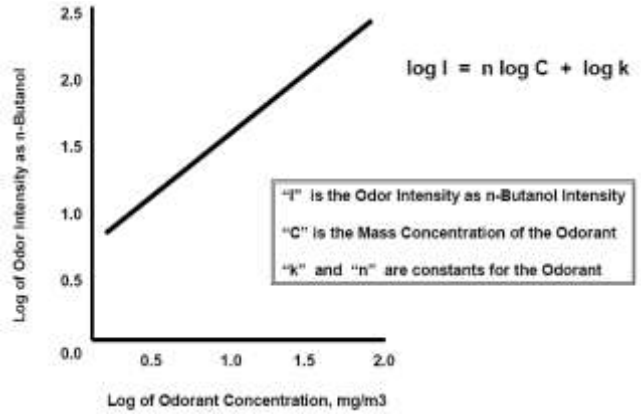

Figure 5.4: "Power Law" for a single odorant [14].

A.3.3 Odour persistency

The persistency of an odour can be represented as a Dose-Response function as shown in Figure 5.5. The Dose-Response function is determined from intensity measurements of an odour at various dilutions and at full strength. Plotted as a straight line on a log-log scale, the result is a linear equation specific for each odour sample. The odorant concentration (dose), expressed as the log of the dilution ratio, and the odour intensity (response), expressed as the log of n-butanol (ppm butanol), produces the log-log plot with a negative slope. The slope of the line represents the relative persistency. The logarithm of the constant k is related to the intensity of the odour sample at full strength, i.e., the y-axis intercept. The comparing line in Figure 5.4 to line in Figure 5.5 has a positive slope, because the concentration (x-axis) is the mass concentration in mg/m^3 of the odorant. The log-log plot in Figure 5.5 has a negative slope because the concentration (x-axis) is the dilution ratio of an odour sample [14].

Odorous air that has a low persistence will have a steep slope, which indicates that it does not take much dilution air to dilute the odorous air to below the detection threshold. Odorous air with a higher persistence will have a shallow slope, which means the sample air requires more dilution air to reach the detection threshold. A more persistent odour will be remembered longer ([14], [17]).

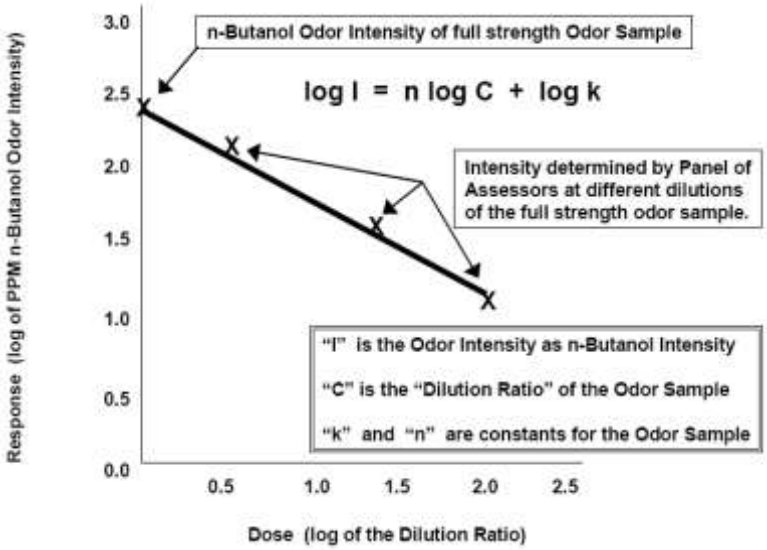

Figure 5.5: The Dose-Response function [14].

A.3.4 Odour characterization

Descriptive analysis is a sensory science term used to describe the action of a panel of assessors describing attributes about a product or sample (qualitative) and scaling the intensity of these attributes (quantitative). The food, beverage, and consumer product industries have formally used descriptive analysis to obtain detailed information about the appearance, aroma, flavour, and texture of products for well over 60 years [14].

Odour character, often called odour quality, is a nominal scale of measurement. Odours can be characterized using reference vocabulary. Standard practice has been to provide assessors with a standard list of descriptor terms, which are organized with like terms in groups. Similarly, terms with negative connotation (unpleasant) would be grouped with other negative terms and positive (pleasant) terms with other positive terms [134].

In the 1970's, American and British brewing and sensory scientists developed a "Beer Flavour Wheel" as a tiered system for describing the flavour (taste and odour) of beers. In the 1980's, the California wine industry developed a wine aroma wheel for the characterization of wines [14].

A descriptor wheel is organized with general descriptors at the centre of the wheel and more specific characters are listed towards the wheel rim. For example, an assessor may identify a flavour as fruity (general first tier description) and move out on the wheel through berry and raspberry. A similar descriptive analysis approach has been used in the environmental odour evaluation industry. Numerous standard odour descriptor lists are available to use as a reference vocabulary by assessors. In 1986, the International Association on Water Pollution Research and Control (IAWPRC) proposed eight major odour descriptor categories for describing odours from natural waters and illustrated the eight categories in an odour wheel: vegetable, fruity, floral, medicinal, chemical, fishy, offensive, and earthy [14].

Figure 5.6: Odour descriptor wheel developed by St. Croix Sensory for use with environmental odour samples [14].

Beyond character descriptors, other attributes of the odour can be characterized using similar profiling methods. For example, the perception of taste is sometimes experienced in the evaluation (sniffing) of a certain odour. The four recognized taste descriptors are salty, sweet, bitter, and sour [12].

A.4 Odour measurement methods

Odour is elicited by chemicals in a gas phase which are detected via olfaction producing recognizable smells (cinnamon, lemon) and/or chemesthesis which mediates pungent sensations (tingling, burning, etc) in response to substances such as ammonia [14].

There are a number of factors which affect odour including the volatile compounds themselves, the number of olfactory receptors available to bind them, the degree to which the compounds become solvated for receptor binding, temperature, humidity, and the matrix in which the odour-producing chemicals are embedded. In addition, individual chemicals may interact (chemically). Odours vary in threshold, intensity, and hedonic tone [14].

Of particular importance has been the characterization and measurement of key potent odorants responsible for the unpleasant odour associated with a specific process. Furthermore, each odorant has a unique odour and odour detection threshold which means that compounds, even if present at the same concentration, may have markedly different odour impacts [18].

Monitoring odours can be accomplished with analytical “chemical” techniques and sensory methods [18].

Analytical techniques:

Chemical analysis – indirect assessment involving the collection of a sample which, when analysed, will give the concentration of the various chemical species present. This includes wet chemistry, as well as sample collection followed by instrumental analysis by means such as gas chromatography (GC).

Direct reading instrumental analysis – provides information on the concentration of specific chemical species or their concentrations relative to each other. This includes portable analysers (including portable GCs and GC-MS) and the "electronic nose", as well as colorimetric tubes.

Sensory methods (relating to human response):

Olfactometry – a sensory assessment – which gives an assessment of the physiological response to a particular mixture – strength, quality, characteristics – which provides information on the likely population response. This is obtained by exposing trained individuals to samples of the odorous air, either in the laboratory or in the field.

These are many divisions of categories for odour measurements techniques and some techniques could fall into more than one. There are a number of different methodologies in use for odour analysis. Selection of a particular method will depend upon: the purpose of the measurement; the frequency of monitoring (once-off, periodic, continuous); the location at which the odour is sampled; whether a point source or area (surface) source; the nature and complexity of the emission – a single compound or a complex mixture [18].

A.4.1 Analytical techniques

A.4.1.1 Gas chromatography

Gas Chromatography (GC) is a widely used analytical technique for separating the components of an odorous air sample for identification and quantification [18]. The GC separation technology is capable of the efficient separation required for analysis of complex gas mixtures. In gas chromatography, a mixture of volatile substances is injected into a column which separates the compounds. The compounds are then detected as peaks which have specific retention times and peak areas which can be used for qualitative and quantitative determinations. A gas chromatograph mass spectrometer (GC-MS) is applied during the early stages of method development to aid in compound (peak) identification. The trace level sulphur-containing compounds are of particular importance because they often have very low odour detection thresholds and possess noxious odour properties. The description of GC methods is presented in more detail in [135] and [136].

A.4.1.2 Electronic noses

The electronic nose is an instrument that consists of an array of electronic chemical receptors which detect volatile chemicals or categories of chemicals, then uses the information to predict sensory-like properties. Electronic noses contain an array of sensors (sintered metal oxides, catalytic metals, conducting polymers, lipid layers, phthalocyanine, organic semi-conductors, surface acoustic wave, etc.) which respond to a wide variety of chemical classes. The sensors are based on conducting composites that change resistance on exposure to a vapor. The change in resistance (ΔR) of individual sensors from baseline resistance (R) produces a pattern of resistance changes ($\Delta R/R$) across the array. The measured response is then converted to a signal using a computer processor. To identify the type, quantity, and quality of the odour the computer uses changes in the pattern generated in the entire sensory array [137].

All these sensors (and their combinations) vary in the magnitude of response to any one compound giving them the discriminatory ability required to analyse odours. The binding and resistance change are rapid and temporary. Response data are exported to a computer which has been trained to use chemometric and "artificial neural network" computer software as a way to recognize the pattern of a mixture of compounds as a specific odour and to discriminate slight differences. Because very large amounts of data are generated, processing it into useful information requires statistical analysis software which can conduct principal component analysis and discriminant factor analysis [137].

Use of arrays of non-specific sensors allows for detection of many thousands of chemical species due to the broad selectivity of the sensory surfaces. The electronic nose can measure a complex group of substances (like the human olfactory system) very rapidly (10-120 seconds), and it can be trained to discriminate “good” from “bad” aromas. However, the electronic nose must be trained for each important component (grassy, smoky) for each application, it must be standardized by both chemical and olfactometric methods, and the “sensor array” is restricted. One of the biggest challenges for electronic noses is detecting complex odours against an intricate background matrix [137].

Electronic noses are finding wide use as a quality control tool, particularly in food, beverage, and perfumery as they can be taught to recognise the “good” product and then reject products whose odour profile do not match the reference standard. Similarly, the quality of drinking water can be monitored as the instrument can be taught to identify various contaminants which might be present. Other applications are in medicine, recognising odours which are characteristic of particular disease processes, for stock control of perishables and for process control in industry where head space volatiles produced during manufacture can be monitored in real time, allowing feedback control loops to be set up [18].

Applications in environmental monitoring are limited at present. In the majority of cases, the technology is unable to give concentration or odour strength information (although calibration may be possible in cases where process and effluent release conditions are tightly defined). Development work is on-going, and it is possible that new environmental odour applications for this technology will emerge [18]. Figure 5.7 shows a schematic presentation of electronic nose network (OdoWatch®) with capability to merge continuously the odour data (can identify the main odour sources) with the incoming weather data to display on the screen the odour plume superimposed on a map of the site and its surroundings.

Figure 5.7: OdoWatch® – Odor Smart Monitoring : 24/7 odour measurement with eNoses, real-time odour plume dispersion modelling & automatic odour alerts [138].

A.4.1.3 Colorimetric detector tubes

Sample of air produces a chemical reaction with chemicals contained in the tube producing a discoloration of the tube. This reaction occurs quickly, (generally within a matter of seconds), and it is possible to determine the amount of sample component reacted within the tube by the extent of discoloration (the reaction is proportional to the mass of the reacting gas). The limits of detection for this technique are typically between 0.2 to 1 ppm, but the detection limit can vary greatly depending on the tube used. From manufacturers’ literature, the relative standard deviation (coefficient of variation) of detector tubes lies between 5 and 20% [18].

A.4.1.4 Portable analysers

A range of different types of portable instruments are available which could be applied to the measurement of odorants: portable FID and GC-MS analysers, gold leaf analysers, paper tape monitors [18].

Portable gold leaf analysers are frequently used on sewage treatment works, effluent plants and landfill sites to monitor hydrogen sulphide. This type of a detector works by drawing odorous air into a sample port and passing it over a “gold leaf”. Reduced sulphide compounds stick to the gold leaf and a small electrical current is generated. The quantity of current generated is proportional to the amount of reduced sulphides collected. Sampling and measurement time depend on the level of sulphides present, but typically it is less than one minute with a reported lower detection limit of 0.003 ppm [18].

Paper tape monitors contain a chemically impregnated tape which, when exposed to a gas sample, changes colour in direct proportion to the amount of gas present. A tape is selected which will react with the gas of interest. The monitor can be set to sample at regular intervals, exposing an unreacted section of the tape each time, and so leaves a permanent record of the concentration of each sample [18].

A.4.2 Olfactometry measurements

Olfactometry uses trained individuals and standardized procedures to measure odour levels. The main advantage of olfactometry is the direct correlation with odour and its use of the human sensitive sense of smell. Olfactometry also has the advantage that it analyses the complete gas mixture, so the contribution of each compound is included [17].

Odours are a combination of gases, some in nearly undetectable concentrations. The human nose can sense these gases and gas combinations at extremely low levels. No instrument can match the sensitivity of the human nose. Several techniques have been employed to assist the human nose in determining detection threshold and intensity. The most popular method of odour measurement uses an instrument called the dynamic olfactometer and an odour panel [17].

A.4.2.1 Dynamic olfactometry

Olfactometer presents three air streams to the trained panellists (standards). One air stream is a mixture of non-odorous air and an extremely small amount of odorous air from a sample. The other two air streams have only non-odorous air. Panellists sniff each air stream and are asked to identify which air stream is different than the other two non-odorous air streams. Initially panellists must guess which air stream is different because the amount of odorous air added is below the detection threshold [17].

In steps, the amount of odorous air added to one of the air streams is doubled until the panellist correctly detects which air stream is different. The air stream with the odour is randomly changed each time. Figure 5.8 illustrates the olfactometry measurement process.

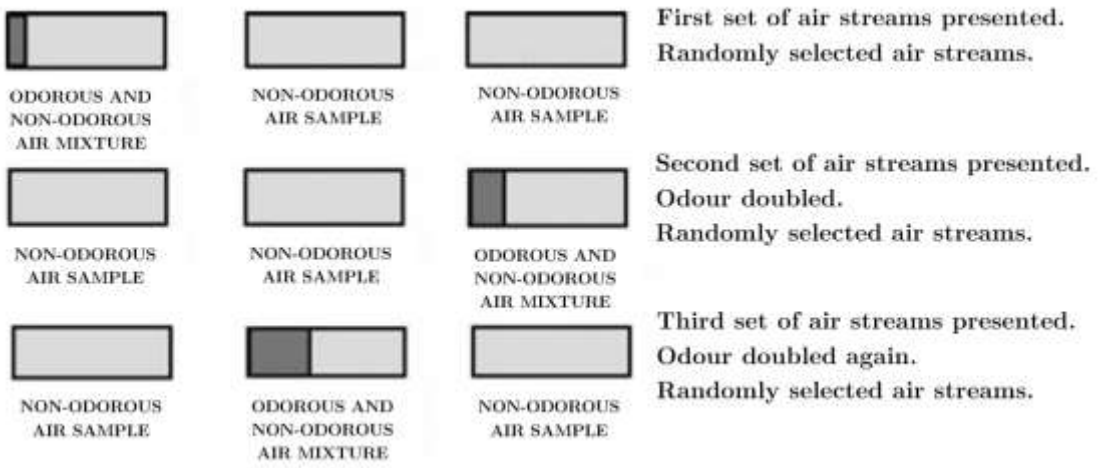

Figure 5.8: Olfactometer dilution sequence example [17].

The detection threshold is the non-odorous airflow rate divided by the odorous airflow rate when the panellist correctly recognizes which air stream is different. A panel of eight trained people is significant enough to analyse each odour sample. The panel's average concentration is reported and used for analysis. This statistical approach is called triangular forced-choice and is standardized with EU standard EN 13275:2003 [139].

Olfactometers as shown in Figure 5.9 and Figure 5.10 are not portable, and an operator closely controls sample delivery. The dilution-threshold ranges are available to be presented at 14 dilutions that represent a range in dilution-to-threshold of 8 to 66,667 (AC'SCENT olfactometer. These units are often used in a laboratory setting by 7 to 10 panellists.

Figure 5.9: The AC'SCENT ® International Olfactometer was designed specifically to meet all requirements of the CEN odour testing standard, EN13725:2003 and ASTM International E679-04. [140].

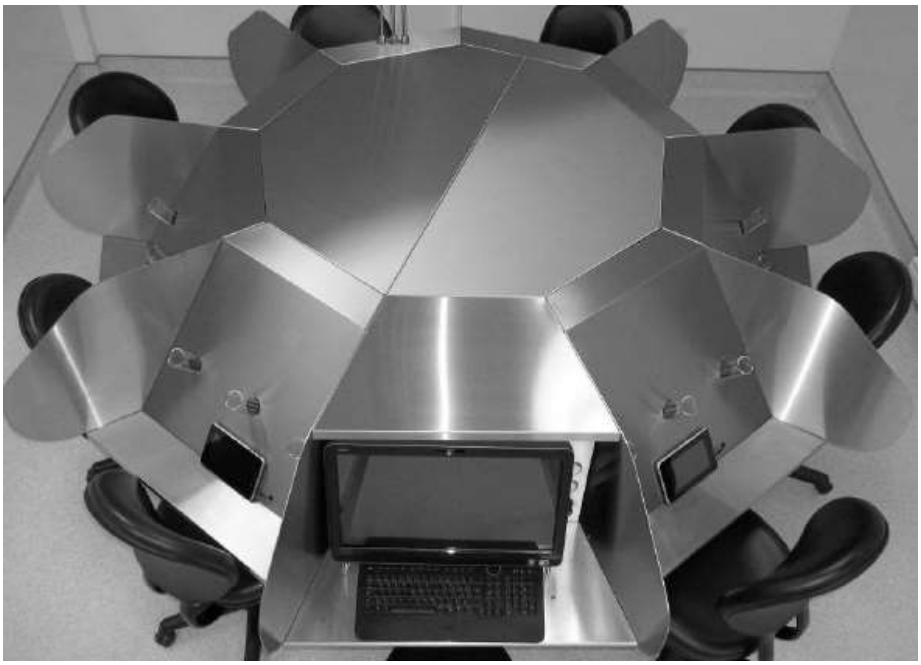

Figure 5.10: Design of a 9-sided (nonagon) ONOSE-8® stationary dynamic olfactometer operated at Consumaj laboratories in Canada. Allows simultaneous olfactometric analyses for 8 panel members, which significantly reduces the duration of the analysis. It meets all requirements of the CEN odour testing standard, EN13725:2003 and ASTM International E679-04. [141].

A.4.2.2 Scentometry

Method of odour concentration evaluation that is available on-site employs the use of a Scentometer®, as seen in Figure 5.11, or a Nasal Ranger®, as seen in Figure 5.12.

The Scentometer® is a plastic box with a number of air inlets and two sniffing ports. Two of the air inlets have activated charcoal filters to remove odours and provide clean air. The remaining inlets are of varying diameter to permit a range of dilutions of odorous air to be sampled. An observer begins by opening the port of the smallest diameter to start with the largest dilution (lowest concentration) of the odour. As successively larger ports are opened, the dilution of the odorous air decreases and the odour concentration increases. When the evaluator can first detect the odour, the odour threshold has been reached. Odour concentrations are expressed as dilutions to threshold. The range of dilutions to threshold possible for the Scentometer® includes 1.5, 2, 7, 15, 31, 170, and 350 [22].

Figure 5.11: The Scentometer Field Olfactometer [22]. Note the two glass nostril ports to the left and the series of orifice holes at the back of the unit to the right in this photo.

The Nasal Ranger® operates on the same principles. Carbon-filtered air is supplied through two replaceable carbon cartridges. An orifice selector dial on the Nasal Ranger® contains six odorous air inlet orifices for six different D/T values (2, 4, 7, 15, 30, and 60). The dial contains six "blank" positions (100% carbon-filtered air) alternating with the D/T orifices. The dial is replaceable for other D/T series (e.g., 60, 100, 200, 300, 400, and 500). The diluted odorous air is sniffed through an ergonomically designed nasal mask, which is constructed of a carbon fibre/epoxy blend with a fluoropolymer (Teflon-like) coating. A check valve is placed in both the inhalation end and exhalation outlet of the nasal mask in order to control the direction of airflow while using the Nasal Ranger [22].

Figure 5.12: The Nasal Ranger Field Olfactometer [22]. The inset picture shows a close-up of the orifice dial, which is located in front Nasal Ranger®.

A.4.2.3 Ranking methods

Odour can be evaluated using panellists to rank samples, a procedure in which an arbitrary scale is used to describe either the intensity or offensiveness of an odour. Typically, a scale of 0 to 10 is used, with 0 indicating no odour or not offensive and 10 representing a very intense or offensive odour. Such methods use either odour adsorbed onto cotton or a liquid sample that has been diluted [14].

A.4.2.4 Referencing methods

This method uses different amounts of n-butanol as a standard to which sample odour intensity is compared, again using a human panel. The range of n-butanol concentrations is often from 0 to 80 ppm. As the concentration of butanol is changed, the sample odour is compared to the butanol to determine at what concentration of butanol the sample's intensity is equivalent. The use of butanol as a reference standard is widely accepted as common practice in Europe and has been incorporated into portable and laboratory scale instrumentation. Most of the methods currently used in the United States employ butanol as a means of assessing panellist suitability rather than as the sole means of determining an odour's strength or acceptability [14].

A.4.2.5 Challenges with olfactometry methods

Odour measurement is a complicated task. While a number of methods are available, none are without drawbacks. However, dilution-to-threshold methods are the most widely accepted methods at the current time [12].

Challenges with current methodology include the use of humans for assessment. Work has shown that the same panellist's response from one day to the next can vary by as much as three-fold, possibly due to health or mood of the individual. Variability in the sensitivity of the individual conducting the evaluation and odour fatigue are further concerns that are commonly addressed in procedural protocol. Odour fatigue is a temporary condition where a person becomes acclimated to an odorant or odour to the point that they are no longer aware that the odour is present. Onsite methods are complicated by the influence that the visual perception might have in an evaluation (smelling with your eyes, so to speak). Each of us has a unique odour acuity. While methods try to minimize panellist variation, the difference in sense of smell from one person is another consideration in human assessment methods. The measurement of odour concentration by dilution is more direct and objective than that of odour quality or intensity. However, each of the above procedures requires the use of the human nose as a detector, so not one is completely objective. The imprecision that results from the large difference between the dilution levels has been identified by researchers as a concern as well. Use of a forced-choice method, such as that used with dynamic olfactometers, in which a panellist must simply identify the presence or absence of an odour, is generally a better method than ranking, as the human nose cannot distinguish small differences between levels of intensity [15].

Odour measurements are often complicated by the variability in meteorological conditions during the sampling period. Odorous emissions change with time and the movement of odorous air. The intensity and location of the odorous air may change with wind speed and direction. At any particular location, the current odour intensity may have little bearing on the odour intensity that was present an hour ago or an hour from now [18].

Odour is measurable using standardized scientific methods in odour-testing laboratories with laboratory olfactometry and in the ambient air with field olfactometry. Point, area, and volume emission sources can be sampled and tested for odour parameters such as odour concentration, intensity, persistence, and descriptors. Presently, international standards are in place, which dictate the scientific methods and practices of odour measurement. These international standard methods for measuring odour are objective, quantitative, dependable, and reproducible [14].

From the Comité Européen de Normalisation (CEN):

EN13725:2003: Air Quality – Determination of Odour Concentration by Dynamic Olfactometry

From ASTM International:

ASTM E679-91: Standard Practice for Determination of Odour and Taste Threshold by a Forced-Choice Ascending Concentration Series Method of Limits

ASTM E544-99: Standard Practice for Referencing Suprathreshold Odour intensity

A.4.3 Comparison of chemical vs sensory assessment techniques

The main factors which influence the choice of technique are [18]:

- *The composition of the odour – mixed or relatively simple.*
- *The reason for which monitoring is being undertaken – for modelling, for assessing annoyance potential, testing of control efficiency etc., compliant.*
- *The level of detail required.*
- *The location of testing – at source, boundary, community.*
- *Frequency – where cost may become a factor.*
- *The need to capture fluctuations or specific events.*

Table 5.1: Characteristics of the odour quantification methods considered [18].

	Subjective observations	Specific chemical tests	GC-MS	Olfactometry	Electronic nose
Application	Simplified olfactometry – "sniff test"	Source sampling	Source sampling/ ambient	Source sampling	Source sampling/ ambient
Analysis	Identifying the presence of odour, offensiveness or identification of source.	Limited to specific compounds	Limited to organic compounds	Fully representative	Fully representative but appropriate sensors must be selected for application.
Sampling methodology	Testing protocol required for repeatability	Direct sampling, e.g. colorimetric tubes or instrumental. Indirect, e.g. collection of sample and lab analysis	Various techniques but will require pre-concentration for ambient air samples	Bag sampling	Direct sampling (but portability is limited)
Limit Of Detection	Typically good, but can vary depending on the environment and the compounds involved.	Depending on test – generally greater than 0.1 ppm	ca. 1.5 ug/m^3	ca. 50 dilutions	Not applicable, but detects differences, not absolute concentrations.
Uncertainty	High, improved by use of standardised protocol.	+/- 5 to 20%	+/- 10%[2]	+/- 40%[1]	Not known
Ease of data interpretation	Reasonable, if protocol is followed.	Depends on the technique, e.g. colorimetric tube results easy to interpret	Often poor	Good	Good.
Relative unit cost	Low	Low to moderate. Depends on specific tests. Sample collection costs may be moderate to high.	Moderate/high. Sample collection costs may be moderate to high..	Moderate/high Sample collection costs may be moderate to high.	Moderate/high

Key
1 - value given in "Odour control a concise guide" for duplicate samples collected and analysed.
2 - typical uncertainty value for thermal desorption and GC-MS analysis.

A.5 Determination of Odour Emission Rates

A.5.1 Odour emission rates

The measurement of the rate of odour discharge involves the collection of a sample of odorous air from the source itself, then the laboratory analysis of that air sample and calculation of the emission rate. The procedures of collection and analysis of the sample are quite separate activities, each with their own issues and problems.

The odour emission rate (OER) has units of "odour per time" (e.g., OU/s or OU/hr), and is used to quantify the rate of odour discharge from odour sources. Two methods can be used to determine the OER, depending on the type of source [34].

Point sources: OER = odour concentration of discharge multiplied by normalised gas flow rate. Normalisation to 20°C is required since that is the temperature of the laboratory where the olfactometry is carried out.

Area sources: Measurement determines the specific odour emission rate (SOER), being the odour discharge per unit area of surface. The SOER has units of "odour per unit area per time" (e.g. OU/m^{2}s or OU/m^{2}h). The OER for an area is then determined by multiplying the SOER by the total exposed area.

Unless appropriate techniques are followed, errors incurred in the process of measuring an OER or SOER may accumulate so that the final calculated emission rate carries a large uncertainty. The most likely sources of error include [34].

Contamination of air samples by the sampling equipment used.

Instability of odour concentration in the air sample.

Erroneous measurement of airflow rates in stacks and sampling hoods.

Additional problems with area source sampling relating to whether the type of sample hood used reflects actual ambient emission conditions.

Uncertainties in odour concentration determined by olfactometry procedure.

The potential for these errors to have occurred should be considered in any odour assessment study which involves odour measurement.

A.5.2 Odour sampling techniques

The precise and correct determination of odorous emissions (odour emission rate) and chemical composition of odour matrix mainly depends on the appropriate sampling technique.

Definitions of source types are defined as follows [34]:

Point source: Discharges from a small opening such as a stack or vent.

Area source: A source with a large surface area such as a landfill surface, a pile of solid material, or a liquid surface.

Volume source: A bulky, diffuse source such as fugitive emissions from within a building.

Line source: A long, narrow source such as a gateroad or roofline vent along a long, narrow building.

A.5.2.1 Point sources

Generally, when collecting samples from stacks, the methodology recommended should be followed for [[34].

Selection of a suitable sampling point in the stack or duct, or confirmation that existing sampling points conform to requirements; and

Measurement of the velocity, temperature, static pressure, and bulk gas properties of the stack gas.

As in the measurement of any other contaminant discharged to air, these stack gas parameters are necessary to calculate the odour emission rate.

The point source emissions can often include particulates and droplets; however, measurement of odour from particles and droplets is not possible due to the principles of olfactory measurements. High temperature discharges will usually need to be diluted before being collected into sample bags to prevent damage to the bag materials and condensation [34].

The OER from a point source (e.g., units of OU/s) is calculated by multiplying the volumetric flow rate from the source (e.g., units of m^3/s) by the odour concentration measured in the sample bag (e.g., units of OU/m^3), corrected for the dilution ratio if necessary. Odour determinations by olfactometry are measured at room temperature (e.g., 20°C), and the volumetric flow rate (usually quoted as "operating temperature" or "standard conditions (0°C)") must be corrected to the same temperature basis as the odour concentration as before this multiplication is carried out. This is called "normalizing" the flow rate (assuming Ideal Gas Law applies) [34].

Sometimes the volumetric flow rate is also corrected for other factors, such as for a dry gas basis (0% moisture), or for combustion sources, to 12% carbon dioxide. These factors must be eliminated (i.e., not included in the calculation) when multiplying the volumetric flow rate by the odour concentration, to give the actual OER at operating conditions [34].

A.5.2.2 Area sources

When dealing with odour emissions, two basic sources are recognised – point sources and area sources. Point sources generally have a well-defined, easily located point from which the odour

is discharged. Examples include artificially ventilated animal housing (e.g., poultry sheds, with large volume fans installed in the shed end-wall) and rendering plants (with a stack for dispersing odorous air into the atmosphere). These are sometimes referred to as “volume sources” [34].

Area sources are less easily quantified. While the area of the emitting surface may be measured, there is no actual flow of contaminated or odorous air through a well-defined discharge point. Consideration of a simple emitting surface, such as the quiescent surface of an anaerobic pond, reveals that a number of different factors will probably control the rate at which odour is emitted from the liquid surface. These will include the surface area of the pond, the difference in concentration between the pond liquor and the air above the pond, the temperature of the liquor and the velocity of wind passing across the surface of the pond [33].

Estimation of rates of emission of volatile materials from area sources is a complicated process. Conceptually, two basic processes may be used [27], [142], [143]:

Device-independent micro-meteorological techniques, where the emission rate is calculated from concentrations measured across the plume of emitted material and local meteorological data, specifically wind velocity profile data.

A sampling device, where a chamber (*Figure 5.13*), *hood or wind tunnel (Figure* 5.14*) is deployed on an emitting surface. The device may be static (sealed or vented) or flushed with contaminant-free carrier at a known velocity or flow rate. The emission rate is calculated as the product of concentration and airflow through the device.*

Figure 5.13: Flux chamber [34].

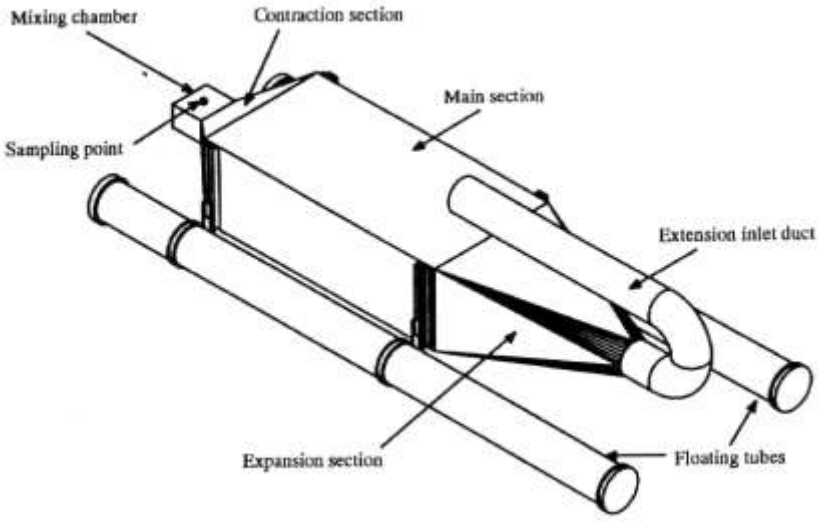

Figure 5.14: Wind tunnel [34].

The design and measurements with flux chambers and wind tunnels are widely debated at present through the scientific community because the estimated emission rates with different devices are very difficult to compare directly [27].

The main differences between chambers and wind tunnels are the ventilation flow rate and airflow dynamics that are established over the measured surface. The SOER calculated from the static flux hood measurement represents emissions during calm wind conditions, while wind tunnel measurements can be conducted to directly measure the effect of wind speed in influencing SOER [34].

However, as the level of understanding grows, it is becoming apparent that the wind tunnel gives a better estimate of odour emissions in real ambient conditions [27].

A.5.2.3 Back-calculation as an alternative to sampling

"Back-calculation" is the estimation of the SOER from an area source by measurement of ambient odour concentrations at a known distance downwind from the source, under known meteorological conditions, with the source OER then determined utilizing a dispersion model. Significant sources of error in this approach mean that this is not often a preferred method, although some consultants do favour it. Sources of error include [34]:

Multiple odour sources and background odour contributing to total odour measurement.

Lower detection limit (LDL) of olfactometer if ambient odour concentrations are low.

Dispersion model inaccuracies if sampling too close to source (e.g., <100m away).

Dispersion model errors (accuracy not better than a factor of 2, could be a factor of 10 or more if trying to predict concentrations at a specified downwind location).

Errors in estimating meteorological conditions and determining exact wind direction and plume centreline.

The greatest flaw with this method is the difficulty in measuring ambient odour concentrations due to limitations of the olfactometry method at low odour concentrations. Back-calculation is not recommended by the authors as a technique for estimating odour

emission rates. However, if no other means of estimation is possible, then back-calculation may be acceptable, but should only be considered if the following conditions prevail [34]:

Odour effects are caused by, or dominated by, only one source of odour.

Odour source discharges a steady, constant emission.

The ambient odour concentrations are strong enough that the LDL is not a problem (suggest >100 OU/m^3 (certainty thresholds) as a rule of thumb), and the ambient sample can be collected far enough from the source that the dispersion model results will be valid (suggest >100m from edge of source).

The terrain in the area is flat, and there are few surface irregularities such as buildings and planted fences to interrupt the plume path.

The wind conditions are steady, atmospheric stability is readily estimated, and inversion layers are sufficiently high that mixing height does not play a part in the dispersion characteristics.

A.5.3 Sample collection methods

The analysis of odorants from ambient air constitutes two phases: firstly, sample collection, then laboratory analysis of these samples. There are four main sample collection methods: gas canisters, solid phase micro-extraction (SPME), sorbent tubes and gas bags [25]. For odorant analysis the human nose is implemented as one of the detectors, complemented with another analytical detector.

A.5.3.1 Solid Phase Micro-Extraction

The use of solid phase micro-extraction (SPME) for non-methane volatile organic compound (NMVOC) and odorant collection provides a compact method of sample collection/pre-concentration. The fibre is exposed to the sample environment for a known time, the target analytes adsorb to the surface of the fibre by either chemisorption or adhesion; the analytes are then liberated from the fibre either by solvent desorption or thermal desorption before chemical speciation by chromatographic techniques.

The collection of odour active compounds by SPME fibres has extensively documented the numerous aroma active constituents in various foods and beverages, including orange juice, simulated beef flavour, and wine.

In contrast to the extent of literature available for food and beverage analysis, the application of SPME to the analysis of environmental samples is moderate. Solid phase micro-extraction has been used in the analysis of indoor air samples, swine house particulate matter and odour emissions, general intensive livestock operations and waste gas emissions [25].

A.5.3.2 Sorbent tubes

The sorbent tubes contain a sorbent of known mass and composition chosen specifically for the target analytes. Sorbent tubes pre-concentrate a sample by passing the odour sample through a sorbent bed such as activated carbon, graphitized carbon blacks, carbon molecular sieves, carbon-based porous polymers, or a multi-sorbent bed. The captured analytes are retained on the sorbent bed in a similar manner to SPME fibres and then thermally liberated for subsequent GC analysis.

Graphitized carbon black (GCB) sorbents are generally nonporous materials that collect analytes on their surface by adsorption, thus their strength is considered to be a function of their specific surface area, that is, the area analytes have to bind to; thus, a lower specific area corresponds to a lower strength. Carbon molecular sieves are porous materials that collect analytes by trapping them within the pores of the material, operating conversely to a conventional sieve, capturing analytes smaller than the size of the pore in the material, and allowing larger molecules to pass through the sorbent bed.

Also termed thermal desorption (referring to the method of extracting the analytes from the sorbent) sorbent tubes have been used for VOC analysis of indoor air, odorous waste gases, food

waste composting plants, biofilter assessment, swine house emissions, dairy farm emissions and other odour emission sources [25].

A.5.3.3 Gas bags and sample canisters

Whole air samples are collected by means of gas bags (polyvinyl fluoride – Tedlar®; polytetrafluoroethylene – Teflon®; polyethylene terephthalate; aluminium foil) or a gas sampling canister. Instead of pre-concentrating the sample (as with SPME or sorbent tubes) the entire sample is collected and kept within the bag or canister. Owing to the logistical constraints of collecting large samples, typically only locations close to the laboratory can be sampled using bags or canisters. Canisters have been used to analyse emissions from swine facilities and wastewater treatment plants, whilst Tedlar® bags have been observed to exhibit significant VOC loss.

The collection of samples with gas bag is most common. Sample collection is based on the "vacuum" or "lung" principle as shown in Figure 5.15. The sample bag is placed inside a rigid container. The air is withdrawn from the container using a vacuum pump. The sampling tube is placed into the sample port and the low pressure in the container causes the bag to fill with a volume from the sample gas stream which is equal to the amount which has been withdrawn from the container. Samples should not be collected by direct pumping because of the risk of adsorption or contamination [25].

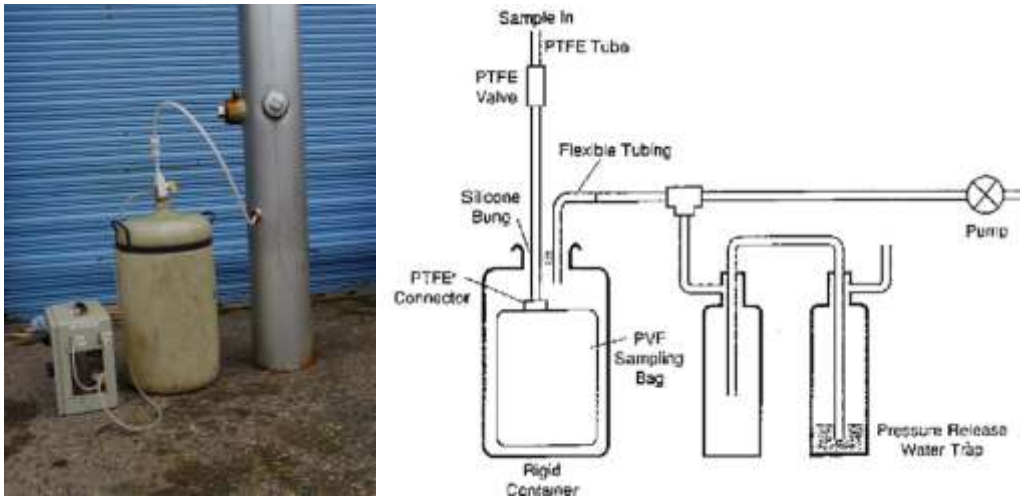

Figure 5.15: Left: odour sampling apparatus; right: schematic of sampling equipment [18].

A.5.3.4 Advantages and limitations of sample collection methods

In Table 5.2, advantages and major limitations of sample collection methods are presented.

Table 5.2: Characteristics of the odour quantification methods considered [25].

Sampling Method	Advantages	Major Limitation(s)
Canisters	Provide a robust method of capturing entire sample matrix	Compound stability, moisture, further sample pre-concentration may be required, difficult to clean canisters, expensive initial setup and maintenance of canisters. Bulky.

Odour Bags	Captures entire sample matrix.	Decay and diffusion of compounds, permeation of moisture into samples promoting further degradation. Sample exposed to light. Large sample size, bulky
Solid Phase Micro-Extraction (SPME)	Convenient for sample pre-concentration – can be desorbed in typical GC injection port. Compact, portable	Selectivity of fibres, quantification of complex matrices. Fibres can be fragile, easily broken if handled incorrectly. Passive sampling may require long time periods with low concentrations, which may result in incorrect chemical representation.
Sorbent Tubes	Convenient for sample collection and pre- concentration. Can be pumped (known volume) or passively collected (known up-take rates) Robust, easily transported	Selectivity of sorbent, moisture trapping on hydrophilic sorbents, quantification needs accurate flow measurements.

A.5.4 New sample collection technologies in development

A.5.4.1 Cryocondensation sampling

In 2009, a new universal, integrative air sampler, named CRYOCORE (CRYOgenic COndensation and REconstitution) was developed with the aim of overcoming many of the limitations of current methodologies for the sampling of airborne VOCs and odours. One of the main objectives was to develop a sampling method allowing the possibility of sample integrity for long periods of time. With CRYOCORE, the samples are condensed in a silanized stainless steel condenser and kept under cryogenic conditions until their analysis in the laboratory [144].

The collected sample is immediately condensed at -196°C into a 50 mL fused-silica-coated stainless-steel condenser and kept under cryogenic conditions (-196°C). The recovery of the cryo-condensed sample is presented in Figure 5.16.

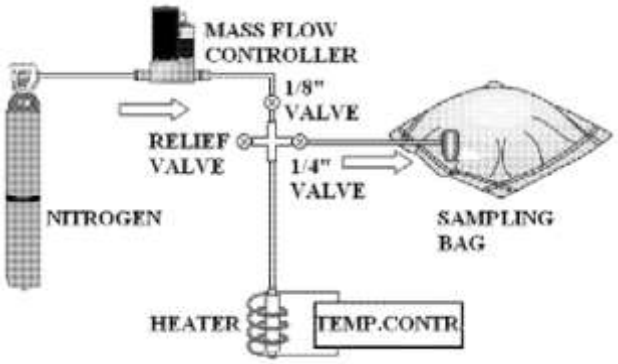

Figure 5.16: Scheme of the recovery setup [144].

A.5.4.2 Adsorptive sampling

The commonly used sampling method in polymeric sample bags has severe disadvantages. Due to adsorption, reaction and diffusion processes, the original concentrations of the species are strongly reduced. The technique of adsorptive sampling and subsequent thermal desorption has shown quantitative collection and recovery for a large number of chemical species [28].

At this principle, multibed adsorbents are used to trap volatiles with differing chemical properties. The recommendations regarding odour sampling are very exact. The biogenic odorants ammonia and hydrogen sulphide are especially critical [28].

Figure 5.17 shows a hypothetical three bed adsorption. The first bed is silica gel for the trapping of water, ammonia, and hydrogen sulphide. The following two beds are made of one weak and one strong adsorbent, Tenax™ and Carbosieve S3™. Tenax has proved to be an efficient adsorbent for the semi volatiles. Carbosieve, on the other hand, can trap the low boiling, high volatile compounds. Hydrogen sulphide, which may have passed the silica gel, is also trapped in the Carbosieve bed to a certain extent [28].

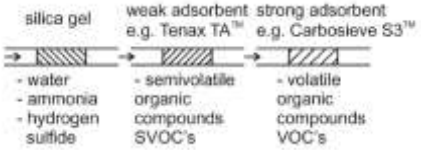

Figure 5.17: Adsorption of odour samples with multiple adsorbents [28].

The trapping of the odorous volatiles is only the first step of the new sampling method. The multi-step desorption and reconstitution method is presented in Figure 5.18. Inert carrier gas is used in the desorption process. This avoids the danger of oxidation reactions of the trapped compounds. To reconstitute the original matrix, the rest of the volume can be complemented with synthetic odourless (humidified) air [28].

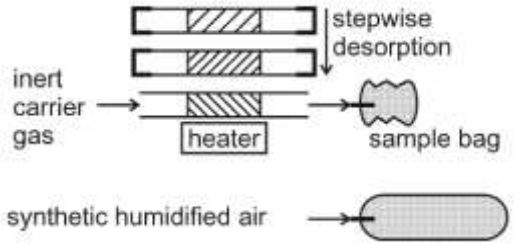

Figure 5.18: Multistep desorption and reconstitution of odour samples [28].

A.5.5 Odour sampling of volatile sulphur compounds

Volatile sulphur compounds (VSC) are odorous compounds that are very malodorous as well at very low gas concentrations (ppb range). Also, VSC are reactive and soluble. Listed characteristics demand careful selection of materials sampling equipment and the implementation of measures to prevent changing of sample matrix during sampling, transport to laboratory and measurements.

Identifying and quantifying VSC in air is challenging due to their volatility, reactivity, and low concentrations [26].

The stability of VSC can also be questionable between odour measurements with olfactometers. Some VSC can react with surfaces of an olfactometers dilution system. The tests in the study of gas mixture stability (H_2S, methanethiol, DMS) in two olfactometers made of glass and other of steel and Teflon [39] showed losses of all compounds of gas mixture. The average loss of H_2S was 60% for the glass olfactometer and 55% for the olfactometer with stainless steel and Teflon. The average loss of methanethiol was 35% in the olfactometer with glass and 27% in the olfactometer with stainless steel and Teflon. DMS was only slightly affected by the dilution system in the olfactometer with glass with an average loss at 9.3%, whereas 21% was lost in the olfactometer with stainless steel and Teflon.

The emission of VSC, in particular from facilities where biological processes are present, can be a major contributor to odour emissions. VSC are often found in emissions from intensive livestock, waste management and wastewater treatment [26]. VSCs have been identified as the dominant odorants emitted from both municipal sewage systems and pulp and paper mill facilities [30].

Field sampling of VSCs for speciation purposes consists of either pre-concentration of select compounds or whole air samples. Pre-concentration of VSC in ambient air using solid-phase microextraction (SPME) has been demonstrated to be inadequate for quantitative purposes due to competitive sorption/reverse diffusion of other volatile compounds, transformation of compounds during analysis, and difficulty of calibrating fibres matching the sampling air matrix. While there has been some success in the use of sorbent tubes for VSC analysis, relative humidity, and transformation of VSC during analysis are still major obstacles faced when using sorbent tubes. Whole air sampling has many of the same issues that pre-concentration techniques have since air samples from these containers must be concentrated with SPME fibres or thermal desorption tubes prior to analysis. In addition, Tedlar bags may be effective at holding VSCs in dry environments; however, in humid environments, this technique has been shown to sorb and potentially degrade VSCs. Drying of air using desiccates has been shown to improve results with Tedlar bags, but the results are short term due to the diffusion of humidity into the bags with storage. Stainless-steel canisters and surfaces have also been found an unsuitable material for the sampling and transferring of VSCs since exposure to these surfaces leads to the rapid loss of the most reactive compounds. The development of fused silica coatings onto stainless steel has reduced the surface reactivity of stainless steel and improved the storage stability and recovery of VSCs from stainless steel canisters [26].

Post collection, the samples must be transported and possibly stored prior to chemical or odour evaluation. The decay, degradation or transformation of the sample may result in incorrect results. Exposure of the sample to light, and/or temperature fluctuations could result in chemical transformation and lead to incorrect conclusions [25].

A.6 Odour Dispersion Modelling

Atmospheric dispersion modelling is a statistical technique which builds up a quantitative model by predicting where emissions will go and at what concentration they will arrive. By predicting this concentration in terms of different atmospheric parameters, it is possible to predict the effect of worst possible conditions or even to simulate a full year of weather changes. Dispersion modelling is usually carried out using internationally recognized computer programs. These models are generally a cost-effective replacement for direct field measurement of ambient air quality and, in the case of new installations or pollution control studies, are the only means of assessing the effects of air discharges on the environment [34].

The ultimate goal of an atmospheric dispersion model applied to odour is to accurately predict concentration downwind of any source under any atmospheric conditions. Atmospheric processes are so complex, and our understanding so elementary, that all currently used models have limitations on their applicability. Models have been developed to evaluate different source types (point, area, and volume), different terrain (simple or complex), different locales (urban, rural), different release rates (plume, puff) and different meteorological conditions (stable, convective). The general suggestion is that the model(s) that most closely approximate the parameters of the source or characteristics of the dispersion process under analysis should be selected [36].

There are several characteristics peculiar to odour which directly affect the modelling process. These are [34]:

Odours are complex and subjective by nature and are difficult to quantify, i.e., it is difficult to get realistic emission rates.

Odorous sources are often characterised by a varied and often complicated network of structures, such as roof vents, stacks, large area sources and door leaks.

Modelling of odours is complex. Some odours mask others, and other odours change in their intensity with distance and exposure to air and light. In some circumstances, the effect of an odour mixture can be less or greater than the sum of its component chemicals (called a "synergistic" effect). Thus, odours are not essentially additive, and it can be incorrect to model assuming they are so. However, there is no quantifiable alternative assumption that can be developed because each mixture of odorous compounds behaves differently. Therefore, the assumption that odours are additive must remain, at least for the present time.

Because of the intermittent nature of odours, a full year of meteorology is recommended for input into dispersion models. This allows more accurate interpretation of the results, such as estimating frequencies of occurrence.

Intensity does not change in direct proportion with dilution.

A.6.1 Models used in odour dispersion modelling

Air dispersion models were broadly divided into Gaussian plume models (steady-state models) and advanced numerical models (unsteady-state models). Gaussian plume models, which have been applied in practical use for a long time, are well understood and have received wide approval. Although created some years later than the Gaussian-plume models, advanced models have been in use for scientific research for decades, and are now getting more and more good appraisement based on their performances in odour dispersion [145].

The characteristic of numerical models is that the area to be examined is divided into individual cells. Instead of a closed solution, the model equations are solved for each cell and time interval. The refinement of the grid as well as intelligent approximations and equation resolvers allow very high calculation precision to be achieved. With regard to the numerical models, a distinction is made between Euler models and Lagrange models. Lagrange models simulate the flow by calculating the trajectories of particles which are subject to the laws of point mechanics in the flow field. Lagrange models have some advantages over the Euler models. The numerical treatment of the advection-diffusion approach leads to the effect of numerical diffusion in Euler models. With the aid of Lagrange models, the behaviour of particles with a mass, as well as ongoing chemical processes, can be described well [38].

A.6.1.1 Gaussian plume models

The Gaussian plume models are the most commonly developed air dispersion model. They are the base for developing most dispersion calculations for the continuous pollution source in the uniform dispersion field. Figure 5.19 shows the approach of typical point source pollution dispersion in the Gaussian plume modelling. It can be observed from the figure that the bell-shaped distribution of the pollution plume is the same in every direction in the three-dimensional space.

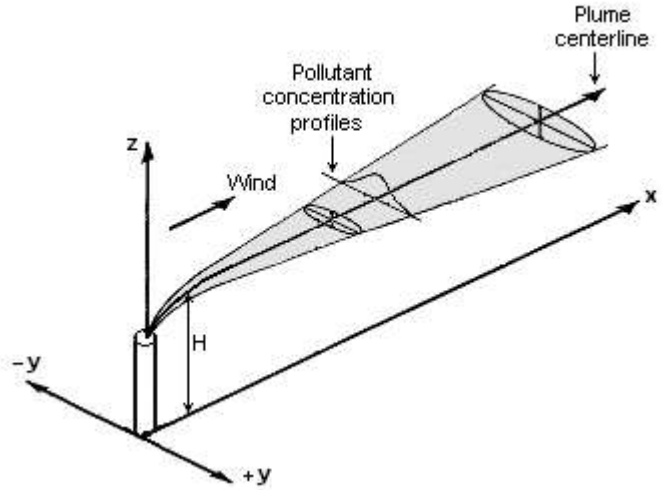

Figure 5.19: A typical plume from an elevated point source in the Gaussian plume modelling [145].

The Gaussian plume equation can be expressed as [38]

$$C_{(x,y,z)} = \frac{Q}{2\pi\,\sigma_y\sigma_z u_h} \cdot e^{\frac{y^2}{2\sigma_y^2}} \cdot \left(e^{\frac{(z-H)^2}{2\sigma_z^2}} + e^{\frac{(z+H)^2}{2\sigma_z^2}} \right) \quad (5.5)$$

Where:

$C_{(x, y, z)}$ is the concentration at the location (x, y, z) in OU/m^3,

Q is the source strength in kOU/m^3,

u_h is the wind speed in m/s in the direction of x axis,

6_y, 6_z are horizontal and vertical dispersion parameters (standard deviations) in meters,

H is effective source height in meters.

For the centreline concentration of ground-level odour source (e.g., agricultural odour source), the value of z = H = y = 0, so we get [145]

$$C_{(x,y,z)} = \frac{Q}{2\pi\,\sigma_y\sigma_z u_h} \quad (5.6)$$

The formula used in Gaussian plume models was derived from the assumption that the whole field where the pollutant disperses is in 'steady-state' condition. Some limitations originally existed because of this assumption.

For example, when calculating each hour's concentration (most of the Gaussian models calculate concentration for each single hour), it excludes the effect of contaminants of previous hours. Due to limitations, this kind of model can be used under situations where the topography is relatively flat without complicated terrain as hills, rivers, or bumps; the meteorology is "simple", i.e., pretty uniform in spatiality, and without many calm conditions [145].

A.6.1.2 LaGrangeian puff models

Advanced models were grouped into three categories: particles, puff, and grid points depending on the way the air pollutants are represented. Puff model is the most widely used advanced model because it can under most circumstances effectively consider the real meteorological condition to be simulated [145].

Puff models address the two disadvantages of plume models. Puff models calculate the distance that a plume can travel based on the wind speed during one simulation time period. A puff model also has memory. The position of the plume at the end of each time period becomes the starting position of the plume for the next time period as shown in Figure 5.20. In this way, puff models have a more realistic presentation of dispersion than plume models [133].

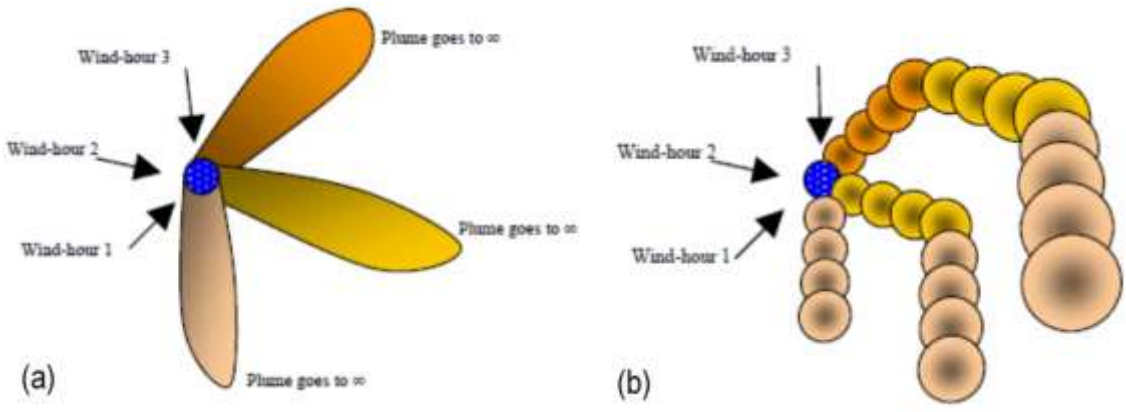

Figure 5.20: Dispersion pattern for different types of models; (a) dispersion from a Gauss steady-state model, (b) dispersion from non-steady state models [145].

Although the puff model requires three-dimensional meteorological data, it can also use the measurements from a weather observation tower as used in other models. Figure 5.21 illustrates the approach puffs travel in atmosphere from a point source adopted by puff models [145].

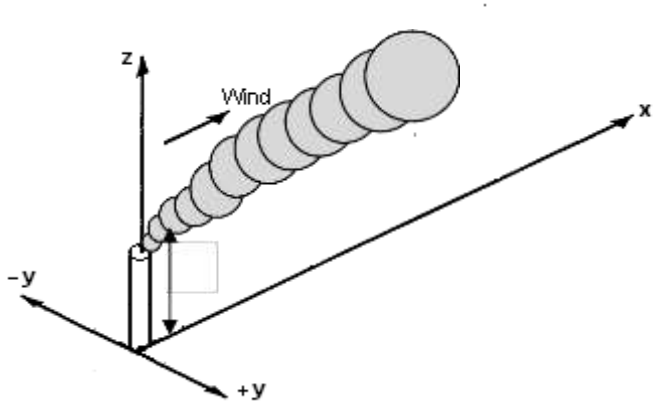

Figure 5.21: A typical plume from an elevated point source in the Lagrangian puff modelling [145].

The Lagrangian puff formula can be expressed as [145]:

$$C_{(x,y,z)}=\frac{Q_{ip}}{(2\pi)^{1,5}\,\sigma_x\sigma_y\sigma_z u_h}\cdot e^{\left[-0,5\left(\frac{x}{\sigma_x}\right)^2-0,5\left(\frac{y}{\sigma_y}\right)^2\right]}\cdot\left(e^{\left[-0,5\left(\frac{z-H}{\sigma_z}\right)^2\right]}+e^{\left[-0,5\left(\frac{z+H}{\sigma_z}\right)^2\right]}\right) \quad (5.7)$$

Where:
Q_{ip} is the instantaneous point source emission rate (source strength).

For centreline concentration of ground-level odour source (e.g., agricultural odour source), the value of y = z = H = 0, so we get [145]:

$$C_{(x,y,z)}=\frac{Q_{ip}}{(2\pi)^{1,5}\,\sigma_x\sigma_y\sigma_z u_h}\cdot e^{\left[-0,5\left(\frac{x}{\sigma_x}\right)^2\right]} \quad (5.8)$$

From upper equations we can see that the theoretical basis of two models for ground-level pollution sources is the same; however, puff models consider time-dependent and longitudinal dispersion. Although puff dispersion model is more sophisticated and can better represent actual weather conditions, it still has some disadvantages compared to plume models. For example, it is more difficult to handle the weather data in puff models. Puff model is suggested to be used in some circumstances, such as when the meteorological condition or terrain is very complicated, or the period of low wind speed happens [145].

Appendix B

Physical and Chemical Properties of DMS, H_2S, CS_2 and COS

Table 5.3: Summary of physical and chemical properties of DMS [47].

Synonym(s):	dimethyl sulphide, dimethyl monosulphide, dimethyl thioether, thiobismethane, DMS
Molecular Formula:	C_2H_6S
Molecular Weight:	62.14 g/mol
CAS Number:	75-18-3
Appearance:	colourless to straw-coloured liquid
Odour:	unpleasant odour
Boiling Point and Melting Point:	310.4 K & 174.8 K
Heat of Vaporization:	28.09 kJ g/mol @ 298 K
Vapour Pressure:	66.9 kPa @ 298 K
Critical Temperature and Pressure:	502 K & 5.68 MPa
Octanol/Water Partition Coefficient:	log Kow = 0.92
Solubility in Water at 298 K:	22 g/dm^3
Specific Gravity as Gas (air = 1):	2.14
Concentration Conversion Factor:	1 ppm = 2.54 mg/m^3

Table 5.4: Summary of physical and chemical properties of H_2S [47].

Synonym(s):	hydrogen sulphide, dihydrogen sulphide, hydrogen sulphur
Molecular Formula:	H_2S
Molecular Weight:	34.08 g/mol
CAS Number:	7783-06-4
Appearance:	colourless gas, sweetish taste
Odour:	offensive strong odour of rotten eggs
Boiling Point and Melting Point:	212.82 K & 187.66 K
Vapour Pressure:	2.08 MPa @ 298 K
Critical Temperature and Pressure:	373 K & 9.01 MPa
Octanol/Water Partition Coefficient:	no data
Solubility in Water at 293 K:	4.13 g/dm^3
Specific Gravity as Gas (Air = 1):	1.19
Dissociation Constant:	$pKa_1 = 7.04$; $pKa_2 = 11.96$
pH:	4.5 in fresh water solution
Heat of Vaporization:	14.08 kJ g/mol @ 298 K
Concentration Conversion Factor:	1 ppm = 1.42 mg/m^3

Table 5.5: Summary of physical and chemical properties of CS_2 [47].

Synonym(s):	carbon bisulfide, carbon sulphide, carbon disulphide
Molecular Formula:	CS_2
Molecular Weight:	76.14 g/mol
CAS Number:	75-15-0
Appearance:	Liquid
Odour:	foul smelling commercial grades, sweetish aromatic when pure
Boiling Point and Melting Point:	319 K & 161.6 K
Heat of Vaporization:	26.72 kJ g/mol @ boiling point
Vapour Pressure:	47.9 kPa @ 298 K
Critical Temperature and Pressure:	552 K & 7.9 MPa
Octanol/water Partition Coefficient:	log Kow = 1.94
Solubility in Water:	2860 mg/dm^3
Specific Gravity as Gas (Air = 1):	2.67
Specific Gravity as Liquid (Water = 1):	1.2632
Concentration Conversion Factor:	1 ppm = 3.16 mg/m^3

Table 5.6: Summary of physical and chemical properties of COS [47].

Synonym(s):	carbon oxysulphide, carbon monoxide monosulphide
Molecular Formula:	COS
Molecular Weight:	60.08 g/mol
CAS Number:	436-58-1
Appearance:	colourless gas
Odour:	typical sulphide when pure
Boiling Point & Melting Point:	223 K & 135 K
Heat of Vaporization:	18.506 kJ g/mol @ 222.9 K
Vapour Pressure:	1.25 MPa @ 298 K
Critical Temperature & Pressure:	378.8 K & 6.35 MPa
Octanol/Water Partition Coefficient:	log Kow = 0.8009 (estimated)
Solubility in Water at 293 K:	1440 mg/dm^3
Specific Gravity as Gas (Air = 1):	2.1
Specific Gravity as Liquid (Water = 1):	1.028
Concentration Conversion Factor:	1 ppm = 2.49 mg/m^3

Appendix C

Modelling of Leakage of Mass Flow from the Ducting

The objective of the modelling is to define leakage of mass flow at the joints of the ventilation ducting. The ducts are 10 m long and for a 500 m long ducting, there are at least 49 joints. Actual ducting for the planned experiment is longer, because the first 30 to 50 m are meant for steadying the flow after the pneumatic fan pushes the air into ducting.

In the experiment with ventilation ducting, if the experiment also allowed to define a decay of DMS while traveling with mine ventilation, then the mass flow must be constant, or it is necessary to find a way to define the DMS loss at the joints.

The modelling was conducted in the Ventsim Visual software. The main characteristics of the model setup are as shown in figures between Figure 5.22 and Figure 5.25:

- Air entering and return shafts, both 160 m deep, with main exhaust fan (default option in software). The main fan was set at 18 % of total power.
- The length of level airway is 1000 m. For modelling reasons (construction of ducting) it is divided in three parts: Airway 1, Airway 2 and Airway 3.
- Approx. 550 m long ducting with diameter 0.6 m consists of 58 ducts (numbers from 0 to 57) with default auxiliary fan in software. The ducting is constructed on the whole length of Airway 2. The leakage was set on “low” (lowest (except nil) of default options of leakage porosity in software). The set value was 25 mm^2/m^2 as total area of hols per area of duct. The leakage porosity is constant throughout the entire ducting length.

The air simulation in the model considers a compressible flow. The airflow rates are approximations of airflow rates in CMV in the area of the planed experiment and as planned for the experiment. The simulation was focused on the leakage of mass flow mainly through joints of ducting.

Three examples were simulated:

- Example 1: Simulates experiment setup with the airflow rates in the ducting as in regular mining activities. That means that they are much higher than airflow rates planned for the experiment.
- Example 2: Simulates experiment setup with the airflow rates in the ducting as planned for the experiment.
- Example 3: Simulates experiment setup with the airflow rates in the ducting as planned for the experiment and in addition to the cross-section reduction at the end of the ducting.

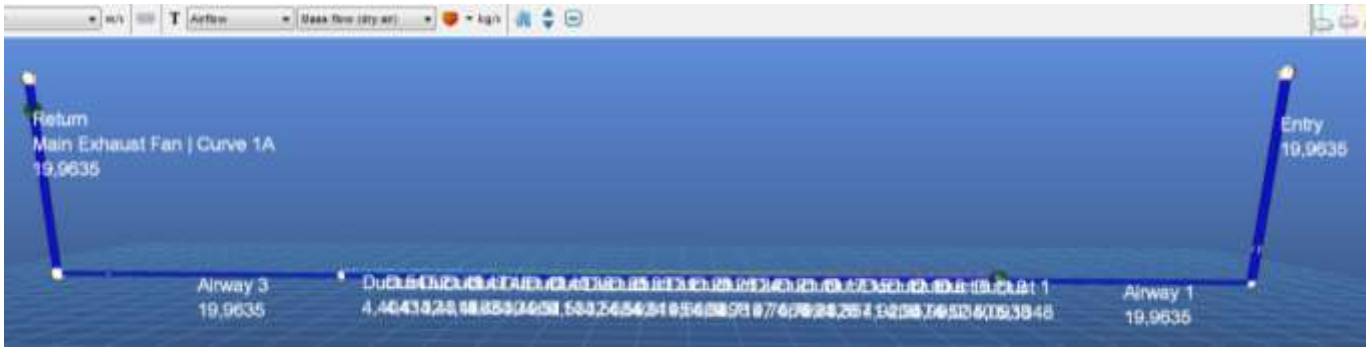

Figure 5.22: Model of planned experiment with entry and return, and the 1000 m long airway with 550 m of forced auxiliary ventilation layout with 0.6 m ducting. Presented mass flows are results of simulation with compressible flows.

Figure 5.23: Zoomed in Figure 5.22 in the ducting area with the auxiliary fan at the start of

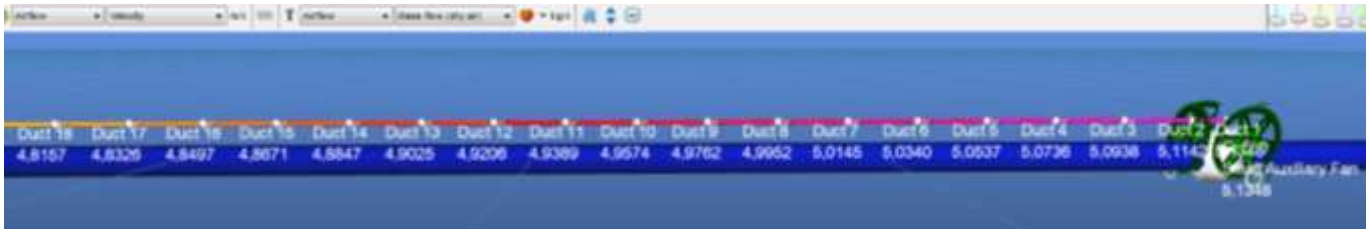

ducting and with the mass flow values in the ducts.

Figure 5.24: Zoomed in Figure 5.22 in the ducting area with the mass flow values in the ducts.

Figure 5.25: Zoomed in Figure 5.22 in the ducting area with an exit of air back into the airway with the mass flow values in the ducts.

Example 1

The simulation results are presented in figures between Figure 5.22 and Figure 5.25 and Table 5.7. The auxiliary fan was set to 100 % power as is usual in mine activities.

The presented mass flow values show the decreasing of mass flow. In Table 1, the last column on the right shows values of leakage for each duct. The values show the decreasing of leakage of mass flow through the ducting. The reason are pressure drops along the ducting for overcoming resistance of ducting and moving the air, and additionally for loss of mass flow.

The total loss of mass flow is 14.3 % or 2.6 % per 100 m of ducting (mass flow losses are comparable to the losses of ducting of brand new ducts, on CMV they were measured as low as 2% per 100 m). The maximum leakage at the first joint is 0.0206 kg/s and the minimum leakage at the last joint is 0.0017 kg/s. The difference between leakages is 91.7 %.

Example 2

The simulation results are presented in Table 5.8: Results of simulation for Example 2. For the actual experiment to maximize the traveling time of DMS, the auxiliary fan was set to only 3 % power to achieve targeted average airflow velocity, approximately 0.7 m/s, which gives a traveling time of approximately 12 minutes.

The presented mass flow values in Table 2 show the decreasing of mass flow due to the same reasons as in example 1. But because of such low fan power which gives such low mass flow rates at the joint between ducts 22 and 23, the direction of the leakage becomes reverse and the “airway starts to leak in the ducting”. In reality, this manifests in the collapse of the soft ducting that is used for the forced auxiliary ventilation layout. This phenomenon also appeared at pre-tests on the previous experiment. The collapsing of the ducting was overcome with the cross-section reduction at the end of ducting.

Example 3

The simulation results are presented in Table 5.9: Results of simulation for Example 3. This simulation is an addition to the simulation of example 2. The targeted average airflow velocity is the same as in example 2. The auxiliary fan was set to only 6 % power to overcome additional resistance due to shock losses of cross-section reduction.

Due to the cross-section reduction/additional resistance, the total loss of mass flow is 28.1 % or 5.1 % per 100 m of ducting.

The decreasing of mass flow leakage is as obvious due to the pressure losses as in example 1 because we are dealing with much less mass flow that we want to move through the ducting. In fact, because of the cross-section reduction, the leakage of mass flow starts to increase towards the end of ducting. The maximum leakage is 0.0014 kg/s and the minimum leakage is 0.0011 kg/s. The difference between leakages is 21.4 %. The difference is much smaller than in example 1. This shows that cross-section reductions help with averaging of mass flow leakages if we assume that each joint of duct is geometrically the same. Taking into account the simulation results, in theory, it is possible to make all joints with the same rate of mass flow leakage with adding additional reduction. But that would also increase the total mass flow loss of the ducting.

Table 5.7: Results of simulation for Example 1.

Airway Name	Profile	Size Dimensions m	Size Length m	Mass flow (dry air) kg/s	Δ Mass flow (dry air) = LEAKAGE kg/s
Entry	Round	6,0 Diameter	160	19.9635	
Return	Round	6,0 Diameter	160	19.9635	
Airway 1	Round	4,0 Diameter	200.1	19.9635	
Airway 2	Round	4,0 Diameter	548.9	15.3026	
Airway 3	Round	4,0 Diameter	251	19.9635	
Duct 0	Round	0,6 Diameter	0	5.1348	
Duct 1	Round	0,6 Diameter	5	5.1348	0.0000
Duct 2	Round	0,6 Diameter	10	5.1142	0.0206
Duct 3	Round	0,6 Diameter	10	5.0938	0.0204
Duct 4	Round	0,6 Diameter	10	5.0736	0.0202
Duct 5	Round	0,6 Diameter	10	5.0537	0.0199
Duct 6	Round	0,6 Diameter	10	5.034	0.0197
Duct 7	Round	0,6 Diameter	10	5.0145	0.0195
Duct 8	Round	0,6 Diameter	10	4.9952	0.0193
Duct 9	Round	0,6 Diameter	10	4.9762	0.0190
Duct 10	Round	0,6 Diameter	10	4.9574	0.0188
Duct 11	Round	0,6 Diameter	10	4.9389	0.0185
Duct 12	Round	0,6 Diameter	10	4.9206	0.0183
Duct 13	Round	0,6 Diameter	10	4.9025	0.0181
Duct 14	Round	0,6 Diameter	10	4.8847	0.0178
Duct 15	Round	0,6 Diameter	10	4.8671	0.0176
Duct 16	Round	0,6 Diameter	10	4.8497	0.0174
Duct 17	Round	0,6 Diameter	10	4.8326	0.0171
Duct 18	Round	0,6 Diameter	10	4.8157	0.0169
Duct 19	Round	0,6 Diameter	10	4.7991	0.0166
Duct 20	Round	0,6 Diameter	10	4.7827	0.0164
Duct 21	Round	0,6 Diameter	10	4.7666	0.0161
Duct 22	Round	0,6 Diameter	10	4.7507	0.0159
Duct 23	Round	0,6 Diameter	10	4.7351	0.0156
Duct 24	Round	0,6 Diameter	10	4.7197	0.0154
Duct 25	Round	0,6 Diameter	10	4.7046	0.0151
Duct 26	Round	0,6 Diameter	10	4.6898	0.0148
Duct 27	Round	0,6 Diameter	10	4.6752	0.0146
Duct 28	Round	0,6 Diameter	10	4.6609	0.0143
Duct 29	Round	0,6 Diameter	10	4.6468	0.0141
Duct 30	Round	0,6 Diameter	10	4.633	0.0138
Duct 31	Round	0,6 Diameter	10	4.6195	0.0135
Duct 32	Round	0,6 Diameter	10	4.6063	0.0132
Duct 33	Round	0,6 Diameter	10	4.5934	0.0129
Duct 34	Round	0,6 Diameter	10	4.5807	0.0127
Duct 35	Round	0,6 Diameter	10	4.5684	0.0123
Duct 36	Round	0,6 Diameter	10	4.5563	0.0121
Duct 37	Round	0,6 Diameter	10	4.5446	0.0117
Duct 38	Round	0,6 Diameter	10	4.5332	0.0114
Duct 39	Round	0,6 Diameter	10	4.5221	0.0111
Duct 40	Round	0,6 Diameter	10	4.5114	0.0107
Duct 41	Round	0,6 Diameter	10	4.5009	0.0105
Duct 42	Round	0,6 Diameter	10	4.4909	0.0100
Duct 43	Round	0,6 Diameter	10	4.4812	0.0097
Duct 44	Round	0,6 Diameter	10	4.4719	0.0093
Duct 45	Round	0,6 Diameter	10	4.463	0.0089
Duct 46	Round	0,6 Diameter	10	4.4544	0.0086
Duct 47	Round	0,6 Diameter	10	4.4463	0.0081
Duct 48	Round	0,6 Diameter	10	4.4387	0.0076
Duct 49	Round	0,6 Diameter	10	4.4315	0.0072
Duct 50	Round	0,6 Diameter	10	4.4249	0.0066
Duct 51	Round	0,6 Diameter	10	4.4187	0.0062
Duct 52	Round	0,6 Diameter	10	4.4132	0.0055
Duct 53	Round	0,6 Diameter	10	4.4083	0.0049
Duct 54	Round	0,6 Diameter	10	4.4043	0.0040
Duct 55	Round	0,6 Diameter	10	4.4011	0.0032
Duct 56	Round	0,6 Diameter	3.9	4.3994	0.0017
Duct 57	Round	0,6 Diameter	0	4.3994	0.0000

Table 5.8: Results of simulation for Example 2.

Airway Name	Profile	Size Dimensions m	Size Length m	Mass flow (dry air) kg/s	Δ Mass flow (dry air) = LEAKAGE kg/s
Entry	Round	6,0 Diameter	160	19.4696	
Return	Round	6,0 Diameter	160	19.4696	
Airway 1	Round	4,0 Diameter	200.1	19.4696	
Airway 2	Round	4,0 Diameter	548.9	19.2201	
Airway 3	Round	4,0 Diameter	251	19.4696	
Duct 0	Round	0,6 Diameter	0	0.2561	
Duct 1	Round	0,6 Diameter	5	0.2561	0
Duct 2	Round	0,6 Diameter	10	0.2555	0.0006
Duct 3	Round	0,6 Diameter	10	0.2549	0.0006
Duct 4	Round	0,6 Diameter	10	0.2542	0.0007
Duct 5	Round	0,6 Diameter	10	0.2536	0.0006
Duct 6	Round	0,6 Diameter	10	0.2531	0.0005
Duct 7	Round	0,6 Diameter	10	0.2525	0.0006
Duct 8	Round	0,6 Diameter	10	0.252	0.0005
Duct 9	Round	0,6 Diameter	10	0.2514	0.0006
Duct 10	Round	0,6 Diameter	10	0.2509	0.0005
Duct 11	Round	0,6 Diameter	10	0.2505	0.0004
Duct 12	Round	0,6 Diameter	10	0.25	0.0005
Duct 13	Round	0,6 Diameter	10	0.2496	0.0004
Duct 14	Round	0,6 Diameter	10	0.2492	0.0004
Duct 15	Round	0,6 Diameter	10	0.2488	0.0004
Duct 16	Round	0,6 Diameter	10	0.2485	0.0003
Duct 17	Round	0,6 Diameter	10	0.2482	0.0003
Duct 18	Round	0,6 Diameter	10	0.2479	0.0003
Duct 19	Round	0,6 Diameter	10	0.2477	0.0002
Duct 20	Round	0,6 Diameter	10	0.2476	0.0001
Duct 21	Round	0,6 Diameter	10	0.2475	1E-04
Duct 22	Round	0,6 Diameter	10	0.2476	-1E-04
Duct 23	Round	0,6 Diameter	10	0.2478	-0.0002
Duct 24	Round	0,6 Diameter	10	0.2481	-0.0003
Duct 25	Round	0,6 Diameter	10	0.2484	-0.0003
Duct 26	Round	0,6 Diameter	10	0.2487	-0.0003
Duct 27	Round	0,6 Diameter	10	0.249	-0.0003
Duct 28	Round	0,6 Diameter	10	0.2494	-0.0004
Duct 29	Round	0,6 Diameter	10	0.2486	0.0008
Duct 30	Round	0,6 Diameter	10	0.2477	0.0009
Duct 31	Round	0,6 Diameter	10	0.2468	0.0009
Duct 32	Round	0,6 Diameter	10	0.246	0.0008
Duct 33	Round	0,6 Diameter	10	0.2452	0.0008
Duct 34	Round	0,6 Diameter	10	0.2444	0.0008
Duct 35	Round	0,6 Diameter	10	0.2436	0.0008
Duct 36	Round	0,6 Diameter	10	0.2428	0.0008
Duct 37	Round	0,6 Diameter	10	0.242	0.0008
Duct 38	Round	0,6 Diameter	10	0.2413	0.0007
Duct 39	Round	0,6 Diameter	10	0.2405	0.0008
Duct 40	Round	0,6 Diameter	10	0.2398	0.0007
Duct 41	Round	0,6 Diameter	10	0.2391	0.0007
Duct 42	Round	0,6 Diameter	10	0.2384	0.0007
Duct 43	Round	0,6 Diameter	10	0.2377	0.0007
Duct 44	Round	0,6 Diameter	10	0.2371	0.0006
Duct 45	Round	0,6 Diameter	10	0.2364	0.0007
Duct 46	Round	0,6 Diameter	10	0.2358	0.0006
Duct 47	Round	0,6 Diameter	10	0.2352	0.0006
Duct 48	Round	0,6 Diameter	10	0.2345	0.0007
Duct 49	Round	0,6 Diameter	10	0.234	0.0005
Duct 50	Round	0,6 Diameter	10	0.2334	0.0006
Duct 51	Round	0,6 Diameter	10	0.2328	0.0006
Duct 52	Round	0,6 Diameter	10	0.2323	0.0005
Duct 53	Round	0,6 Diameter	10	0.2318	0.0005
Duct 54	Round	0,6 Diameter	10	0.2313	0.0005
Duct 55	Round	0,6 Diameter	10	0.2308	0.0005
Duct 56	Round	0,6 Diameter	3.9	0.2303	0.0005
Duct 57	Round	0,6 Diameter	0	0.2303	0

Table 5.9: Results of simulation for Example 3.

Airway Name	Profile	Size Dimensions m	Size Length m	Mass flow (dry air) kg/s	Δ Mass flow (dry air) = LEAKAGE kg/s
Entry	Round	6,0 Diameter	160	19.457	
Return	Round	6,0 Diameter	160	19.457	
Airway 1	Round	4,0 Diameter	200.1	19.457	
Airway 2	Round	4,0 Diameter	548.9	19.2374	
Airway 3	Round	4,0 Diameter	251	19.457	
Duct 0	Round	0,6 Diameter	0	0.2534	
Duct 1	Round	0,6 Diameter	5	0.2534	0
Duct 2	Round	0,6 Diameter	10	0.252	0.0014
Duct 3	Round	0,6 Diameter	10	0.2507	0.0013
Duct 4	Round	0,6 Diameter	10	0.2493	0.0014
Duct 5	Round	0,6 Diameter	10	0.248	0.0013
Duct 6	Round	0,6 Diameter	10	0.2467	0.0013
Duct 7	Round	0,6 Diameter	10	0.2454	0.0013
Duct 8	Round	0,6 Diameter	10	0.2441	0.0013
Duct 9	Round	0,6 Diameter	10	0.2428	0.0013
Duct 10	Round	0,6 Diameter	10	0.2415	0.0013
Duct 11	Round	0,6 Diameter	10	0.2402	0.0013
Duct 12	Round	0,6 Diameter	10	0.2389	0.0013
Duct 13	Round	0,6 Diameter	10	0.2377	0.0012
Duct 14	Round	0,6 Diameter	10	0.2364	0.0013
Duct 15	Round	0,6 Diameter	10	0.2351	0.0013
Duct 16	Round	0,6 Diameter	10	0.2339	0.0012
Duct 17	Round	0,6 Diameter	10	0.2327	0.0012
Duct 18	Round	0,6 Diameter	10	0.2314	0.0013
Duct 19	Round	0,6 Diameter	10	0.2302	0.0012
Duct 20	Round	0,6 Diameter	10	0.229	0.0012
Duct 21	Round	0,6 Diameter	10	0.2278	0.0012
Duct 22	Round	0,6 Diameter	10	0.2266	0.0012
Duct 23	Round	0,6 Diameter	10	0.2254	0.0012
Duct 24	Round	0,6 Diameter	10	0.2243	0.0011
Duct 25	Round	0,6 Diameter	10	0.2231	0.0012
Duct 26	Round	0,6 Diameter	10	0.2219	0.0012
Duct 27	Round	0,6 Diameter	10	0.2208	0.0011
Duct 28	Round	0,6 Diameter	10	0.2196	0.0012
Duct 29	Round	0,6 Diameter	10	0.2182	0.0014
Duct 30	Round	0,6 Diameter	10	0.2168	0.0014
Duct 31	Round	0,6 Diameter	10	0.2154	0.0014
Duct 32	Round	0,6 Diameter	10	0.214	0.0014
Duct 33	Round	0,6 Diameter	10	0.2126	0.0014
Duct 34	Round	0,6 Diameter	10	0.2112	0.0014
Duct 35	Round	0,6 Diameter	10	0.2098	0.0014
Duct 36	Round	0,6 Diameter	10	0.2085	0.0013
Duct 37	Round	0,6 Diameter	10	0.2071	0.0014
Duct 38	Round	0,6 Diameter	10	0.2057	0.0014
Duct 39	Round	0,6 Diameter	10	0.2044	0.0013
Duct 40	Round	0,6 Diameter	10	0.203	0.0014
Duct 41	Round	0,6 Diameter	10	0.2017	0.0013
Duct 42	Round	0,6 Diameter	10	0.2004	0.0013
Duct 43	Round	0,6 Diameter	10	0.199	0.0014
Duct 44	Round	0,6 Diameter	10	0.1977	0.0013
Duct 45	Round	0,6 Diameter	10	0.1964	0.0013
Duct 46	Round	0,6 Diameter	10	0.195	0.0014
Duct 47	Round	0,6 Diameter	10	0.1937	0.0013
Duct 48	Round	0,6 Diameter	10	0.1924	0.0013
Duct 49	Round	0,6 Diameter	10	0.1911	0.0013
Duct 50	Round	0,6 Diameter	10	0.1898	0.0013
Duct 51	Round	0,6 Diameter	10	0.1885	0.0013
Duct 52	Round	0,6 Diameter	10	0.1872	0.0013
Duct 53	Round	0,6 Diameter	10	0.186	0.0012
Duct 54	Round	0,6 Diameter	10	0.1847	0.0013
Duct 55	Round	0,6 Diameter	10	0.1834	0.0013
Duct 56	Round	0,6 Diameter	3.9	0.1821	0.0013
Duct 57	Round	0,6 Diameter	0	0.1821	0

In conclusion, the simulations show that leakage of mass flow varies at joints between ducts. Even if all joints are geometrically the same, they have the same number of holes, and their sizes and shapes are the same. The leakage of mass flow also depends on pressure drops along the ducting to overcome resistance of ducting and air movement, and on the same parameters in the airway in which the ducting is mounted. Also, the total resistance of a specific duct can greatly vary from duct to duct if for example shock losses are added in the form of cross-section reduction for example.

The modelling data show that cross-section reductions are necessary to inflate the soft ducting and that such a reduction at the end of ducting can help average the leakage at joint because it actually increases the leakages towards the end of ducting as shown in example 3 and interrupts the leakage reduction along the ducting as shown in example 1.

The data revealed that, in theory, shock losses such as reduction of cross-sections can be arranged so that all ducting joints have the same mass flow leakage rate.

On the other side, such a setup with leakage of mass flow will not allow the detection of possible decay of DMS based on changes in mass flow rates.

Regarding the stability of DMS, it makes sense to monitor only gas concentrations in the ducting. And if DMS concentrations are constant throughout the ducting, then no DMS decay occurs.

There is a need for an experiment that supports the DMS dilution model. According to the literature data, DMS is not expected to decay in the mine, at least during the 10-15 minutes of travel to the surface. However, it should be taken into account that the travel time from the development heading is much longer, up to 1 hour.

The solution to this problem is in the ventilation ducts, which take control over the mine conditions, since it is assumed that the mixture of gasses in the turbulent flow will be constant regardless of mass flow losses.

Therefore, in the doctoral dissertation, it was proposed to test a constant gas mixture throughout the ducting channel despite the leakage of mass flow using two steps:

Step 1: First, to test the sensors, while the DMS 1 and DMS 2 sensors are mounted at location 1 (see locations 1 and 2 in Figure 3.4 and Figure 3.5 in Chapter 3.3.1.

Step 2: To move the DMS 2 sensor to location 2 while DMS 1 remains at location 1.

Appendix D

Results of 30-Minute Intervals

Table 5.10: Analysis results of 30-minute intervals of airflow rates and gases concentrations and emissions classified regarding production rates at zero production, e.g., standstill of longwall face or performing of support working phases, respectively.

Production intensity	DMS	CH_4	CO_2	Production rate	Airflow rate	DMS emission	CH_4 emission	CO_2 emission
0	[mg/m³]	[g/m³]	[g/m³]	[t/30min]	[m³/s]	[mg/s]	[kg/s]	[kg/s]
Num. of events	2725	2725	2725	2725	2725	2725	2725	2725
MAX	53.0	8.48	45.10	0	59.6	1692	0.162	0.967
MEAN	**13.2**	**3.52**	**17.89**	**0**	**25.7**	**334**	**0.088**	**0.442**
MIN	3.8	0.91	6.63	0	8.5	77	0.022	0.162
Std	6.9	0.87	5.01	0	8.2	200	0.028	0.152
97.5th percentile	31.2	5.40	28.24	0	39.6	817	0.135	0.760
75th percentile	16.5	4.12	21.25	0	31.9	441	0.107	0.550
50th percentile	12.0	3.42	17.30	0	25.5	297	0.093	0.434
25th percentile	7.4	2.95	14.17	0	22.3	160	0.071	0.315
2.5th percentile	5.4	2.06	9.81	0	10.9	116	0.034	0.204

Table 5.11: Analysis results of 30-minute intervals of airflow rates and gases concentrations and emissions classified regarding production rates between 1 and 100 tonnes per 30 minutes.

Production intensity	DMS	CH_4	CO_2	Production rate	Airflow rate	DMS emission	CH_4 emission	CO_2 emission
1-100	[mg/m³]	[g/m³]	[g/m³]	[t/30min]	[m³/s]	[mg/s]	[kg/s]	[kg/s]
Num. of events	442	442	442	442	442	442	442	442
MAX	44.9	6.16	32.87	100	47.3	1672	0.161	0.924
MEAN	**12.4**	**3.34**	**18.20**	**40**	**30.8**	**378**	**0.099**	**0.542**
MIN	2.2	1.34	7.92	1	9.8	82	0.035	0.171
Std	5.9	0.98	5.77	32	6.2	196	0.022	0.147
97.5th percentile	25.8	5.64	30.46	98	41.3	910	0.144	0.826
75th percentile	15.2	3.82	22.15	67	35.7	472	0.114	0.655
50th percentile	11.6	3.11	17.21	35	30.7	349	0.098	0.540
25th percentile	8.4	2.65	13.73	9	25.7	246	0.084	0.444
2.5th percentile	4.0	1.94	8.64	1	19.8	104	0.059	0.267

Table 5.12: Analysis results of 30-minute intervals of airflow rates and gases concentrations and emissions classified regarding production rates between 101 and 200 tonnes per 30 minutes.

Production intensity	DMS	CH_4	CO_2	Production rate	Airflow rate	DMS emission	CH_4 emission	CO_2 emission
101-200	[mg/m³]	[g/m³]	[g/m³]	[t/30min]	[m³/s]	[mg/s]	[kg/s]	[kg/s]
Num. of events	335	335	335	335	335	335	335	335
MAX	39.0	6.35	35.15	200	45.5	1328	0.159	1.038
MEAN	**13.4**	**3.33**	**18.78**	**149**	**30.6**	**406**	**0.098**	**0.556**
MIN	3.9	1.44	8.63	101	11.7	93	0.041	0.205
Std	6.4	0.94	5.86	30	6.0	214	0.022	0.151
97.5th percentile	29.9	5.49	31.24	199	40.4	1049	0.142	0.862
75th percentile	16.7	3.82	22.90	175	35.4	497	0.112	0.671
50th percentile	12.2	3.13	18.31	149	30.9	356	0.098	0.555
25th percentile	8.7	2.73	14.47	124	25.4	263	0.084	0.455
2.5th percentile	4.8	1.90	9.26	102	19.5	145	0.056	0.289

Table 5.13: Analysis results of 30-minute intervals of airflow rates and gases concentrations and emissions classified regarding production rates between 201 and 300 tonnes per 30 minutes.

Production intensity	DMS	CH_4	CO_2	Production rate	Airflow rate	DMS emission	CH_4 emission	CO_2 emission
201-300	[mg/m³]	[g/m³]	[g/m³]	[t/30min]	[m³/s]	[mg/s]	[kg/s]	[kg/s]
Num. of events	314	314	314	314	314	314	314	314
MAX	44.3	6.24	36.73	300	40.9	1642	0.162	1.048
MEAN	**17.0**	**3.54**	**21.52**	**250**	**30.5**	**516**	**0.105**	**0.639**
MIN	5.6	0.85	8.24	202	11.8	161	0.026	0.163
Std	6.9	0.95	5.62	29	5.6	245	0.021	0.147
97.5th percentile	33.1	5.77	32.36	298	39.6	1184	0.147	0.917
75th percentile	20.9	4.05	25.22	276	35.1	604	0.118	0.730
50th percentile	16.2	3.35	21.28	249	30.6	478	0.105	0.642
25th percentile	12.0	2.90	17.88	226	25.5	336	0.092	0.550
2.5th percentile	7.2	2.08	10.53	206	21.7	209	0.057	0.315

Table 5.14: Analysis results of 30-minute intervals of airflow rates and gases concentrations and emissions classified regarding production rates between 301 and 400 tonnes per 30 minutes.

Production intensity	DMS	CH_4	CO_2	Production rate	Airflow rate	DMS emission	CH_4 emission	CO_2 emission
301-400	[mg/m³]	[g/m³]	[g/m³]	[t/30min]	[m³/s]	[mg/s]	[kg/s]	[kg/s]
Num. of events	291	291	291	291	291	291	291	291
MAX	50.4	6.45	36.50	400	42.0	1876	0.162	1.065
MEAN	**18.4**	**3.65**	**22.42**	**349**	**30.7**	**565**	**0.109**	**0.670**
MIN	5.6	0.92	9.49	301	18.2	150	0.027	0.260
Std	8.0	1.03	6.01	29	5.1	280	0.022	0.145
97.5th percentile	38.8	6.00	33.87	399	39.0	1274	0.148	0.955
75th percentile	22.6	4.19	26.46	375	35.1	668	0.122	0.766
50th percentile	16.5	3.35	21.75	345	31.5	498	0.109	0.670
25th percentile	12.5	2.98	18.01	325	26.2	374	0.094	0.573
2.5th percentile	7.3	2.14	11.59	302	22.8	242	0.068	0.391

Table 5.15: Analysis results of 30-minute intervals of airflow rates and gases concentrations and emissions classified regarding production rates between 401 and 500 tonnes per 30 minutes.

Production intensity	DMS	CH_4	CO_2	Production rate	Airflow rate	DMS emission	CH_4 emission	CO_2 emission
401-500	[mg/m³]	[g/m³]	[g/m³]	[t/30min]	[m³/s]	[mg/s]	[kg/s]	[kg/s]
Num. of events	227	227	227	227	227	227	227	227
MAX	81.2	6.56	37.65	500	41.4	2232	0.163	1.015
MEAN	**20.2**	**3.70**	**23.73**	**450**	**30.8**	**620**	**0.112**	**0.713**
MIN	5.9	0.98	11.97	401	21.0	193	0.031	0.378
Std	9.9	0.97	5.66	27	5.0	314	0.020	0.134
97.5th percentile	45.0	5.94	34.80	496	39.5	1530	0.156	0.973
75th percentile	23.9	4.20	28.12	469	34.9	734	0.125	0.814
50th percentile	18.0	3.47	23.34	453	31.4	541	0.110	0.719
25th percentile	13.9	3.03	19.25	427	26.0	415	0.098	0.614
2.5th percentile	9.3	2.34	13.52	404	22.9	266	0.082	0.474

Table 5.16: Analysis results of 30-minute intervals of airflow rates and gases concentrations and emissions classified regarding production rates between 501 and 600 tonnes per 30 minutes.

Production intensity	DMS	CH_4	CO_2	Production rate	Airflow rate	DMS emission	CH_4 emission	CO_2 emission
501-600	[mg/m³]	[g/m³]	[g/m³]	[t/30min]	[m³/s]	[mg/s]	[kg/s]	[kg/s]
Num. of events	113	113	113	113	113	113	113	113
MAX	67.3	6.94	37.60	600	41.1	1881	0.170	1.060
MEAN	**22.7**	**3.90**	**25.12**	**541**	**30.2**	**674**	**0.116**	**0.740**
MIN	7.1	1.04	11.01	501	17.5	217	0.034	0.402
Std	11.8	1.04	5.88	28	5.4	346	0.023	0.141
97.5th percentile	58.0	6.16	35.69	598	40.0	1700	0.163	0.987
75th percentile	25.7	4.38	29.54	563	34.6	774	0.129	0.840
50th percentile	19.8	3.62	24.55	533	30.7	574	0.115	0.753
25th percentile	15.7	3.13	19.97	518	26.1	438	0.101	0.631
2.5th percentile	8.8	2.70	15.18	501	21.7	268	0.071	0.498

Table 5.17: Analysis results of 30-minute intervals of airflow rates and gases concentrations and emissions classified regarding production rates between 601 and 671 tonnes per 30 minutes.

Production intensity	DMS	CH_4	CO_2	Production rate	Airflow rate	DMS emission	CH_4 emission	CO_2 emission
601-671	[mg/m³]	[g/m³]	[g/m³]	[t/30min]	[m³/s]	[mg/s]	[kg/s]	[kg/s]
Num. of events	15	15	15	15	15	15	15	15
MAX	46.2	4.90	31.45	671	37.5	1731	0.160	1.091
MEAN	**20.4**	**3.44**	**22.46**	**633**	**33.7**	**692**	**0.115**	**0.749**
MIN	10.1	2.66	16.20	603	23.7	370	0.094	0.579
Std	9.3	0.72	4.75	23	3.9	364	0.020	0.151
97.5th percentile	42.4	4.82	30.64	669	37.4	1580	0.152	1.024
75th percentile	21.1	3.81	25.65	649	36.5	674	0.129	0.844
50th percentile	17.8	3.21	23.06	624	34.4	566	0.104	0.766
25th percentile	15.0	2.83	17.43	614	33.2	516	0.097	0.601
2.5th percentile	10.7	2.70	16.49	604	24.7	381	0.094	0.579

Table 5.18: Analysis results of all 30-minute intervals of airflow rates and gases concentrations and emissions classified regarding production rates between 1 and 671 tonnes per 30 minutes.

Production intensity	DMS	CH_4	CO_2	Production rate	Airflow rate	DMS emission	CH_4 emission	CO_2 emission
1-671	[mg/m³]	[g/m³]	[g/m³]	[t/30min]	[m³/s]	[mg/s]	[kg/s]	[kg/s]
Num. of events	1737	1737	1737	1737	1737	1737	1737	1737
MAX	81.2	6.94	37.65	671	47.3	2232	0.168	1.091
MEAN	**16.2**	**3.51**	**20.83**	**242**	**30.6**	**493**	**0.104**	**0.621**
MIN	2.2	0.85	7.92	1	9.8	82	0.026	0.163
Std	8.3	0.99	6.23	166	5.7	273	0.022	0.162
97.5th percentile	36.8	5.87	33.30	563	40.3	1245	0.149	0.927
75th percentile	20.0	4.02	25.21	374	35.1	590	0.119	0.730
50th percentile	14.6	3.28	20.19	231	31.1	435	0.104	0.622
25th percentile	10.7	2.83	16.36	99	25.9	314	0.090	0.512
2.5th percentile	4.9	2.00	9.51	2	21.1	147	0.059	0.292

Appendix E

The Procedure for Calculating Correlations in Relation to Working Phases of Velenje Mining Method

The correlation analysis based on specific pairs of monitored sensors in relation to actual workflow of working phases of extraction process and also in relation to locations of the sensors. The working phases (see Figure 1.7 in Chapter 1.4.2) were established on the basis of daily reports of longwall face mining supervisors. Every work shift the mining supervisor has produced a graph of the workflow (part of a daily report), which serves for daily chronological overview of the main extraction features on the longwall face as shown in Figure 3.2 (see Chapter 3.2) for a work day on 12 October 2012. From the workflow it is visible that working phases follow the technological process as envisaged (Figure 5.26); after two cuts with the shearer and advancing of transporters (AFC and BSL) and hydraulic shield supports, the top coal caving part follows. The production on the longwall face was active in the first and second work shift, the third shift was not in operation as planned according to the production of other longwall faces on CMV and coal consumption of the Šoštanj thermal plant.

During the analysed period (from 5 October 1012 (6:00) to 25 October 2012 (6:00)) the excavation on the longwall face took place in two eight-hour shifts per working day.

Technological cycle of excavation on longwall panel K.-130/B consisted of the following main working phases:

- *dismantling of steel arch support units at crossroads,*
- *transport of steel arch support,*
- *cutting of longwall face with a shearer,*
- *advancing of transporters (AFC and BSL),*
- *advancing of hydraulic shield supports (53 pieces),*
- *top coal caving of sectors (longwall face was divided in two sectors as shown in Figure 5),*
- *shortening of the rubber conveyor, pipe lines and power lines.*

The major working phases with coal crushing are cutting and top coal caving. Technological cycle on longwall panel K.-130/B consisted of four cuts and top coal caving in two sectors as shown in Figure 5.26.

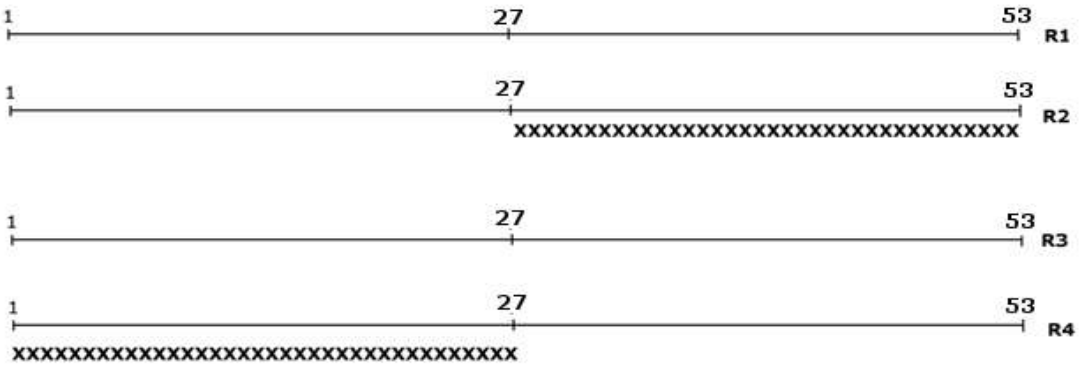

Figure 5.26: Technological cycle on longwall panel K.-130/B: the order of cutting and top coal caving.

The calculation of hourly correlation coefficients was calculated with MS Excel. After the preview of data for the analysed period (21 days between 5 October 1012 (6:00) to 26 October 2012 (6:00)). Correlation coefficients were calculated for 36 sensors and differences (see Table 3.2 in Chapter 3.2). Each parameter had 30,240 measurements. The data was rearranged in a way that it was possible to produce the matrix of correlation coefficients (36x36) for each monitored hour (480 matrices). For the matrix of correlation coefficients (e.g., in Table 5.20 for 12 October 2012 (12-13h)) we used the »Correlation« function which is in MS Excel add-in package »Analysis ToolPak«. Such matrices contain the correlation coefficients for each inter-relationship of all the sensors and sensor differences. For further data processing the specific correlation coefficients are hereinafter rearranged in terms of automation of calculations with MS Excel; the focus was to automate as much as possible the processing of tables (e.g. Table 5.20) and charts (e.g. figures between Figure 5.27 and Figure 5.30) that represent the average specific correlation coefficients in relation to a specific working phase.

Table 5.19: Hourly values of coal production, airflow and DMS, CH4, CO2 emissions for 12 October 2012.

	DMS	CO_17	CO_24	CH4_51	CO2_07	CH4_67	CO2_22	CH4_06	CO2_23	CH4_22	CO2_24	CH4_20	CO2_25	CH4_24	CO2_34	RO32_SUM	VP_34	[m3/min]	CO (17-24)	CH4 (67-5	CO2 (22-0	CH4 (06-6	CO2 (23-2	CH4 (22-0	CO2 (24-2	CH4 (29-2	CO2 (25-3	CH4 (24-2	CO2 (34-2	CH4 (22-3	CO2 (24-4	CH4 (29-4	CO25-4	5-CH4	(24+5-CO(
DMS	1																																		
CO_17	-0,0812	1																																	
CO_24	0,509656	-0,0582	1																																
CH4_51	0,057766	-0,0364	0,07836	1																															
CO2_07	-0,1248	-0,0364	-0,3003	-0,0348	1																														
CH4_67	0,766245	-0,2470	0,499655	0,07585	-0,0133	1																													
CO2_22	0,874262	-0,1725	0,411943	0,138631	-0,0330	0,824551	1																												
CH4_06	-0,1474	-0,0955	0,173486	-0,0742	0,070841	-0,1716		1																											
CO2_23	0,545601	-0,2901	0,196678	0,010695	-0,0081	0,565202	0,387562		1																										
CH4_22	0,766228	-0,2428	0,285456	0,035365	0,010104	0,615338	0,792127	0,019468	0,803416	1																									
CO2_24	0,75622	-0,2282	0,2476	0,01709	0,017709	0,554837	0,758522	0,000726	0,798144	0,962992	1																								
CH4_20	0,816645	-0,1234	0,393116	0,056643	-0,0343	0,608523	0,7739	-0,05659	0,675941	0,917027	0,915179	1																							
CO2_25	0,790995	-0,1390	0,3207	-0,0284	-0,0059	0,552063	0,766899	-0,09822	0,644637	0,908711	0,936637	0,993952	1																						
CH4_24	0,900144	-0,0623	0,425586	-0,0325	-0,0075	0,710889	0,808353	-0,19085	0,418123	0,713002	0,710297	0,782674	0,773573	1																					
CO2_34	0,894575	0,040257	0,445957	-0,0209	-0,0209	0,648828	0,782107	-0,15544	0,43424	0,717186	0,732157	0,786757	0,792249	0,953436	1																				
RO32_SUM	0,786366	-0,0426	0,308275	-0,0829	-0,0575	0,640435	0,719636	-0,13784	0,21125	0,5784	0,577414	0,622646	0,649633	0,873806	0,794413	1																			
[t/min]	0,755799	-0,2245	0,380965	0,130207	-0,0412	0,612886	0,775174	-0,18839	0,572014	0,770984	0,785744	0,754816	0,689008	0,687151	0,566994	1																			
VP_34	-0,1825	0,232491	-0,0873	-0,1309	-0,0620	-0,0211	-0,2485	0,167538	-0,3071	-0,3471	-0,4154	-0,3065	-0,3476	-0,1569	-0,1981	0,001794	-0,3980	1																	
[m3/min]	-0,1825	0,232491	-0,0873	-0,1309	-0,0620	-0,0211	-0,2485	0,167538	-0,3071	-0,3471	-0,4154	-0,3065	-0,3476	-0,1569	-0,1981	0,001794	-0,3980	1	1																
CO (17-24)	-0,1824	0,979121	-0,2797	-0,0505	0,005562	-0,3407	-0,2506	-0,12583	-0,3207	-0,2931	-0,2701	-0,9947	-0,1998	-0,1469	-0,0518	-0,1039	-0,2964	0,242674	1																
1=CH4 (67-51)	0,122238	-0,0218	0,044889	-0,9726	0,031007	0,159046	0,055825	0,091852	0,106801	0,109079	0,112889	0,086415	0,157418	0,198687	0,172201	0,232081	0,014599	0,124737	-0,03022	1															
1=CO2 (22-07)	0,63275	-0,0780	0,408815	0,111718	-0,7890	0,517102	0,640023	-0,07253	0,352459	0,479111	0,453086	0,502047	0,475973	0,520625	0,496818	0,486537	0,508198	-0,10506	-0,15836	0,010476	1													
2=CH4 (06-67)	-0,5832	0,068132	-0,1521	-0,1084	-0,0284	-0,5312	-0,6386	0,803116	0,029753	-0,3512	-0,3306	-0,4117	-0,4134	-0,5870	-0,5186	-0,6698	-0,5263	0,155	0,09669	-0,017	-0,3706	1												
2=CO2 (23-22)	-0,0944	-0,1985	-0,1158	-0,1052	0,018348	-0,1048	0,807378	0,711139	0,282346	0,304683	0,14516	0,117212	-0,1900	-0,1485	-0,3690	0,021347	-0,5412	-0,1542	-0,1685	0,079631	-0,1250	0,578813	1											
3=CH4 (22-06)	0,696023	-0,1317	0,147414	0,074841	0,035102	0,434542	0,731725	-0,61769	0,386614	0,774246	0,757001	0,75713	0,776938	0,681635	0,662499	0,668805	0,725682	-0,3790	-0,15082	0,027656	0,422768	-0,7846	-0,16237	1										
3=CO2 (24-23)	0,7029	-0,1078	0,207762	0,017248	0,032918	0,431074	0,691802	-0,32076	0,389613	0,804875	0,865826	0,838398	0,894791	0,738569	0,7586	0,707344	0,717924	-0,3800	-0,38003	-0,14665	0,088873	0,399008	-0,53022	-0,12484	0,836132	1								
4=CH4 (29-22)	-0,2119	0,343527	0,102518	0,028935	-0,095	-0,2667	-0,3629	-0,16331	-0,5922	-0,5803	-0,4933	-0,2074	-0,2770	-0,1915	-0,1546	-0,3477	-0,3887	0,225453	0,311421	-0,0911	-0,1505	0,020663	-0,3962	-0,3533	-0,2623	1								
4=CO2 (25-24)	-0,4964	0,308313	-0,0531	-0,0848	-0,0491	-0,4081	-0,5401	-0,15789	-0,8233	-0,7889	-0,8304	-0,9753	-0,5826	-0,4176	-0,4386	-0,3064	-0,1601	0,430937	0,410987	0,309062	-0,0115	-0,2942	0,109722	-0,5204	-0,5206	-0,5857	0,71519	1						
5=CH4 (24-29)	0,348661	0,060779	0,153949	-0,1219	0,032101	0,321591	0,261794	-0,22188	-0,2134	-0,0667	-0,0686	-0,0956	-0,0272	0,570854	0,498887	0,554395	0,126415	0,147577	0,147577	0,027038	0,196085	0,136233	-0,3807	-0,4767	0,08792	0,072377	-0,0351	0,115751	1					
5=CO2 (34-29)	0,249793	0,271499	0,234226	0,008916	-0,0245	0,210223	0,10611	-0,10185	-0,2701	-0,2088	-0,2265	-0,1748	-0,2250	0,36974	0,416264	0,300466	-0,0275	0,201677	0,201677	0,214929	0,040401	0,084069	-0,2122	-0,4118	-0,0998	-0,1219	0,155396	0,167669	0,790976	1				
2+3=CH4 (22-67)	0,421062	-0,1304	0,003878	-0,0099	0,022388	0,06251	0,412073	-0,03135	0,658001	0,825187	0,822043	0,750515	0,754945	0,393339	0,44452	0,273402	0,53698	-0,42435	-0,42485	-0,12684	0,024138	0,236568	-0,064	0,432634	0,668909	0,710174	-0,54365	-0,70653	-0,315	-0,41513	1			
2+3=CO2 (24-22)	0,556031	-0,2151	0,110781	-0,0490	0,039905	0,312417	0,493953	0,089913	0,773142	0,874483	0,941274	0,820187	0,852389	0,528907	0,571673	0,39757	0,639632	-0,42556	-0,42556	-0,23062	0,121702	0,272929	-0,11031	0,500023	0,630827	0,796817	-0,47024	-0,83818	-0,22718	-0,35729	0,883335	1		
2+3+4=CH4(29-67)	0,371131	0,05586	0,067039	0,006348	-0,0317	-0,0895	-0,1377	0,419482	0,625895	0,675629	0,735851	0,733012	0,350628	0,493265	0,234997	0,400456	-0,3667	-0,3667	0,040383	-0,0274	0,188873	-0,0635	0,271648	0,579482	0,684444	-0,0327	-0,4017	-0,3944	-0,3988	0,856638	0,762839	1		
2+3+4=CO(25-22)	0,439866	-0,0614	0,13041	-0,1590	0,018911	0,126374	0,298084	-0,00145	0,487244	0,684157	0,754008	0,774929	0,841193	0,469487	0,593979	0,359894	0,469544	-0,3077	-0,30771	-0,08598	0,187101	0,168678	-0,07676	0,336362	0,539066	0,747984	-0,09581	-0,4115	-0,26118	-0,42411	0,775674	0,851639	0,86479	1	
2+3+4+5=CH4(24-67)	0,654175	0,305962	0,202166	-0,1044	-1,5E-16	0,208726	0,481069	-0,32632	0,190504	0,511652	0,555429	0,586007	0,64539	0,836195	0,8214	0,715656	0,480169	-0,2018	-0,2018	0,061333	0,15226	0,295688	-0,4020	-0,18254	0,608988	0,690862	-0,0583	-0,2625	0,543021	0,350209	0,49821	0,491845	0,557397	0,554295	1
2+3+4+5=CO(34-22)	0,642775	0,395448	0,339674	-0,1400	-0,0051	0,313564	0,376785	-0,09617	0,202924	0,443603	0,492291	0,55997	0,575035	0,782063	0,871905	0,615391	0,412305	-0,0992	-0,09923	0,119893	0,212107	0,235578	-0,2691	-0,07903	0,409803	0,584029	0,065305	-0,2276	0,492764	0,535391	0,336964	0,461635	0,435257	0,537817	0,842976	1

The determination of specific working phases for this analysis was done for each hour of analysed period accordingly as:

- *Cutting: cutting of longwall face with a shearer.*
- *Advancing: advancement of chain transporters (AFC and BSL) and hydraulic shield supports (HSS).*
- *Caving 1/2: top coal caving in sector from 1 to 27 HSS.*
- *Caving 2/2: top coal caving in sector from 28 to 53 HSS.*
- *Not in operation: work shift s or day not in operation.*
- *Shift change: in an 8-hour shift; the first hour is mostly used for entering the mine through the shaft, the walk to the work site (extraction phases start up to 10 to 15 minutes before the end of the first hour after the coal transport system is periodically checked between shifts); the last hour starts (10-15 minutes past the hour) with site inspection, walk to the shaft and exit.*
- *Undefined: Usually, individual work phases do not precisely last hour by hour. For hours which cannot be determined characteristic work phases are left undefined.*

The identification of working phases for the correlation study from the daily workflow Figure 3.2 (see Chapter 3.2) was done as shown in Table 5.20 for 12 October 2012.

Table 5.20: Characteristic work phases identified on the basis of the workflow report for 12 October 2012.

12.10.2012	(6-7)	(7-8)	(8-9)	(9-10)	(10-11)	(11-12)	(12-13)	(13-14)	(14-15)	(15-16)	(16-17)	(17-18)	(18-19)	(19-20)	(20-21)	(21-22)	(22-23)	(23-24)	(0-1)	(1-2)	(2-3)	(3-4)	(4-5)	(5-6)
Cutting		1		1							1													
Advancing			1		1							1												
Caving 1/2													1	1	1									
Caving 2/2						1	1																	
Not in operation																	1	1	1	1	1	1	1	1
Shift change	1							1	1							1								
Undefined	0	0	0	0	0	0	0	0	0	1	0	0	0	0	0	0	0	0	0	0	0	0	0	0

The correlation study results in relation to working phases are presented as values in tables (e.g., Table 5.20) and visualized as in figures between Figure 5.27 and Figure 5.30. Hourly correlation coefficients for the period of 5 October 2012 to 25 October 2012 were arranged according to the working phases, while the specific average hourly correlation coefficients were calculated for each working phase. Results are presented in

Table 4.3 (see Chapter 4.2). Specific relationships are interpreted by the size of the correlation coefficients according to the presented "rule of thumb" (Table 3.3). Both the calculation and visualization of the hourly correlation coefficients were made also for each sensor location and for the areas between sensor locations.

The detailed results of correlation analysis of the monitoring campaign on longwall panel k.-130/B are presented in [146].

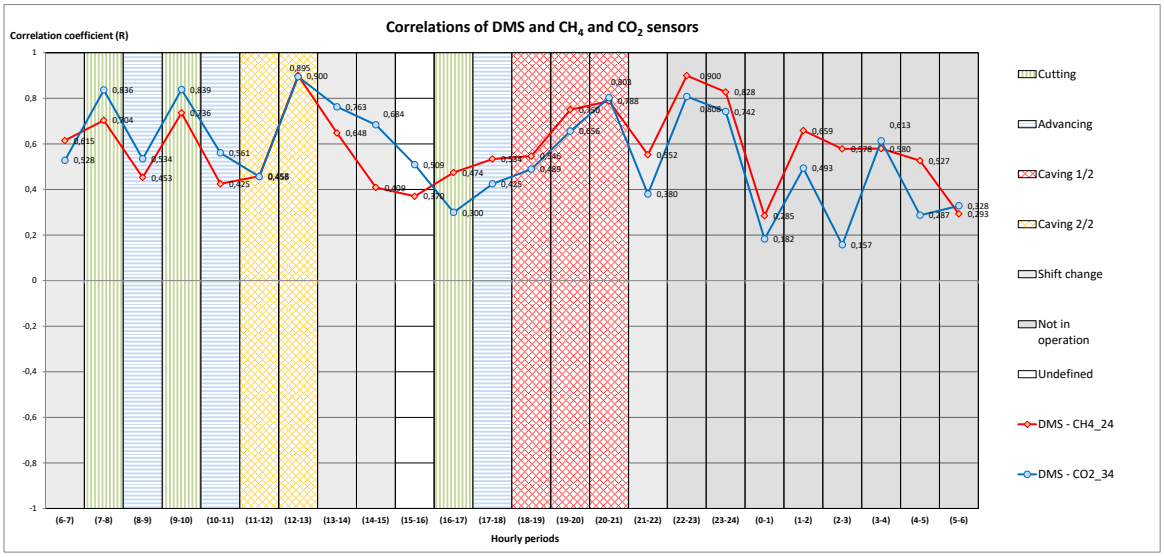

Figure 5.27: Hourly correlation coefficients of DMS-CH4_24 and DMS-CO2_34 in relation to work phases for 12 October 2012.

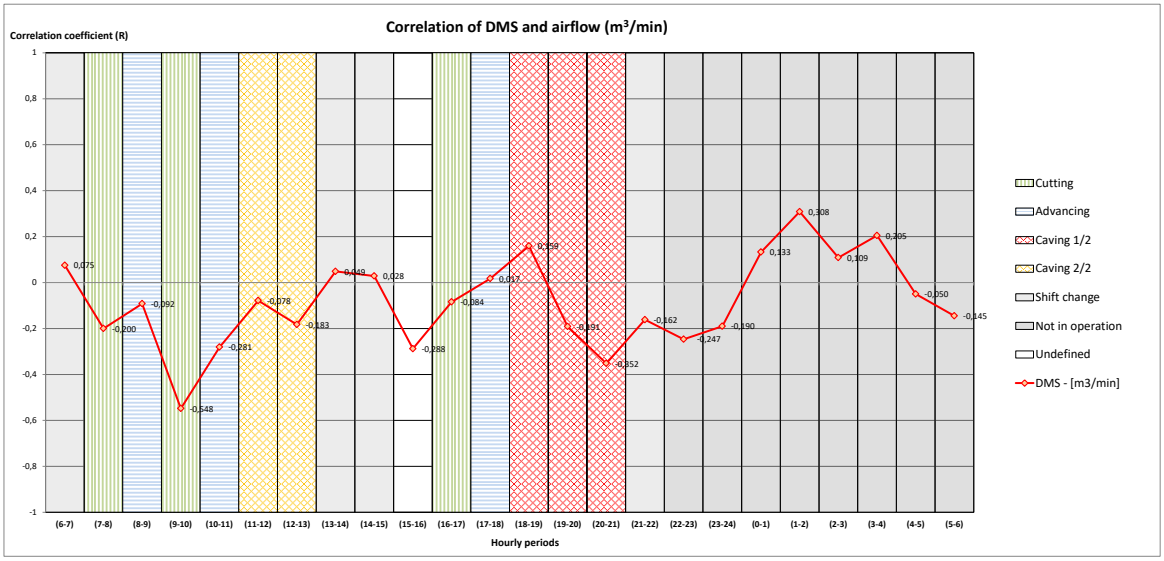

Figure 5.28: Hourly correlation coefficients of DMS and airflow [m^3/min] in relation to work phases for 12 October 2012.

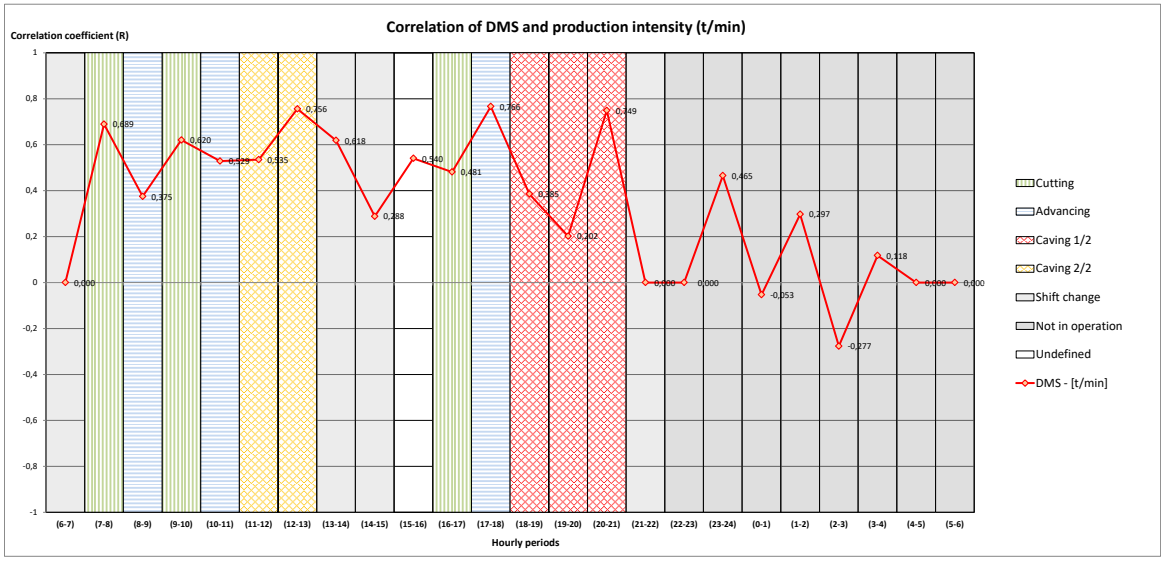

Figure 5.29: Hourly correlation coefficients of DMS and production intensity [t/min] in relation to work phases for 12 October 2012.

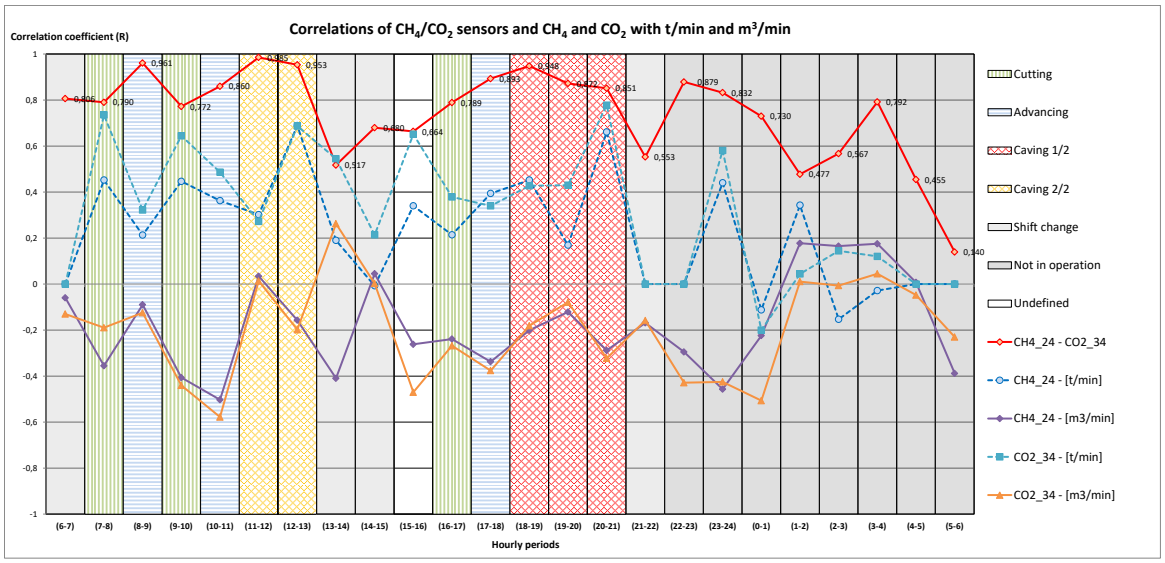

Figure 5.30: Hourly correlation coefficients of CH4_24-CO2_34 and CH4 and CO2 with coal intensity [t/min] and airflow [m3/min] in relation to work phases for 12 October 2012.

References

[1] G. Uranjek, M. Horvat, R. Milačič, J. Rošer and J. Kotnik, "Assessment of dimethyl sulphide odorous emissions during coal extraction process in Coal Mine Velenje," *Environmental Monitoring and Assessment,* vol. Volume 195, p. 19, 2023.

[2] Brattoli M., Cisternino E., De Gennaro G., Giungato P., Mazzone A., Palmisani J. and Tutino M., "Gas chromatography analysis with olfactometric detection (gc-o): an innovative approach for chemical characterization of odor active volatile organic compounds (vocs) emitted from a consumer products," *Chemical Engineering Transactions,* vol. 40, pp. 121-126, 2014.

[3] Rosenkranz H. S. and Cunningham A. R., "Environmental odors and health hazards," *Science of The Total Environment,* vol. 313 Issues 1–3., p. 15–24, 2003.

[4] Nagata Y., "Measurement of Odour Threshold by Triangle Odour Bag Method," *Odor Measurement Review. Office of Odor, Noise and Vibration, Environmental Management Bureau, Ministry of the Environment, Government of Japan,* vol. 150, p. 118–128, 2003.

[5] R. Fisher, R. Barczak, I. Suffet, J. Hayes and R. Stuetz, "Framework for the use of odour wheels to manage odours throughout wastewater biosolids processing," *Science of The Total Environment,* vol. Volume 634, pp. 214-223, 2018.

[6] R. Barczak, R. Fisher, N. Le-Minh and R. Stuetz, "Identification of volatile sulfur odorants emitted from ageing wastewater biosolids," *Chemosphere,* Vols. Volume 287, Part 2., 2022.

[7] Qiao L., Chen J. and Yang X., "Potential particulate pollution derived from UV-induced degradation of odorous dimethyl sulfide," *Journal of Environmental Sciences,* vol. 23(1), pp. 135-154, 2011.

[8] Kozinc J., "Defining and identifying the origin of volatile sulphur compounds on coal stock piles," *University of Ljubljana, Faculty of chemistry and chemical technology. (Ph.D. Dissertation),* 2005.

[9] Finster K., King G.M. and Bak F., "Formation of methylmercaptan and dimethylsulfide from methoxylated aromatic compounds in anoxic marine and fresh water sediments," *FEMS Microbiology Letters,* vol. 74/4, p. 295–301, 1990.

[10] M. Markič, "Petrology and genesis of the Velenje lignite," *University of Ljubljana, Faculty of Natural Sciences and Engineering, Department of Geology. (Ph.D. Dissertation),* 2009.

[11] Markič M. and Sachsenhofer R. F., "The Velenje lignite - Its petrology and genesis," *Geological Survey of Slovenia,* p. 218, 2010.

[12] W. Powers and M. Corzangeno, "The Science of Smell Part 1: Odour perception and physiological response," *Iowa State University Extension and Outreach,* 2004.

[13] W. Powers and M. Corzangeno, "The Science of Smell Part 2: Odour chemistry, Iowa State University, May 2004," *Iowa State University Extension and Outreach,* 2004.

[14] St. Croix Sensory, *A detailed assessment of the science and technology of odour measurement,* 2003.

[15] W. Powers, J. McGuire and M. Carlson, "The Science of Smell Part 3: Odour detection and measurement," *Iowa State University Extension and Outreach,* 2004.

[16] Powers W., McGuire J. and Carlson M., "The Science of Smell Part 4: Principles of odour control," *Iowa State University,* 2004.

[17] Nicolai R. and Pohl S., “Understanding livestock odours,” *South Dakota State University,* 2005.

[18] *Integrated Pollution Prevention and Control (IPPC) – Horizontal Guidance for Odour: Part 2 – Assessment and Control,* Scottish Environmental Protection Agency, 2002.

[19] Department for Environment, Food and Rural Affairs, UK, *Odour Guidance for Local Authorities,* 2010.

[20] J. Gebicki, H. Byliński and J. Namieśnik, “Measurement techniques for assessing the olfactory impact of municipal sewage treatment plants,” *Environmental Monitoring and Assessment,* vol. Volume 188, p. 32, 2016.

[21] C. Conti, M. Guarino and J. Bacenetti, “Measurements techniques and models to assess odor annoyance: A review,” *Environment International,* vol. Volume 134, 2020.

[22] McGinley M. A. and McGinley C. M., “Comparison of Field Olfactometers in a Controlled Chamber using Hydrogen Sulfide as the Test Odorant,” in *International Water Association 2nd International Conference on Odour and VOCs : Measurement, Regulation, and Control Techniques*, Singapore, 2003.

[23] D. Karakaya, O. Ulucan and M. Turkan, “Electronic Nose and Its Applications: A Survey,” *International Journal of Automation and Computing,* vol. Volume 17, p. 179–209., 2020.

[24] C. Kim, K. Lee and K. M.S., “Artificial olfactory sensor technology that mimics the olfactory mechanism: a comprehensive review,” *Biomaterials Research,* vol. Volume 26, p. 40, 2022.

[25] Parcsi G., “Chemical analysis of odorants from poultry facilities (Ph.D. Dissertation),” *University of New South Wales,* p. 250, 2005.

[26] Trabue S., Scoggin K., Mitloehner F., Li H., Burns R. and Xin H., “Field sampling method for quantifying volatile sulfur compounds from animal feeding operations,” *Atmospheric Environment,* vol. 42, p. 3332–3341, 2008.

[27] Hudson N. A., “Investigation of mechanisms governing emissions of odorants (Ph.D. Dissertation),” *Queensland University of technology,* 2009.

[28] Boeker P., Haas T., Diekmann B. and Schulze Lammers P., “New odour sampling method: adsorption and reconstitution of odours,” *Chemical Engineering Transactions,* vol. 23, pp. 49-54, 2010.

[29] Juarez-Galan J. M., Martinez J. V. and Valor I., “Stability assurance of odour concentration by cryocondensation sampling,” *Chemical Engineering Transactions,* vol. 23, pp. 79-86, 2010.

[30] Parcsi G., Gouézigou J.le, Sivret E. C., Wang X. and Stuetz R. M., “Fate of sulphur odorants in odour collection,” 2010.

[31] H. Bylinski, R. Barczak and J. Gebicki, “Monitoring of odours emitted from stabilized dewatered sludge subjected to aging using proton transfer reaction–mass spectrometry,” *Environmental Science and Pollution Research,* vol. Volume 26, p. 5500–5513, 2019.

[32] Benzo M., Pittarello A., Giacetti W., Gandini C. and Caccialanza G., “Full application of odour field inspection according to VDI 3940 in Italy: odour impact evaluation of an anaerobic digestion plant,” *Chemical Engineering Transactions,* vol. 23, pp. 219-224, 2010.

[33] Kost W.J. and Richter C.J., “On the accuracy of the measured odour impact by field inspection (grid method) specific for every single grid. an additional worthwhile information to evaluate the data set,” *Chemical Engineering Transactions,* vol. 23, pp. 285-290, 2010.

[34] Freeman T., Needham C. and Schulz T., "Analysis of Options for Odour Evaluation for Industrial or Trade Processes," *CH2M Beca Ltd,* p. 146, 2000.

[35] Scire J. S., Strimaitis D.G. and Yamartino R.J., "A User's Guide for CALPUFF Dispersion Model (Version 5)," *Earth Tech. Inc.,* 2000.

[36] Xing Y., "Evaluation f commercial air dispersion models for livestock odour dispersion simulation (Master of Science Thesis)," *Department of Agricultural and Bioresource Engineering. University of Saskatchewan. Saskatoon (Canada),* p. 138, 2006.

[37] Li Y., "Evaluation of Aermod and Calpuff air disersion models for livestock odour dispersion simulation," *Department of Agricultural and Bioresource Engineering. University of Saskatchewan. Saskatoon (Canada), (Master of Science Thesis),* p. 156, 2009.

[38] Boeker P., Wallenfang O., Koster F., Croce R., Diekmann B., Griebel M. and Lammers P. S., "The Modelling of Odour Dispersion with Time-Resolved Models," *Agrartechnische Forschung,* vol. 6 (4), pp. 84 - 89, 2000.

[39] Koziel J., Lo Y.C.M., Cai L. and Wright D.W., "Simultaneous characterization of VOCs and livestock odors using solid-phase microextraction-ultidimensional gas chromatography-mass spectrometry-olfactometry," *Chemical Engineering Transactions,* vol. 23, pp. 73-78, 2010.

[40] Fischer C., Maurice C. and Lagerkvist A., "Gas Emission from Landfills: An overview of issues and research needs," Stockholm : AFN. Naturvårdsverket, (AFR-report; No. 264), 1999.

[41] McKendry P., Looney J. H. and McKenzie A., "Managing Odour Risk at Landfill Sites: Main Report," MSE Ltd& Virdis, 2002.

[42] Kenneth R. F., Dennis Y., Palczynski R., Dixon E., Jackson W. and Kinneburgh C., "Assessment report on reduced sulphur compounds for developing ambient air quality objectives," AMEC Earth & Environmental Limited and University of Calgary, 2004.

[43] Zagustina N. A., Krikunova N. I., Kulikova A. K., Misharina T. A., Romanov M. E., Ruzhitsky A. O., Terenina, M. B., Veprizky A. A., Zhukov V. G. and Popov V. O., "Composition of the air emission from a tobacco factory and development of the biocatalyst for odour control," *Journal of Chemical Technology and Biotechnology,* pp. 320 - 327, 2010.

[44] Vanek M., Mitterpach J. and Zacharova A., "Odour control in biogas plant – case study," *15th International Multidisciplinary Scientific GeoConference SGEM,* vol. Book4, pp. 353-360, 2015.

[45] Kellaghan R., *Air quality impact assessment – BHP Billiton Illawarra coal – ventilation shaft No. 6 project,* Queensland Environment Pty Ltd trading as PAEholmes, Australia, 2010, p. 48.

[46] Kellaghan R., *Tasman extension project - Air quality and greenhouse gas assessment,* Queensland Environment Pty Ltd trading as PAEholmes, Australia, 2012, p. 80.

[47] Cox J. and Isley C., *Analysis of odour complaints and ambient air quality in Wollar and Cooks Gap,* Pacific Environment Operations Pty Ltd, Australia, 2014, p. 35.

[48] P. f. E. P. a. R. -. L. o. Mine, *ML6345 and ML6436 Kanmantoo Copper Mine - Main report,* 2016, pp. 318..

[49] Abdul-Wahab S. and Marikar F., "The environmental impact of gold mines: pollution by heavy metals," *Central European Journal of Engineering,* pp. 304-313, 2012.

[50] Kupczewska-Dobecka M., Czerczak S., Gromiec J. P. and Konieczko K., "Assessment of potential health hazard during emissions of hydrogen sulphid from the mine exploiting copper ore deposit – case study," *Central European Journal of Public Health,* vol. 23(2), pp. 161-165, 2015.

[51] MineARC systems, “MineARC stench gas,” [Online]. Available: https://minearc.com/. [Accessed 2021].

[52] Park E. B., *Fires and ignition in mine,* vol. 4(3), Loyabad Colliery, Manbhum, 1940, pp. 451-456.

[53] Pone J. D. N. , Hein K. A. A., Stracher G. B. , Annegarn H. J. , Finkleman R. B. , Blake D. R. , McCormack J. K. and Schroeder P., “The spontaneous combustion of coal and its by-products in the Witbank and Sasolburg coalfields of South Africa,” *International Journal of Coal Geology,* vol. 72, p. 124–140, 2007.

[54] Cox J. L. and Nelson C. R., *Coal weathering: causes, effects and implications,* Gas Research Institute, Chicago, USA, 1984, p. 6.

[55] Shao D., Hutchinson E. J., Heidbrink J., Wei-Ping P. and Shou C.-L. , “Behavior of sulphur during coal pyrolysis,” *Journal of Analytical and Applied pyrolysis,* pp. 91-100, 1994.

[56] Johnson D. B. and Hallberg K. B., “Acid mine drainage remediation options: a review,” *Science of the Total Environment,* vol. 338, p. 12, 2005.

[57] Zhou Q., Hu H., Liu Q. and S. Zhu, *Effect of atmospheres on evolution of sulphur containing gases during coal pyrolysis,* American Chemical Society, Division of Fuel Chemistry ed., vol. 49 (2), Institute of Coal Chemical Engineering, Dalian University of Technology, China, 2004.

[58] Day S., *Spontaneous Combustion in Open Cut Coal Mines,* CSIRO Energy Technology, 2008.

[59] M. c. mine, “Muswellbrook coal mine - Annual Environment Management Report 2016,” [Online]. Available: https://www.idemitsu.com.au/mining/wp-content/uploads/2016/01/2016-Annual-Environmental-Management-Report.pdf. [Accessed 17 januar 2021].

[60] “Muswellbrook coal mine - Annual Environment Management Report 2017,” [Online]. Available: https://www.idemitsu.com.au/mining/wp-content/uploads/2016/01/2017-Annual-Environmental-Management-Report.pdf. [Accessed 17 januar 2021].

[61] “Muswellbrook coal mine - Annual Environment Management Report 2018,” [Online]. Available: https://www.idemitsu.com.au/mining/wp-content/uploads/2016/01/2018-Annual-Environmental-Management-Report.pdf. [Accessed 20 januar 2021].

[62] “Muswellbrook coal mine - Annual Environment Management Report 2019,” [Online]. Available: https://www.idemitsu.com.au/mining/wp-content/uploads/2016/01/2019-Annual-Environmental-Management-Report.pdf. [Accessed 20 januar 2021].

[63] “Austar Coal Mine Community Complaints Register 2020,” [Online]. Available: https://www.austarcoalmine.com.au/icms_docs/314433_austar-community-complaints-register-2020.pdf. [Accessed 17 Januar 2021].

[64] “Wambo cole mine - Annual Environmental Management Report 2014,” [Online]. Available: https://www.peabodyenergy.com/Peabody/media/MediaLibrary/Operations/Australia%20Mining/New%20South%20Wales%20Mining/Wambo%20Mine/WCM%20AEMR%202014. [Accessed 17 januar 2021].

[65] “Wambo cole mine - Annual Environmental Management Report 2019,” [Online]. Available: https://www.peabodyenergy.com/Peabody/media/MediaLibrary/Operations/Australia%20Mining/New%20South%20Wales%20Mining/Wambo%20Mine/WCM%20AEMR%202019. [Accessed 17 januar 2021].

[66] “Mt Arthur coal mine - Annual Environmental Management Report 2014,” [Online]. Available: https://www.bhp.com/-/media/bhp/regulatory-information-media/coal/new-south-wales-energy-coal/mt-arthur-coal/annual-environmental-management-reviews/140929_coal_nswec_mtarthur_annualenvironmentalmanagementreportfy14.pdf. [Accessed 17 januar 2021].

[67] “Tahmoor coal mine - Annual Environmental Management Report 2018,” [Online]. Available: https://www.resourcesregulator.nsw.gov.au/sites/default/files/documents/annual-report-2018_tahmoor-colliery_tahmoor-coal-pty-ltd.pdf. [Accessed 17 januar 2021].

[68] “Tahmoor coal mine - Annual Environmental Management Report 2019,” [Online]. Available: https://www.resourcesregulator.nsw.gov.au/sites/default/files/documents/annual-report-2019_tahmoor-colliery_tahmoor-coal-pty-ltd.pdf. [Accessed 17 januar 2021].

[69] “Canyon Coal Mine Community Complaints Register 2006,” [Online]. Available: https://whitehavencoal.com.au/Documentations/Canyon%20Mine/Community/Community%20Complaints%20Register/CAN-Complaint%20Register%202006%20(1%20complaint).pdf. [Accessed 17 januar 2021].

[70] “Canyon Coal Mine Community Complaints Register 2007,” [Online]. Available: https://whitehavencoal.com.au/Documentations/Canyon%20Mine/Community/Community%20Complaints%20Register/CAN-Complaint%20Register%202007%20(3%20complaints).pdf. [Accessed 17 januar 2021].

[71] “Canyon Coal Mine Community Complaints Register 2008,” [Online]. Available: https://whitehavencoal.com.au/Documentations/Canyon%20Mine/Community/Community%20Complaints%20Register/CAN-Complaint%20Register%202008%20(0%20complaints).pdf. [Accessed 17 januar 2021].

[72] “Canyon Coal Mine Community Complaints Register 2009,” [Online]. Available: https://whitehavencoal.com.au/Documentations/Canyon%20Mine/Community/Community%20Complaints%20Register/CAN-Complaint%20Register%202009%20(0%20complaints).pdf. [Accessed 17 januar 2021].

[73] “Moolarben Coal Mines - Annual Environmental Management Report 2011-2012,” [Online]. Available: https://minedocs.com/20/Moolarben_Coal_Operations_AR_12312012.pdf. [Accessed 17 januar 2021].

[74] “Moolarben Coal Mines - Annual Environmental Management Report 2019,” [Online]. Available: https://www.moolarbencoal.com.au/icms_docs/319544_2019-annual-review.pdf. [Accessed 17 januar 2021].

[75] “Drayton coal mine - Annual Environmental Management Report 2013,” [Online]. Available: https://australia.angloamerican.com/~/media/Files/A/Anglo-American-Australia-V2/Attachments/environment/Drayton-AEMR-2013.pdf. [Accessed 17 januar 2021].

[76] “Drayton coal mine - Annual Environmental Management Report 2015,” [Online]. Available: https://australia.angloamerican.com/~/media/Files/A/Anglo-American-Australia-V3/document/drayton-environtment/2016/AEMR%202015_FINAL_compressed.pdf. [Accessed 17 januar 2021].

[77] “Drayton coal mine - Annual Environmental Management Report 2016,” [Online]. Available: https://australia.angloamerican.com/~/media/Files/A/Anglo-American-Australia-V3/document/drayton-environtment/2016/AEMR%202016_FINAL_compressed.pdf. [Accessed 17 januar 2021].

[78] “Duralie Coal Mine - Complaints Register 2016-2017,” [Online]. Available: https://www.duraliecoal.com.au/content/Document/Duralie_Complaint_Register%20-%20June%202017.pdf. [Accessed 17 januar 2021].

[79] “Duralie Coal Mine - Complaints Register 2019,” [Online]. Available: https://www.duraliecoal.com.au/content/Document/Duralie_Complaint_Register%20-%20February%202019.pdf. [Accessed 17 januar 2021].

[80] A. E. Regulator, Ed.“Recurrent Human Health Complaints Technical Information Synthesis (Fort McKay Area),” p. 257, 2016.

[81] Kozinc J., Treeby M. and Zupančič–Kralj L., “Determination of Sulfur Gases From Velenje Coal Stockpile,” *Acta Chimica Slovenica,* vol. 51, p. 529−536, 2004.

[82] Zapušek A. and Marsel J., “Determination of dimethyl sulfide in coal mine atmosphere by gas chromatography,” in *22nd International Symposium on Chromatography*, Rome, 1998.

[83] Zhang X., *Gaseous emissions from coal stockpiles,* IEA Clean Coal Centre, 2013, p. 29.

[84] *Eight individual reports: Results from gas desorbtion measurements from boreholes samples, ERICo Velenje, Inštitut za ekološke raziskave, 1998 and 1999..*

[85] G. Uranjek, S. Zavšek, I. Pohorec and L. Golob, “Odour emissions from the technological processes of coal extraction in Coal mine Velenje = Emisije vonjav pri tehnoloških postopkih pridobivanja premoga v Premogovniku Velenje.,” *RMZ - Materials and geoenvironment,* vol. Volume 60/2, pp. 131-142, 2013.

[86] R. J. McGorrin, “The Significance of Volatile Sulphur Compounds in Food Flavors,” *ACS Symposium Series. ACS Publications.,* vol. 1068, p. 1–3, 2011.

[87] Stafisso A., Marconi O., Perretti G. and Fantozzi P., “Determination of dimethyl sulphide in brewery samples by headspace gas chromatography mass spektrometry (HS – GC/MS),” *Italian Journal of Food Science,* vol. 23(1), p. 19–27.

[88] Lytra G., Tempère S., Marchand S., de Revel G. and Barbe J. C., “How do esters and dimethyl sulphide concentrations affect fruity aroma perception of red wine? Demonstration by dynamic sensory profile evaluation,” *Food Chemistry,* vol. 194, pp. 196-200, 2016.

[89] Feng T., Shui M., Song S., Zhuang H., Sun M. and Ya L., “Characterization of the Key Aroma Compounds in Three Truffle Varieties from China by Flavoromics Approach,” *Molecules,* Vols. 24(18), 3305, 2019.

[90] Breeden D. C. and Juvik J. A., “An extraction method for the determination of dimethyl sulfide in cooked corn,” *Journal of Food Composition and Analysis,* vol. 5 (2), pp. 134-138, 1992.

[91] Schäfer H., Myronova N. and Boden R., “Microbial degradation of dimethylsulphide and related C1-sulphur compounds: organisms and pathways controlling fluxes of sulphur in the biosphere,” *Journal of Experimental Botany,* Vols. 61, No. 2, p. 315–334, 2009.

[92] Burbank H. and Qian M. C., “Development of volatile sulfur compounds in heat-shocked and pasteurized milk cheese,” *International Dairy Journal,* Vols. 18, Issue 8, pp. 811-818, 2008.

[93] Catalan L. J. J., Liang V., Walton C. and Jia C. Q., “Effects of process changes on concentrations of individual malodorous sulphur compounds in ambient air near a Kraft pulp plant in Thunder Bay, Ontario, Canada,” *Ecology and the Environment,* vol. 101, 2007.

[94] Drimal M., Lewis C. and Fabianova E., "Health risk assessment of environmental exposure to malodorous sulfur compounds in central Slovakia (Ružomberok area)," *Carpathian Journal of Earth and Environmental Sciences,* Vols. 5, No. 1, p. 119 – 126, 2010.

[95] Feilberg A., Hansen M. J., Liu D. and Nyord T., "Contribution of livestock H2S to total sulphur emissions in a region with intensive animal production," *Nature Communications,* Vols. 8,1069, 2017.

[96] M. Wiśniewska, A. Kulig and K. Lelicińska-Serafin, "Comparative analysis of preliminary identification and characteristic of odour sources in biogas plants processing municipal waste in Poland," *SN Applied Sciences. ,* Vols. 1, 550, 2019.

[97] "ASK Piearcey Ltd," [Online]. Available: https://askpiear1991cey.wordpress.com/2013/07/30/odour-control-systems-one-of-uks-largest-sewage-ocus/. [Accessed 2014].

[98] Uranjek G., Zavšek S., Pohorec I. and Golob L., "Odour emissions from the technological processes of coal extraction in Coal mine Velenje," *Materials and geoenvironment,* vol. 60 (2), pp. 131-142, 2013.

[99] Hansen M., Feilberg A. and Adamsen A., "Stability of volatile reduced sulphur compounds in the dilution system of an olfactometer," *Chemical Engineering Transactions,* vol. 23, pp. 67-72, 2010.

[100] Gauer A.,, *The CLAW hypothesis - A role for Dimethylsulfide in climate?,* Institute of Biogeochemistry and Pollutant Dynamics, Department of Environmental Sciences, ETH Zürich, 2009, p. 20.

[101] Boucher O., Moulin C., Belviso S., Aumont O., Bopp L., Cosme E., von Kuhlmann R., Lawrence M. G., Pham M., Reddy M. S., Sciare J. and Venkataraman C., "DMS atmospheric concentrations and sulphate aerosol indirect radiative forcing: a sensitivity study to the DMS source representation and oxidation," *Atmospheric Chemistry and Physics,* vol. 3, p. 49–65, 2003.

[102] von Glasow R. and Crutzen P. J., "Model study of multiphase DMS oxidation with a focus on halogens," *Atmospheric Chemistry and Physics,* vol. 4, p. 589–608, 2004.

[103] L. Catalan, V. Liang and A. Johnson, "Emissions of reduced sulphur compounds from the surface of primary and secondary wastewater clarifiers at a Kraft Mill.," *Environmental Monitoring and Assessment.,* vol. 156, p. 37, 2009.

[104] Liu J., Geng C., Mu Y., Zhang Y. and Wu H., "Exchange of carbonyl sulfide (COS) between the atmosphere and various soils in China," *Biogeosciences Discussions,* vol. 6, p. 10557–10582, 2009.

[105] Brezigar A., Ogorelec B., Rijavec L. and Mioč P., "Geologic setting of the Pre-Pliocene basement of the Velenje depression and its surroundings," *Geologija,* vol. 30, p. 31–65, 1987.

[106] Medved M., Golob L. and Kotnik A., "Velenje Coal Mine (VCM) Mining Method and Modern Mechanized Faces," in *3rd Balkan mining congress*, İzmir-Turkey, 2009.

[107] Seher A., The history of Coal Mine Velenje Vol. 1, vol. Vol. 1, Velenje: Coal Mine Velenje, 1995.

[108] Lenart M., Veber I., Blažič A. and Lajlar B., *Velenje Mining Method, Mining project of Coal Mine Velenje, Mining project No.: RP – 36/95 LM,* Velenje: Coal Mine Velenje, 1996.

[109] Likar J., Medved M., Lenart M., Mayer J., Malenković V., Jeromel G. and Dervarič E., "Analysis of geomechanical changes in hanging wall caused by longwall multi top caving in coal mining," *Journal of Mining Science,* Vols. 48, no. 1, pp. 135-145, 2012.

[110] Jeromel G., Medved M. and J. Likar, “An analysis of the geomechanical processes in coal mining using the Velenje Mining Method,” *Acta Geotechnica Slovenica,* vol. 1, pp. 31-45, 2010.

[111] Si G., Jamnikar S., Lazar J., Shi J.Q., Durucan S., Korre A. and Zavšek S., “Monitoring and modelling of gas dynamics in multi-level longwall top coal caving of ultra-thick coal seams, Part I: Borehole measurements and a conceptual model for gas emission zones,” *International Journal of Coal Geology,* vol. 144, pp. 98-110, 2015.

[112] Dervarič E., Vukelić Ž. and Medved M., “Modernization of technological process and equipment at floor level roadways execution in Velenje coal mine,” *Materials and geoenvironment,* vol. 58, p. 437–450, 2011.

[113] Silvester S. A., *The integration of CFD and VR methods to assist auxiliary ventilation practice (PhD thesis),* School of Chemical, Environmental and Mining Engineering, The University of Nottingham, 2002, p. 319.

[114] Murphy T. M., *A method for evaluating the application of variable frequency drives with coal mine ventilation fans (Master of Science),* Blacksburg, VA: Department of Mining and Minerals Engineering, Virginia Polytechnic Institute and State University, 2006.

[115] M. McPherson, Subsurface Ventilation and Environmental Engineering, Springer Netherlands, 1993, p. 905.

[116] Erico Ltd, *Monthly reports of chemical analysis of mine air for period 2008-2013 (in Slovene),* Velenje, Slovenia: ERICO Velenje d.o.o..

[117] D. B. Parker, J. A. Koziel, C. L., L. D. Jacobson, N. Akdeniz, T. T. Lim, E. A. Caraway, S. Zhang, S. J. Hoff, A. J. Heber, K. Y. Heathcote and B. Hetchler, “Odor and Odorous Chemical Emissions from Animal Buildings: Part 6. Odor Activity Value,” *Journal of the ASABE,* vol. Vol. 55(6), pp. 2357-2368, 2012.

[118] H. Bylinski, P. Kolasinska and T. Dymerski, “Determination of odour concentration by TD-GC×GC–TOF-MS and field olfactometry techniques,” *Monatshefte für Chemie - Chemical Monthly,* vol. 148, no. DOI: 10.1007/s00706-017-2023-8, p. 1651–1659, 2017.

[119] M. Brattoli, G. De Gennaro, V. De Pinto, A. Demarinis Loiotile, S. Lovascio and M. Penza, “Odour Detection Methods: Olfactometry and Chemical Sensors,” *Sensors,* vol. Volume 11, pp. 5290-5322, 2011.

[120] D. Hinkle, W. Wiersma and S. Jurs, Applied statistics for the behavioral sciences - 5th ed, Boston, Mass., [etc.] : Houghton Mifflin, 2003, p. 756.

[121] Ventsim software, *Ventsim Visual™, User Guide v3.2,* 2012.

[122] Z. Žibert, “Determination of ventilation parameters according to barometric method.,” in *8th Mining and Geotechnology Scientific Conference at "40th jump over the leather*", University of Ljubljana, Faculty of Natural Sciences and Engineering., 2006.

[123] B. Salobir, “Optimisation of mine fans operation in conditions of stagnation the pit.,” *RMZ – Materials and Geoenvironment. ,* vol. Vol. 56. No. 3., p. 364–373, 2009.

[124] B. Salobir, “Influence of air conditioning at high productive mining field in ventilation area of the Velenje Coal Mine,” *RMZ – Materials and Geoenvironment,* vol. Vol. 56. No. 2., p. 230–239, 2009.

[125] S. Zavšek, *Model for research of structural and petrographically changes of the Velenje lignite depending on various stress states and presence of gases (PhD thesis),* University of Ljubljana, Faculty of Natural Sciences and Engineering, 2004.

[126] J. Lazar, T. Kanduč, S. Jamnikar, F. Grassa and S. Zavšek, “Distribution, composition and origin of coalbed gases in excavation fields from the Preloge and Pesje mining areas, Velenje Basin, Slovenia,” *International Journal of Coal Geology,* vol. Volume 131, p. 363–377, 2014.

[127] T. Kanduč, S. Zavšek, S. Jamnikar and T. Verbovšek, “Spatial distribution and origin of coalbed gases at the working faces of the Velenje Coal Basin, Slovenia, since the year 2000,” *RMZ-materials and geoenvironment,* vol. Volume 63, pp. 213-225, 2016.

[128] M. Mastalertz, H. Gluskoter and R. J., “Carbon dioxide and methane sorption in high volatile bituminous coals from Indiana,” *USA - International Journal of Coal Geology,* vol. Volume 60/1, pp. 43-55, 2004.

[129] T. Chen and M. Jang, “Chamber simulation of photooxidation of dimethyl sulfide and isoprene in the presence of NOx,” *Atmospheric Chemistry and Physics,* vol. Volume 12, p. 10257–10269, 2012.

[130] e. a. f. (. National laboratory of health, “Report: Odour measurements on ventilation station Šoštanj,” National laboratory of health, environment, and food (NLHEF). Slovenia., 2017.

[131] N. I. o. P. H. (NIPH), “Report: Emissions from ventilation station Šoštanj in Coal mine Velenje,” National Institute of Public Health. Slovenia, 2008.

[132] McGinley C. M., Mahin T. D. and Pope R. J., “Elements of Successful Odor / Odour Laws,” in *WEF Odor / VOC 2000 Specialty Conference*, Cincinnati, OH., USA, 2000.

[133] Xing Y., *Evaluation f commercial air dispersion models for livestock odour dispersion simulation (Master of Science Thesis),* Department of Agricultural and Bioresource Engineering, University of Saskatchewan. Saskatoon, Canada, 2006, p. 138.

[134] Powers W., McGuire J. and Carlson M., *The Science of Smell Part 4: Principles of odour control,* Iowa State University, 2004.

[135] Uranjek G., *Seminar 1,* Jožef Stefan International Postgraduate School, Ljubljana, 2012, p. 65.

[136] Uranjek G., *Seminar 2,* Jožef Stefan International Postgraduate School, Ljubljana, 2012, p. 75.

[137] *Odour Guidance for Local Authorities,* Department for Environment: Food and Rural Affairs, UK, 2010.

[138] OdoWatch®. [Online]. Available: http://www.odotech.com/en/odowatch/. [Accessed 2015].

[139] McGinley M. A. and McGinley C. M., “The New European Olfactometry Standard: Implementation, Experience, and Perspectives,” in *Air and Waste Management Association, 2001 Annual Conference*, 2001.

[140] “Ac´scent olfactometer,” [Online]. Available: http://www.fivesenses.com/Prod_ACSCENT.cfm. [Accessed 2015].

[141] Choinière D. and Giard D., “A New State of the Art Stationary Dynamic Dilution Olfactometer,” *Chemical engineeing transactions,* vol. 30, p. 6, 2012.

[142] Hudsona N. and Ayoko G. A., “Odour sampling 1. Physical chemistry considerations,” *Bioresource Technology,* vol. 99(10), pp. 3982-3992, 2008.

[143] N. Hudson and Ayoko, G.A., “Odour sampling 2. Comparison of physical and aerodynamic characteristics of sampling devices,” *Bioresource Technology,* vol. 99(10), pp. 3993-4007, 2008.

[144] Juarez-Galan J. M., Martinez J. V., Amo A., and Valor I., “Stability assurance of odour concentration by cryocondensation sampling,” *Chemical Engineering Transactions,* vol. 23, pp. 79-86, 2010.

[145] Yuguo L., *Evaluation of AERMOD and CALPUFF air dispersion models for livestock odour dispersion simulation (Master of Science Thesis),* Department of Agricultural and Bioresource Engineering, University of Saskatchewan, Saskatoon, Canada, 2009, p. 156.

[146] G. Uranjek, *Seminar 3: Data analysis report of Monitoring setup on longwall panel k.-130/B in Preloge pit,* Ljubljana: Jožef Stefan International Postgraduate School, 2013, p. 156.

[147] Scottish Environmental Protection Agency, *Integrated Pollution Prevention and Control (IPPC) – Horizontal Guidance for Odour: Part 2 – Assessment and Control,* 2002.

[148] McGinley M. A. and McGinley C. M., "Comparison of Field Olfactometers in a Controlled Chamber using Hydrogen Sulfide as the Test Odorant," *International Water Association 2nd International Conference on Odour and VOCs: Measurement Regulation and Control Techniques, Singapore,* pp. 14-17, 2003.

[149] Capellia L., Sironia S., del Rossoa R. and Guillo J.M., "Measuring odours in the environment vs. dispersion modeling: A review," *Atmospheric Environment,* vol. 79, p. 731–743, 2013.

[150] Videmšek B., *Monitoring the flow of material and controlling the concentration of harmful gases in Velenje Coal Mine (BSc thesis),* vol. 109, Maribor, Slovenia: University of Maribor, Faculty of Electrical Engineering and Computer Science, 2010.

Bibliography

Publications Related to the Thesis

Journal Articles

G. Uranjek, M. Horvat, R. Milačič, J. Rošer, J. Kotnik, "Assessment of dimethyl sulphide odorous emissions during coal extraction process in Coal Mine Velenje," *Environmental monitoring and assessment*, 2023, vol. 195, str. 1269-1-1269-19. ISSN 1573-2959. https://repozitorij.uni-lj.si/IzpisGradiva.php?id=152577, DOI: 10.1007/s10661-023-11755-z. [COBISS.SI-ID 167107075]

G. Uranjek, S. Zavšek, I. Pohorec, L. Golob, "Odour emissions from the technological processes of coal extraction in Coal mine Velenje = Emisije vonjav pri tehnoloških postopkih pridobivanja premoga v Premogovniku Velenje," *RMZ - Materials and geoenvironment*, ISSN 1408-7073, 2013, let. 60, št. 2, str. 131-142, ilustr. [COBISS.SI-ID 1416031]

Conference Paper

G. Uranjek, S. Zavšek, L. Golob, I. Pohorec, "Emisija vonjav pri procesu podzemnega pridobivanja premoga in deponiranja premoga na površini," V: KORTNIK, Jože (ur.). *11. posvetovanje rudarskih in geotehnoloških strokovnjakov ob 43. Skoku čez kožo, Ljubljana, 05. april 2013*. Ljubljana: Slovensko rudarsko društvo inženirjev in tehnikov - SRDIT, 2013, str. 1-11. [COBISS.SI-ID 1286495]

G. Uranjek, S. Zavšek, L. Golob, „Emisije vonjav pri procesu podzemnega pridobivanja premoga in deponiranja premoga na površini = Odour emission from the processes of underground coal ecxavation and surface coal deposition," V: 3. Mednarodna konferenca Energetika in klimatske spremembe = 3rd International Conference Energy Technology and Climate Changes, [Slovenija, Velenje, 20.-21. 6. 2013]. AVSEC, Jurij (ur.). *Zbornik povzetkov referatov*. Velenje: Coal Mine, 2013, str. 127-128. [COBISS.SI-ID 27212583]

Other Publications

G. Uranjek, "Priloga k spremljanju objektov s simultanimi meritvami različnih tipov = An addition to construction monitoring with simultaneous application of varius types of observations," *diplomsko delo*. Ljubljana: [G. Uranjek], 2007. 102 str., priloge, grafični prikazi. [COBISS.SI-ID 697439]

G. Uranjek, "Priloga k spremljanju objektov s simultanimi meritvami različnih tipov," *Prešernova nagrada*. Ljubljana: [G. Uranjek], 2007. XVI, 102 str., pril., ilustr., graf. prikazi. [COBISS.SI-ID 765023]

M. Vulić, G. Uranjek, “A contribution to construction monitoring with simultaneous application of various types of observations = Prispevek k spremljanju objektov s simultanimi meritvami različnih tipov,” *RMZ - Materials and geoenvironment*, ISSN 1408-7073, 2007, vol. 54, no. 2, str. 247-263. [COBISS.SI-ID 745055]

M. Vulić, G. Uranjek, D. Potočnik, „A deformation monitoring with simultaneous heterogeneous observation system,” V: *Mednarodna konferenca "Gospodarjenje z odpadki, okoljska geotehnologija in trajnostni razvoj" = International Conference "Waste Management, Environmental Geotechnology and Global Sustainable Development" : ICWMEGGSD'07 - GzO'07, Avgust 28.-30.,2007, Ljubljana, Slovenija*. Ljubljana: Naravoslovnotehniška fakulteta, Oddelek za geotehnologijo in rudarstvo, 2007, 10 str. [COBISS.SI-ID 742495]

J. Lazar, S. Zavšek, S. Jamnikar, J. Žula, G. Uranjek, L. Golob, “Research of innovative technologies for degasification of lignite seam,” V: 4. študentska konferenca Mednarodne podiplomske šole Jožefa Stefana = 4th Jožef Stefan International Postgraduate School Students Conference, 25. maj 2012, Ljubljana, Slovenija. PETELIN, Dejan (ur.), TAVČAR, Aleš (ur.), KALUŽA, Boštjan (ur.). *Zbornik = Proceedings*. Ljubljana: Mednarodna podiplomska šola Jožefa Stefana, 2012, str. 51-58. [COBISS.SI-ID 26831911]

J. Lazar, S. Zavšek, S. Jamnikar, J. Žula, G. Uranjek, L. Golob, “Execution of RFCS CoGasOUT project,” V: 4th Balkan Mining Congress, Ljubljana, Slovenia, 18th-20th October 2011. MEDVED, Milan (ur.), VULIĆ, Milivoj (ur.). *Paper's book*. Velenje: Coal Mine, 2011, str. 681-686. [COBISS.SI-ID 26831399]

J. Lazar, S. Zavšek, S. Jamnikar, J. Žula, G. Uranjek, L. Golob, “Čiste premogovne tehnologije in projekt CoGasOUT,” V: 3. študentska konferenca Mednarodne podiplomske šole Jožefa Stefana = 3rd Jožef Stefan International Postgraduate School Students Conference, 25. maj 2011, Ljubljana, Slovenija. PETELIN, Dejan (ur.), et al. *Zbornik prispevkov = Proceedings*. Ljubljana: Mednarodna podiplomska šola Jožefa Stefana, 2011, str. 22-28. [COBISS.SI-ID 26831143]

JAMNIKAR, Sergej, LAZAR, Jerneja, ZAVŠEK, Simon, URANJEK, Gregor. “Execution and results of RFCS funded project CoGasOUT at Coal-Mine Velenje” *: 5. Študentska konferenca Mednarodne podiplomske šole Jožefa Stefana, 23. maj 2013, Ljubljana, Slovenija*. 2012. [COBISS.SI-ID 26889767]

J. Lazar, S. Jamnikar, S. Zavšek, L. Golob, J. Žula, G. Uranjek, “Results of in-situ measurements, laboratory experiments on lignite samples and numerical modeling of coal pillar, performing under research projects CoGasOUT and GHG2E” *: . 4. Študentska konferenca Mednarodne podiplomske šole Jožefa Stefana, 25. maj 2012, Ljubljana, Slovenija*. 2012. [COBISS.SI-ID 26889511]

J. Lazar, S. Zavšek, S. Jamnikar, G. Uranjek, L. Golob, *“*Clean coal technologies*” : presented at Fifth International Conference on Clean Coal Technologies CCT 2011, Zaragoza, Spain*. 2011. [COBISS.SI-ID 26889255]

Biography

Gregor Uranjek was born on 04/20/1976 in Slovenj Gradec, Slovenia. He Attended primary and high school in Velenje and in 1991 followed mechanical technician training. In 1995, he started his studies of Mining and Geotechnology at the Faculty of Natural Sciences. In 2007, he successfully defended a bachelor's thesis entitled "An addition to construction monitoring with simultaneous application of various types of observation" for which he received "Student Prešeren Award". The same year he passed the English language examination at the Faculty of Arts in Ljubljana and was accepted for a three-year habilitation as assistant in the field of Mine Survey and Applied Geophysics at the Faculty of Natural Sciences. During the entire study period, he has carried out various student works to support himself. Since 2007, he has been employed at Premogovnik Velenje, d.o.o. (the Velenje Coal Mine). In 2010, he began his PhD studies in Ecotechnology at the Jožef Stefan International Postgraduate School. Since 2017, he has been working at the Velenje Coal Mine in management or technical management positions, respectively.

His research is dedicated to developing approaches to quantifying odorous emissions from the extraction process in the coal mine and to developing technical odour abatement measures for underground mines.

Membership in associations:
Between 1989 and 2001 he was training fencing at the Rudolf Cvetko Fencing Club in Velenje. As a member of the Slovenian National Youth Team he participated in one World Championship and two European Championships. Between 2007 and 2011 was a coach at the fencing club. Between 2009 and 2011, he was a technical director of the Fencing Association of Slovenia.